Talanta

The International Journal of Pure and Applied Analytical Chemistry

Publication information: *Talanta* (ISSN 0039-9140). For 2007, volumes 71–73 are scheduled for publication. Subscription prices are available upon request from the Publisher or from the Regional Sales Office nearest you or from this journal's website (http://www.elsevier.com/locate/talanta). Further information is available on this journal and other Elsevier products through Elsevier's website: (http://www.elsevier.com). Subscriptions are accepted on a prepaid basis only and are entered on a calendar year basis. Issues are sent by standard mail (surface within Europe, air delivery outside Europe). Priority rates are available upon request. Claims for missing issues should be made within six months of the date of dispatch.

Orders, claims, and journal enquiries: please contact the Customer Service Department at the Regional Sales Office nearest you:
Orlando: Elsevier, Customer Service Department, 6277 Sea Harbor Drive, Orlando, FL 32887-4800, USA; phone: (+1) (877) 8397126 [toll free number for US customers], or (+1) (407) 3454020 [customers outside US]; fax: (+1) (407) 3631354; e-mail: usjcs@elsevier.com
Amsterdam: Elsevier, Customer Service Department, PO Box 211, 1000 AE Amsterdam, The Netherlands; phone: (+31) (20) 4853757; fax: (+31) (20) 4853432; e-mail: nlinfo-f@elsevier.com
Tokyo: Elsevier, Customer Service Department, 4F Higashi-Azabu, 1-Chome Bldg, 1-9-15 Higashi-Azabu, Minato-ku, Tokyo 106-0044, Japan; phone: (+81) (3) 5561 5037; fax: (+81) (3) 5561 5047; e-mail: jp.info@elsevier.com
Singapore: Elsevier, Customer Service Department, 3 Killiney Road, #08-01 Winsland House I, Singapore 239519; phone: (+65) 63490222; fax: (+65) 67331510; e-mail: asiainfo@elsevier.com

USA mailing notice: *Talanta* (ISSN 0039-9140) is published monthly by Elsevier B.V. (P.O. Box 211, 1000 AE Amsterdam, The Netherlands). Annual subscription price in the USA US$ 3,818 (valid in North, Central and South America), including air speed delivery. Application to mail at periodical postage rate is paid at Rathway, NJ and additional mailing offices.
USA POSTMASTER: Send address changes to *Talanta*, Publications Expediting Inc., 200 Meacham Avenue, Elmont, NY 11003.
AIRFREIGHT AND MAILING in the USA by Publications Expediting Inc., 200 Meacham Avenue, Elmont, NY 11003.

Available online at www.sciencedirect.com
ScienceDirect
Talanta 72 (2007) 1847–1852
Talanta
www.elsevier.com/locate/talanta

Short communication

Simultaneous spectrophotometric determination of Sn(II) and Sn(IV) by mean centering of ratio kinetic profiles and partial least squares methods

Tayyebeh Madrakian [a,*], Abbas Afkhami [a], Roshanak Moein [a], Morteza Bahram [b]

[a] *Faculty of Chemistry, Bu-Ali Sina University, Hamadan, Iran*
[b] *Department of Chemistry, Faculty of Science, Urmia University, Urmia, Iran*

Received 8 November 2006; received in revised form 3 February 2007; accepted 3 February 2007
Available online 21 February 2007

Abstract

Two spectrophotometric methods are described for the simultaneous determination of binary mixtures of Sn(II) and Sn(IV) in water samples and fruit juice samples, without prior separation steps, using the mean centering of ratio kinetic profiles and partial least squares (PLS) methods. The methods are based on the difference in the rate of the reactions of Sn(II) and Sn(IV) with pyrocatechol violet at pH 4.0. The methods allow rapid and accurate determination of Sn(II) and Sn(IV). The analytical characteristics of the methods for the simultaneous determination of binary mixtures of Sn(II) and Sn(IV) were calculated. The results showed that the methods were capable to simultaneous determination of 0.1–1.80 mg L^{-1} each of cations. The proposed methods were successfully applied to the simultaneous determination of Sn(II) and Sn(IV)in an orange juice sample.

Keywords: Sn(II) and Sn(IV); Simultaneous determination; Orange juice; Water

1. Introduction

Tin is a toxic metal, which could gather in a human's body and the tissue of animals [1]. There are mainly two chemical species of inorganic tin (Sn(II) and Sn(IV)) in environmental samples. Sn(II) seems to be more toxic than Sn(IV) [2]. Differential toxicities of the different forms of an element have dictated an increasing development and use of analytical determination of the chemical species. Several methods including atomic absorption spectrometry [3–6], atomic emission spectrometry [7,8], spectrophotometry [9–13], electrochemical methods [14–17], spectrofuorimetry [18,19] have been developed for the determination of tin. To the best of our knowledge there is no report on the simultaneous determination of Sn(II) and Sn(IV).

Simultaneous determination of two or more compounds in the same mixtures without preliminary separation is the main problem of spectrophotometric multicomponent analysis. Several spectrophotometric determination methods have been used for resolving mixtures of compounds with overlapping spectra. The methods, such as derivative spectrophotometry [20], partial least squares regression (PLSR) [21,22], principal component regression (PCR) [23], multi-wavelength linear regression analysis (MLRA) [24], H-point standard addition method (HPSAM) for binary [25] and ternary [26] mixtures have been utilized.

Differences in kinetic behavior have also been used extensively for the simultaneous determination of two or more components in mixtures. Many differential kinetic methods have been proposed for the analysis of mixtures of closely related species without prior separation [27,28].

Recently, some new approaches have been presented for simultaneous analysis of binary and ternary mixtures, which called "mean centering of ratio spectra" [29–33].

Pyrocatechol violet (pyrocatechol sulfonaphthalein or 3,3′,4′-trihydrooxyfuchsone-2′-sulfonic acid, PCV), a dye in the triphenylmethane series has been used for spectrophotometric determination of some cations including Al(III) [34], Fe(II) [35], U(VI) [36] and Sn(IV) [37].

In this paper, we discuss two different methods, for the simultaneous analysis of binary mixtures of Sn(II) and Sn(IV) based on the difference in the rate of complex formation of these metal

* Corresponding author. Tel.: +98 811 8272404; fax: +98 811 8272404.
E-mail address: madrakian@basu.ac.ir (T. Madrakian).

0039-9140/$ – see front matter © 2007 Published by Elsevier B.V.
doi:10.1016/j.talanta.2007.02.023

ions with PCV without any preliminary separation. The methods are mean centering of ratio kinetic profiles and partial least squares (PLS) methods. The aim of this work on the one hand is to present a sensitive and selective chemical system for simultaneous determination of Sn(II) and Sn(IV), and on the other hand to compare the applicability of mean centering of ratio kinetic profiles and PLS for simultaneous analysis of binary mixtures.

2. Experimental

2.1. Apparatus

A Perkin-Elmer Lambda 45 UV–vis spectrometer was used for recording and storage of UV–vis absorbance spectra using 1 cm quartz cells and slit width of 0.5 nm. A Metrohm model 713 pH-meter with a combined glass electrode was used for pH measurements. All calculations in the computing process were done in Matlab 6.5 and Microsoft Excel for Windows.

2.2. Reagents

Distilled water and analytical-reagent grade chemicals were used. A 100 mg L^{-1} of Sn(II) and Sn(IV) were prepared by dissolving appropriate amounts of $SnCl_2{\cdot}2H_2O$ (Merck) and $SnCl_4{\cdot}5H_2O$ (Fluka) in 0.2 mol L^{-1} HCl solution. A 1.0×10^{-3} mol L^{-1} PCV (Merck) solution was prepared daily by dissolving 0.0386 g of this indicator in water and diluting to the mark in a 100 mL volumetric flask. Acetic acid–acetate (1.0 mol L^{-1}) buffer solution of pH 4.0 was prepared from acetic acid and sodium acetate (Merck).

2.3. Procedure

Aliquots of Sn(II) and Sn(IV) solutions was transferred into a 5 mL volumetric flask containing 2.0 mL of pH 4.0 acetate buffer solution and 1.68 mL of 1.0×10^{-3} mol L^{-1} PCV and finally, the solution was diluted to the mark with distilled water. A portion of the solution was transferred into a quartz cell to record the absorption kinetic profile of the solution at 550 nm in the time range 0–600 s with 4 s intervals. Kinetic profiles for the solutions contain Sn(II) and Sn(IV) with different concentrations was recorded.

3. Results and discussion

3.1. Reaction of Sn(IV) and Sn(II) with PCV

PCV forms at least two complexes with Sn(IV) [38]. The absorption spectra of PCV in the presence of two different amounts of Sn(IV) show that at low ratios of Sn(IV): PCV the predominant form of the complex is a 1:2 Sn(IV): L complex with a λ_{max} at 550 nm, while at high ratios of Sn(IV): PCV both the 1:1 and 2:1 Sn(IV): L complexes are present in the solution [39]. The absorption behavior of PCV in the presence of Sn(II) was also recorded. The results (Fig. 1) show that the absorption spectra obtained by the addition of Sn(II) to PCV solution are exactly the same as those obtained by the addition of Sn(IV). The absorbance-time diagrams for Sn(IV)–PCV mixture and Sn(II)–PCV at 550 nm are given in Fig. 2. As Fig. 2 shows the complexation reaction of Sn(IV) is more rapid than that of Sn(II). PCV oxidizes Sn(II) to Sn(IV) and the produced Sn(IV) ions then react with PCV to form complexes. The difference in the kinetic behavior of Sn(II) and Sn(IV) in the reaction with PCV can be used to their simultaneous determination.

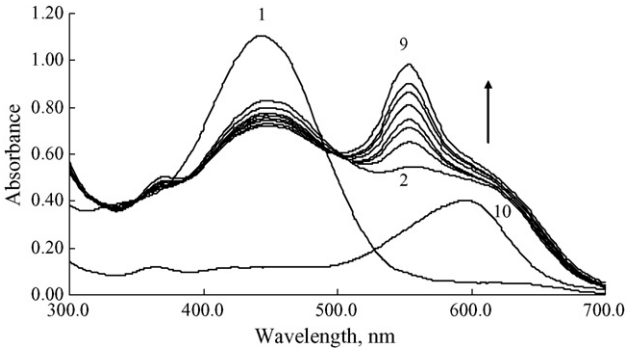

Fig. 1. The absorption spectra for (1) 5.0×10^{-4} mol L^{-1} PCV, (2–9) 5.0×10^{-4} mol L^{-1} PCV in the presence of 5.0×10^{-5} mol L^{-1} of Sn(II) at different times (time intervals 1 min) at pH 4.0 and (10) 1.0×10^{-3} mol L^{-1} of Sn(II) in the presence 1.0×10^{-4} mol L^{-1} PCV at pH 4.0 at 10 min after mixing.

3.2. The optimum experimental conditions

The complex formation reactions of Sn(II) and Sn(IV) ions with PCV depend on pH. In order to find the optimum pH, the effect of pH in the range of 2–6 and different buffer solutions on the rate of the complex formation reactions and spectral characteristics of the complex of a constant concentration of each cation with PCV was investigated. The results show, the absorbance change in the range of 1–10 min after initiation of the reaction increases by increasing pH of the solution up to 4.0 and decreases at higher pH values. Therefore, pH 4.0 was selected as optimum pH. Citrate Phthalate and acetate buffer solutions of pH 4.0 were tested and the acetate buffer solution was found as the best. A 3.2×10^{-4} mol L^{-1} PCV, at least 10-fold excess over maximum concentration of metal ions, was applied to obtain a pseudo-first order reaction with respect to each cation.

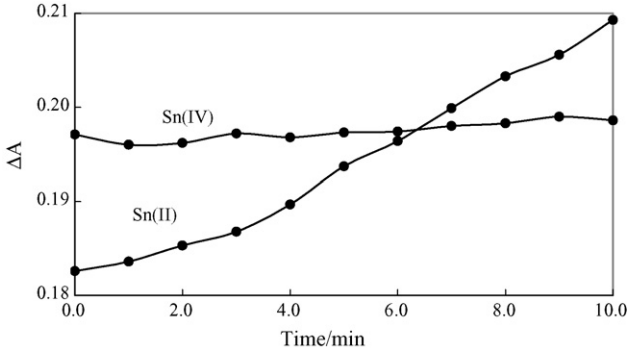

Fig. 2. The kinetic profiles of complexation reactions of Sn(II) and Sn(IV) with PCV at 550 nm, conditions: PCV concentration 3.2×10^{-4} mol L^{-1}, the concentration of Sn(II) and Sn(IV) was 0.60 mg L^{-1} at pH 4.0.

3.3. Mean centering of ratio kinetic profiles

The theoretical background of this work has been described previously [30,32]. Mean centering of ratio kinetic profiles was used to the simultaneous determination of Sn(II) and Sn(IV) based on the difference in the rate of their complexation reaction with PCV in aqueous media without any preliminary separation.

The kinetic profiles of complexation reactions of Sn(II) and Sn(IV) with PCV at 550 nm and 25 °C are presented in Fig. 2. As Fig. 2 shows the kinetic profiles of the complexation reactions of Sn(II) and Sn(IV) with PCV are different and this difference could be used to their simultaneous determination.

A calibration graph for Sn(II) was obtained by recording and storing the kinetic profiles of standard solutions containing different concentrations of Sn(II) and Sn(IV). The stored kinetic profiles for the solutions of Sn(II) were divided by normalized kinetic profile of Sn(IV) and the ratio profiles were obtained. Then mean centering of these vectors with respect to time were obtained. The minimum or maximum of the mean centering of ratio profiles with respect to time was used for the construction of calibration graph for Sn(II). For the prediction of concentration of Sn(II) in synthetic binary mixtures and real samples the same procedure was used except that the kinetic profiles of the mixtures were used instead of the kinetic profiles of standard solution of Sn(II). The construction of calibration curves for Sn(IV) was performed as described for Sn(II).

The absorption kinetic profiles of the standard solutions of Sn(II) and Sn(IV) with different concentrations were recorded at 550 nm in the time range 0–600 s (Figs. 3a and 4a) with 4 s intervals and divided by the normalized kinetic profile of the Sn(IV) and Sn(II), respectively, and the ratio profiles were obtained (Figs. 3b and 4b). Mean centering of the ratio profiles for Sn(II) were obtained in the time range of 64–94 s (Fig. 3c). The concentration of Sn(II) was determined by measuring the amplitude at 64 s corresponding to a maximum amount in the mean centering of ratio profiles as shown in Fig. 3c. For the prediction of concentration of Sn(II) in synthetic binary mixtures and real samples the same procedure was used except that the kinetic profiles of the mixture were used instead of the kinetic profiles of standard solutions of Sn(II). Mean centering of the ratio profiles were obtained in the time range of 32–64 s (Fig. 3c). The concentration of Sn(IV) was determined by measuring the amplitude at 32 s corresponding to a maximum amount in the mean centering of ratio profiles as shown in Fig. 4c. For the prediction of concentration of Sn(IV) in synthetic binary mixtures and real samples the same procedure was used except that the kinetic profiles of the mixtures were used instead of the kinetic profiles of standard solutions of Sn(IV).

3.3.1. Analytical characteristics

In the proposed method, Beer's law was obeyed in the concentration range 0.10–1.80 mg L^{-1} for both Sn(II) and Sn(IV) ions. Table 1 shows the linear regression parameters for calibration data for simultaneous determination of Sn(II) and Sn(IV) in their binary mixtures. Limit of detection of the method for determination of Sn(II) and Sn(IV) (defined as the concentration equivalent to three times the standard deviation of five replicate measurements of the blank) are also shown in Table 1. To check the reproducibility of the method five replicate resolving of Sn(II) and Sn(IV) mixtures were performed. The mean recoveries for simultaneous determination of these species in binary mixtures were 104 and 101% for Sn(II) and Sn(IV), respectively.

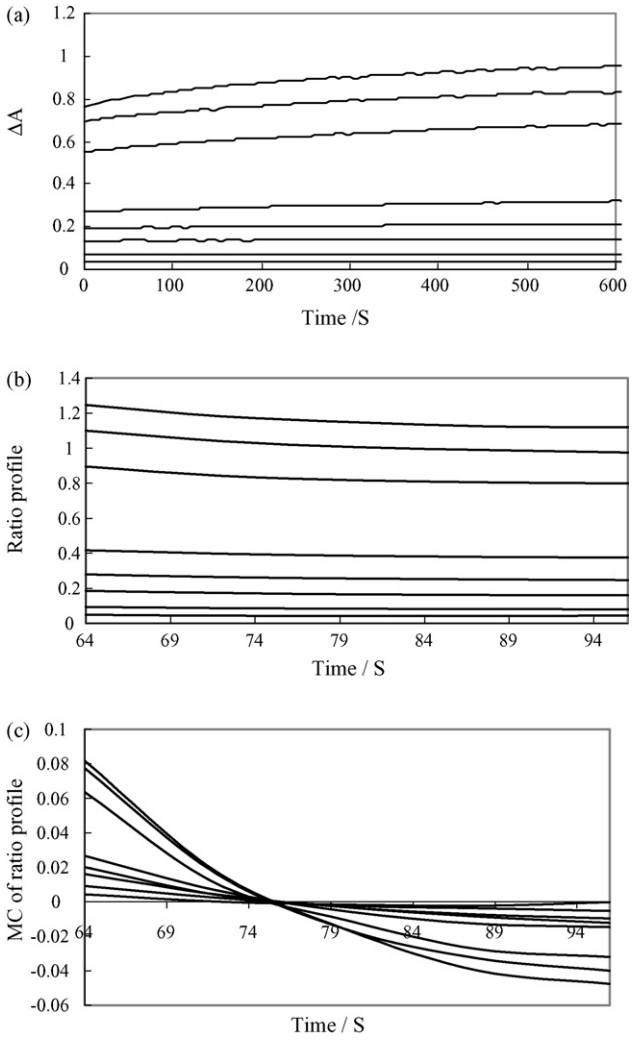

Fig. 3. The absorption kinetic profiles of the standard solutions of the Sn(II) with different concentrations (0.10, 0.20, 0.40, 1.00 and 1.80 mg L^{-1}) were recorded at 550 nm (a), the ratio profiles obtained by dividing the normalized kinetic profile of the Sn(IV) (b) and the mean centering of ratio profiles (c).

The effect of time range on the analytical parameters such as slope, intercept and correlation coefficient of the calibration graphs was also tested. It was observed that changing the time range had significant effect on the analytical parameters. The best time range is that provides the maximum slope, the minimum intercept and the best correlation coefficient. Therefore, selection of the time range was performed for Sn(II) and Sn(IV) separately. Different time ranges were used and the best time range for Sn(II) and Sn(IV) by the proposed method was obtained as 64–96 s and 32–64 s, respectively. The effect of divisor concentration on the analytical parameters such as detection limit, slope, intercept and correlation coefficient of the calibration graphs was also tested. It was observed that changing the concentration of divisors in their linear calibration range had no

Table 1
Analytical characteristics for analysis of Sn(II) and Sn(IV) in binary mixture by the mean centering of ratio kinetic profiles method

Analyte	Calibration equation	R^a	Linear range (mg L^{-1})	LOD (mg L^{-1})[b]
Sn(II)	$Y = 0.0483X - 0.0029$	0.9985	0.10–1.80	0.03
Sn(IV)	$Y = 0.0428X + 0.0009$	0.9991	0.10–1.80	0.05

[a] Correlation coefficient.
[b] Limit of detection.

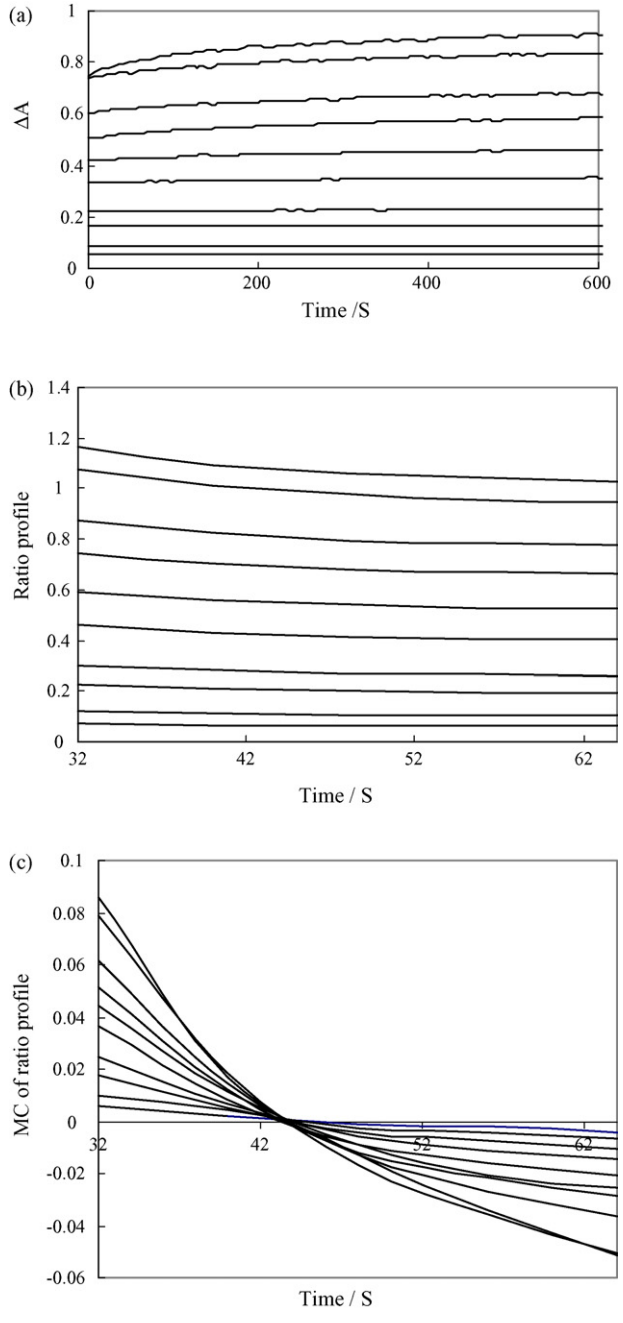

Fig. 4. The absorption kinetic profiles of the standard solutions of the Sn(IV) with different concentrations (0.10, 0.20, 0.40, 1.00 and 1.80 mg L^{-1}) were recorded at 550 nm (a), the ratio profiles obtained by dividing the normalized kinetic profile of the Sn(II) (b) and the mean centering of ratio profiles (c).

significant effect on the analytical parameters. Therefore, a normalized kinetic profile of each of the Sn(II) and Sn(IV) was used as divisor profile in the proposed method. In order to obtain the accuracy and precision of the method, several synthetic mixtures with different concentration ratios of Sn(II) and Sn(IV) were analyzed using the proposed method. The prediction error of a single component in the mixtures was calculated as the relative standard error (R.S.E.) for the prediction concentration [29]:

$$\text{R.S.E.}(\%) = \left(\frac{\sum_{j=1}^{N} (\hat{C}_j - C_j)^2}{\Sigma_{J=1}^{N} (C_j)^2} \right)^{1/2} \times 100 \quad (1)$$

where N is the number of samples, C_j the concentration of the component in the jth mixture and $\hat{C}_j$ is the estimated concentration. The total prediction error (R.S.E.$_t$) of N samples is calculated as follows:

$$\text{R.S.E.}_t(\%) = \left(\frac{\sum_{i=1}^{M} \sum_{j=1}^{N} (\hat{C}_{ij} - C_{ij})^2}{\sum_{i=1}^{M} \sum_{j=1}^{N} (C_{ij})^2} \right)^{1/2} \times 100 \quad (2)$$

where C_{ij} is the concentration of the component in the jth sample and $\hat{C}_{ij}$ is its estimated value. The reasonable single relative errors for Sn(II) and Sn(IV) were 3.76 and 3.80%, respectively, and total relative error was 3.78%.

3.4. Partial least squares regression

Under the optimum conditions described in Section 3.2, calibration graphs for Sn(II) and Sn(IV) were constructed by plotting absorbance change values during 0–600 s as a function of the analyte concentration. The calibration graphs were linear in the range of 0.10–2.00 mg L^{-1} for both Sn(II) and Sn(IV) ions, respectively.

The PLS-1 calibration for both ions was constructed by using the NIPALS algorithm. To choose the calibration samples, the components to be determined have been selected in order to span all dimensions. A training set of 26 standard samples (17 samples as calibration set and 9 samples as prediction set) in aqueous media was taken from different mixtures of Sn(II) and Sn(IV) ions. Each concentration was varied between 0.10 and 2.00 mg L^{-1} through the calibration and prediction matrices. The correlation between the different calibration samples has to be avoided because colinear components in the training set data will tend to cause under-fitting in the PLS models. The obtained model was validated with a nine synthetic mixture set

containing the considered metal ions in different proportion. The kinetic profile between 0 and 600 s was selected for analysis.

3.4.1. Statistical parameters

Some statistical parameters were given for the validation of the constructed calibrations for the training set and the synthetic binary mixtures of both ions. The application ability of a calibration model can be explained in various ways. The prediction error of a single component in the mixture and the total prediction error were calculated by using Eqs. (1) and (2). The reasonable single relative errors for Sn(II) and Sn(IV) were 4.5 and 1.80%, respectively, and total relative error was 3.40%. To select the number of factors in the PLS algorithm a cross-validation method leaving out one sample at a time, was employed [40]. For the mentioned sets of 17 calibration kinetic profiles, PLS calibration on 16 calibration kinetic profiles was performed and using this calibration the concentration of the sample left out during the calibration process was calculated. This process was repeated 20 times and each sample has been left only once. The concentration of each sample was then predicted and compared with the know concentration of this reference sample, the prediction residual error sum of squares (PREES) was calculated (Eq. (3)).

$$\mathrm{PRESS} = \sum_{i}^{N} (C_i^{\mathrm{added}} - C_i^{\mathrm{found}})^2 \quad (3)$$

Fig. 5 shows the plot of the PREES versus the number of factor for each individual component in aqueous media. For finding the smallest number of factors, the *F*-statistic test was used to carry out to significant determination. PLS modeling obtained the number of factors of three for both elements.

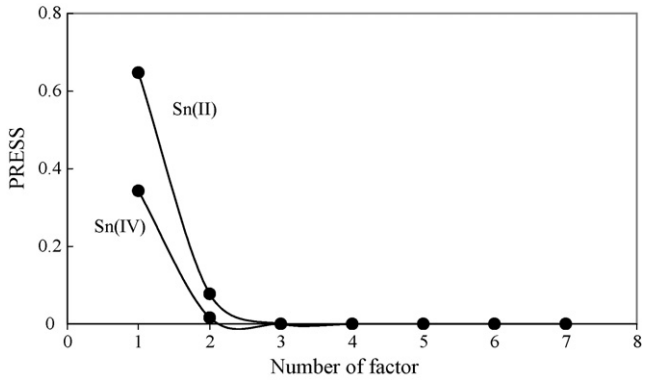

Fig. 5. Plot of PRESS against the number of factors for Sn(II) and Sn(IV) in aqueous media.

Table 2
Tolerance ratio of diverse ions on the determination of mixtures of 1.00 mg L^{-1} each of Sn(II) and Sn(IV)

Ions	Tolerance ratio
Ni^{2+}, Co^{2+}, Na^{+}, K^{+}, NO_3^{-}, Be^{2+}, Mg^{2+}, Cd^{2+}, Ca^{2+}, Ba^{2+}, Mn^{2+}, Zn^{2+}, Pb^{2+}, Hg^{2+}, SO_4^{2-}	1000
Al^{3+}, Fe^{3+}, Bi^{3+}	100[a]
Cu^{2+}, Ag^{+}	50[a]
F^{-}, CN^{-}, $Cr_2O_7^{2-}$	10

[a] After addition EDTA 0.05%.

3.5. Interference study

The effects of different ions on the simultaneous determination of 1.0 mg L^{-1} each of the Sn(II) and Sn(IV) by proposed method was studied. An ion was considered as interferent, when it caused a variation in the recovery of analytes by the proposed method greater than ±5%. As the results (Table 2) show, most of the cations and anions did not interfere in the determination of Sn(II) and Sn(IV) even when present 1000-fold excess over Sn(II) and Sn(IV). Some of the species tried such as Al^{3+}, Fe^{3+}, Bi^{3+}, Cu^{2+} and Ag^{+} interfered on the determination of Sn(II) and Sn(IV) at 10–50-fold excess. The interfering effect of Al^{3+}, Fe^{3+} and Bi^{3+} ions was completely removed up to 100-fold in the presence of 0.05% of EDTA, as a proper masking agent. The interfering effect of Cu^{2+} and Ag^{+} ions was completely removed up to 50-fold in the presence of 0.05% of EDTA. The ions F^{-}, CN^{-} and $Cr_2O_7^{2-}$ interfered at 10-fold excess over Sn(II) and Sn(IV).

3.6. Application

The proposed methods were successfully applied to the simultaneous determination of mixtures of Sn(II) and Sn(IV) in canned orange juice samples. For digestion of the sample, five milliliters of orange juice was transferred into a 250 mL Erlenmeyer flask and 10 mL concentrated sulfuric acid was added.

Table 3
Determination of Sn(II) and Sn(IV) mixtures in an orange juice sample by the mean centering of ratio profiles (method I) and PLS (method II) methods

Method	Sn(II) (mg L^{-1})			Sn(IV) (mg L^{-1})			Total Sn[b]
	Added	Found[a]	Recovery (%)	Added	Found[a]	Recovery (%)	
I	–	24.2	–	–	32.6		57.1
	5.0	29.5	106.0	10.0	42.1	95.0	
	15.0	38.8	97.3	20.0	53.2	103.0	
II							
	–	23.9	–	–	32.7	–	55.6
	5.0	28.8	98.0	10.0	42.4	97.0	
	15.0	38.0	94.0	20.0	53.9	106.0	

[a] Mean ± S.D. ($n = 3$).
[b] Determined by atomic absorption spectrometry.

The solution was diluted to about 75 mL by distilled water. Then, it was cooled, filtered and washed with water and the filtrate was collected in a 100 mL calibrated flask and diluted to the volume with water. The concentration of Sn(II) and Sn(IV) was determined by the proposed methods. Total concentration of tin in the samples was also determined by flame atomic absorption spectrometry (FAAS). The total amount of Sn(II) and Sn(IV) obtained by the proposed method is in good agreement with those obtained by FAAS. The results are shown in Table 3. The results show the applicability of the proposed methods for simultaneous determination of Sn(II) and Sn(IV) in such samples.

The proposed methods were also successfully applied to the simultaneous determination of mixtures of Sn(II) and Sn(IV) after addition to tap water samples. The obtained recoveries were in the ranges of 96.5–106% and 95.0–107.0% for Sn(II) and Sn(IV), respectively.

4. Conclusion

The proposed methods, PLS-1 and mean centering of ratio kinetic profiles, are very suitable for simultaneous determination of Sn(II) and Sn(IV) by kinetic spectrophotometric method and can be applied to the analysis of water samples and fruit juice samples. The results show that accuracy, precision, reproducibility, sensitivity and linear range are nearly the same for both the methods. These methods are very simple, rapid, accurate and cost effective. These methods can be used for resolving binary mixtures in the complex samples with unknown matrices.

The mean centering of ratio kinetic profiles method is simple, very sensitive and easy to understand and apply. Standard addition can be simply used in the proposed method and matrix effects can be removed easily. Therefore, this method can be used for resolving binary and ternary mixtures in the complex samples with unknown matrices.

References

[1] M.E. Malla, M.B. Alvarez, D.A. Batistoni, Talanta 57 (2002) 277.
[2] B. Pawlik Skowronska, R. Kaczorowska, T. Skowronski, Environ. Pollut. 97 (1997) 65.
[3] M. Burguera, J.L. Burguera, C. Rivas, P. Carrero, R. Brunetto, M. Gallignani, Anal. Chim. Acta 308 (1995) 339.
[4] W. Horwitz (Ed.), Official Methods of Analysis of AOAC International, Method 973.36, seventeenth ed., AOAC international, Gaithersburg, MD, 2000.
[5] J. Moreda-Piñeiro, P. Lopez-Mahia, S. Muniategui-Lorenzo, E. Fernandez-Fernandez, D. Prada-Rodriguez, Anal. Chim. Acta 461 (2002) 261.
[6] I. Lopez-Garcia, I. Arnau-Jerez, N. Campillo, M. Hernandez-Cordoba, Talanta 62 (2004) 413.
[7] L. Perring, M. Basic Dvorzak, Anal. Bioanal. Chem. 374 (2002) 234.
[8] A.S. Ribeiro, A.L. Moretto, M.A.Z. Arruda, S. Cadore, Microchim. Acta 141 (2003) 149.
[9] A.M. Gutierrez, C. Perez-Conde, M.P. Rebollar, Talanta 32 (1985) 927.
[10] S.P. Arya, A. Bansal, Microchim. Acta 116 (1994) 63.
[11] L.F. Capitán-Vallvey, M.C. Valencia, G. Mirón, Anal. Chim. Acta 289 (1994) 365.
[12] A.C. Spinola Costa, L.S.G. Teixeira, S.L.C. Ferreira, Talanta 42 (1995) 1973.
[13] X. Huang, W. Zhang, S. Han, X. Wang, Talanta 44 (1997) 817.
[14] M. Taher, B. Puri, Talanta 48 (1999) 355.
[15] L. Clinio, T. Giancarlo, Microchem. J. 78 (2004) 175.
[16] Y. Li, H. Long, F. Zhou, Anal. Chim. Acta 554 (2005) 86.
[17] E.A. Hutton, S.B. Hočevar, L. Mauko, B. Ogorevc, Anal. Chim. Acta 580 (2006) 244.
[18] S. Rubio, A. Gomez-Hens, M. Valcarcel, Analyst 110 (1985) 43.
[19] J.L. Manzoori, M. Amjadi, D. Abolhasani, J. Hazard. Mater. B137 (2006) 1631.
[20] T. Madrakian, A. Afkhami, M. Borazjani, M. Bahram, Bull. Korean Chem. Soc. 25 (2004) 1764.
[21] T. Madrakian, A. Afkhami, M. Borazjani, M. Bahram, Spectrochim. Acta A 61 (2005) 2988.
[22] A. Afkhami, M. Bahram, Microchim. Acta 155 (2006) 403.
[23] E. Dinc, C. Yucesoy, F. Onur, J. Pharm. Biomed. Anal. 28 (2002) 1091.
[24] M. Blanco, J. Gene, H. Iturriaga, S. Maspoch, J. Riba, Talanta 34 (1987) 987.
[25] A. Afkhami, M. Bahram, Spectrochim. Acta A 60 (2004) 181.
[26] M. Hasani, L. Yaghoubi, H. Abdollahi, Talanta 68 (2006) 1628.
[27] A. Afkhami, A.R. Zarei, Talanta 60 (2003) 63.
[28] A. Afkhami, A.R. Zarei, Talanta 62 (2004) 559.
[29] A. Afkhami, M. Bahram, Talanta 66 (2005) 712.
[30] A. Afkhami, M. Bahram, Anal. Chim. Acta 526 (2004) 211.
[31] A. Afkhami, M. Bahram, Talanta 68 (2006) 1148.
[32] A. Afkhami, T. Madrakian, M. Bahram, J. Hazard. Mater. 123 (2005) 250.
[33] A. Afkhami, T. Madrakian, E. Bozorgzadeh, M. Bahram, Talanta 71 (2007) 1103.
[34] S. Tagashira, Anal. Chim. Acta 157 (1984) 343.
[35] M. Tarek, M. Zaki, W.H. Mahmoud, Talanta 35 (1988) 253.
[36] T. Madrakian, A. Afkhami, A. Mousavi, Talanta 71 (2007) 610.
[37] A.C. Spinola Costa, L.S.G. Teixeira, S.L.C. Ferreria, Talanta 42 (19995) (1973).
[38] W.D. Wakley, L.P. Varga, Anal. Chem. 44 (1972) 169.
[39] H.B. Corbin, Anal. Chem. 45 (1973) 534.
[40] H. Abdollahi, Anal. Chim. Acta 442 (2001) 327.

Available online at www.sciencedirect.com
ScienceDirect
Talanta 72 (2007) 1618–1624
Talanta
www.elsevier.com/locate/talanta

Flocculation-ultrasonic assisted extraction and solid phase clean-up for determination of polycyclic aromatic hydrocarbons in water rich in colloidal particulate with high performance liquid chromatography and ultraviolet-fluorescence detection

Shun-Li Fan [a,b], Lixia Zhao [a], Jin-Ming Lin [a,*]

[a] *State Key Laboratory of Environmental Chemistry and Ecotoxicology, Research Center for Eco-Environmental Sciences, Chinese Academy of Sciences, P.O. Box 2871, Beijing 100085, China*

[b] *Henan Key Laboratory for Environmental Pollution Control, College of Chemistry and Environmental Sciences, Henan Normal University, Xinxiang 453007, China*

Received 23 November 2006; received in revised form 1 January 2007; accepted 14 January 2007
Available online 20 January 2007

Abstract

In the present work, a simple method of sample preparation for the determination of polycyclic aromatic hydrocarbons (PAHs) in water rich in colloidal particulate was developed. The technique was mainly based on the effect of the flocculation of aluminum sulfate and the adsorption of the flocculation aid florisil. The method contained three steps: flocculation, ultrasonic extraction, and solid-phase extraction cleanup. Major parameters of the procedure were optimized with high performance liquid chromatography (HPLC) separation and ultraviolet-fluorescence detection. When 250 mL model sample containing 16 EPA PAHs was processed, the developed method provided detection limits in the range of 0.02–5 ng/L. Both spiked and non-spiked polluted river water samples rich in suspended particles and organic matters were analyzed. Recoveries and relative standard deviations for the 16 PAHs were in ranges of 86–94% and 3–13% ($n = 5$), respectively.

Keywords: Flocculation; Ultrasonic extraction; Solid-phase extraction; Polycyclic aromatic hydrocarbons; High performance liquid chromatography

1. Introduction

Polycyclic aromatic hydrocarbons (PAHs) are a special group of organic compounds originating from anthropogenic combustion processes and biogenic activities. Because of their mutagenic, carcinogenic, toxic nature and environmental ubiquitous occurrence, 16 PAHs have been selected as priority pollutants by the US Environmental Protection Agency (EPA) and consequently are monitored worldwide in environmental matrices. Although analytical instrumentations such as gas chromatography with mass spectrometry detection (GC/MS) and high performance liquid chromatography with fluorescence or ultraviolet detection (HPLC/FL or UV) have matured, determination of trace PAHs in aqueous samples is still often a difficult task as analytes enrichment and isolation are required. Sample preparation has become, in effect, a bottleneck in the laboratory processes nowadays [1,2].

Commonly used methods for aqueous PAHs sample preparation are liquid–liquid extraction (LLE) and solid-phase extraction (SPE) [1–6]. LLE has many well-known disadvantages such as emulsion and large volume consumption of toxic and flammable solvents, there is therefore an increasing tendency to replace LLE by SPE due to its advantages of selectivity of extraction and significant reduction of solvents consumption. SPE can be also used for solid samples by combination with other techniques like ultrasonic extraction [2,7,8]. However, SPE has drawbacks for water analysis, such as particle blockage, small cross-sectional area and slow sample processing rate, etc. [3]. It only works well with "clean" samples and has not yet been directly applied to polluted waters rich in colloidal particulate [1,4,5]. Furthermore, for water sample containing large amount

* Corresponding author. Present address: Department of Chemistry, Tsinghua University, Beijing 100084, China. Tel.: +86 10 62792343; fax: +86 10 62792343.
E-mail address: jmlin@mail.tsinghua.edu.cn (J.-M. Lin).

0039-9140/$ – see front matter © 2007 Elsevier B.V. All rights reserved.
doi:10.1016/j.talanta.2007.01.034

of particles and colloidal matter, preliminary filtration of the sample before SPE is proved not only time consuming but also unreliability because considerable PAHs may be lost in the step owing to the rather intensive adsorption on the solid particulate matter [1].

In recent years, some new techniques including solid-phase micro-extraction (SPME) [9–11] and stir bar sorptive extraction (SBSE) [12–14] and liquid-phase micro-extraction (LPME) [15–17] have been developed rapidly. Since they are all equilibrium methods, based on the PAHs partitioning between the aqueous and the extraction phases, rather than exhaustive method like LLE or SPE, problems like extraction stability and sensitivity are often reported. In addition, there also remain other evident defects of them unsolved. For example, SPME has inherent disadvantage of severe sample carry-over between runs, and LPME usually suffers from interference of particles contained in the aqueous water [15,16]. Generally, these techniques are more suitable for determination of free PAHs in relatively "clean" water [18].

It is well-known that coagulation–flocculation process is widespread used for removal of colloidal particulate and organic matter in engineering of water or wastewater treatment. According to the literatures reported, with this process, 80% of organic compounds and at least 85% of suspended solid could be removed from water [19]. And additions of some adsorbents or flocculant aids such as activated carbon [20], organobenite [21], metal oxides [22] to the system may considerably promote the removal further due to the synergetic effect of the accelerated kinetics of coagulation–flocculation, sedimentation, and particularly of adsorption. To our knowledge, however, no work about using the coagulation–flocculation process as a sample preparation tool for the purpose of analytical specific organic compounds such as PAHs in water has been done.

Due to their hydrophobicity and poor solubility, PAHs present a great affinity for colloidal particles and organic matter in water and are partitioned a significant proportion in these matrices [1,18]. It can be expected that an appropriate coagulation–flocculation process will effectively "remove" PAHs from water into the floc sediment. In this study, an attempt at employing coagulation–flocculation process as one of the sample preparation steps for determination of EPA 16 PAHs from polluted water in rich colloidal particles has been made. In the process, PAHs in the water sample were first "removed" to the floc sediment using aluminum sulfate and florisil as coagulant and flocculant aid, respectively. Then, in combination with ultrasonic extraction and solid phase clean-up, PAHs were enriched from the sediment and were finally determined by HPLC with ultraviolet-fluorescence detection.

2. Experiment

2.1. Reagents and materials

The 16 PAHs, naphthalene (Nap), acenaphthylene (Acy), acenaphthene (Ace), fluorene (Flue), phenanthrene (Phe), anthracene (An), fluoranthene (Flut), pyrene (Py), benz[*a*]anthracene (BaA), chrysene (Chy), benzo[*b*]fluoranthene (BbF), benzo[*k*]fluoranthene (BkF), benzo[*a*]pyrene (Bap), dibenz[*a,h*]anthracene (DBA), benzo[[*a*]]perylene (Bper), indeno[1,2,3-*cd*]pyrene (IP), were purchased from Aldrich (Milwaukee, WI, USA) and Supelco (Bellefonte, PA, USA). Individual stock solutions of these PAHs were made in acetonitrile at concentrations of approximately 250 μg/mL. These solutions were used to make a PAHs mixture for chromatography experiment and sample spiking test. A standard solution of the 16 PAHs (200 μg/mL for each compound) in methanol/methylene chloride (1:1, v/v) was delivered from Accustandard (New Haven, CT, USA). HPLC grade acetonitrile and methanol were from Fisher (Fair Lawn, NJ, USA). Pesticide grade dichloromethane and acetone were obtained from Dikma (Beijing, China). Aluminum sulfate, sodium sulfate and ammonium hydroxide (25–28%) were from Beijing Chemical Reagents Company (Beijing, China). Florisil (100–200 mesh) was from Jixiang Chemical Reagents Company (Shanghai, China). Sodium sulfate and Florisil were baked at 420 and 650 °C, respectively, for at least 12 h and stored in seal containers. All other reagents were analytical grade and deionized ultrapure water (EasyPureTM LF, Barnstead, Iowa, USA) was used throughout. The glasswares were cleaned by successive acetone and dichloromethane rinsing, soaking in a detergent bath, water washing and stored at 120 °C until use.

2.2. Apparatus and method

For the sample preparation, the procedures were mainly comprised three steps, flocculation, ultrasonication and SPE (Fig. 1).

In the flocculation step, a homemade conventional jar-test apparatus consisted of a beaker of 500 mL and an adjustable speed stirrer were employed. Coagulant of 6.0 mL 10% aluminum sulfate solution and flocculation aid of 4.0 g florisil were added directly to the beaker containing 250 mL water sample during the phase of agitation and the acidity was controlled at pH 6.0 using ammonium hydroxide or hydrochloric acid. The solution was stirred rapidly at 150 rpm for *ca.* 10 s during the reagents addition, followed by slow stirring at 60 rpm for 20 min and quiescent settling for 15 min. The supernatant was withdrawn as completely as possible by siphoning.

In the ultrasonication step, the precipitate was centrifuged at 3500 rpm for 5 min with a TDL-40B centrifuge (Shanghai Anting Scientific Instrument Factory, Shanghai, China), then mixed with 8 g anhydrous sodium sulfate, extracted with 30 mL acetone-dichloromethane (1:1, v/v) for 15 min at room temperature (*ca.* 25 °C) in a ultrasonic bath (40 kHz, Kunshan Ultrasonic Instrument Co., Jiangsu, China) with an occasional swirl to prevent its sticking to the bottom of the flask. The extract was filtered through a Whatman glass fiber filter and the filtrate was evaporated to half volume in a water bath so as to exclude the water-nonmiscible component of dichloromethane in the solvents.

The SPE was performed with Supelclean Envi-18 (3 mL) cartridges (Supelco, USA) on a set of Visiprep^{TM} Solid Phase

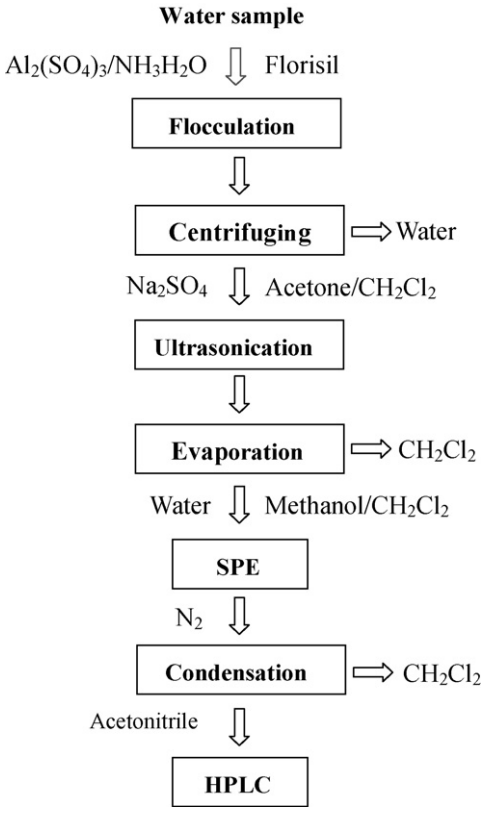

Fig. 1. Extraction procedures for the recovery of PAHs from waters.

Extraction Vacuum Manifolds (Supelco, USA). Prior to the SPE, the above solution obtained (about 15 mL) was reconstituted by addition 35 mL of water to make the extraction solution to be 30% (v/v) acetone in water. The SPE cartridge was conditioned with 5 mL dichloromethane, 5 mL acetone and 5 mL water in succession. The reconstituted solution was loaded at a flow rate of 4–6 mL/min. The cartridge was washed with 20 mL 40% acetone, dried by applying a vacuum (*ca.* 1 min) and passing through 0.3 mL methanol, then slowly eluted by application of 2.5 mL of dichloromethane. The eluate was evaporated to about 100 μL under a gentle stream of ultrapure nitrogen and the final volume of the residue was adjusted to 1 mL with acetonitrile before HPLC analysis.

For the PAHs analyses, a Shimadzu HPLC-10Avp system (Shimadzu, Tokyo, Japan) equipped with time-programmable ultraviolet-fluorescence detectors and an automatic sample injector was used. The PAHs were separated in a Nucleosil-100-5C18 PAH (250 mm × 4.6 mm ID) column (Macherey-Nagel, German). The chromatographic separation was performed with a mobile phase linear gradient comprising acetonitrile and water from 55% (v/v) acetonitrile to 100% acetonitrile within 20 min and then the final composition was maintained for further 10 min. The injection volume was 10 μL. The mobile phase flow rate was 1.3 mL/min and the column temperature was controlled at 30 °C. Fifteen PAHs were detected by the FL detector except that Acy by UV due to the lack of fluorescence. The detection wavelength programme used is given in Table 1.

Table 1
Wavelength programing in UV and FL detection

Time (min)	λ_{UV} (nm)	λ_{ex} (nm)	λ_{em} (nm)	PAHs
0	254	296	430	
8.40	220	280	340	Nap
9.30	229			Acy, Ace
11.45	254			Flue
12.40		250	350	Phen
13.55			400	An
14.76	235	280	450	Flut
15.75	240		393	Py
18.00	287		405	BaA
19.57	267	268		Chy
21.24	256	296	430	BbF
22.83	296			BkF Bap
25.58			395	DBA
27.00			418	Bper
28.00	249		500	IP

3. Results and discussion

3.1. Optimization of SPE procedure

In the SPE of PAHs, some operational parameters such as conditioning of the cartridge, flow rate of the sample loaded were directly determined according to the cartridge manufacturer's advice without further optimization. Since the techniques of elution PAHs from the cartridge and dryness of the eluate have matured, the conditions of these used in this work mainly referenced the previous investigations with some minor modification [2]. Other parameters were investigated by using 100 mL mixing standard solution containing 0.5–50 ng respective PAHs as a model sample. Each experiment was repeated three times and the data shown in the paper were the mean values.

One parameter studied was the concentration of the organic modifier added into the sample because the organic modifier could not only increase the solubility of PAHs thereby preventing them from adsorption onto the walls and surfaces of the system, but also keep the octadecyl chains of the C_{18} SPE cartridge in activated form [2]. In our experiments, acetone was used as the organic modifier. The recoveries of PAHs of the modified solution containing different percentages of acetone are shown in Fig. 2. The procedure for this investigation was

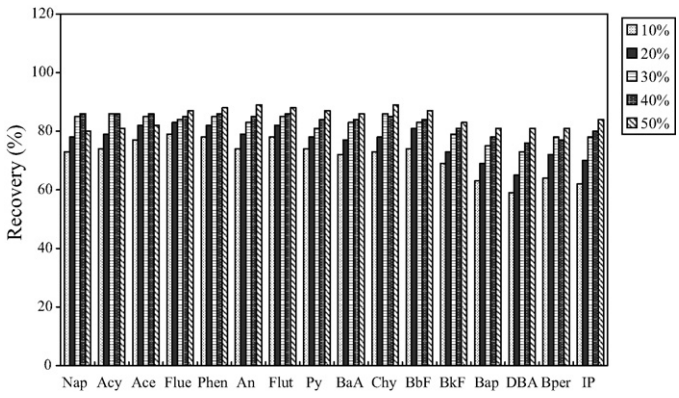

Fig. 2. Effect of acetone concentration on the recovery of PAHs.

almost the same as that described in Section 2.2, except that the step of washing cartridge was omitted and the cartridge drying was carried out by only applying a vacuum (20 min). From Fig. 2 it is clear that the recoveries for PAHs increased with the increase of acetone concentration up to 40%, which was especially more evident for the high molecular weight PAHs (5–6 rings). However, when the concentration of acetone was 50%, the recoveries for the low molecular weight PAHs (2–3 rings) became lower. This can be simply explained by the increases of both solubility of PAHs and the eluotropic strength of the sample when the acetone content was increased. The increase of solubility of PAHs is mainly conducive to higher recoveries for the high molecular weight PAHs due to their more hydrophobicity, while the increase of the eluotropic strength resulted in smaller breakthrough volumes for the low molecular weight PAHs that have relatively high solubilities in water. Since the difference of the recoveries obtained with 30% and 40% acetone content was not significant, 30% acetone in the sample was used as an organic modifier in the following experiment.

A clean-up step is necessary before the analytes are eluted from the cartridge when real sample is considerably contaminated. According to the results of our experiments, 20 mL 40% acetone was suitable to be the solvent because it has eluotropic strength higher than that of the sample loaded and lower than that of the solvent (dichloromethane) used for eluting PAHs. More importantly, the results showed that this was the maximum concentration of acetone and amount used under the condition that the recoveries of the 16 PAHs were in the acceptable ranges after the clean-up step. Therefore, 20 mL 40% acetone was used as SPE clean-up solvent in the real sample preparation.

After the cartridge clean-up, the cartridge drying is also an important aspect to be considered since an apolar solvent was used to elute the PAHs and the residue water on the cartridge can result in lower recovery and lower repeatability. Although water aspirator, flow of nitrogen or air, centrifuging are commonly used methods for drying the SPE cartridge nowadays, disadvantages are still present among them. All these methods are time consuming. Kiss et al. [6] found that about half amount of the residue water could be removed within 1 min with a water aspirator, but the other half seemed more refractory and still needed removal with nitrogen flow for 15 min. Moreover, long time suction may result in the loss of volatile PAHs, trace impurity in nitrogen or air leads to interference in the following detection, centrifuging usually cannot remove the water utterly [6]. In this work, we tested a new method for dry the cartridge. The method is simply carried out by applying a vacuum for 1 min first, then passing through an appropriate amount of methanol to the cartridge. The influence of the amount of methanol on the PAHs recoveries was studied. The results (Fig. 3) showed that good recoveries (93–102%) could be obtained when 0.3 mL methanol was applied. While Nap began to be eluted out and its recovery decreased significantly from 98% to 62% when 0.5 mL methanol was used. Compared with the results without applying methanol, it can be seen that methanol could efficiently remove the refractory water retained in the pores of the C_{18} sorbent due to its excellent miscibility.

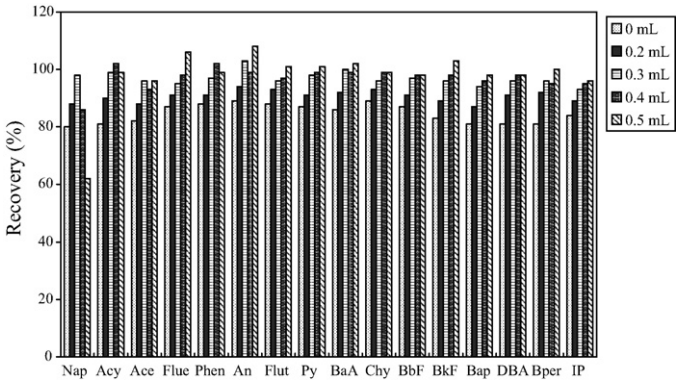

Fig. 3. Effect of cartridge drying with methanol on the recovery of PAHs.

3.2. Optimization of ultrasonic extraction

To optimize the ultrasonic extraction, the precipitate was initially obtained by flocculation of the model sample under almost the same conditions as that described in the first paragraph in Section 2.2, except that 2.0 mL $Al_2(SO_4)_3$ (10%), 2.0 g florisil were used and slow stirring time was 10 min. A mixture of acetone and dichloromethane (1:1, v/v), which is often used as a solvent for ultrasonic extraction of PAHs from solid sample [23], was applied to the procedure. The effect of the amount of acetone–dichloromethane on the recoveries of PAHs was examined in the range of 20–40 mL. As presented in Fig. 4, 30 mL of acetone–dichloromethane could almost reach maximum recoveries 63–80% for all PAHs. More Consumption of solvent did not increase the recoveries significantly. So, 30 mL solvent of acetone–dichloromethane was chosen for the ultrasonic extraction.

3.3. Optimization of flocculation procedure

Flocculation is a two-step serial process that consists of destabilization of colloid particles or organic matter via charge neutralization by coagulant and agglomeration of destabilized particles into larger settleable flocs via sweep flocs, adsorption and inter-particle bridging. In this process it is essential that the coagulant agent be added by rapid mixing for dispersion it throughout the liquid and subsequently slow mixing encourages collision of the particles to agglomerate into larger flocs. More-

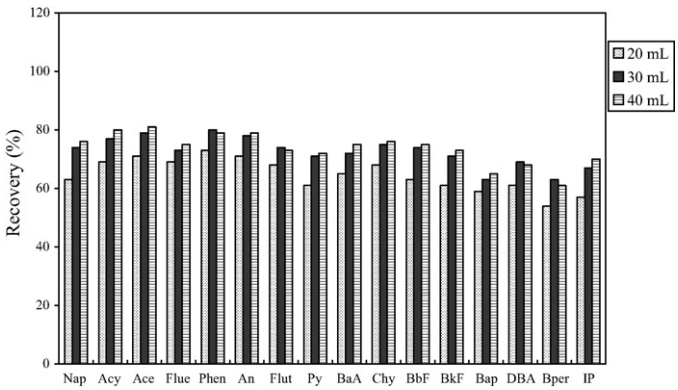

Fig. 4. Effect of solvent amount on the ultrasonic extraction of PAHs.

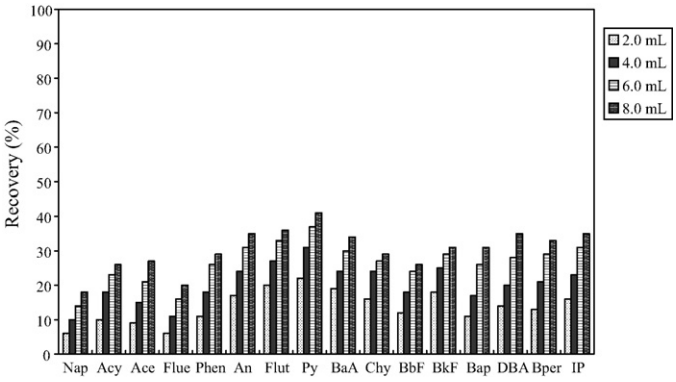

Fig. 5. Effect of 10% aluminum sulfate on the recovery of PAHs in the flocculation procedure.

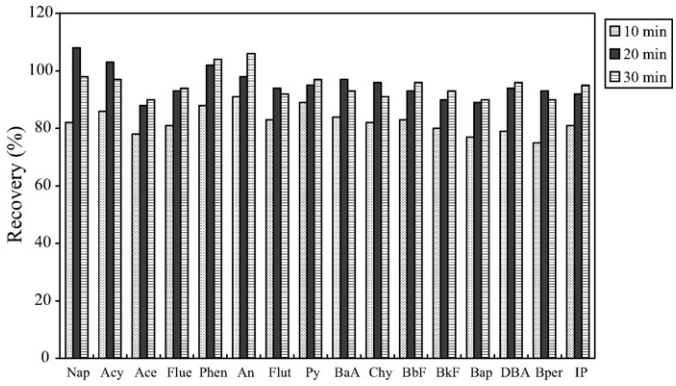

Fig. 7. Effect of floculation time on the recoveries of PAHs.

over the dosages of the coagulants (including flocculation aid), pH of the liquid and flocculation time were important factors in removal of colloids and pollutants. The study was conducted with 250 mL water spiked with 16 PAH (0.5–50 ng, respectively). And aluminum sulfate was selected as coagulant and florisil as flocculant aid due to their wide utilities in flocculation for wastewater treatment and adsorptive separation for analytical chemistry, respectively. The acidity of the liquid was always controlled at pH 6.0 with ammonium hydroxide or hydrochloric acid according to the literature reported pH 5.5–8.0 [24]. Optimizations of the dosage of coagulants and flocculation time were described bellow.

The result of the effect of the dosage of 10% aluminum sulfate is shown as Fig. 5. It can be seen that the efficiency of the PAHs recoveries was low when only aluminum sulfate was used as coagulant. Although the recoveries increased with the increase dosage added, product of hydrous aluminum oxide floc increased too correspondingly, and the floc settleablity was found to become poor when the coagulant dosage used was above 6.0 mL. For the addition of 6.0 mL of 10% aluminum sulfate, the recoveries were 14–37%, the precipitation time was 32 min. To promote the efficiency of the flocculation, flocculation aid of florisil was added simultaneously with the coagulant of aluminum sulfate. The results (Fig. 6) revealed that addition of florisil not only significantly increased the recoveries but also saved the time of the precipitation. With the addition of 4.0 g florisil and 10 min slow stirring (60 rpm), almost maximum PAHs recoveries, 75–91%, were yielded and the precipitation time was reduced to 15 min. This performance suggested that florisil played an important part in removal of PAHs in the process.

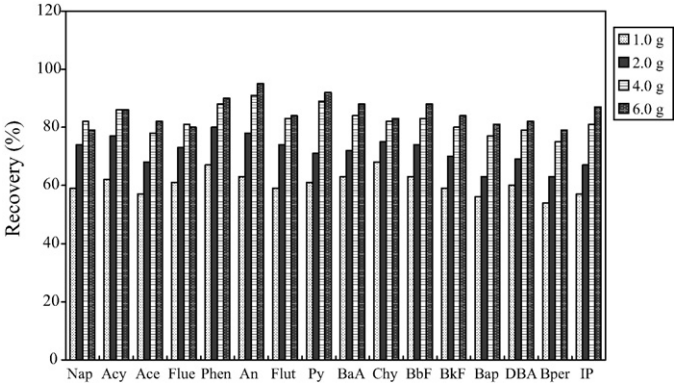

Fig. 6. Effect of florisil as flocculation aid on the recovery of PAHs.

The effect of floculation time on the recoveries of PAHs was examined in the range of 10–30 min with slow stirring operation. And the dosage of 10% aluminum sulfate and florisil were 6.0 mL and 4.0 g, respectively. The results (Fig. 7) demonstrated that the recoveries increased with the increase of flocculation time in the range 10–20 and 20 min flocculation provided almost the maximum recoveries (88–108%), and 30 min flocculation did not give much difference with that. Comparing the results with that obtained under without use of florisil, we can conclude that most part of the PAHs was removed likely by florisil adsorption due to its large specific surface area and a small part by flocculation. Furthermore, the florisil particles might also serve as nuclei for the formation of flocs during the process, which improved the agglomeration of the flocs and consequently facilitated their settling if the fact that precipitation time was evidently reduced with the addition of florisil was considered.

In summary, the optimal condition of the flocculation procedure was that 6.0 mL 10% aluminum sulfate and 4.0 g florisil were added simultaneously into 250 water sample at pH 6.0 with *ca.* 10 s of rapid mixing (150 rpm), 20 min of slow stirring (60 rpm) for flocculation and then settled 15 min for precipitation.

3.4. Analytical performance

To understand the analytical performance of the proposed method, 250 mL of PAHs standard solutions covering each of their linear ranges were enriched and determined under the optimized conditions. Two typical chromatograms were shown as Fig. 8. Peak heights were used to evaluate the linearity, precision and sensitivity of the method and the results were presented in Table 2. Good linearity was observed over the ranges tested. The regression coefficients obtained were between 0.9908 and 0.9973. The relative standard deviations (R.S.D.) measured by five repeated determination of a standard solution containing 50 ng/L for each PAHs, except for An 25 ng/L, ranged from 2% to 12%. The limits of detection calculated with a signal to noise ratio of three were less than 0.7 ng/L for 14 PAHs and 5 ng/L and 3 ng/L for Acy and IP respectively.

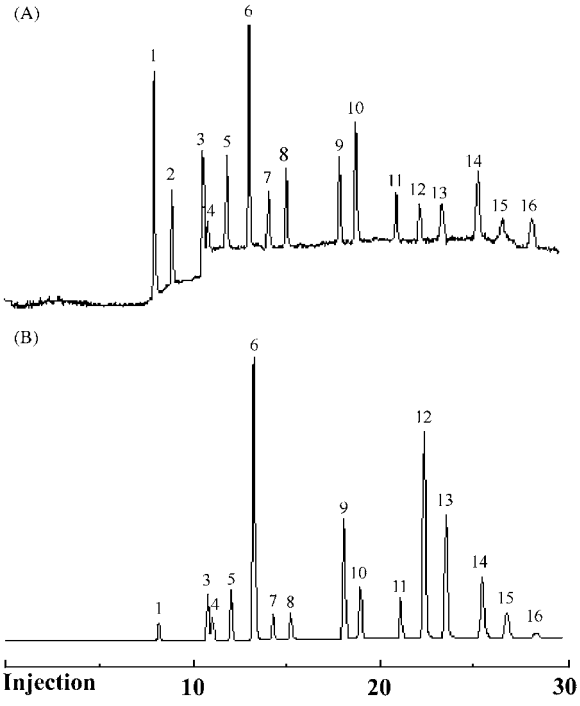

Fig. 8. Chromatograms for determination of 16 PAHs: (A) UV detection; (B) FL detection, 250 mL standard solution containing 50 ng/L for each PAHs enriched with the proposed method. 1: Nap; 2: Acy; 3: Ace; 4: Fue; 5: Phen; 6: An; 7: Flut; 8: Py; 9: BaA; 10: Chy; 11: BbF; 12: BkF; 13: Bap; 14: DBA; 15: Bper; 16: IP.

3.5. Application to polluted water analysis

The developed method had been applied to determine the 16 EPA PAHs in real water samples collected from the Qinghe River (Beijing, China). The water is polluted mainly with suspended particles and organic matters due to domestic wastewater discharge and urban rainfall-runoff. Concentrations of suspended particles and organic matters in the water determined by standard gravimetric analysis and potassium dichromate oxidization method (CODcr) were 79.5 and 38.8 mg/L, respectively. In order to validate the method, recoveries were also determined by spiking the sample with standard solution. The results are shown in Table 3. Chromatogram of the sample determined with FL detection is shown as Fig. 9. It can be seen that good recoveries (86–94%) were obtained for 16 EPA PAHs. The relative standard deviations were in the range 3–13% ($n = 5$). So, the developed method was applicable for determination of PAHs in water rich in colloidal particulate.

Table 2
Some analytical characteristics of the proposed method

PAHs	LODs[a] (ng/L)	R.S.D.[b] (%)	Range (ng/L)	Regression coefficient
Nap	0.7	12	5–500	0.9916
Acy[c]	5	9	20–500	0.9923
Ace	0.5	5	2–100	0.9958
Flue	0.5	6	2–100	0.9968
Phen	0.2	3	1–100	0.9945
An	0.02	7	0.1–50	0.9921
Flut	0.2	4	1–100	0.9937
Py	0.4	2	2–100	0.9962
BaA	0.2	3	1–100	0.9942
Chy	0.2	2	1–100	0.9973
BbF	0.4	4	2–100	0.9966
BkF	0.04	3	0.2–100	0.9925
Bap	0.2	5	1–100	0.9944
DBA	0.2	6	1–100	0.9929
Bper	0.5	8	2–100	0.9940
IP	3	9	10–500	0.9908

[a] LOD: limit of detection(N/S = 3)
[b] R.S.D.: relative standard deviation, 50 ng/L for each PAHs, except for An 25 ng/L ($n = 5$)
[c] UV detection.

Table 3
Determination of PAHs in polluted water (250 mL, $n = 5$)

PAHs	Original found (ng/L)	Added (ng/L)	Total found (ng/L)	Recovery (%)	R.S.D. (%)
Nap	113	100	202	89	13
Acy[a]	<DOL	100	88	88	11
Ace	93	100	187	94	7
Flue	34	50	80	92	6
Phen	75	50	120	90	4
An	6	10	15	90	8
Flut	36	50	79	86	5
Py	34	50	77	86	3
BaA	37	50	81	88	4
Chy	64	50	107	86	3
BbF	69	50	112	86	4
BkF	57	50	101	88	4
Bap	30	50	73	86	5
DBA	52	50	95	86	9
Bper	56	50	101	90	9
IP	57	50	100	86	10

[a] UV detection.

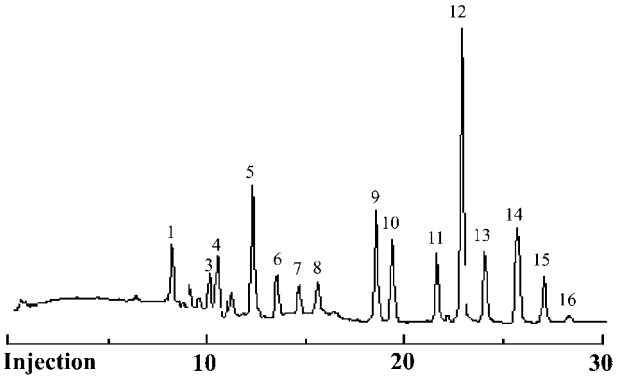

Fig. 9. HPLC-FL Chromatogram of polluted water sample concentrated by the proposed method, 250 mL river water was enriched under the optimal conditions. The peak numbers are same as in Fig. 8.

4. Conclusions

It was found that flocculation process could be used for recovery PAHs from polluted water rich in colloidal particulate. Employing aluminum sulfate as coagulant, florisil as flocculation aid, and combining with ultrasonic extraction, solid-phase clean-up techniques, we have studied the influence factors on the process and developed a new sample preparation method

for determination of PAHs in water. The method was successfully applied to determine the 16 EPA PAHs in polluted river water using HPLC ultraviolet-fluorescence detection. Compared with SPE technique, the developed method has several advantages: Firstly, overcoming the problem of particle blockage often encountered by SPE. Secondly, saving time. In SPE, the time consumption is proportional to the volume of sample loaded, while flocculation is operated at a confined scale of time, thus, large sample volume (e.g. >500 mL) will make the process consume relatively less time provided that SPE should carry out the same task, although the whole time required by the current method (*ca*. 70 min*)* is comparable with that of SPE. Finally, determination of total PAHs. The proposed method could be used for determination of total PAHs in very contaminated water, whereas SPE is usually used to determine dissolved or free PAHs in "clean" water and PAHs adsorbed on particles in water is excluded during the period of the sample preliminary filtration.

Although the experiments showed that the developed method was useful for water sample preparation, aluminum sulfate used only, as a coagulant, was proved not much effective for recovery of PAHs in water and a relative large amount of flocculation aid florisil was still required. Therefore, search and exploring new flocculation systems were needed to study further.

Acknowledgements

The authors gratefully acknowledge financial support of the National Natural Science Foundation of China (Nos. 20437020 and 20575073) and Major Research Program of Chinese Academy of Sciences (KZCX3-SW-432).

References

[1] E. Manoli, C. Samara, Trends Anal. Chem. 18 (1999) 417.
[2] R.M. Marce, F. Borrull, J. Chromatogr. A 885 (2000) 273.
[3] Z.S. Ferrera, C.P. Sanz, C.M. Santana, J.J.S. Rodriguez, Trends Anal. Chem. 23 (2004) 469.
[4] F. Busetti, A. Heitz, M. Cuomo, S. Badoer, P. Traverso, J. Chromatogr. A 1102 (2006) 104.
[5] E. Manoli, C. Samara, Chromatographia 43 (1996) 135.
[6] G. Kiss, Z. Varga-Puchony, J. Hlavay, J. Chromatogr. A 725 (1996) 261.
[7] Dugay, C. Herrenknecht, M. Czok, F. Guyon, N. Pages, J. Chromatogr. A 958 (2002) 1.
[8] F. Sun, D. Littlejohn, M.D. Gibson, Anal. Chim. Acta 364 (1998) 1.
[9] Mohammadi, Y. Yamini, N. Alizadeh, J. Chromatogr. A 1063 (2005) 1.
[10] P. Popp, C. Bauer, M. Moder, A. Paschke, J. Chromatogr. A 897 (2000) 153.
[11] R. Doong, S. Chang, Y. Sun, J. Chromatogr. A 879 (2000) 177.
[12] E. Baltussen, P. Sandra, F. David, C. Cramers, J. Microcol. Sep. 11 (1999) 737.
[13] B. Kolahgar, A. Hoffmann, A.C. Heiden, J. Chromatogr. A 963 (2002) 225.
[14] P. Popp, C. Bauer, L. Wennrich, Anal. Chim. Acta 436 (2001) 1.
[15] L. Zhao, H.K. Lee, Anal. Chem. 74 (2002) 2486.
[16] S. Shariati-Feizabadi, Y. Yamini, N. Bahramifar, Anal. Chim. Acta 489 (2003) 21.
[17] L. Hou, H.K. Lee, J. Chromatogr. A 976 (2002) 377.
[18] M.S. Garcia-Falcon, C. Perez-Lamela, J. Simal-Gandara, Anal. Chim. Acta 508 (2004) 177.
[19] M.I. Aguilar, J. Saez, M. Llorens, A. Soler, J.F. Ortuno, V. Meseguer, A. Fuentes, Chemosphere 58 (2005) 47.
[20] J.W. Lee, S.P. Choi, R. Thiruvenkatachari, W.G. Shim, H. Moon, Dyes Pigments 69 (2006) 196.
[21] Y.H. Shen, Environ. Technol. 23 (2002) 553.
[22] L.O. Kolarik, Water Res. 17 (1983) 141.
[23] Y.F. Song, X. Jing, S. Fleischmann, B.-M. Wilke, Chemosphere 48 (2002) 993.
[24] T. Nandy, S. Shastry, P.P. Pathe, S.N. Kaul, Water, Air, Soil Pollut. 148 (2003) 15.

Available online at www.sciencedirect.com
ScienceDirect
Talanta 72 (2007) 1687–1692
Talanta
www.elsevier.com/locate/talanta

Synthesis of titania and titanate nanomaterials and their application in environmental analytical chemistry

Guang-Sheng Guo *, Chao-Nan He, Zhi-Hua Wang, Fu-Bo Gu, Dong-Mei Han

State Key Laboratory of Chemical Resource Engineering, Beijing University of Chemical Technology, Beijing 100029, China

Received 3 October 2006; received in revised form 12 March 2007; accepted 21 March 2007
Available online 25 March 2007

Abstract

TiO_2 nanoparticles and $H_2Ti_2O_5{\cdot}H_2O$, $Na_2Ti_2O_4(OH)_2$ nanotubes were synthesized by solvothermal method and their applications in the degradation of active Brilliant-blue (KN-R) solution were investigated. The experimental results revealed that the synthesized TiO_2 nanoparticles had a good crystallinity and a narrow size distribution (about 4–5 nm); the obtained $H_2Ti_2O_5{\cdot}H_2O$, $Na_2Ti_2O_4(OH)_2$ were tubelike products with an average diameter of ~20–30 and ~200–300 nm length. The three catalysts we synthesized had some hydroxyl groups and the maximum absorption boundaries of the samples were all red-shifted, which indicated the samples had a promising prospect in photocatalysis.

The results of the photocatalytic experiments indicated that the photocatalytic activity of the samples was: $TiO_2 > H_2Ti_2O_5{\cdot}H_2O > Na_2Ti_2O_4(OH)_2$, which was in good accordance with the fact of FTIR and UV–vis absorption spectra. The formation mechanism of these nanostructures was also discussed.

Keywords: Solvothermal method; Titania; Nanotube; Photocatalyst

1. Introduction

The wastewaters, containing organic dyes, cannot be biodegraded readily, which results in potentially environmental problems [1–5]. Photocatalytic processes are rapidly developing for the degradation of aqueous organic contaminates and air pollutants. In 1993, Legrini et al. and Anne Fox and Dulay introduced photochemical technology, in which the mechanism of the TiO_2-photocatalyzed oxidative degradation, the TiO_2/UV process efficiency and the problems in the development of the TiO_2/UV process were included [6,7]. Hoffmann et al. expatiated semiconductor photocatalysis in environmental applications and they were interested in quantum-sized TiO_2 semiconductor [8]. Hidaka et al. discussed the photodegradation kinetics in terms of Langmuir–Hinshelwd model by comparing of photocatalytic processes between anionic sodium dodecylbenzenesulfonate and cationic benzyldodecyldlmethylammonlum chloride on the TiO_2 surface [9]. Chen et al. studied the effect of transition metal ions on the TiO_2-assisted photodegradation of dyes under visible irradiation and deduced that the reduction of O_2 was essential for the photodegradation of dyes under visible irradiation [10]. Zhao et al. suggested that TiO_2/Pt co-catalyst exhibited greater catalytic activity than P25 TiO_2 alone [11]. Li et al. demonstrated TiO_2 nanoparticles dispersed in silicate had a good photocatalytic activity and the ability to be readily separated from the reaction system and exhibited the potential to be effective in the treatment of dye pollutants in aqueous systems [12]. They also studied photodegradation of dye pollutants on one-dimensional TiO_2 nanoparticles under UV and visible irradiation and found that the nanorods had a superior ability to utilize less energetic but more abundant visible light [13].

Titania and titanate photocatalysts, which are nontoxic, insoluble, cheap and can be activated by sunlight, have attracted increasing attention for their decoloring and oxidizing dyes in wastewater, degradation of hazardous volatile organic and malodorous compound, direct decomposition of NO_x and SO_x and purification of air and water [14–16]. In addition, titania nanoparticles and titanate nanotubes exhibit desirable properties for their applications in lithium-ion-battery, electrochemical capacitors, solar energy conversion and gas sensors [17–20].

The unique properties of nanoparticles are highly dependent upon the crystallinity, the morphology, the size and the size

* Corresponding author. Tel.: +86 1064434808; fax: +86 1064423089.
E-mail addresses: guogs@mail.buct.edu.cn, hcn2005@gmail.com (G.-S. Guo).

0039-9140/$ – see front matter © 2007 Elsevier B.V. All rights reserved.
doi:10.1016/j.talanta.2007.03.039

distribution of the nanoparticles. With the decrease of particle size, the photocatalytic activity of titania can be increased dramatically, which is probably due to the significant particle-size effect and the large specific surface.

Several different methods have been developed for the preparation of titania nanoparticles, such as sol–gel process, hydrothermal method and emulsion precipitation. However, most of the nanoparticles produced with the methods have a poor crystalline and an imperfect morphology. In order to obtain a good crystallinity and perfect morphology, further calcination is required, which frequently results in particle agglomeration and size change. In previous studies, the titanate nanotubes were usually synthesized through the dissolution of TiO_2 powders in high concentrated NaOH solution at a high reaction temperature and then post-treated with hydrochloric acid or water. The obtained products were $Na_2Ti_3O_7$ [20–23], H_2TiO_3 [24], $H_2Ti_2O_4(OH)_2$ or $Na_2Ti_2O_4(OH)_2$ [25–28] and it was proposed that the titanate nanotubes were formed during the washing procedures [22–28]. However, the proposition is still a controversial topic. Further investigation on the exact formation mechanism of titanate nanotubes is required.

Solvothermal method can usually provide access to uniform and distinct morphologies in large scales. In this study, by solvothermal method, small-sized TiO_2 nanoparticles and $H_2Ti_2O_5{\cdot}H_2O$, $Na_2Ti_2O_4(OH)_2$ nanotubes were synthesized without any post-processing. The formation mechanism of the nanomaterials was discussed and their photocatalytic activity in the degradation of organic dye solution was investigated.

2. Experimental

2.1. Chemical

The chemicals included tetrabutyl orthotitanate (TBOT), stearic acid (SA), NaOH, HCl, ethanol, active Brilliant-blue (KN-R). All reagents, supplied by Beijing Chemical Reagents Company, were of AR grade and used without further purification. Deionized water was used throughout the whole experiment.

2.2. Preparation of TiO_2 nanoparticles and $H_2Ti_2O_5{\cdot}H_2O$, $Na_2Ti_2O_4(OH)_2$ nanotubes

The appropriate conditions required for the preparation of different samples are shown in Table 1. In a typical process, 10 mL of TBOT and certain amount SA were added into a 50 mL flask which contained 20 mL of ethanol, and then the mixture was heated at 40 °C with magnetic stirring for 20 min. Then the deionized water was added to the mixture until the appearance of large amounts of white precipitates. The pH value of the solution was adjusted by addition of aqueous NaOH or HCl. Then the white precipitates were transferred into a 100 mL Teflon-lined stainless steel autoclave, in which 40 mL ethanol was input firstly, and sealed. The autoclave was put into an oven, heated to 130 °C for a few hours, then cooled naturally in air. After that, the mixtures were centrifuged at a speed of 4000 rpm and the precipitates were collected. The precipitates were washed with ethanol four times and then dried at 60 °C overnight.

2.3. Photocatalytic degradation experiments

The photocatalytic tests were taken as follows: 0.1 g catalysts was put into 600 mL 0.05 mg/L solution of active Brilliant-blue (KN-R), and then stirred at room temperature for 10 min. The mixture was put into a photocatalysis reactor and radiated by UV illumination with the power of 11 W. The aqueous system of suspended catalyst was oxygenated to ensure the system had enough oxygen. The sample solution was taken at certain reaction intervals and centrifuged at 3000 rpm for 5 min to separate the catalysts particles. Concentrations of the dye solution were measured by UV–vis spectrophotometer.

2.4. Characterizations of the samples

X-ray power diffraction (XRD) patterns were recorded with a D/Max 2500 V diffractometer (Cu Kα, $\lambda = 1.5406$ Å). The morphologies and structures of the samples were determined by Hitachi Model JEM-100 CX transmission electron microscopy (TEM) and high-resolution transmission electron microscopy (HRTEM) (JEM-2010). UV–vis absorption spectra were obtained by using a Shimadzu UV-2501PC spectrophotometer. Energy dispersive X-ray analysis (LEO-435VP LINKISIS EDS) was to confirm the elements of the sample.

3. Results and discussion

3.1. Shape, crystal structure and composition of the samples

When the pH values were lower than 8, the typical XRD patterns of the samples, synthesized with different molar ratio of TBOT to SA, are shown in Fig. 1. It could be seen that when

Table 1
Summary of experimental conditions and results

Experimental conditions	Samples		
	TiO_2 nanoparticles	$H_2Ti_2O_4(OH)_4$ nanotubes	$Na_2Ti_2O_4(OH)_2$ nanotubes
TBOT:SA	2:1	2.24:1	1.5:1
Initial pH	3–4	8–9	12–13
Temperature	130 °C	130 °C	130 °C
Reaction time	12 h	24 h	24 h
Post-treatment	Washed with ethanol	Washed with ethanol	Washed with ethanol and deionized water

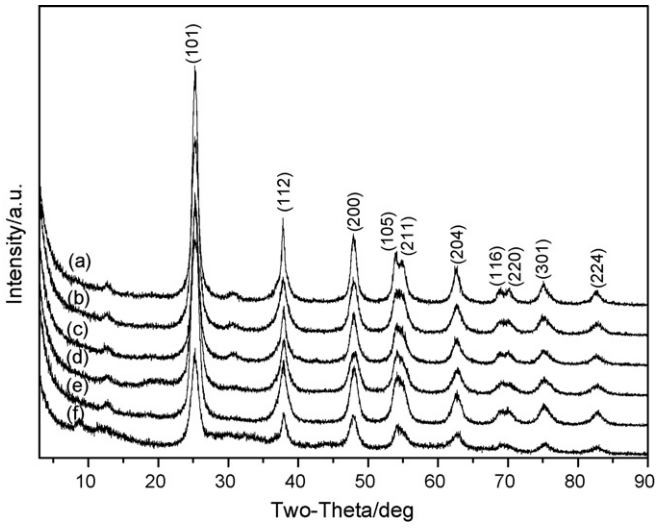

Fig. 1. XRD patterns of anatase TiO_2 synthesized with various pH value and TBOT/SA (mole ratio): pH ~ 3–4, TBOT/SA (a) 2.5:1; (b) 2:1; (c) 1:1 and pH ~ 7–8, TBOT/SA (d) 2.5:1; (e) 2:1; (f) 1:1.

the molar ratio was between 1 and 2.5, all of the samples were assigned to anatase TiO_2. According to the XRD data, the calculated lattice parameters of the samples were $a = 7.5936$ Å, $b = 1.9019$ Å, $c = 9.5024$ Å, which were well consistent with the literature data ($a = 7.5540$ Å, $b = 1.8889$ Å, $c = 9.5012$ Å) (JCPDS card: 21–1272). The broadening of diffraction peaks indicated the nanosized crystalline domain and the strong diffraction peaks revealed that the obtained products were highly crystalline.

Fig. 2 shows the TEM and HRTEM images of TiO_2 nanoparticles. The samples were obtained when the pH value was ~3–4, TBOT/SA was 2:1. The image showed (Fig. 2a) that the sample had a narrow size distribution with an average diameter of ~4–5 nm. HRTEM showed (Fig. 2b) that the TiO_2 nanoparticles were highly crystalline, with an interplanar spacing of ~0.3509 nm, which was in correspondence with the (1 0 1) plane of TiO_2. These results were in agreement with the XRD results.

Fig. 3 is the XRD pattern and the TEM image of the sample, which was synthesized when the TBOT/SA was 2.24:1, the pH value was ~8–9 and the reaction time was 24 h. The sample was assigned to $H_2Ti_2O_5 \cdot H_2O$ (JCPDS card: 47–0124) (Fig. 3a).

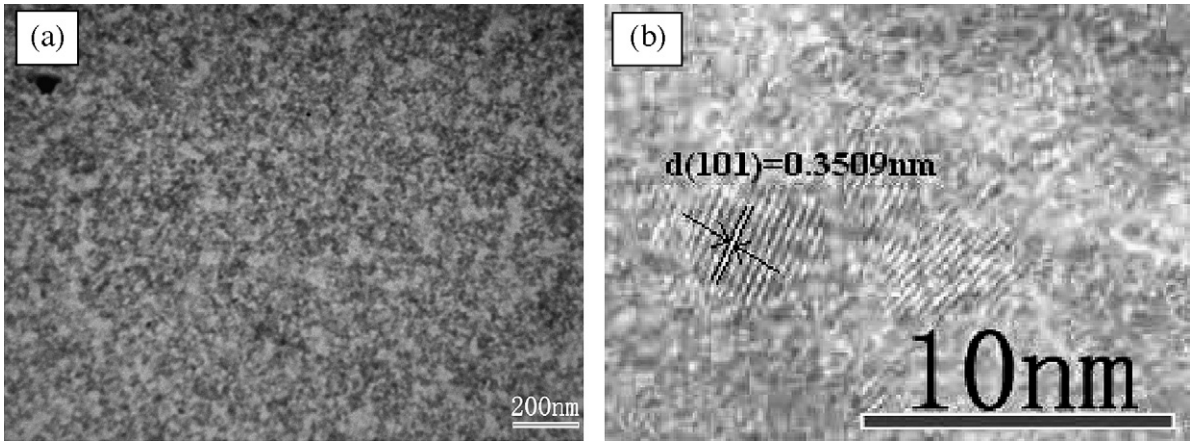

Fig. 2. TEM (a) and HRTEM (b) images of TiO_2 nanoparticles.

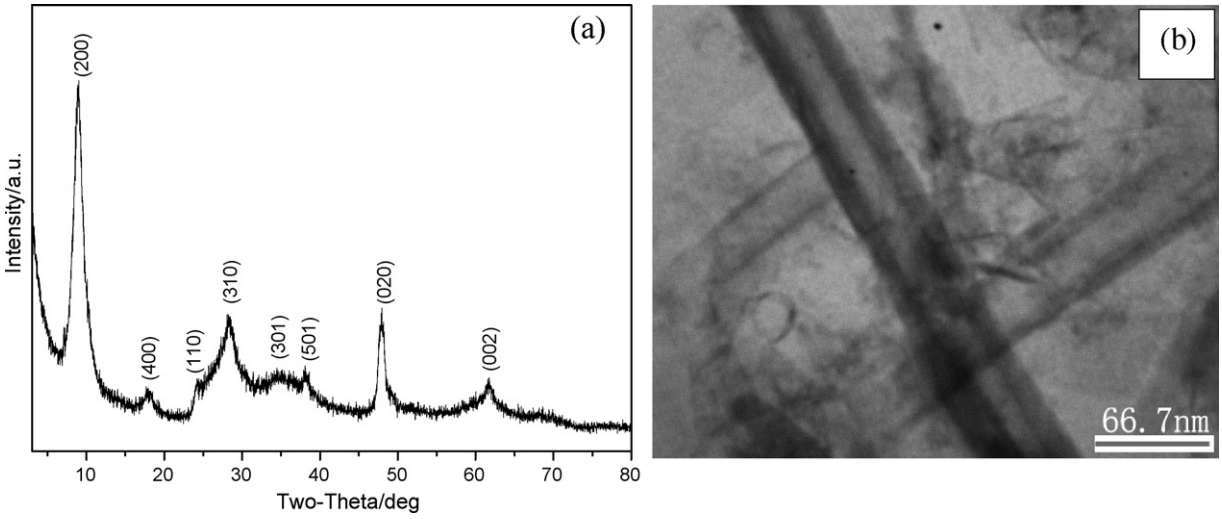

Fig. 3. XRD pattern (a) and TEM (b) of $H_2Ti_2O_5 \cdot H_2O$.

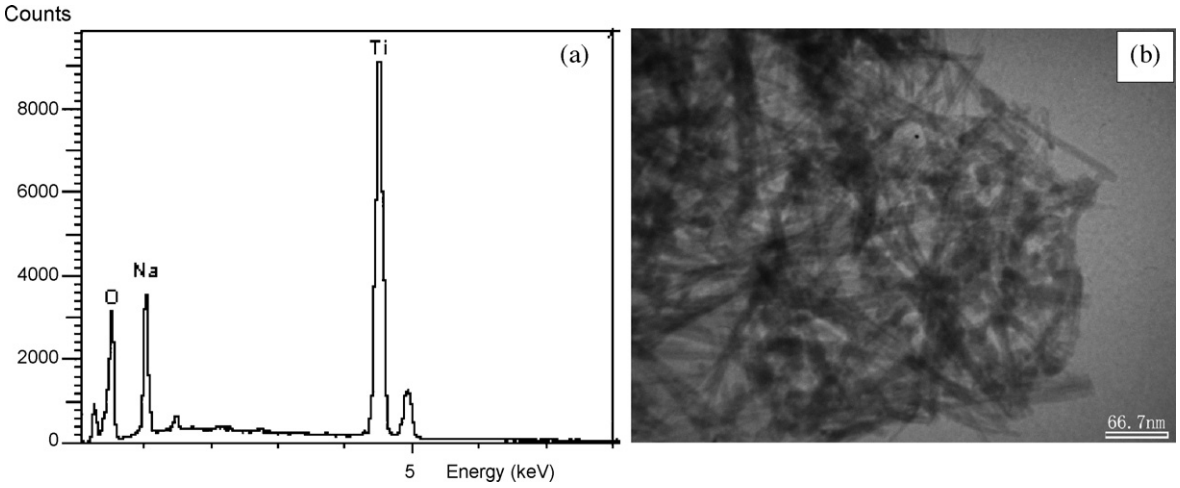

Fig. 4. EDS spectrum (a) and the TEM image (b) of $Na_2Ti_2O_4(OH)_2$ nanotubes.

Fig. 3b shows the TEM image of several $H_2Ti_2O_5{\cdot}H_2O$ nanotubes. Tubelike structures with inner diameters of ~25–40 nm, outer diameters of ~30–50 nm dominated the field of vision, and some nanosheets were observed, simultaneously.

Fig. 4 shows the energy dispersive X-ray analysis (EDS) and the TEM image of the sample which was synthesized when BOT/SA was 1.5:1, the pH value was ~12–13, the reaction temperature was 130 °C and the reaction time of 24 h. The result showed that the existence of Ti, Na and O elements in the product (Fig. 4a). The molar ratio of Ti to Na was 1:1.08, which was very close to theoretical value (1:1). TEM image of the $Na_2Ti_2O_4(OH)_2$ showed that the sample was tubelike structures with a diameter of ~10–20 nm, a length of ~300–500 nm were obtained (Fig. 4b).

3.2. Formation mechanism of the nanotubes

In the solvothermal reaction system, pH was an important impact factor on the composing of the products. In the synthesis process, when the deionized water was dropped into the mixture of TBOT and SA, the TBOT hydrolyzed quickly, and then the nanocrystal of $Ti(OH)_4$ formed. When the pH value was lower than 8, the $Ti(OH)_4$ were intended to decompose to form TiO_2 nanoparticles under a high temperature and high pressure conditions [29]. When the NaOH solution was added to adjust the pH value to 8–10, parts of SA would react with NaOH, which resulted in the formation of sodium stearate. Then the –O–H bond of one $Ti(OH)_4$ would react with one –O–H bond of another $Ti(OH)_4$ to form one H_2O molecule, the rest of the two $Ti(OH)_4$ molecules were connected via –O–Ti– bond. When a large amounts of $Ti(OH)_4$ took part in the reaction, sheetlike (or layer) structures of $H_2Ti_2O_5{\cdot}H_2O$ would form. Under certain conditions, a sheetlike structure began to curl and finally the $H_2Ti_2O_5{\cdot}H_2O$ tubelike structure formed. The driving force for the curling of sheetlike structure may come from the thermal stress existing at high temperature and high pressure, which reduced the interlayer forces at the edges and scrolled the sheets into tubes [30]. When the pH was ~11–13, some NaOH reacted with SA absorbed on the surface of $Ti(OH)_4$ to produce sodium stearate. Then the interaction occurred between the –O–H bond of NaOH and the –O–H bond of the $Ti(OH)_4$ to form one H_2O molecule. With abundant NaOH in solvothermal system, the intermediate of $H_2Ti_2O_5{\cdot}H_2O$ would react with the rest of NaOH to form $Na_2Ti_2O_4(OH)_2$. Finally, $Na_2Ti_2O_4(OH)_2$ nanosheets formed via –Ti–O–Na bond. The formation process of $Na_2Ti_2O_4(OH)_2$ nanosheets rolling into nanotubes was similar to that of $H_2Ti_2O_5{\cdot}H_2O$. The formation process of titanate nanotubes and TiO_2 nanoparticles are summarized in Scheme 1.

3.3. FTIR and UV–vis spectra of different catalysts

The FTIR and UV–vis spectra of different catalysts were shown in Fig. 5. It was shown that the FTIR spectra of different catalysts were similar (Fig. 5a–c). Hence, as an example, the FTIR spectra of $H_2Ti_2O_5{\cdot}H_2O$ (Fig. 5b) were explained here in detail. It was believed that the broad peak at 3300 cm^{-1} and the peak at 1650 cm^{-1} correspond to the surface-adsorbed water and hydroxyl groups [31]. The broad band (from about

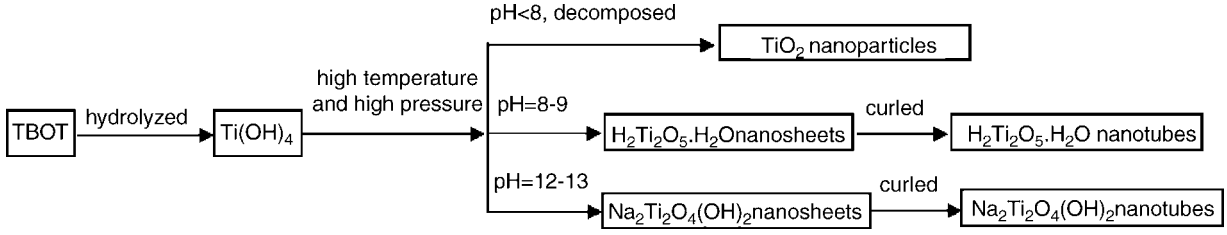

Scheme 1. The formation process of titanate nanotubes and TiO_2 nanoparticles.

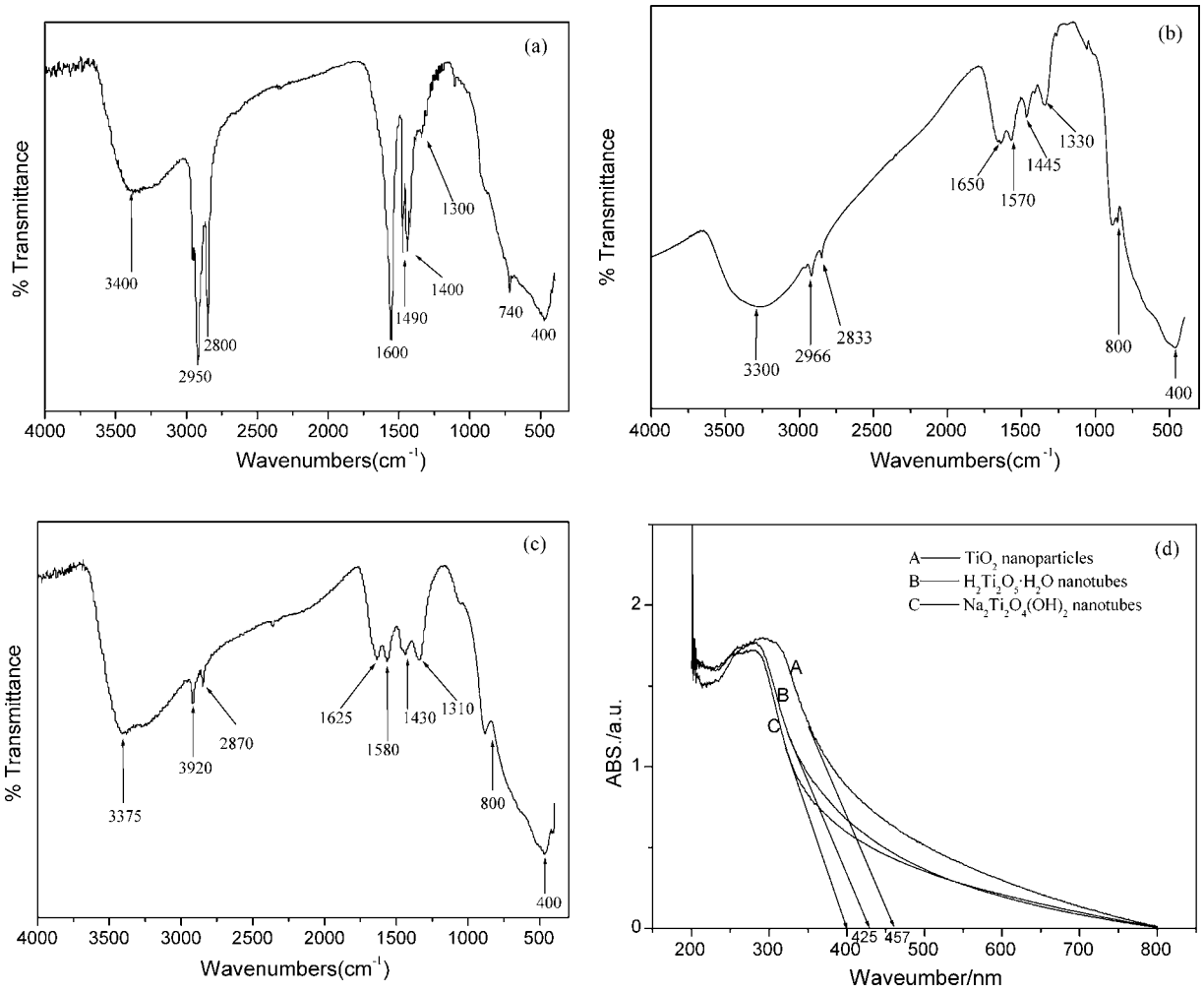

Fig. 5. FTIR spectra (a) TiO_2, (b) $H_2Ti_2O_5{\cdot}H_2O$, (c) $Na_2Ti_2O_4(OH)_2$ and UV–vis spectra (d) of different catalysts.

800 till 400 cm^{-1}) was assigned to Ti–O and Ti–O–Ti skeletal frequency region [32]. Two weak bands at 2966 and 2833 cm^{-1} (νCH and νCH_2) could be ascribed to the characteristic frequencies of residual organic species (SA), which was not completely removed by ethanol and distilled water washing. The peaks at 1330–1570 cm^{-1} region could be attributed to carboxyl (C=O) and methylene groups [31]. The carboxyl and methylene groups might also be resulted from residual organic species (SA).

Fig. 5d shows the UV–vis absorption spectra of different samples. The absorption intensity for the samples was: $TiO_2 > H_2Ti_2O_5{\cdot}H_2O > Na_2Ti_2O_4(OH)_2$. The maximum absorption boundaries of TiO_2 nanoparticles (457 nm), $H_2Ti_2O_4(OH)_2$ nanotubes (425 nm), $Na_2Ti_2O_4(OH)_2$ nanotubes (400 nm), were all red-shifted relative to the bulk anatase TiO_2 (387 nm) [33], which indicated that the samples had a promising prospect in photocatalysis. The maximum absorption boundaries and absorption intensity of the sample indicated that photocatalytic activity of them may be $TiO_2 > H_2Ti_2O_5{\cdot}H_2O > Na_2Ti_2O_4(OH)_2$.

The mechanism of photodegradation of dyes under visible light using TiO_2 is shown as follows [13]:

$$\text{dye} + h\nu \rightarrow \text{dye}^* \quad (1)$$

$$\text{dye}^* + TiO_2 \rightarrow \text{dye}^{\bullet +} + TiO_2(e) \quad (2)$$

$$TiO_2(e) + O_2 \rightarrow TiO_2 + O_2^{\bullet -} \quad (3)$$

$$O_2^{\bullet -} + TiO_2(e) + 2H^+ \rightarrow H_2O_2 \quad (4)$$

$$H_2O_2 + TiO_2(e) \rightarrow OH^{\bullet} + OH^- \quad (5)$$

$$\text{dye}^{\bullet +} + O_2 \text{ (or } O_2^{\bullet -}, \text{ or } {}^{\bullet}OH) \rightarrow \text{peroxylated or hydroxylated intermediates} \rightarrow \text{degraded or mineralized products} \quad (6)$$

According to the above formulae, the radicals and the hydroxyl groups play a key role in the degradation process and the more radicals or hydroxyl groups means the better photocatalytic activity. In our experiments, the synthesized three catalysts, which had similar mechanism of photodegradation of dyes, had some hydroxyl groups (Fig. 5a–c), which mean the samples had a promising prospect in photocatalysis. The red-shifted maximum absorption boundaries of the samples (Fig. 5d) mean that the samples can absorb more photons under UV light or sunlight. Then the red-shifted maximum absorption peaks of three catalysts mean a better photocatalytic activity.

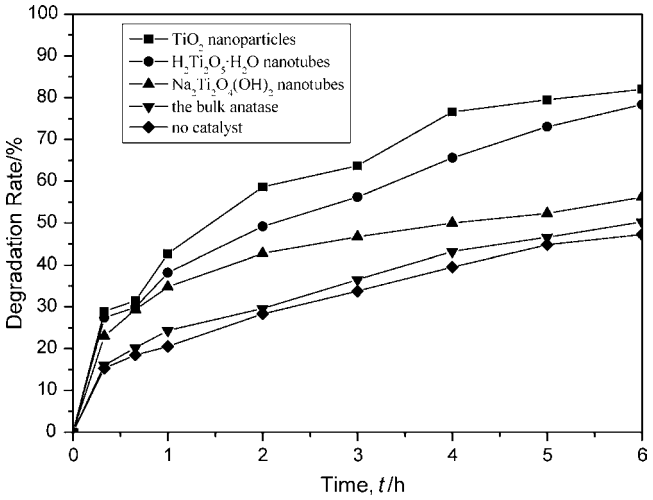

Fig. 6. Degradation rate curves of dye solution with different catalysts.

3.4. Photocatalytic activity of the samples

The degradation rate curves of dye solution with different catalysts were shown in Fig. 6. After 6 h irradiation, the photocatalytic degradation rate of the active Brilliant-blue (KN-R) were 80% (TiO_2 nanoparticles), 76% ($H_2Ti_2O_4(OH)_2$ nanotubes) and 55% ($Na_2Ti_2O_4(OH)_2$ nanotubes) while the photocatalytic degradation rate were 50% using the bulk anatase as catalysts and 45% without catalyst. The above results showed that the photocatalytic degradation rates were enhanced by the addition of the catalysts we synthesized and the photocatalytic activity of the samples was: $TiO_2 > H_2Ti_2O_5{\cdot}H_2O > Na_2Ti_2O_4(OH)_2 >$ the bulk anatase, which was in good accordance with the fact of FTIR and UV–vis absorption spectra. With the photocatalytic reaction continuing, the catalysts were usually passivated and lost their photocatalytic activity. Fig. 6 also shows that the photocatalytic degradation rates of the catalysts decreased with the prolongation of the photocatalytic reaction time.

4. Conclusions

In summary, TiO_2 nanoparticles and $H_2Ti_2O_5{\cdot}H_2O$, $Na_2Ti_2O_4(OH)_2$ nanotubes were prepared with one-step synthesis by solvothermal method. The formation mechanism of nanotubes was attributed to the curling of the nanosheet to tubelike structure under the high temperature and high pressure in the solvothermal system, and it was believed that the nanotubes were formed during the reaction course. The samples all had some hydroxyl groups. Compared with the bulk TiO_2, the maximum absorptions of our samples were red-shifted. The results of photocatalytic degradation of organic dye solution indicated that the photocatalytic activity of the samples was: $TiO_2 > H_2Ti_2O_5{\cdot}H_2O > Na_2Ti_2O_4(OH)_2$, which was in good accordance with the fact of FTIR and UV–vis absorption spectra.

Acknowledgement

This work was financially supported by the National Nature Science Foundation of China (No. 20571007) and Beijing Natural Science Foundation (No. 2073029).

References

[1] K. Swaminathan, S. Sandhya, A.C. Sophia, K. Pachhade, Y.V. Subrahmanyam, Chemosphere 50 (2003) 619–625.
[2] H. Zhang, X. Quan, S. Chen, H. Zhao, Y. Zhao, Sep. Purif. Technol. 50 (2006) 147–155.
[3] A. Aleboyeh, H. Aleboyeh, Y. Moussa, Dyes Pigments 57 (2003) 67–75.
[4] S. Chakrabarti, B.K. Dutta, J. Hazard. Mater. 112 (2004) 269–278.
[5] P.K. Malik, S.K. Sanyal, Sep. Purif. Technol. 36 (2004) 167–175.
[6] O. Legrini, E. Oliveros, A.M. Braun, Chem. Rev. 93 (1993) 671–698.
[7] M. Anne Fox, M.T. Dulay, Chem. Rev. 93 (1993) 341–357.
[8] M.R. Hoffmann, S.T. Martin, W. Choi, D.W. Bahnemannt, Chem. Rev. 95 (1995) 69–96.
[9] H. Hidaka, J. Zhao, E. Pelizzetti, N. Serpone, J. Phys. Chem. 96 (1992) 2226–2230.
[10] C. Chen, X. Li, W. Ma, J. Zhao, H. Hidaka, N. Serpone, J. Phys. Chem. B 106 (2002) 318–324.
[11] W. Zhao, C. Chen, X. Li, J. Zhao, J. Phys. Chem. B 106 (2002) 5022–5028.
[12] J. Li, C. Chen, J. Zhao, H. Zhu, J. Orthman, Appl. Catal. B 37 (2002) 331–338.
[13] J. Li, W. Mab, C. Chenb, J. Zhao, H. Zhu, X. Gao, J. Mol. Catal. A 261 (2007) 131–138.
[14] M. Muruganandhaml, M. Swaminathan, Sep. Purif. Technol. 48 (2006) 297–303.
[15] E. Beyers, P. Cool, E.F. Vansant, J. Phys. Chem. B 109 (2005) 10081–10086.
[16] A.B. Prevot, E. Pramauro, Talanta 48 (1999) 847–857.
[17] A.R. Armstrong, G. Armstrong, J. Canales, P.G. Bruce, Angew. Chem. Int. Ed. 43 (2004) 2286–2288.
[18] J. Li, L. Li, L. Zheng, Y. Xian, L. Jin, Talanta 68 (2006) 765–770.
[19] A.Y.H. Lo, R.W. Schurko, M. Vettraino, B.O. Skadtchenko, M. Trudeau, D.M. Antonelli, Inorg. Chem. 45 (2006) 1828–1838.
[20] B. Elizabetha, P. Sylvester, A. Clearfield, Environ. Sci. Technol. 32 (1998) 101–107.
[21] Q. Chen, W. Zhou, G. Du, L.M. Peng, Adv. Mater. 14 (2002) 1208–1211.
[22] Z.R. Tian, J.A. Voigt, J. Liu, B. Mckenzie, H. Xu, J. Am. Chem. Soc. 125 (2003) 12384–12385.
[23] A. Thorne, A. Kruth, D. Tunstall, J.T.S. Irvine, W. Zhou, J. Phys. Chem. B 109 (2005) 5439–5444.
[24] Y.V. Kolen'ko, K.A. Kovnir, A.I. Gavrilov, A.V. Garshev, J. Frantti, O.I. Lebedev, B.R. Churagulov, G.V. Tendeloo, M. Yoshimura, J. Phys. Chem. B 110 (2006) 4030–4038.
[25] M. Zhang, Z. Jin, J. Zhang, X. Guo, J. Yang, W. Li, X. Wang, Z. Zhang, J. Mol. Catal. A: Chem. 217 (2004) 203–210.
[26] J. Yang, Z. Jin, X. Wang, W. Li, J. Zhang, S. Zhang, X. Guo, Z. Zhang, Dalton Tans. (2003) 3898–3901.
[27] M. Wei, H. Zhou, Y. Konishi, M. Ichihara, H. Sugiha, H. Arakawa, Inorg. Chem. 45 (2006) 5684–5690.
[28] C.C. Tsai, H. Teng, Chem. Mater. 18 (2006) 367–373.
[29] Y. Murakami, T. Matsumoto, Y. Takasu, J. Phys. Chem. B 103 (1999) 1836–1840.
[30] Y.D. Li, X.L. Li, R.R. He, J. Zhu, Z.X. Deng, J. Am. Chem. Soc. 12 (2002) 1411–1416.
[31] G.J. de, A.A. Soler-Illia, A. Louis, C. Sanchez, Chem. Mater. 14 (2002) 750–759.
[32] A.M. Peiro, J. Peral, C. Domingo, X. Domenech, J.A. Ayllon, Chem. Mater. 13 (2001) 2567–2573.
[33] A. Hattor, M. Yamamoto, H. Tada, Chem. Lett. 32 (1998) 707–708.

Available online at www.sciencedirect.com
ScienceDirect
Talanta 72 (2007) 1675–1680
Talanta
www.elsevier.com/locate/talanta

Flow-injection spectrofluorometric determination of trace amounts of formaldehyde in water after derivatization with acetoacetanilide

Qiong Li, Mitsuko Oshima, Shoji Motomizu *

Department of Chemistry, Faculty of Science, Okayama University, 3-1-1 Tsushimanaka, Okayama 700-8530, Japan

Available online 1 February 2007

Abstract

A novel fluorophotometric method for formaldehyde determination in environmental waters was developed: the method does not require any enrichment procedures. A flow-injection analysis method for the spectrofluorometric determination of formaldehyde in waters, which is based on the reaction of formaldehyde with acetoacetanilide and ammonia, is proposed. The proposed method shows a good linearity from 0.50 to 40 × 10^{-7} M, and the limit of detection (LOD) of 3 × 10^{-9} M (0.09 ppb) is achievable. The sample throughput is 15 h^{-1}. One of the main advantages in the proposed method is that the reaction can be carried out at room temperature without any heating system. The effect of various interferences possibly present in the real water samples was investigated. Most cations and anions, as well as organic compounds, do not interfere with the determination of formaldehyde in environmental water samples. The proposed method is very simple, rapid, less expensive, and highly sensitive, and can be applied to the environmental water samples, such as rain, tap water and river water, at low concentration levels without any enrichment procedure.

Keywords: Spectrofluorometric; Water samples; Flow-injection; Formaldehyde determination; Acetoacetanilide

1. Introduction

The organic compound, formaldehyde, is a gasous substance with a pungent smell, and it is the simplest aldehyde. Formaldehyde is unfavorable for our health because at low concentration levels, formaldehyde can cause irritation of eyes, nose, throat, and skin. Further, people with asthma may be more sensitive to the effects of inhaled formaldehyde. Therefore, formaldehyde is one of the analytically interesting substances in aquatic and air environment as an environmental pollutant. Although formaldehyde is a gas at room temperature, it is readily soluble in water. In an aqueous media, formaldehyde can polymerize, and formalin actually contains only a little formaldehyde in the form of H_2CO monomer. Oral administration of large amounts of formaldehyde can cause severe pain, vomiting, coma, and possible death. Formaldehyde can enter drinking water as a result of human activities, major sources being the discharge of industrial wastes and oxidative water treatment processes such as ozonation and chlorination [1].

Due to the influence of HCHO to nature and human bodies, a number of analytical methods have been proposed. Trace amounts of formaldehyde have been commonly determined by spectrophotometric methods [2–8]. However, some of them are not sensitive enough for the analysis of real water samples and are sometimes subject to numerous interferences, which are serious problems. HPLC with 2,4-dinitrophenylhydrazine (DNPH) as a derivatization agent [9–12] is one of the most frequently used methods. Recently, Burini and Coli [13] reported a HPLC system coupled with a diode array detector for formaldehyde determination after derivatization with ethyl 3-oxobutanoate: the limit of detection (LOD) was 0.024 μg ml^{-1}. HPLC procedures, however, are time-consuming and are less adaptable to water samples.

The fluorometric methods based on the Hantzsch reaction, which involve the cyclization of amine, aldehyde and β-diketone to form a dihydropyridine derivative, have often been used for the detection of formaldehyde in aqueous solutions. Nash [14] introduced a colorimetric method into analytical chemistry for HCHO, which was based on the Hantzsch reaction of formaldehyde with acetylacetone (AA) or 2,4-pentanedione

* Corresponding author. Tel.: +81 86 251 7846; fax: +81 86 251 7846.
E-mail address: motomizu@cc.okayama-u.ac.jp (S. Motomizu).

0039-9140/$ – see front matter © 2007 Elsevier B.V. All rights reserved.
doi:10.1016/j.talanta.2007.01.054

in the presence of ammonia to form a yellow product of 3,5-diactyl-1,4-dihydrolutidine (DDL). Later, Belman [15] found that without any other changes, highly sensitive measurement could be made by fluorometry, instead of spectrophotometry. This detection reaction with AA gave less product of lutidine with all aliphatic aldehydes except formaldehyde because of the mildness of the reaction conditions of analysis. However, this method is in general time-consuming and needs high temperature. Later, Sawicki and Carnes [16] proposed other reagents for the fluorometric detection of formaldehyde: 5,5-dimethyl-1,3-cyclohexnedione (dimedone) and 1,3-cyclohexanedione (CHD). Both of them can offer excellent sensitivity for the detection of HCHO, though such reactions require high temperature for the reaction, and furthermore, the CHD methods can suffer from positive interference from H_2O_2 [17]. Aiming at developing sensitive methods of analysis for HCHO, flow-injection analysis (FIA) has been frequently used. Fluorometric FI methods have been studied with 4-amino-3-penten-2-one (Fluoral P) [18], 1,3-cyclohexanedione (CHD) [19], 5,5-dimethylcyclohexane-1,3-dione (dimedone) [20], acetylacetone [21] and acridine yellow-bromate [22]. In addition, Li et al. [23] developed an FI chemiluminescence method with bromate–rhodamine 6G system, which showed a detection limit of 0.3 $\mu g\,l^{-1}$ (0.3 ppb). However, they are simple but are not sensitive enough and are subject to interferences from other compounds.

In Japan, the maximum concentration of HCHO, which is allowed in drinking water, is now 80 ppb (2.7 μM). In general, concentrations of HCHO in tap waters range from 0.15 to 15 ppb in Japan [1], and therefore, any enrichment procedures are always necessary for the preconcentration of formaldehyde before measurement [1,24,25]. Now, a simple and highly sensitive method for formaldehyde determination is required for the direct analysis of water samples without any preconcentration techniques.

Recently, the authors examined several detection reactions for formaldehyde based on the Hantzsch reaction using novel reagents, which were benzoylacetone, *N*-methylacetoacetamide, *n*-acetoacetyl-*o*-toluidine and acetoacetanilide (AAA) [26]. Of these, AAA was found to be most reactive, selective and sensitive by a batchwise/spectrofluorometry. Furthermore, AAA is more sensitive than the ones reported so far.

In this paper, a novel detection reagent, AAA, for the determination of formaldehyde is proposed for the flow-injection method coupled with spectrofluorometry: the detection is based on the Hantzsch reaction, which involves the cyclization between AAA and formaldehyde in the presence of ammonium acetate. The reaction conditions were optimized by a flow-injection method, and the method was applied to the determination of trace amounts of formaldehyde in environmental waters.

2. Experimental

2.1. Reagents

All chemicals used in this work were of analytical reagent grade, and the water purified with a Milli Q Labo (Millipore, Japan) was used throughout the experiments for the preparation of all solutions. A 0.2 M acetoacetanilide stock solution was prepared by dissolving 3.544 g of acetoacetanilide (Wako Pure chemicals, Osaka) in 50 ml of ethanol and diluting it to 100 ml with the purified water. An ammonium acetate stock solution was prepared by dissolving 77.10 g of ammonium acetate (Wako Pure chemicals, Osaka) in the purified water and diluting it to 250 ml with the purified water. A 0.10 M standard solution of formaldehyde was prepared by diluting 0.78 ml of 36.0–38.0% HCHO solution (Wako Pure chemicals, Osaka) to 100 ml with purified water, followed by an accurate concentration determination using the iodometric method. The working standard solutions were daily prepared by accurate dilution of the standard stock solution. For interference testing, the following compounds were used: sodium chloride, sodium nitrate, sodium nitrite, sodium sulfate, sodium sulfite, sodium carbonate, copper(II) chloride, iron(III) nitrate, hydrogen peroxide, acetic acid, acetone, propionaldehyde and acetaldehyde.

2.2. Apparatus

A schematic diagram of a flow-injection analysis (FIA) system is shown in Fig. 1. A double-plunger micropump (Sanuki Kogyo, RX-703T, Japan), P, was used for propelling a carrier solution (CS) and a reagent solution (RS). A six-way valve (Sanuki Kogyo, Japan), V, was used for introducing standard formaldehyde solutions and samples into the carrier stream. A 0.5 mm i.d. PTFE tubing was used for flow lines. A thermostating dry bath (Iuchi, EB-303, Japan) was used throughout the whole experiment. Peaks for HCHO determination were measured at $\lambda_{ex} = 370$ nm and $\lambda_{em} = 470$ nm by a fluorescence detector (Shimadzu, RF-10A XL, Japan) with a micro flow-though cell (16 μl). Peak height was recorded with a chart strip recorder (TOA, FBR-251A, Japan). All measurements were performed in a temperature-controlled room ($25.0 \pm 0.1\,^{\circ}C$).

2.3. Flow-injection procedure for the determination of HCHO in aqueous solutions

The manifold of the flow-injection system used in this work is shown in Fig. 1. In the proposed method, the flow rate of the

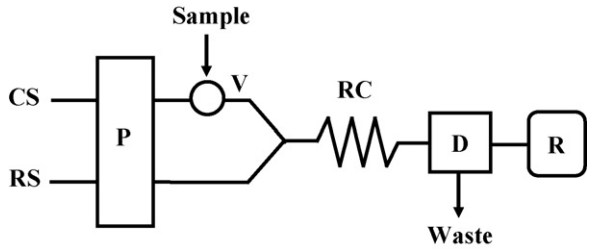

Fig. 1. FIA system for the determination of HCHO using acetoacetanilide as a reagent. CS: carrier solution (distilled water); RS: 0.05 M acetoacetanilide and 2.0 M ammonia acetate solution in 40% ethanol solution (pH 7.5); P: pump RX-703T; V: six ways valves with 300 μl loop; RC: reaction coil (10 m × 0.5 mm i.d.); D: fluorometric detector FP-920; R: recorder; temperature: 25 °C.

carrier and the reagent solution was set up at 0.3 ml min^{-1}. A six-way valve with a sample loop (300 μl) was used for introducing the working standard solutions of HCHO into the carrier stream for the preparation of a calibration graph. The standard HCHO solution was mixed with the reagent solutions, and flowed into the reaction coil (RC). Fluorescence changes of the reaction product were measured with the fluorescence detector: an excitation and an emission wavelength were 370 and 470 nm, respectively. The flow signals were recorded with a chart strip recorder.

3. Results and discussion

3.1. Optimization manifold parameters for spectrofluorometric determination of formaldehyde

The optimization of manifold parameters was performed using the FIA manifold with fluorometric detector in Fig. 1. The effect of reaction temperature on signal intensity was examined by varying the temperature from 25 to 80 °C using the dry heating bath. The results obtained are shown in Fig. 2. The results showed that at temperature of 50 °C gave the strongest intensity, while above 50 °C, the baseline is not stable and some air bubbles occurred. When higher sensitivity is required, heating system can be used. However, for convenient operation, 25 °C (room temperature) was selected as a compromise between the sensitivity and the convenience of the flow system in this work.

At room temperature, reaction time is very important for improving the reaction efficiency of the detection reaction. The effect of the flow rate of the carrier and the reagent solution was investigated in the range of 0.2–0.6 ml min^{-1}. The results obtained (Fig. 3) indicates that with increasing flow rate from 0.2 to 0.6 ml min^{-1}, the sensitivity of the detection of HCHO is lowered though the sampling frequency is higher. Considering the sensitivity and the sample throughput, 0.3 ml min^{-1} of the flow rate was chosen in the further experiments.

The effect of mixing coil length was examined by varying the length from 4 to 14 m. As shown in Fig. 4, the signal intensity increased with increasing the mixing coil length up to 10 m, and above 10 m, signal intensity was almost identical. A reaction coil length of 10 m was chosen as a compromise with respect of the sensitivity and the sample throughput.

The sample injection volumes of 100, 200, 300, 400 and 500 μl were examined by changing the length of the sample loop of the injection valve. From the results obtained (Fig. 5), it can be seen that larger volumes were preferable to obtain higher peak, and the volumes above 300 μl gave only a small increase in peak height. The sample volume of 300 μl was selected as a compromise of the sensitivity, the sample throughput and the sample size.

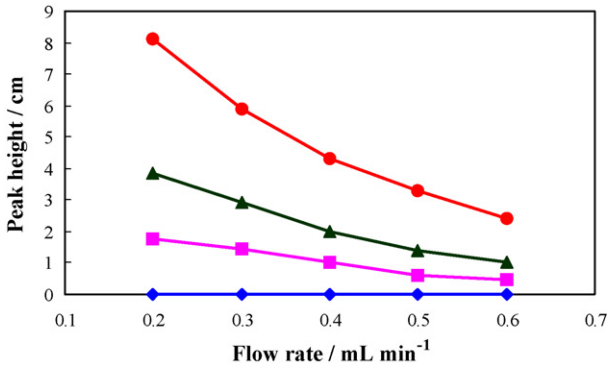

Fig. 3. Effect of flow rate. HCHO concentration (♦) 0 (blank); (■) 1×10^{-6} M; (▲) 2×10^{-6} M; (●) 4×10^{-6} M.

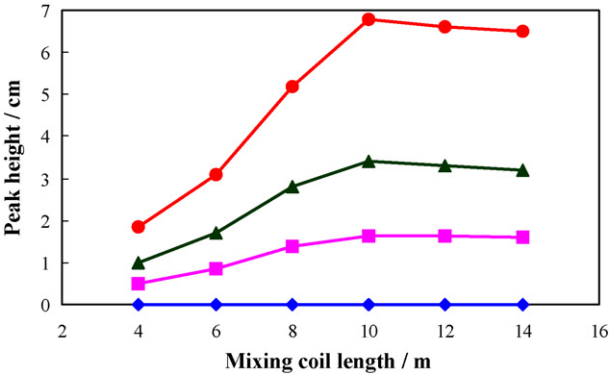

Fig. 4. Effect of mixing coil length. HCHO concentration (♦) 0 (blank); (■) 1×10^{-6} M; (▲) 2×10^{-6} M; (●) 4×10^{-6} M.

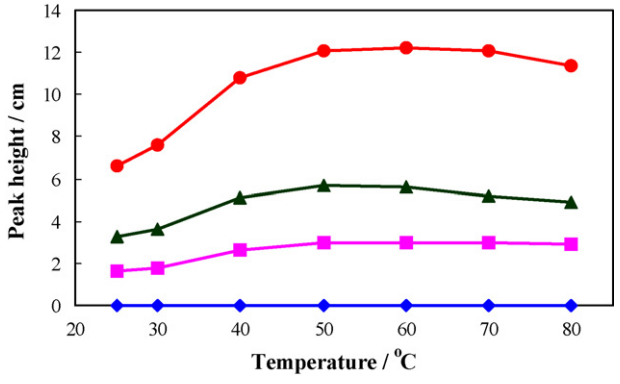

Fig. 2. Effect of reaction temperature. HCHO concentration (♦) 0 (blank); (■) 1×10^{-6} M; (▲) 2×10^{-6} M; (●) 4×10^{-6} M.

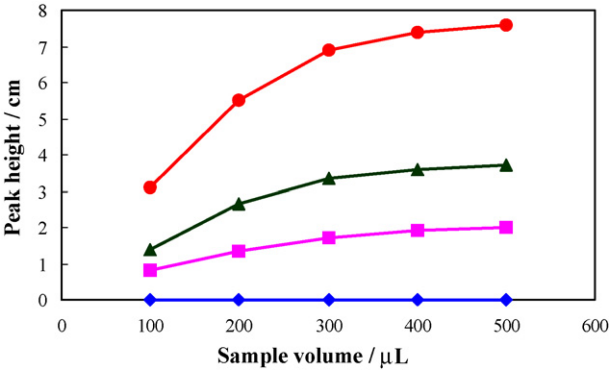

Fig. 5. Effect of sample volume. HCHO concentration (♦) 0 (blank); (■) 1×10^{-6} M; (▲) 2×10^{-6} M; (●) 4×10^{-6} M.

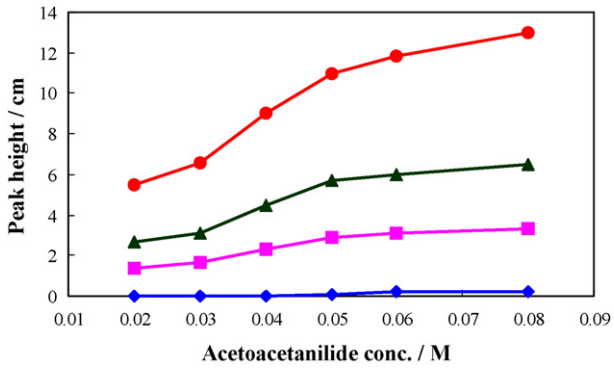

Fig. 6. Effect of concentration of acetoacetanilide. HCHO concentration (♦) 0 (blank); (■) 1×10^{-6} M; (▲) 2×10^{-6} M; (●) 4×10^{-6} M.

3.2. Optimization of reagent concentrations for spectrofluorometric determination of formaldehyde

In this work, acetoacetanilide was proposed for formaldehyde detection based on Hantzsch reaction. Two molecules of an acetoacetanilide were initially involved in the unprecedented transformation: one reacts with formaldehyde and the other one reacts with ammonia to form an enamine-type intermediate, followed by a cyclodehydration to afford the dihydropyridine derivative [26]. Therefore, the effect of acetoacetanilide concentrations in the range of 0.02–0.08 M on the fluorescence intensity was studied. The results in Fig. 6 indicates that the peak height increased with increasing acetoacetanilide concentration up to 0.05 M, above which the signal intensity was almost identical. In this study, 0.05 M acetoacetanilide was selected.

Experimental results demonstrated that the reaction could proceed better in some organic solvents. A comparison of ethanol, methanol and acetone was examined. The results implies that higher and more constant sensitivity could be obtained in ethanol solution medium. Therefore, the effect of ethanol concentration in the range of 10–50% on fluorescence intensity was studied. Fig. 7 shows that with increasing concentration of ethanol, the peak height increased. However, high reagent blank and noisy background was obtained when ethanol concentration was more than 40%. Therefore, 40% ethanol solution was chosen for the further experiments.

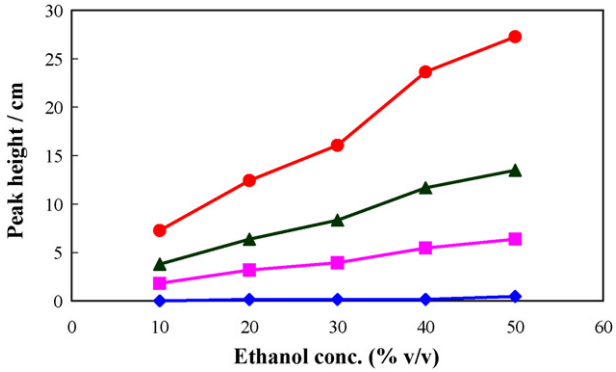

Fig. 7. Effect of concentration of ethanol. HCHO concentration (♦) 0 (blank); (■) 1×10^{-6} M; (▲) 2×10^{-6} M; (●) 4×10^{-6} M.

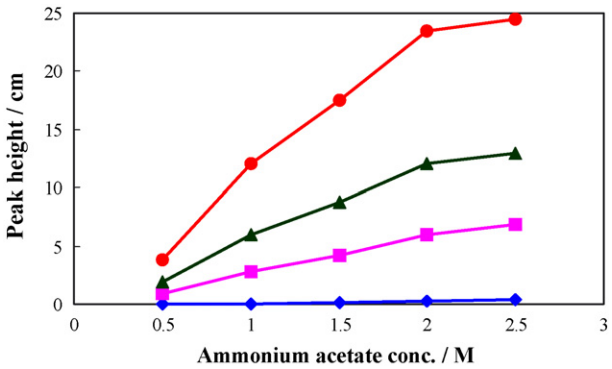

Fig. 8. Effect of concentration of ammonium acetate. HCHO concentration (♦) 0 (blank); (■) 1×10^{-6} M; (▲) 2×10^{-6} M; (●) 4×10^{-6} M.

Ammonium acetate works as both buffer and one of the components of the reagents in the proposed method. The effect of ammonium acetate concentration was examined in the range of 0.5–2.5 M. The results obtained are shown in Fig. 8. It was found that the peak height increased with increasing ammonium acetate concentration. In the proposed method, 2.0 M ammonium acetate concentration was selected because of stronger capacity, higher sensitivity and better baseline.

In the reaction of formaldehyde with the proposed reagents, pH of the reagent solution is very important for the reaction efficiency. The effect of pH on the sensitivity was investigated in the range of pH 5.0–8.0 using ammonium acetate as buffers: the pH was adjusted with acetic acid and NaOH solution. The results obtained are shown in Fig. 9, which indicates that in the pH range over 6.5–7.5, the peak height is almost identical, and below pH 6.5 and above pH 7.5, the peak height becomes shorter. From these results, the pH of 7.5 was chosen for further experiments.

3.3. Interference from foreign substances

The investigation of possible interferences was conducted with regard to possible chemical interferences and the problem of selectivity. The interference from low-molecular-weight aldehydes and other substances was investigated. It was found that their interferences with the determination of HCHO in water

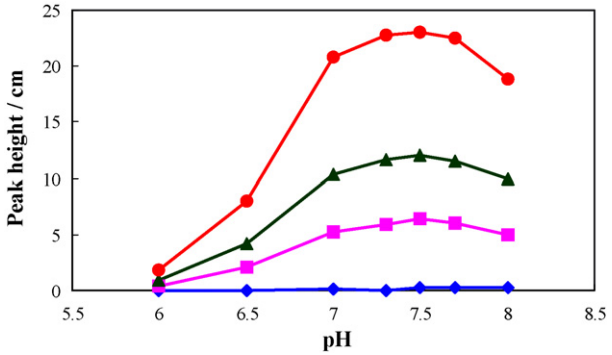

Fig. 9. Effect of pH. HCHO concentration (♦) 0 (blank); (■) 1×10^{-6} M; (▲) 2×10^{-6} M; (●) 4×10^{-6} M.

Table 1
Tolerable concentrations of foreign species for the determination of 1×10^{-6} M HCHO

Foreign substances	Tolerable concentration (M)	Tolerable limit ([species]/[HCHO])	Relative error (%)
Na^+	1×10^{-2}	10,000	+4.2
Cl^-	1×10^{-2}	10,000	+4.2
H_2O_2	1×10^{-2}	10,000	−4.2
NO_3^-	1×10^{-2}	10,000	+4.7
HAc	1×10^{-2}	10,000	−3.7
NO_2^-	5×10^{-3}	5,000	−4.4
SO_4^{2-}	2×10^{-3}	2,000	−3.8
Acetone	2×10^{-3}	2,000	+3.7
Propionaldehyde	1×10^{-3}	1,000	+4.2
CO_3^{2-}	1×10^{-3}	1,000	+4.7
Acetaldehyde	5×10^{-4}	500	+3.0
Cu^{2+}	2.5×10^{-5}	25	+2.7
Fe^{3+}	1×10^{-5}	10	+4.3
SO_3^{2-}	2×10^{-6}	2	−3.8

samples were negligible even when interfering substances were added at higher concentrations than commonly existing ones. However, the HCHO signal decreased seriously with the addition of more than two-fold of sulfite ion. This interference is due to the reaction of HCHO with sulfite. Since sulfite is easily oxidized to sulfate, only a low concentrations of sulfite can remain in natural waters. Therefore, the proposed method is free from interference with the determination of formaldehyde in environmental waters. In Table 1, the tolerable concentration is defined as the concentrations of foreign substances causing less than ±5% relative error.

Table 2
Summary of the optimal conditions for the proposed method

Parameter	Range examined	Optimal conditions
Reaction temperature (°C)	25–80	25
Flow rate (ml min^{-1})	0.2–0.6	0.3
Mixing coil length (m)	4–14	10
Sample volume (μl)	100–500	300
Acetoacetanilide concentration (M)	0.02–0.08	0.05
Ethanol concentration (%, v/v)	10–50	40
Ammonium acetate concentration (M)	0.5–2.5	2.0
pH	6.0–8.0	7.5

3.4. Calibration graph and analytical features

Under the optimal conditions summarized in Table 2, the calibration graph was prepared over the range of 0.50–40 × 10^{-7} M HCHO with a correlation coefficient of 0.9999. The peak profile of HCHO for the calibration graph obtained are shown in Fig. 10. The equation of the calibration graph was expressed as $Y = 0.57X + 0.19$, where Y is the peak height and X is the HCHO concentration in 10^{-7} M. The standard deviation and the relative standard deviation of 12 replicate injections of 5.0×10^{-7} M were 0.052% and 1.7%, respectively.

The limit of detection, calculated as the concentration corresponding to three times of the baseline noise (S/N = 3), was 3×10^{-9} M (0.09 ppb). The proposed method is superior in terms of sensitivity compared with other flow-injection spectrofluorometric methods as shown in Table 3.

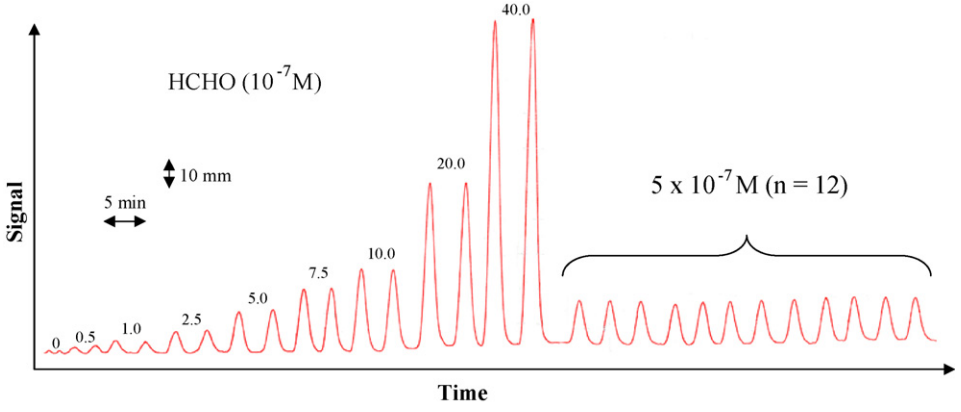

Fig. 10. Flow signals for HCHO determination. HCHO concentration: 0–40 × 10^{-7} M; 0.05 M acetoacetanilide; 40% ethanol solution; 2.0 M ammonium acetate; pH 7.5; flow rate: 0.3 ml min^{-1}; reaction coil length: 10 m; sample injection volume: 300 μl; reaction temperature: 25 °C.

Table 3
Comparison of flow-injection spectrofluorometric method for the determination of formaldehyde

Reagent	Reaction temperature (°C)	Working range (M)	Detection limit (M)	Sample throughput (h^{-1})	Reference
4-Amino-3-penten-2-one (Fluoral P)	60	0.5–100 × 10^{-6}	–	12	[18]
1,3-Cyclohexanedione (CHD)	95	0.14–1.4 × 10^{-7}	6 × 10^{-9}	–	[19]
5,5-Dimethycyclohexane-1,3-dione (Dimedone)	130	1.7–3.3 × 10^{-7} and 0.83–3.3 × 10^{-6}	3 × 10^{-8}	20	[20]
Acetylacetone (AA)	60	1.5–15 × 10^{-7}	8 × 10^{-9}	20	[21]
Acetoacetanilide (AAA)	25	0.50–40 × 10^{-7}	3 × 10^{-9}	15	This work

Table 4
Recovery tests of formaldehyde in environmental waters

Sample	Concentration added (ppb)	Concentration recovered (ppb)	Recovery (%)
Rain	0	15.7	–
	7.5	22.6	96.2
	15.0	31.0	101.9
	30.0	45.2	96.8
River water	0	3.53	–
	1.5	5.25	106.2
	3.0	6.83	108.4
	6.0	9.67	104.0
Tap water 1	0	1.13	–
	1.5	2.9	110.2
	3.0	4.2	106.2
Tap water 2	0	1.29	–
	1.5	2.91	107.6
	3.0	4.36	105.4

All values are means ($n = 4$).

3.5. Application of the proposed method to environmental water samples

The proposed method was applied to the determination of formaldehyde in rain, river and tap water samples. All samples were filtered using filter papers before introducing to the flow-injection system. In order to evaluate the validity of the proposed method for the determination of formaldehyde, the recovery test was performed. The samples were spiked with known amounts of formaldehyde solutions from 1.5 to 30.0 ppb, which covers the usual concentration ranges of formaldehyde in environmental water samples. Significantly high recoveries from 96.2% to 110.2% were obtained from the determination of formaldehyde in water samples (Table 4).

4. Conclusions

A new reagent, acetoacetanilide, is first introduced for the sensitive determination of trace amounts of formaldehyde.

The proposed method has several advantages over the previously reported methods: (1) simpler analysis system, (2) higher sensitivity and (3) less toxicity of the reagents used.

The proposed method can be directly applied to the determination of HCHO in the environmental water samples (rain, tap water and river water) at low concentration levels without any enrichment procedure.

Acknowledgement

This work was supported partially by the Grant-in-Aid for Scientific Research (B) (no. 16350044) from Japan Society for the Promotion of Science (JSPS).

References

[1] N. Kiba, L.M. Sun, S. Yokose, M.T. Kazue, T.T. Suzuki, Anal. Chim. Acta 378 (1999) 169.
[2] A.C. Rayner, C.M. Jephcott, Anal. Chem. 33 (1961) 627.
[3] E. Sawicki, T.R. Hauser, S. McPherson, Anal. Chem. 34 (1962) 1460.
[4] B.W. Bailey, J.M. Rankin, Anal. Chem. 43 (1971) 782.
[5] R.R. Miksch, D.W. Anthon, L.Z. Fanning, C.D. Hollowell, K. Revzan, J. Glanville, Anal. Chem. 53 (1981) 2118.
[6] A. Afkhami, M. Rezaei, Microchem. J. 63 (1999) 243.
[7] A.A. Ensafi, S. Abassi, Fresen. J. Anal. Chem. 363 (1999) 376.
[8] J.M. Bosque-Sendra, S. Pescarolo, L. Cuadros-Rodríguez, A.M. García-Campaña, E.M. Almansa-López, Fresen. J. Anal. Chem. 369 (2001) 715.
[9] R.K. Beasley, C.E. Hoffman, M.L. Rueppel, J.W. Worley, Anal. Chem. 52 (1980) 1110.
[10] D. Grosjean, K. Fung, Anal. Chem. 54 (1982) 1221.
[11] K. Kuwata, M. Uebori, H. Yamasaki, Y. Kuge, Y. Kiso, Anal. Chem. 55 (1983) 2013.
[12] F. Sandner, W. Dott, J. Hollender, Int. J. Hyg. Environ. Health 203 (2001) 275.
[13] G. Burini, R. Coli, Anal. Chim. Acta 511 (2004) 155.
[14] T. Nash, Biochem. J. 55 (1953) 416.
[15] S. Belman, Anal. Chim. Acta 29 (1963) 120.
[16] E. Sawicki, R.A. Carnes, Mikrochim. Acta (1968) 148.
[17] J. Li, P.K. Dasgupta, W. Luke, Anal. Chim. Acta 531 (2005) 51.
[18] H. Tsuchiya, S. Ohtani, K. Yamada, M. Akagiri, N. Takagi, Analyst 119 (1994) 1413.
[19] Q. Fan, P.K. Dasgupta, Anal. Chem. 66 (1994) 551.
[20] T. Sakai, S. Tanaka, N. Teshima, S. Yasuda, N. Ura, Talanta 58 (2002) 1271.
[21] P. Sritharathikhun, M. Oshima, S. Motomizu, Talanta 67 (2005) 1014.
[22] T. Pérez-Ruíz, C. Martínez-Lozana, V. Tomáa, J. Fenoll, Anal. Bioanal. Chem. 375 (2003) 661.
[23] B. Li, M. Liu, Z. Zhang, C. Xu, Anal. Sci. 19 (2003) 1643.
[24] E. Cotsaris, B.C. Nicholson, Analyst 118 (1993) 265.
[25] K. Takami, K. Kuwata, A. Sugimae, M. Nakamoto, Anal. Chem. 57 (1985) 243.
[26] Q. Li, P. Sritharathikhum, M. Oshima, S. Motomizu, Proceedings of the 67th Symposium of the Japan Society for Analytical Chemistry, Akita, Japan, May 13–14, 2006, p. P196.

Available online at www.sciencedirect.com
ScienceDirect
Talanta 72 (2007) 1704–1709
Talanta
www.elsevier.com/locate/talanta

Ultrasensitive electrogenerated chemiluminescence detection of DNA hybridization using carbon-nanotubes loaded with tris(2,2′-bipyridyl) ruthenium derivative tags

Yan Li, Honglan Qi, Fang Fang, Chengxiao Zhang *

Key Laboratory of Analytical Chemistry for Life Science of Shaanxi Province, School of Chemistry and Materials Science, Shaanxi Normal University, Xi'an 710062, PR China

Available online 9 February 2007

Abstract

An ultrasensitive electrogenerated chemiluminescence (ECL) detection method of DNA hybridization based on single-walled carbon-nanotubes (SWNT) carrying a large number of ruthenium complex tags was developed. The probe single strand DNA (ss-DNA) and ruthenium complex were loaded at SWNT, which was taken as an ECL probe. When the capture ss-DNA with a thiol group was self-assembled onto the surface of gold electrode, and then hybridized with target ss-DNA and further hybridized with the ECL probe to form DNA sandwich conjugate, a strong ECL response was electrochemically generated. The ECL intensity was linearly related to the concentration of perfect-matched target ss-DNA in the range from 2.4×10^{-14} to 1.7×10^{-12} M with a detection limit of 9.0×10^{-15} M. The ECL signal difference permitted to discriminate the perfect-matched target ss-DNA and two-base-mismatched ss-DNA. This work demonstrates that SWNT can provide an amplification platform for carrying a large number of ECL probe and thus resulting in an ultrasensitive ECL detection of DNA hybridization.

Keywords: DNA hybridization; Electrogenerated chemiluminescence; Amplification; Carbon nanotubes; Tris(2,2′-bipyridyl) ruthenium derivatives

1. Introduction

Development of highly sensitive detection method for DNA hybridization has been received much attention due to its important applications in clinical diagnosis, medicine, epidemic prevention, environmental protection and bioengineering [1–3]. A variety of techniques have been developed for DNA hybridization detection, including fluorescence imaging [4,5], electrochemical [6–8], micro-gravimetrical [9], bioluminescence [10], chemiluminescence [11] and electrogenerated chemiluminescence (ECL) techniques [12,13]. ECL technique has many distinct advantages over fluorescence technique because it does not involve a light source and avoids the attendant problems of scattered light and impurities luminescent. Moreover, the specificity of the ECL reaction associated with the ECL label and the coreactant species decreases problems with side reactions and is characterized by good spatial and temporal resolution [13]. Recently, ECL detection of DNA hybridization, combining the base-pair recognition of nucleic-acid probes with the advantages of ECL technique, is currently receiving a considerable attention [13–18]. Miao and Bard [13] developed an ECL method for the detection of ss-DNA by immobilizing DNA on gold electrode and using tris(2,2′-bipyridyl) ruthenium(II) as a ECL label. Fang and co-workers [12] reported an ECL detection method for DNA hybridization based on *N*-(4-aminobutyl)-*N*-ethylisoluminol labeled a probe ss-DNA for the recognition of a target ss-DNA immobilized on PPy modified electrode. Firrao [17] reported an ECL detection method similar to Bard's method [13], except at a glassy carbon electrode covalently attached a probe ss-DNA. These reported protocols are all based on one ECL label per hybridizing with ss-DNA [13–18].

Great efforts have been made to improve the sensitivity of DNA hybridization detection using nanomaterials including silica, metal nanoparticles and polymeric microbeads for carrying multiple reporters externally or internally [14,19–23]. Miao and Bard [14] utilized polystyrene microspheres/beads as the carriers of the ECL labels of $Ru(bpy)_3[B(C_6F_5)_4]$. Tris(2,2′-bipyridyl) ruthenium(II)-doped silica nanoparticles for ECL detection of DNA [19], fluorophores dye-doped silica nanoparticles for fluorescent detection of DNA [20], cobalt(III) tris(2,2′-bipyridyl) doped silica nanoparticles for electrochemical detection of DNA

* Corresponding author. Tel.: +86 29 85303825; fax: +86 29 85307774.
E-mail address: cxzhang@snnu.edu.cn (C. Zhang).

0039-9140/$ – see front matter © 2007 Elsevier B.V. All rights reserved.
doi:10.1016/j.talanta.2007.01.062

[21], and microsphere tags loaded internally with ferrocenecarboxaldehyde marker for electrochemical detection of DNA [22] were also reported. These approaches offer a remarkable amplification of single hybridization events. However, the sensitivity of established ECL detection for DNA hybridization based on doping signal compound into nanoparticles is limited because the ECL emission of signal compound is electrochemically generated from the surface of the nanoparticles. Recently, our group developed a novel ECL method for the detection of DNA hybridization based on gold nanoparticles carrying multiple ECL probes [23]. New nanomaterial-based schemes coupling of multiple amplification units and processes on surface are highly desired for meeting the high sensitivity of ECL detection of DNA hybridization.

Carbon nanotubes (CNT) have been proved to be a novel type of nanostructure materials with attractive properties including unique mechanical, electronic and chemical properties [24]. The attractive properties of CNT make them promising candidates for DNA hybridization detection [25–27]. Wang et al. [28] demonstrated the use of CNT loaded alkaline phosphatase through cross linking for dramatically amplifying enzyme-based bioaffinity electrical sensing of proteins and DNA. Khairoutdinov et al. [29] and Panhuis and co-workers [30] reported the approach to covalent attachment of ruthenium complex to carboxylated single-wall carbon-nanotubes (SWNT) and to amino functionalized multiwall carbon nanotubes, respectively.

In the present work, it was proposed that SWNT was used as carrier platform for load of the ss-DNA probe and ruthenium complex in order to amplify ECL signal for the detection of DNA hybridization. In this paper, the ECL behavior of SWNT loaded with the ss-DNA probe and ruthenium complex was investigated. The optimization of the analytical conditions and characteristics for DNA hybridization detection were presented. To our knowledge, this is the new example of ECL detection of DNA hybridization using carbon nanotube as a carrier for ECL tags and probe DNA.

2. Experimental

2.1. Reagents

N-Hydroxysuccinimide (NHS), 4,4′-dicarboxylic acid-2,2′-bipyridyl (dcbpy), 1-ethyl-3-(3-dimethylaminopropyl) carbodiimide (EDC), *N*,*N*′-dicyclohexyl carbodiimide (DCC) and sodium hexafluorophosphate were purchased from Sigma (USA). Ruthenium(III) chloride hydrate was obtained from ACROS Organics (Japan). 2,2′-Bipyridine, tri-*n*-propylamine (TPA), ethylenediamine were obtained from First Reagent Company of Shanghai (Shanghai, China). Single-wall carbon nanotubes (SWNT) were from Shenzhen Nanotech Port Co. Ltd. (Shenzhen, China).

Synthetic ss-DNA was obtained from Shenggong Bioengineering Co. Ltd. (Shanghai, China) and has the following sequences: capture DNA: 5′-TGG AAA ATC TCT AGC AGT CGT-$(CH_2)_6$-SH-3′; probe DNA: 5′-NH_2-$(CH_2)_6$-ATG TCC CTC AGA CCC TTT-3′; perfect-matched (PM) target DNA: 5′-ACT GCT AGA GAT TTT CCA CAC TGA CTA AAA GGG TCT GAG GGA-3′; non-complementary sequence: 5′-ACT GCT AGA GAT TTT CCA CAC TGA CTA CTT CAA CAG TGC CCC-3′; two mismatched (TM) target DNA: 5′-ACT GCT AGA GAT TTT CCA CAC TGA CTA AAA GCG TCT GTG GGA-3′.

The ss-DNA stock solution was prepared using water and was kept at −18 °C in refrigerator. 0.10 M phosphate buffer solutions (PBS, pH 7.4) were used for the hybridization and wash solution. All other reagents were of analytical grade and Millipore filtered water (>18 ΩM cm^{-1}) was used throughout.

2.2. Apparatus

The experimental set-up for ECL measurement consisted of a CHI-600B electrochemical system (Shanghai Chenhua Instrument Co. Ltd., Shanghai, China) and an ultra-weak chemiluminescence analyzer controlled by a personal computer with the BPCL program (Institute of Biophysics, Chinese Academy of Science, Beijing, China, operated at −900 V). A commercial cylindroid's glass cell was used as ECL cell and employed with a three-electrode system composed of a disk gold electrode ($\phi = 2$ mm) or a disk gold electrode immobilized DNA as a working electrode, a platinum plate as counter-electrode, and an Ag/AgCl (saturated KCl) as reference electrode. All potentials were referred to the reference electrode. For detecting ECL, the cell was placed directly in front of a photomultiplier (PMT) and the PMT window was only opened towards the working electrode to eliminate the blank chemiluminescence and the ECL from the counter-electrode.

2.3. Preparation of SWNT–Ru 1–DNA conjugates

According to Refs. [31,32], ruthenium bis(2,2′-bipyridine) (2,2′-bipyridine-4,4′-dicarboxylic acid)-*N*-hydroxysuccinimide ester (Ru 2) was synthesized and the concentration of Ru 2 was estimated to be 6.34×10^{-2} M by means of UV–vis spectrum. Two hundred microlitres of 1.0×10^{-3} M Ru 2 was added to 50 μL of ethylenediamine with shaking at room temperature for 30 min, stirring for 12 h. After several filtration/centrifugation steps, Ru 1 solid was obtained.

The SWNT–Ru 1–DNA conjugates were prepared with a modified literature protocol [28–30]. This process includes a SWNT purification step, a SWNT activation step and a SWNT covalent attachment of Ru 1 to carboxylated SWNT step. SWNT (50 mg) were purified by refluxing in 100 mL of 2 M HNO_3 for 48 h, followed by several ultracentrifugation and ultrafiltration steps in the presence of 0.2% *N*,*N*-dimethylformamide (DMF) to further remove small particles. The purified SWNT were shortened by treating them with a 1:3 HNO_3/H_2SO_4 mixture for 2 h in an ultrasonic bath, followed by washing with water, filtration and drying.

Activation of the SWNT with carboxylic acids was achieved by sonicating a 5 mL of 0.2% DMF suspension containing 0.5 mg SWNT purified, 100 mM NHS, and 100 mM EDC (set to pH 6.0 with 0.1 M HCl), for 1 h at room temperature [28]. Following the activation, the pH was adjusted to 8.5, and the probe DNA and the Ru 1 were added to the above suspension,

resulting at a final concentrations of 6.15×10^{-6} M probe DNA and 6.34×10^{-6} M Ru 1, respectively. The reaction mixture was stirred overnight at room temperature. Following this incubation, the mixture was washed with 0.5 M NaCl during several centrifugation cycles at 12,000 rpm. Subsequently, the resulting solution was allowed to stand at room temperature for few hours, and the supernatant fractions were collected to obtain SWNT–Ru 1–DNA conjugate. For comparison, Ru 2–DNA conjugate was also synthesized according to Refs. [23,33,34].

2.4. ECL detection for target DNA

A gold disk electrode was pretreated according to Ref. [23]. Subsequently, the cleaned electrode was immersed in 1.0 mL of capture DNA (5.12×10^{-6} M) for 4 h to form capture DNA self-assembled electrode and then washed twice with 0.1 M PBS. The resulting electrodes were then immersed in 1.0 mL of target DNA solution having different concentrations for 30 min at 37 °C to hybridize with target DNA. After that, the hybridized electrode was washed with the same buffer and then immersed into 1 mL of SWNT–Ru 1–DNA conjugate for 30 min at 37 °C, followed by washing with the same buffer to remove the unbinding the ECL probe on the electrode, which was employed as the working electrode. ECL measurement was performed at a constant potential of +1.30 V in 2.0 mL of 0.10 M PBS (pH 7.4) containing 0.10 M TPA. The concentration of target DNA was quantified by the integrated ECL intensity for 30 s after the potential was applied.

3. Results and discussion

Schematic diagram of the ECL detection for DNA hybridization is demonstrated in Fig. 1. The ECL method is designed to utilize a sandwich DNA detection model and the ECL probes of carbon-nanotubes loaded with probe ss-DNA and Ru 1 tags. The probe ss-DNA and Ru 1 were loaded at SWNT, which was taken as an ECL probe. When the capture ss-DNA with a thiol group was self-assembled onto the surface of gold electrode, and then hybridized with target ss-DNA and further hybridized with the ECL probe to form DNA sandwich conjugate, a strong ECL response was electrochemically generated. The great advantages of the sandwich technique over conventional hybridization formats are the speed and ease with which it can be applied to the analysis of crude biological samples, with a minimum of sample preprocessing [35]. Such assays are extremely flexible, because they are not limited to the use of a modified target ss-DNA (analyte) for the immobilization on the solid support. The obvious advantages of the sandwich assay will be a high specificity compared with direct hybridization assay because two hybridization events must be curried out in sandwich assay and will be combined with a high sensitivity associated with signal amplification. In present work, therefore, approach of sandwich mode with signal amplification was chosen to assay the specific DNA sequences.

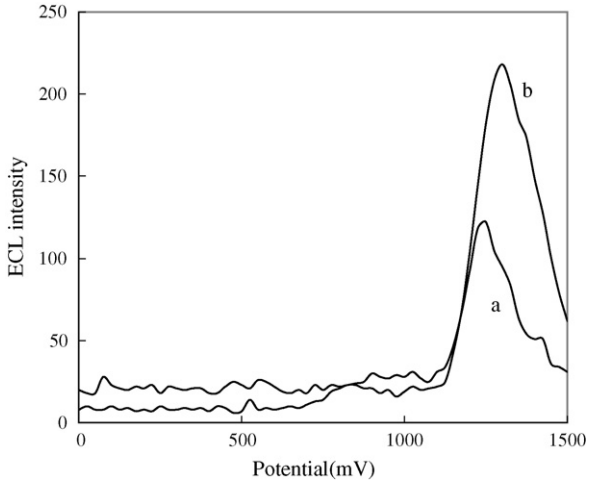

Fig. 2. ECL profiles of 2.0×10^{-9} M Ru 1 (a) and 1.0×10^{-8} M SWNT–Ru 1–DNA (b) at a gold electrode in 0.10 M PBS (pH 7.4) containing 0.10 M TPA. Scan rate: 50 mV s^{-1}.

3.1. ECL behavior of SWNT–Ru 1–DNA conjugate

ECL behavior of SWNT–Ru 1–DNA conjugate was investigated using linear potential scan technique with a scan rate of 50 mV s^{-1} at a gold electrode. Fig. 2 shows the ECL profiles of Ru 1 and the SWNT–Ru 1–DNA conjugate in 0.10 M PBS containing 0.10 M TPA. From Fig. 2, it can be seen that the strong ECL emissions of both Ru 1 and the SWNT–Ru 1–DNA conjugate are generated and the ECL peak appears at +1.25 V for Ru 1 and at +1.30 V for SWNT–Ru 1–DNA conjugate, respectively. This indicates that ECL behavior of SWNT–Ru 1–DNA conjugate is similar with that of Ru 1 and

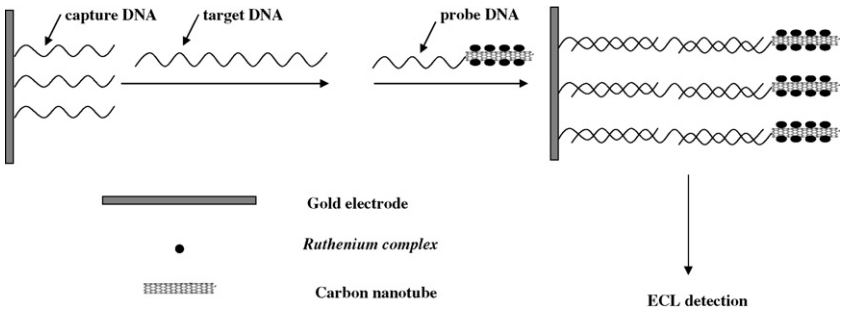

Fig. 1. Schematic diagram of the ECL detection for DNA hybridization using sandwich DNA detection model and the ECL probes of carbon-nanotubes loaded with probe ss-DNA and Ru 1 tags.

SWNT–Ru 1–DNA conjugate maybe used as an ECL probe. It was found that the maximum ECL intensity was obtained when a constant potential of +1.30 V was employed. Therefore, a constant potential of +1.30 V was chosen in this work because of its excellent sensitivity. When the constant potential was applied, 1.0 s from the potential applied to the ECL peak was only needed and it took 20 s for the signal to return to stable value, and when applied potential was switched off, it took 5.0 s to return to background signal (data not shown). This indicates that this ECL process is a quick emission process. Therefore, the integrated ECL intensity for 30 s after the potential applied was used to obtain a high accurate for quantitative analysis.

3.2. Comparison of ECL intensity of SWNT–Ru 1–DNA conjugate with Ru 2–DNA conjugate

The signal amplification associated with the SWNT carrier tris(2,2′-bipyridyl) ruthenium derivative tags was showed in Fig. 3, which displays the hybridization ECL response of Ru 2–DNA conjugate (a) for 1.7×10^{-10} M PM target DNA and SWNT–Ru 1–DNA conjugate (b) for 1.7×10^{-12} M PM target DNA, respectively. The result showed that the ECL emission peak obtained after the 1.7×10^{-10} M PM target DNA hybridization with Ru 2–DNA conjugate was 299 and that 1.7×10^{-12} M PM target DNA with SWNT–Ru 1–DNA conjugate was 4927. The SWNT–Ru 1–DNA conjugate based protocol exhibits a substantially (∼16 times) larger ECL signal for the significantly (100-fold) lower target DNA concentration. This indicates that the ECL probe SWNT–Ru 1–DNA conjugate employing multiple reporters per hybridization event can greatly enhance the ECL detection sensitivity due to its offering a remarkable amplification of hybridization events. Therefore, the ECL probe SWNT–Ru 1–DNA conjugate can amplify ECL signal during ECL detection of DNA hybridization.

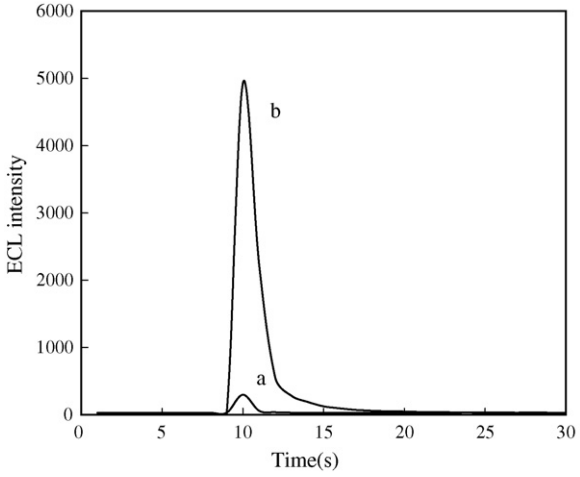

Fig. 3. ECL profile for target DNA hybridized with Ru 2–DNA conjugate (a) and SWNT–Ru 1–DNA conjugate (b). Concentration of PM target DNA: 1.7×10^{-10} M (a) and 1.7×10^{-12} M (b). Self-assembled time of capture DNA: 4 h; hybridization time: 30 min; hybridization temperature: 37 °C. The ECL measurement condition was performed at an applied potential of +1.30 V in 0.10 M PBS (pH 7.4) containing 0.10 M TPA.

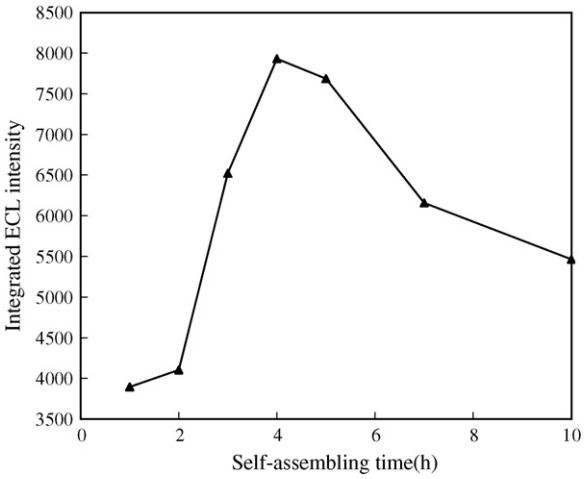

Fig. 4. Effect of self-assembled time of capture DNA on the ECL intensity. 5.12×10^{-6} M capture DNA; 2.4×10^{-13} M PM target DNA; 1.0×10^{-8} M SWNT–Ru 1–DNA probe. Other conditions were same as Fig. 3.

3.3. Optimization of self-assembling time and hybridization time

Fig. 4 shows the effect of self-assembled time of capture DNA on the ECL intensity. From Fig. 4, it can be seen that the ECL intensity increased significantly with increasing self-assembled time from 2 to 4 h and reached a maximum at about 4 h, attributed to an increased amount of SWNT–Ru 1–DNA probe on the surface of the electrode with increasing self-assembled time. With further increasing the self-assembled time, however, the ECL intensity decreased. This was attributed to steric and electrostatic hindrance arising from the more tightly packed DNA monolayer. Similar phenomena were reported for immobilization of ss-DNA on a microtiter plate [36] and on a gold surface [37]. Therefore, a self-assembled time of 4 h was chosen in following experiments to obtain an excellent sensitivity.

Fig. 5 shows the effect of hybridization time on the ECL intensity. The results showed that the ECL intensity increased with

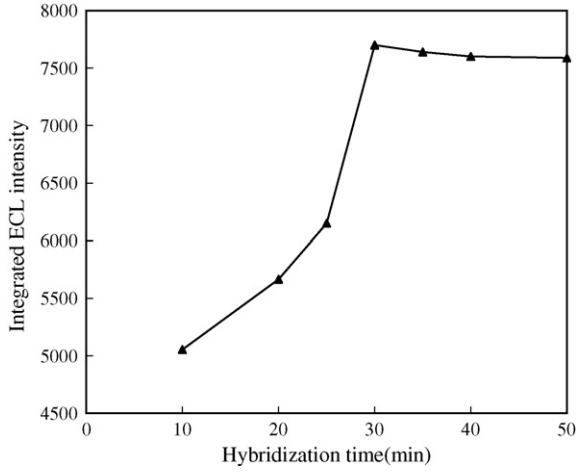

Fig. 5. Effect of hybridization time on the ECL intensity. 2.4×10^{-13} M PM target DNA; 1.0×10^{-8} M SWNT–Ru 1–DNA probe; self-assembled time: 4 h. Other conditions were same as Fig. 3.

increasing the hybridization time from 10 to 30 min and reached a maximum at 30 min, and then reached a constant value after 30 min. This suggests that the hybridization reaction completes within 30 min. Therefore, the hybridization time of 30 min was employed in following experiments.

3.4. ECL detection of DNA hybridization

The quantitative behavior was assessed by measuring the dependence of the SWNT–Ru 1–DNA ECL hybridization signal upon the concentration of PM target DNA. Under the optimized conditions, the linear range for PM target DNA was measured. Fig. 6 shows the ECL profiles of the different concentrations of PM target DNA after hybridization with the ECL probe SWNT–Ru 1–DNA conjugate. The integrated ECL intensity had a linear relationship with the concentration of PM target DNA in the range from 2.4×10^{-14} to 1.7×10^{-12} M. The linear regression equation was $S = 2959 + 174.5C$ (unit of C is 10^{-14} M) and the correlation coefficient was 0.9946. The detection limit for the PM target DNA was 9.0×10^{-15} M. This is considerably lower than that reported using single $Ru(bpy)_3^{2+}$ tag (1×10^{-11} M) [17]. The substantial (~1000-fold) lowering of the detection limit reflects the amplification of SWNT carrying lots of Ru 1. The precision was estimated for seven successive measurements of 2.4×10^{-13} M PM target DNA that yielded reproducible the integrated ECL intensity with a relative standard deviation of 5.9%.

3.5. The recognition of target DNA

To assay the specificity of proposed method, a large excess of non-complementary DNA and TB target DNA were used, respectively. Fig. 7 compares the response of the SWNT–Ru 1–DNA based on the protocol for 2.4×10^{-13} M PM target DNA (d), 2.4×10^{-11} M TM target DNA (c) and 2.4×10^{-11} M non-complementary DNA (b), respectively. As shown in Fig. 7, only PM target DNA gives significant ECL response. Despite its 100-fold excess, the non-complementary DNA yields a substantially smaller response compared with the PM target DNA, which were equivalent to that of the blank measurement (without DNA on the electrode). Although TM target DNA had slight response, it still could be identified with PM target DNA. This proved that the prepared SWNT–Ru 1–DNA probe in this work was highly selective to the target DNA sequence and could be used to identify the DNA sequence with TM target DNA sequence.

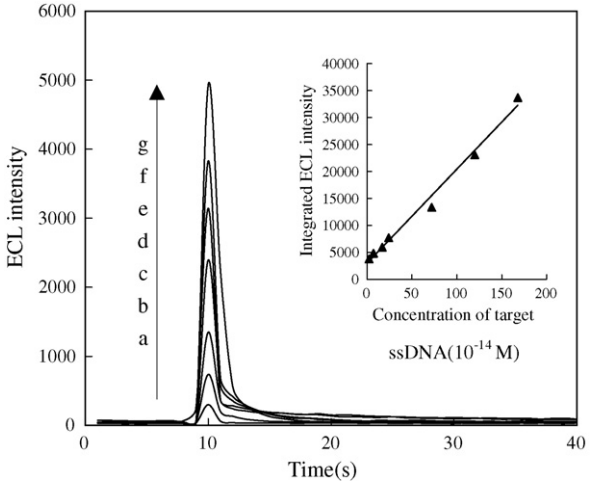

Fig. 6. The ECL profiles of the different concentration of PM target DNA sequence after hybridization with the ECL probe. The concentration of PM target DNA sequence: (a) 2.4×10^{-14} M, (b) 7.2×10^{-14} M, (c) 1.7×10^{-13} M, (d) 2.4×10^{-13} M, (e) 7.2×10^{-13} M, (f) 1.2×10^{-12} M, and (g) 1.7×10^{-12} M. Other conditions were same as Fig. 3.

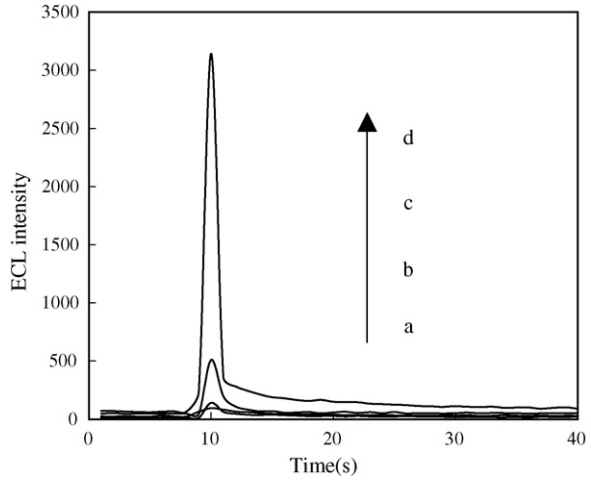

Fig. 7. The ECL response for different DNA sequences. (a) Blank (without DNA on the electrode); (b) non-complementary sequence (2.4×10^{-11} M); (c) TM target DNA sequence; (d) PM target DNA sequence (2.4×10^{-13} M). Other conditions were same as Fig. 3.

4. Conclusions

An ultrasensitive ECL method for the detection of DNA hybridization based on carbon-nanotubes loaded with tris(2,2′-bipyridyl) ruthenium derivative tags has been developed. SWNT loaded with large of tris(2,2′-bipyridyl) ruthenium derivative tags exhibits excellent ECL signaling ability in the presence of a trace amount of DNA targets and the developed ECL method based on the multiple reporters per hybridization event offer a high sensitivity for the detection of DNA hybridization. In addition, the carbon-nanotubes loaded with tris(2,2′-bipyridyl) ruthenium(II) derivative tags based DNA bioanalysis assay can effectively discriminate two-base mismatched DNA sequences. The CNT-derived amplification bioassays offer great promise for ultrasensitive detection of other biorecognition events.

Acknowledgements

Financial supports from the National Science Foundations of China (No. 20375025, No.90607016) are gratefully acknowledged.

References

[1] N. Chistodoulides, M. Tran, P.N. Floriano, M. Rodriguez, A. Goodey, M. Ali, D. Neikirk, J.T. McDevitt, Anal. Chem. 74 (2002) 3030.
[2] F. Lucarelli, A. Kicela, I. Palchetti, G. Marrazza, M. Mascini, Bioelectrochemistry 58 (2002) 113.
[3] G. Marrazza, I. Chianella, M. Mascini, Anal. Chim. Acta 387 (1999) 297.
[4] V. Benoit, A. Steel, M. Torres, Y.-Y. Yu, H. Yang, J. Cooper, Anal. Chem. 73 (2001) 2412.
[5] Y. Dharmadi, R. Gonzales, Biotechnol. Prog. 20 (2004) 1309.
[6] J. Wang, Electroanalysis 13 (2000) 635.
[7] R. Gasparac, B.J. Taft, M.A. Lapierre-Delvin, A.D. Lazareck, J.M. Xu, S.O. Kelley, J. Am. Chem. Soc. 126 (2004) 12270.
[8] E.L.S. Wong, F.J. Mearns, J.J. Gooding, Sens. Actuators B 111–112 (2005) 515.
[9] X. Su, R. Robelek, Y.J. Wu, G.Y. Wang, W. Knoll, Anal. Chem. 76 (2004) 489.
[10] L.J. Kricka, Clin. Chem. 45 (1999) 453.
[11] B.J. Cheek, A.B. Steel, M.P. Torres, Y.-Y. Yu, H. Yang, Anal. Chem. 73 (2001) 5777.
[12] M.L. Yang, C.Z. Liu, K.J. Qian, P.G. He, Y.Z. Fang, Analyst 127 (2002) 1267.
[13] W.J. Miao, A.J. Bard, Anal. Chem. 75 (2003) 5825.
[14] W.J. Miao, A.J. Bard, Anal. Chem. 76 (2004) 5379.
[15] A.M. Spehar, S. Koster, S. Kulmala, E. Verpoorte, N. de Rooij, M. Koudelka-Hep, Luminescence 19 (2004) 287.
[16] C. Bertolino, M. MacSweeney, J. Tobin, B. O'Neill, M.M. Sheehan, S. Coluccia, H. Berney, Biosens. Bioelectron. 21 (2005) 565.
[17] G. Firrao, Int. J. Environ. Anal. Chem. 85 (2005) 609.
[18] A.M. Spehar-Deleze, L. Schmidt, R. Neier, S. Kulmala, N. de Rooij, M. Koudelka-Hep, Biosens. Bioelectron. 22 (2006) 722.
[19] Z. Chang, J.G. Zhou, K. Zhao, N.G. Zhu, P.G. He, Y.Z. Fang, Electrochim. Acta 52 (2006) 575.
[20] X.J. Zhao, R. Tapec-Dytioco, W.H. Tan, J. Am. Chem. Soc. 125 (2003) 11474.
[21] N.N. Zhu, H. Cai, P.G. He, Y.Z. Fang, Anal. Chim. Acta 481 (2003) 181.
[22] J. Wang, R. Polsky, A. Merkoci, K.L. Turner, Langmuir 19 (2003) 989.
[23] H. Wang, C.X. Zhang, Y. Li, H.L. Qi, Anal. Chim. Acta 575 (2006) 205.
[24] D. Tasis, N. Tagmatarchis, A. Bianco, M. Prato, Chem. Rev. 106 (2006) 1105.
[25] R.H. Baughman, A. Zakhidov, W.A. de Heer, Science 297 (2002) 787.
[26] Q. Zhao, Z.H. Gan, Q.K. Zhuang, Electroanalysis 14 (2002) 1609.
[27] J.N. Wohlstadter, J.L. Wilbur, G.B. Sigal, H.A. Biebuyck, M.A. Billadeau, L.W. Dong, A.B. Fischer, S.R. Gudibande, S.H. Jameison, J.H. Kenten, J. Leginus, J.K. Leland, R.J. Massey, S.J. Wohlstadter, Adv. Mater. 15 (2003) 1184.
[28] J. Wang, G. Liu, M.R. Jan, J. Am. Chem. Soc. 126 (2004) 3010.
[29] R.F. Khairoutdinov, L.V. Doubova, R.C. Haddon, L. Saraf, J. Phys. Chem. B 108 (2004) 19976.
[30] F. Frehill, J.G. Vos, S. Benrezzak, A.A. Koos, Z. Konya, M.G. Ruther, W.J. Blau, A. Fonseca, J.B. Nagy, L.P. Biro, A.I. Minett, M. in het Panhuis, J. Am. Chem. Soc. 124 (2002) 13694.
[31] T. Shimdzu, T. Iyoda, K. Izaki, J. Phys. Chem. 89 (1985) 642.
[32] K. Kalyanasundaram, Md.K. Nazeeruddin, M. Grätzel, G. Viscardi, P. Savarino, E. Barni, Inorg. Chim. Acta 198–200 (1992) 831.
[33] E. Terpetschnig, H. Szmacinski, H. Malak, J.R. Lakowicz, Biophys. J. 68 (1995) 342.
[34] C. Xu, H. Cai, P.G. He, Y.Z. Fang, Fresen. J. Anal. Chem. 367 (2000) 593.
[35] P.J. Nicholls, A.D.B. Malcolm, J. Clin. Lab. Anal. 3 (1989) 122.
[36] N.H.L. Chin, T.K. Christopoulos, J. Peltier, Analyst 123 (1998) 1315.
[37] T.M. Herne, M.J. Tarlov, J. Am. Chem. Soc. 119 (1997) 8916.

Available online at www.sciencedirect.com
ScienceDirect
Talanta 72 (2007) 1600–1608
Talanta
www.elsevier.com/locate/talanta

On-line preconcentration of trace carcinogenic polycyclic aromatic hydrocarbons (PAHs) in microcolumn liquid chromatography via large volume injection

Lee Wah Lim *, Yuki Okouchi, Toyohide Takeuchi

Department of Chemistry, Faculty of Engineering, Gifu University, 1-1 Yanagido, Gifu 501-1193, Japan

Received 15 November 2006; received in revised form 9 January 2007; accepted 22 February 2007
Available online 7 March 2007

Abstract

The ability and efficiency of micro precolumns made of C30 particles, monolithic silica C18 stationary phase and quartz wool coated with C30, which act as novel solid phase absorbing materials, for the on-line enrichment of aqueous polycyclic aromatic hydrocarbons (PAHs) in microcolumn liquid chromatography (LC) was investigated. The enrichment unit was designed in such a way that micro precolumns were directly connected to a 6-port micro injection valve via fused-silica tubing (0.05 mm I.D.) in order to minimize band broadening of the samples, and the enrichment efficiency of the three materials was tested using 14 PAHs, which are selected by the US Environmental Protection Agency (US EPA), as the analytes. The separation of PAHs was evaluated by using laboratory-made C30 or ODS capillary columns and the results were compared. There were no significant differences showed from the separation of PAHs in terms of peak signal between the C30 and ODS capillary columns, but the C30 capillary column was chosen for the following experiment due to its ability to produce better repeatability than the ODS column. By using the three kinds of precolumn materials, results showed that the precolumn packed with C30 particles as well as the capillary monolithic C18 precolumns (0.1 or 0.2 mm I.D.) provided better recovery than those of the quartz wool's. As long as the recovery and separation of the PAHs were concerned, 0.1 mm I.D. monolithic C18 precolumn showed the best results and the R.S.D.s ($N = 7$) for the retention time, peak area and peak height were between 0.70–1.5, 2.3–5.8 and 2.4–6.6%, respectively. Large volume injection up to 0.5 mL, i.e. 2500-fold enrichment, was possible and no negative effect on the separation profile was found. The LOD (S/N = 3) were between 0.10 and 4.6 pg mL^{-1}, while the LOQ (S/N = 10) were in the range of 0.32–15 pg mL^{-1}, which showed that the system is comparable to many major analytical techniques and is sensitive enough for the trace analysis of PAHs in environmental samples. The system was then applied to the determination of trace PAHs present in soil sample which was randomly taken from a nearby highway.

Keywords: Microcolumn LC; On-line preconcentration; PAHs; Trace analysis; Large volume injection

1. Introduction

Polycyclic aromatic hydrocarbons (PAHs) are a group of approximately 10,000 compounds, and the famous ones are acenaphthene (ACE), acenaphthylene (ACY), anthracene (ANTH), benzo[*a*]anthracene (BaA), benzo[*a*]pyrene (BaP), benzo[*k*]fluoranthene (BkF), fluoranthene (FLT), naphthalene (NAPH), phenanthrene (PHEN), etc. PAHs are colorless, white or pale yellow-green solid organic compounds that contain at least two fused 6-sided benzene rings which include only carbon and hydrogen. They may also contain other rings of carbon that are not 6-sided. Most of PAHs do not dissolve easily into water, but some are readily evaporated into the air.

Although about 10,000 of PAHs exist in the environment, only 16 of them have been selected by the US Environmental Protection Agency (US EPA) as priority pollutants due to their carcinogenic properties. These 16 PAHs are NAPH, ACY, ACE, fluorene (FLU), ANTH, FLT, pyrene (PYR), BaA, chrysene (CHR), benzo[*b*]fluoranthene (BbF), BkF, BaP, dibenzo[*a*,*h*]anthracene (DiahA), benzo[*g*,*h*,*i*]perylene (BghiP), and indeno[1,2,3-*cd*]pyrene (INPY) [1]. Besides CHR and BbF, 14 other selected PAHs are shown in Fig. 1 and these 14 compounds were used as the samples in the present research.

* Corresponding author. Tel.: +81 58 293 2815; fax: +81 58 293 2815.
E-mail address: leewahlim@apchem.gifu-u.ac.jp (L.W. Lim).

0039-9140/$ – see front matter © 2007 Elsevier B.V. All rights reserved.
doi:10.1016/j.talanta.2007.02.033

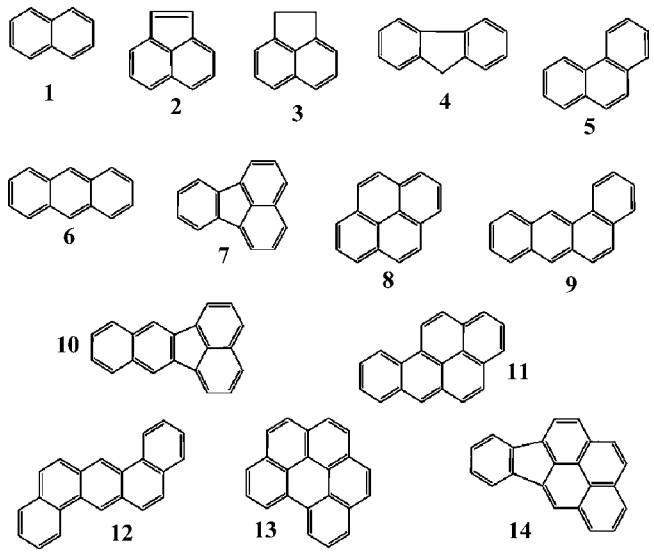

Fig. 1. Chemical structures of US EPA 14 priority pollutant PAHs. 1: naphthalene (NAPH), 2: acenaphthylene (ACY), 3: acenaphthene (ACE), 4: fluorene (FLU), 5: phenanthrene (PHEN), 6: anthracene (ANTH), 7: fluoranthene (FLT), 8: pyrene (PYR), 9: benzo[*a*]anthracene (BaA), 10: benzo[*k*]fluoranthene (BkF), 11: benzo[*a*]pyrene (BaP), 12: dibenzo[*a,h*]anthracene (DiahA), 13: benzo[*g,h,i*]perylene (BghiP), and 14: indeno[1,2,3-*cd*]pyrene (INPY).

PAHs are formed in any type of incomplete combustion of oil, coal, petrol, wood, garbage, tobacco, meats, or other carbon-containing organic materials. Most of PAHs have no known use, only a few such as NAPH, which is known as mothballs, and ANTH are used in making dyes, explosives, plastics, lubricants, and moth repellent. PAHs are also found at low concentrations in some special-purpose skin products and shampoos that contain coal tars. The primary sources of emission of PAHs are smoke, automobile emissions and industrial exhausts from petroleum refineries, fossils fuel power plants, coking plants, paper mills, etc. Naturally occurring fire, such as bush or forest fires, also forms PAHs, and they are also emitted from active volcanoes.

From the above-mentioned facts, there is no doubt that PAHs have been given much attention and there are numerous reports regarding the analysis of PAHs that have been made up till present. The common determination methods of PAHs are usually based on HPLC [1–5] as well as GC–MS [6–8] or GC–FID [9,10], with pre-treatment methods such as solid phase extraction (SPE) [1,4,5,8–10], supercritical fluid extraction [2], liquid phase micro extraction [3,6], and accelerated solvent extraction [7], etc. SPE is the most widely used method due to its simplicity and relatively good efficiency, as well as its ability to preconcentrate components to be analyzed and clean-up matrices from sample prior to analysis.

With the increasing concern of environmentally friendly analysis, miniaturization of separation column in LC has been undertaken since the 1970s and the development of capillary LC has been described [11,12]. Owning to its smaller diameter, i.e. approximately 0.1–0.8 mm I.D., compared to conventional column size, i.e. 4.0–6.0 mm I.D., the use of microcolumns in LC possesses advantages such as increased mass sensitivity due to a decrease in column's cross-sectional area, low consumption of solvent, reagent and packing material, use of exotic mobile phase and mobile phase additives, etc. The most significant feature of microcolumn LC is its ability for the direct coupling to mass spectrometry (MS), which is an ultimate detector for chromatography. However, decreasing the size of the separation column also decreases its concentration sensitivity due to the limit in the sample injection, i.e. usually 0.2 μL for most injectors. In order to overcome this drawback, sample enrichment has been proposed and it has been widely employed in HPLC in order to achieve higher sensitivity.

In our previous studies, we had developed on-line precolumn enrichment systems for the highly sensitive determination of trace analytes in microcolumn LC using packed or monolithic precolumns [13–16]. Those systems have one major and most significant similarity, i.e. they allowed large volume injection of sample analytes in order to improve the sensitivity of the detection. In the case of PAHs, since they are present in air, soils, sediments, etc., at the low μg/g level, preconcentration and clean-up of PAHs from the samples are indispensable prior to the determination. Even though there have been a significant number of researches dealing with the determination of PAHs, very few have reported on improving overall sensitivity of the analytical method via large volume injection. In the most recent report on large-volume-injection-GC–MS of PAHs [7], 35-fold enrichment was achieved with increased sensitivity of 10–50 times compared with the conventional 2 μL splitless injection.

The aim of the present study was to develop a sensitive novel procedure for the determination of PAHs at trace level via precolumn enrichment in μLC, and its application to the trace analysis of PAH in soil sample taken from a nearby highway, which was exposed to the automobile emissions. The evaluation of three kinds of solid phase sorption materials for the enrichment of PAHs was carried out after a suitable stationary phase for the micro separation column was selected.

2. Experimental

2.1. Apparatus

The eluent, which was also used as the desorption solvent, was supplied by a micro pump Model micro21PU-01 (Jasco, Tokyo, Japan). Sample was loaded by using an M435 micro injection valve (Upchurch Scientific, Oak Harbor, WA, USA). A model UV-2070 Plus UV detector (Jasco) was used and the analytes were detected at a wavelength of 254 nm. All data were collected by a C-R7Ae plus Chromatopac processor (Shimadzu, Kyoto, Japan). When operating at the gradient elution mode, the eluents were supplied by using two micro pumps (micro21PU-01) equipped with a degasser model DG-2080-54S (Jasco).

The laboratory-made separation column was prepared by using fused silica capillary (100 mm × 0.32 mm I.D. × 0.45 mm O.D. or 500 mm × 0.53 mm I.D. × 0.65 mm O.D.; GL Sciences, Tokyo, Japan) as reported previously [17]. The packing particles used were Develosil Spherical Porous Silica ODS and C30 (5 μm particle diameter; Nomura Chemical, Seto, Japan).

2.2. Reagents

Acetonitrile and distilled water were of HPLC grade and obtained from Wako Pure Chemical Industries (Osaka, Japan). Other reagents were of reagent grade and were used as received, unless otherwise noted. ACE was purchased from Tokyo Chemical Industry (Tokyo, Japan) while CHR and BghiP were purchased from Sigma–Aldrich Japan (Tokyo, Japan). NAPH, FLU, PHEN, ANTH, FLT, PYR and BaP were obtained from Nacalai Tesque (Kyoto, Japan). ACY, BaA, BkF, DiahA and INPY were purchased from Wako Pure Chemical Industries.

The reagents used for making monolithic silica C18 stationary phase were mainly obtained from Nacalai Tesque, except tetramethoxysilane (TMOS) and PEG 10,000 which were purchased from Tokyo Chemical Industry and Sigma–Aldrich Japan, respectively.

2.3. Fabrication of micro precolumns

The micro precolumns were basically made of three kinds of materials, i.e. Develosil Spherical Porous Silica C30 (15–30 μm particle diameter; Nomura Chemical), quartz wool fibers coated with C30 (abbreviated as C30-fiber; Nomura Chemical) and laboratory-made monolithic silica C18 stationary phase. The Develosil C30 particles as well as the C30-fibers were packed into 0.25 mm I.D. PTFE tubes and the effective length of the precolumn was 10 mm, as shown in Fig. 2, while the monolithic silica capillary columns were directly connected via PTFE tubes and fused-silica capillaries (50 μm I.D. × 375 μm O.D.; GL Sciences, Tokyo, Japan) to an M435 micro injection valve (Upchurch Scientific, Oak Harbor, WA, USA). Fig. 3 shows the magnification of the C30-fiber, in which the size of the diameter was approximately 20 μm, and each precolumn was packed with approximately 90 pieces of fibers.

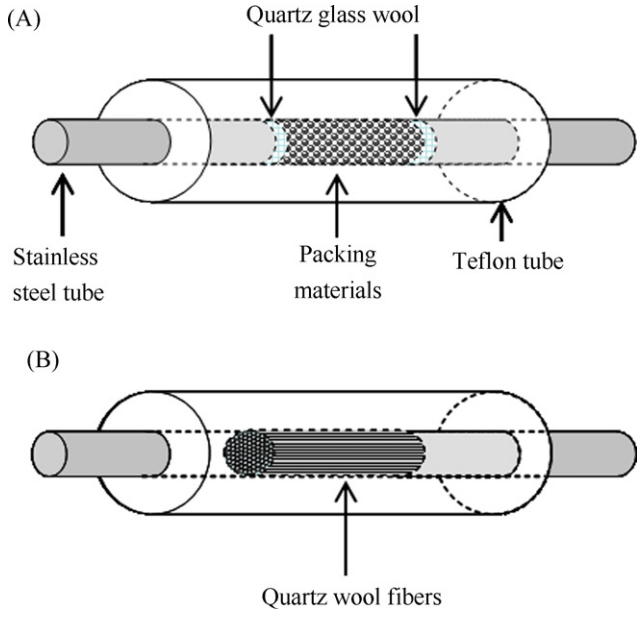

Fig. 2. Diagrams of the micro precolumns packed with particles (A) as well as the C30 coated fiber (B).

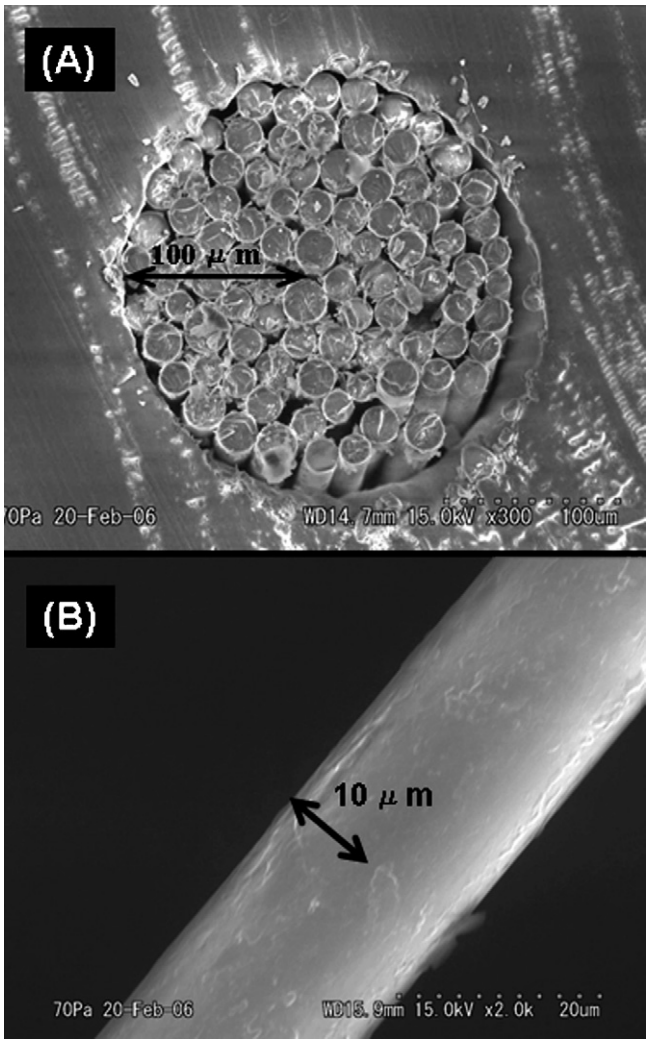

Fig. 3. SEM photographs of the micro precolumn packed with 90 pieces of C30-fiber (A) and the C30-fiber (B).

Monolithic silica capillary columns were in situ prepared in fused-silica capillary with 0.1 and 0.2 mm I.D. (GL Sciences) according to the sol–gel method previously reported [15,18]. Fused-silica capillary tubes were treated with 1 M sodium hydroxide at 60 °C for 2 h, followed by washing with 1 M hydrochloric acid and methanol before they were dried at 120 °C in nitrogen stream for 30 min. Sol–gel solution was prepared by dissolving 0.53 g of PEG 10,000 in a mixture of 2 mL of TMOS and 5 mL of 0.01 M acetic acid, followed by agitation in an ice water-bath for 40 min. The solution was then degassed under vacuum for 10 min before it was filled into the above-pretreated capillary tubes. The fused-silica capillary tubes filled with the sol–gel solution were kept at 40 °C for 20 h, and nitrogen was passed to remove the reagent from the column after the reaction, followed by washing with water and 0.1 M ammonia aqueous solution. The monolithic silica capillary columns were then filled with 0.1 M ammonia aqueous solution and kept at 60 °C for 45 h. After washing with 60% ethanol aqueous solution, the capillary columns were finally heated at 330 °C for 5 h, followed by purging with nitrogen gas at 110 °C for 1 h. The capillaries were then reacted with 10%

dimethyloctadecylchlorosilane in toluene solvent at 140 °C for 24 h. After that they were washed with toluene, THF and methanol prior to use.

Since the use of TMOS alone failed to produce excellent monolithic columns with diameter larger than 0.1 mm I.D. and gap along the inner surface was frequently observed, in the preparation of 0.2 mm I.D. monolithic columns, a hybrid of TMOS and methyltrimethoxysilane (39:1) was used and the effects of shrinkage during the gelation process were minimized. Under the observation of SEM, there was no distinct difference shown between the both monolithic columns in terms of their structural profiles. However, the methyl-containing monolith should be more hydrophobic than the purely inorganic monolith.

2.4. Sample enrichment

In our previous research, i.e. ref. [13–16], we found that sample enrichment was significantly effected by the sample solvent. The recovery of enrichment increased with increasing water content in the enriched sample as long as the peak signal was concerned. In other words, the higher the water concentration in the sample, the better the recovery could be achieved. Thus, in this study, all of the samples were diluted with water at the final stage and sample in water:ACN = 98:2 was used for enrichment purposes.

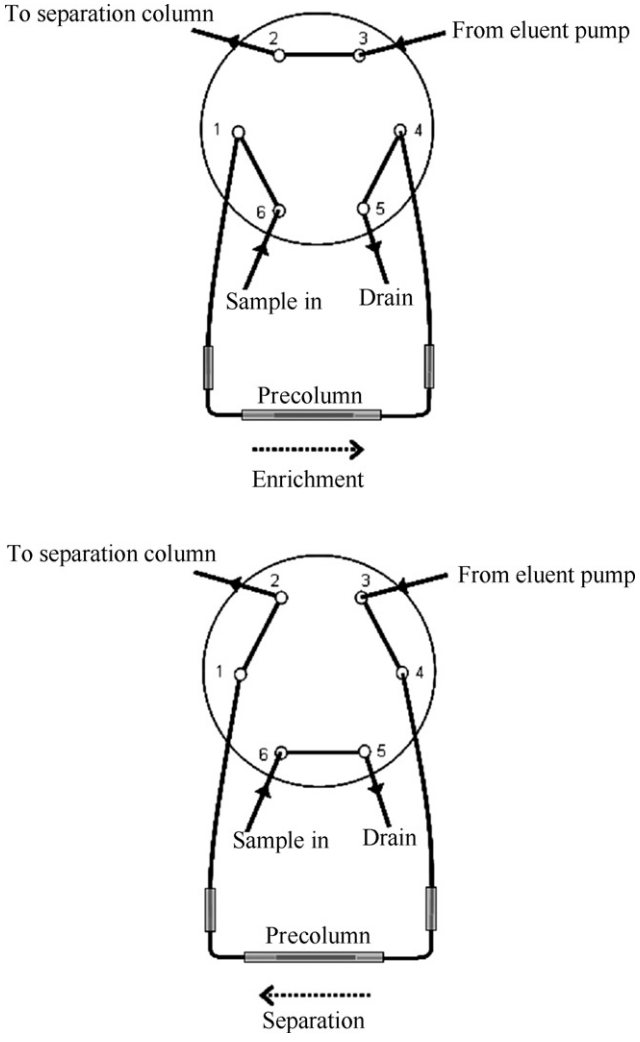

Fig. 4. Illustrated diagrams of the enrichment unit when loading the sample (enrichment) or when injecting the sample (separation).

The flow of the eluent, which also acts as the desorption solvent, was controlled by switching the micro injection valve (M435) in order to introduce the enriched sample into the separation column. Fig. 4 shows the diagrams of the enrichment unit when loading (enrichment) or injecting (separation) the sample. The sample was loaded via a hand-made rubber band-driven pumping device during all concentrations and the enriched sample was back-eluted into the separation column. Comparing to our previous work as in ref. [15] which used monolithic precolumns, the usage of Develosil C30 and C30-fiber as the enrichment media was also investigated in this study.

2.5. Extraction of PAHs in soil

Soil sample was randomly taken from a nearby highway that is normally used by diesel engine trucks. Among all the reported methods on the extraction of soil samples, we have chosen to use the conventional easy and time-saving extraction method by the mean of mechanical shaking [19] which is more environmentally friendly and cost-effective. Only 20 mL of toluene was needed as the extraction solvent and 10 g of un-treated soil was used. After the analytes were totally extracted from soil, the solution was then centrifuged at 3000 rpm for 5 min. A 10 mL of the upper solution was taken and dried in a draft chamber at 25 °C and the residue was then dissolved in 5 mL of ACN. After filtration with a 0.45 μm membrane, the solution was diluted 50-fold with HPLC-grade water to make the final sample solution contain 2% of total ACN.

3. Results and discussion

3.1. Isocratic separation of PAHs using a 10-cm microcolumn

The separation of PAHs was first carried out at isocratic mode using laboratory-made 10-cm C30 or ODS capillary columns, and the PAHs were divided into Groups A and B, for shorter and longer retention PAHs, respectively. Group A of PAHs containing NAPH, ACY, ACE, FLU, PHEN, ANTH, FLT and PYR, and Group B consisted of BaA, BkF, BaP, DiahA, BghiP and INPY. Mixture of ACN-water solutions of 70 and 90% were used for the isocratic separation of Group A and B, respectively, and the flow-rate was set at 4.2 μL min^{-1} while the wavelength of UV detection was 254 nm. 0.2 mL of 2 and 20 ppb for each PAHs of Group A and B were enriched using a C30 micro precolumn.

Fig. 5 shows the chromatograms of Group A analytes obtained by the both columns. The separation profiles observed in Fig. 5 were quite similar, however C30 showed relatively shorter retention time with slightly better resolution and background noise. The same phenomenon was also observed in the separation of Group B analytes. Table 1 shows the repeatability

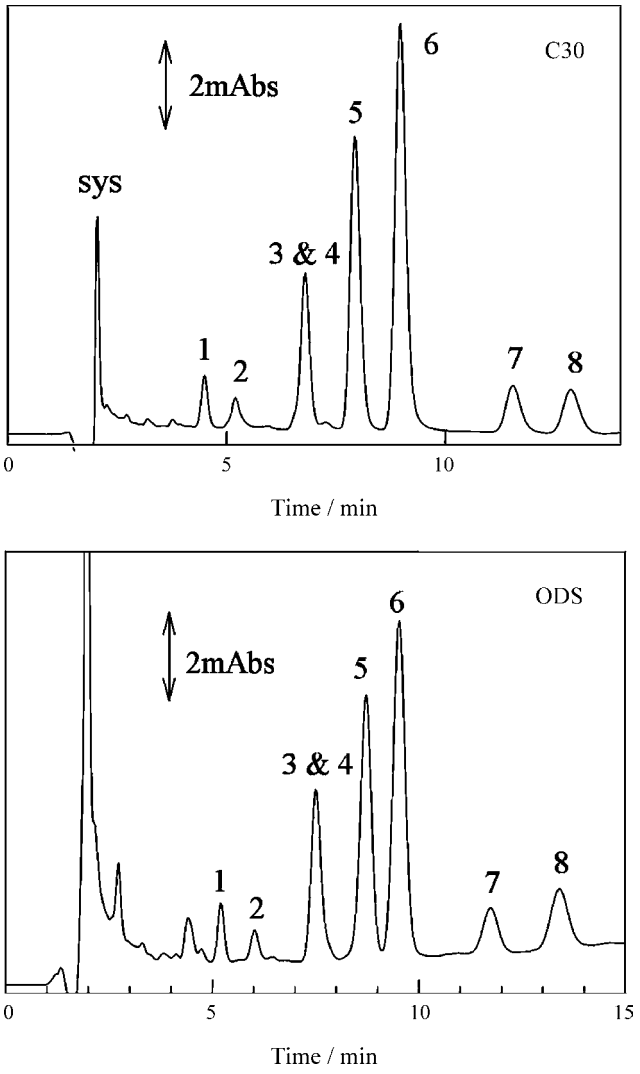

Fig. 5. Separation of an authentic mixture of eight PAHs using laboratory-made C30 and ODS microcolumns. Separation column: Develosil Spherical Porous Silica C30 or ODS (100 mm × 0.32 mm I.D.). Eluent: 70% ACN. Flow-rate: 4.2 μL min^{-1}. Wavelength of UV detection: 254 nm. Analyte: 2 ppb for each PAHs; number abbreviations as in Fig. 1. Micro precolumn: Develosil C30 (10 mm × 0.25 mm I.D.). Injection volume: 0.2 mL.

of retention time and peak signals obtained by the columns. The relative standard deviation (R.S.D.) values for seven successive measurements obtained using the ODS microcolumn were between 0.17 and 2.35% for the retention time, whereas those for the peak height and peak area were in the range of 0.89–7.83 and 2.34–6.94%, respectively. Comparing to these values, those obtained by using the C30 microcolumn were less than 1.15, 5.46 and 4.75% for the retention time, peak height and peak area, respectively. Considering these results, C30 microcolumn was chosen for the following experiments.

3.2. Gradient elution of PAHs using a 10-cm microcolumn

As can be seen from Fig. 5, the isocratic elution could not separate ACE and FLU, and in order to separate all the 14 PAHs in a single chromatographic run, eluents with different compositions are needed. Therefore, we investigated the use of gradient elution for the simultaneous separation of the PAHs. Under optimum conditions, the separation of 14 PAHs was achieved within 40 min with the ACN composition being gradually increased from 55 to 100% in 30 min. The chromatograms of the separation are shown in Fig. 6 and repeatability results are summarized in Table 2.

3.3. Effects of the enrichment media: C30, C30 coated micro fiber and monolithic C18 (0.1 mm I.D.)

Fig. 6 shows the separation profiles for the gradient elution of 14 PAHs by the same 10-cm microcolumn using three kinds of enrichment materials, i.e. C30 particles, C30-fiber as well as the monolithic C18 stationary phase. Obviously, the enrichment media had a significant effect on the separation of the column due to different enrichment efficiencies. Normally, the separation of the analytes is improved by enrichment [15]. It was found that the recovery as well as the relative intensities of the analytes obtained using the C30-fiber precolumn were approximately 1/2 comparing to those obtained using the C30 as well as the monolithic C18 precolumns. This might be due to the fact that the coating of the C30 was only on the surface of the fibers and thus reduced its adsorbing power compared to the C30 particles alone. Another possibility could be due to the sample breakthrough that might have occurred. This problem could be improved by packing more fibers into the precolumn.

As summarized in Table 2, the R.S.D. values for seven successive measurements obtained using the C30-fiber precolumn for the retention time, peak height and peak area were in the range of 0.36–1.26, 2.53–11.1 and 3.31–10.2%, respectively. Similarly, those obtained by using the C30 precolumn were between 0.80–1.64, 1.53–13.6 and 1.98–12.7% for the retention

Table 1
Comparison of the repeatability of retention time, peak area and peak height for the laboratory-made C30 and ODS microcolumns

PAHs	R.S.D. (%, $n=7$)					
	Retention time		Peak area		Peak height	
	C30	ODS	C30	ODS	C30	ODS
NAPH	0.97	0.85	4.13	2.34	4.98	0.89
ACY	0.87	0.48	3.76	4.16	2.78	2.73
ACE	–	–	–	–	–	–
FLU	–	–	–	–	–	–
PHEN	0.71	0.32	3.36	2.94	3.5	2.97
ANTH	0.71	0.20	4.75	4.39	4.58	3.80
FLT	0.64	0.17	4.04	4.19	5.36	5.40
PYR	0.61	0.22	4.63	3.63	5.02	1.33
BaA	0.62	0.54	4.56	4.21	4.73	4.28
BkF	0.79	1.54	2.95	4.58	1.03	5.28
BaP	1.03	1.79	4.18	5.44	4.79	5.15
DiahA	1.12	1.39	3.55	6.94	4.02	7.83
BghiP	1.14	1.16	3.63	4.34	5.46	6.40
INPY	1.15	2.35	2.89	5.89	3.33	1.16

Separation column: Develosil Spherical Porous Silica C30 or ODS (100 mm × 0.32 mm I.D.). Eluent: 70% ACN for Group A (NAPH–PYR) and 90% ACN for Group B (BaA–INPY). Flow-rate: 4.2 μL min^{-1}. Wavelength of UV detection: 254 nm. Analyte: 2 and 20 ppb each for Group A and B, respectively. Micro precolumn: Develosil C30 (10 mm × 0.25 mm I.D.). Injection volume: 0.2 mL.

Table 2
Effects of the enrichment media on the repeatability of retention time, peak area and peak height

PAHs	R.S.D. (%, $n=7$)								
	Retention time			Peak area			Peak height		
	C30	C30-fiber	M*1 C18	C30	C30-fiber	M*1 C18	C30	C30-fiber	M*1 C18
NAPH	1.64	1.16	1.48	2.93	9.75	5.38	5.75	8.68	6.55
ACY	1.16	0.89	1.39	2.07	8.08	2.48	1.53	5.43	3.10
ACE	1.19	1.10	1.52	1.98	9.53	2.34	2.24	8.24	3.88
FLU	1.00	0.93	1.52	2.66	4.10	2.69	2.81	4.55	2.42
PHEN	1.39	1.03	0.96	2.38	3.69	3.00	3.46	3.83	3.65
ANTH	1.16	1.23	0.86	3.60	4.22	4.40	3.79	4.48	2.91
FLT	1.05	0.92	1.16	2.82	4.87	3.99	3.82	3.60	3.20
PYR	0.79	0.97	1.30	4.73	3.31	3.26	4.49	2.53	3.43
BaA	0.80	0.83	0.98	5.65	4.75	3.22	10.7	4.04	2.61
BkF	0.92	0.99	0.70	8.92	4.90	3.92	13.6	7.38	3.20
BaP	1.31	1.00	0.73	8.66	8.26	2.65	11.0	10.8	3.56
DiahA	1.00	1.26	0.97	12.7	9.27	5.83	10.6	7.29	3.95
BghiP	1.14	0.36	0.94	8.94	6.87	3.54	13.0	11.0	2.90
INPY	1.46	0.86	1.01	11.4	10.2	3.18	13.6	11.1	4.15

Operating conditions as in Fig. 5. M*1: Monolithic column with 0.1 mm I.D.

time, peak height and peak area, respectively. On the other hand, those R.S.D.s of the retention time, peak height and peak area obtained using the monolithic C18 precolumn were in the range of 0.70–1.52, 2.42–6.55 and 2.48–5.83%, respectively. The reason why monolithic precolumn gave much better repeatability values lies in the fact that it possesses higher permeability compared with common densely packed column, i.e. in this case was the C30 precolumn. This property is very important not only for rapid separation but also for sample clean-up as well as sample enrichment [15].

3.4. Effects of the monolithic enrichment media: monolithic silica (0.1 mm I.D.) and C18 (0.2 mm I.D.)

From the above results, the enrichment efficiency of the monolithic media was further investigated. We used two more similar monolithic materials, i.e. the monolithic silica support without modification with C18 as well as the modified C18 microcolumn with a bigger inner diameter (0.2 mm I.D.). The chromatograms obtained using these two microcolumns are shown in Fig. 7 and the repeatability values are summarized in Table 3. These chromatograms are similar to the one obtained by using the monolithic C18 with 0.1 mm I.D. but higher recovery of several analytes are obtained by the monolithic C18 with 0.2 mm I.D. However, the R.S.D.s of these two microcolumns are not better but worse than those obtained from the 0.1 mm I.D. monolithic C18 microcolumn. The R.S.D.s of the retention time, peak height and peak area obtained using the monolithic silica precolumn were in the range of 0.75–1.93, 4.90–8.84 and 2.85–9.70%, respectively, and those of the monolithic C18 (0.2 mm I.D.) were in the range of 0.56–2.58, 5.06–13.7 and 2.83–8.97%, respectively.

Table 3
Effects of the monolithic supports as the enrichment media on the repeatability of retention time, peak area and peak height

PAHs	R.S.D. (%, $n=7$)					
	Retention time		Peak area		Peak height	
	M*1 Silica	M*2 C18	M*1 Silica	M*2 C18	M*1 silica	M*2 C18
NAPH	1.49	2.58	9.70	7.49	8.35	5.06
ACY	1.57	2.41	5.46	2.83	6.46	7.91
ACE	1.59	1.69	6.15	3.10	6.35	6.05
FLU	0.97	1.94	5.13	4.24	5.76	8.88
PHEN	1.54	1.06	5.59	4.72	6.09	5.58
ANTH	1.89	1.04	5.08	4.09	7.74	5.60
FLT	0.75	1.61	2.85	6.91	4.90	7.97
PYR	1.38	0.80	4.31	5.45	8.84	8.28
BaA	1.29	1.33	6.24	5.68	7.07	8.63
BkF	1.93	1.03	5.24	8.72	6.77	9.42
BaP	1.37	0.56	7.67	7.70	8.80	6.97
DiahA	0.86	1.44	8.40	8.97	8.46	11.7
BghiP	0.90	1.47	6.10	8.17	7.83	13.0
INPY	1.16	1.73	8.49	7.96	7.99	13.7

Operating conditions as in Fig. 6. M*1: Monolithic column with 0.1 mm I.D. M*2: monolithic column with 0.2 mm I.D.

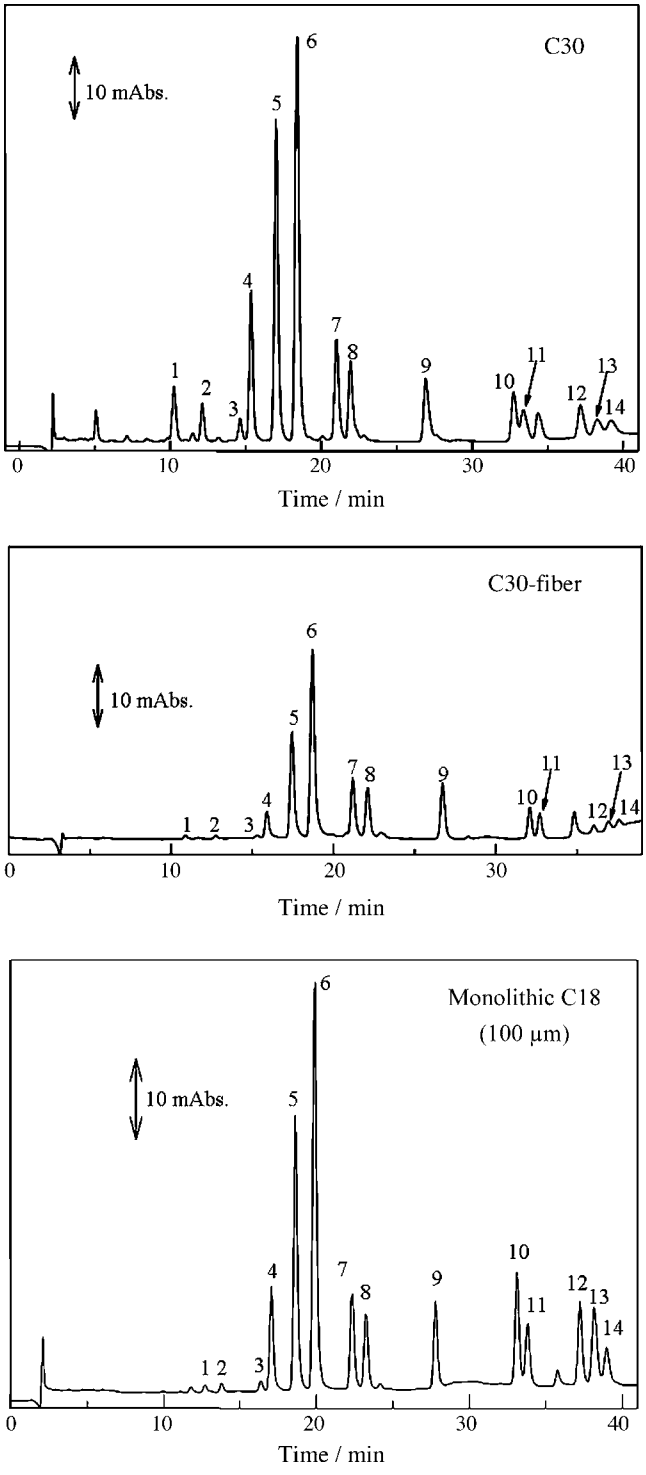

Fig. 6. Gradient elution of an authentic mixture of 14 PAHs by using the C30, C30-fiber or monolithic C18 micro precolumns as the enrichment media. Separation column: Develosil Spherical Porous Silica C30 (100 mm × 0.32 mm I.D.). Eluent: 55% ACN linearly increased to 100% ACN in 30 min. Flow-rate: 4.2 μL min^{-1}. Wavelength of UV detection: 254 nm. Analyte: 20 ppb for each PAH. Micro precolumn: Develosil C30, C30-fiber (10 mm × 0.25 mm I.D.) or monolithic C18 (10 mm × 0.10 mm I.D.). Injection volume: 0.2 mL.

We expected that without C18 modification, the retention and enrichment of PAHs could not be possible on the silica precolumn, however, the upper trace of Fig. 7 shows us that some analytes might have entered and retained in the double-pore structure of silica. Nevertheless, the R.S.D.s results were not satisfactory. On the other hand, the 0.2 mm I.D. monolithic C18 column could retain more analytes than the 0.1 mm I.D. column, as can be seem from Figs. 6 and 7, but this column was not stable as we could notice some loss in the stationary phase after six enrichments and thus causing the undesired R.S.D.s values. This might be due to the fact that the methyl-containing monolith, i.e. the 0.2 mm I.D. monolithic C18 column, is less stable than the purely TMOS-based monolith. Considering these results, we could conclude that 0.1 mm monolithic C18 is the best enrichment media compared to all tested materials in this study.

3.5. Gradient elution of PAHs using a 50-cm microcolumn

In order to improve the resolution of PAHs, we tried to pack the C30 particles into a longer column of about 50 cm in length.

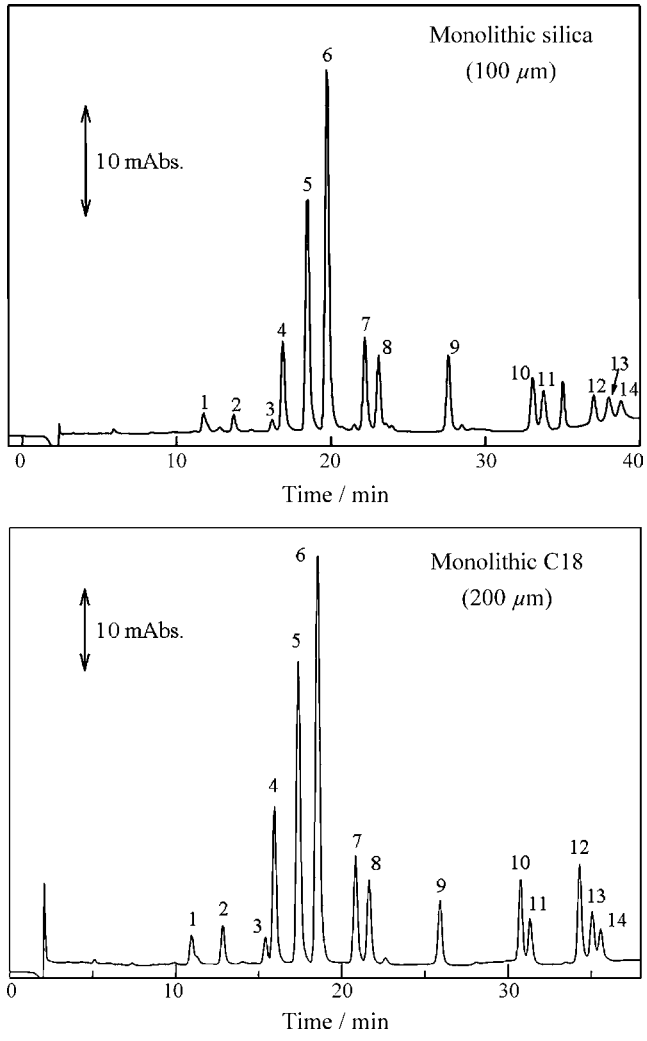

Fig. 7. Gradient elution of an authentic mixture of 14 PAHs by using monolithic silica supports (with and without modification of C18) as the enrichment media. Micro precolumn: Monolithic silica (10 mm × 0.10 mm I.D.) or monolithic C18 (10 mm × 0.20 mm I.D.). Other operating conditions are the same as in Fig. 5.

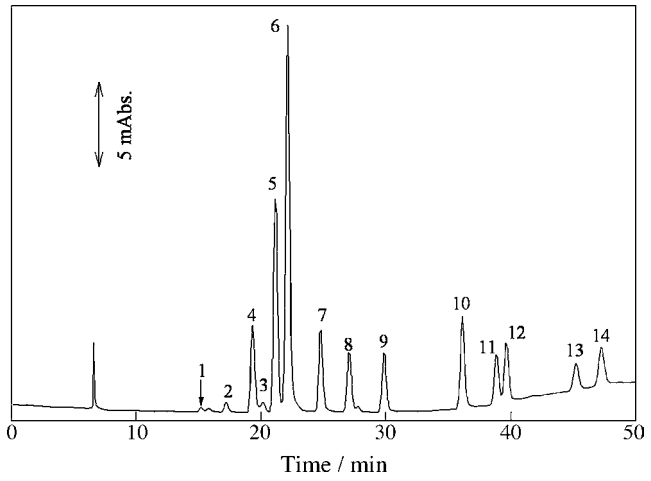

Fig. 8. Gradient elution of an authentic mixture of 14 PAHs by using a laboratory-made 50-cm C30 micro separation column with monolithic C18 precolumns as the enrichment media. Separation column: Develosil Spherical Porous Silica C30 (500 mm × 0.53 mm I.D.). Eluent: 85% ACN linearly increased to 100% ACN in 30 min. Flow-rate: 10.0 μL min^{-1}. Wavelength of UV detection: 254 nm. Analyte: 20 ppb for each PAHs. Micro precolumn: monolithic C18 (10 mm × 0.10 mm I.D.). Injection volume: 0.2 mL.

For this purpose, a 0.53 mm I.D. fused capillary was used instead of 0.32 mm I.D. By using the monolithic C18 (0.1 mm I.D.) as the enrichment column, the separation of the PAHs is shown in Fig. 8. Under these optimum conditions, the separation of about half of the 14 PAHs was improved if compared with the 10-cm column. And relatively good R.S.D.s results were also obtained, as summarized in Table 4.

The calculated values for the limit of detection (LOD) (S/N = 3) as well as the limit of quantitation (LOQ) (S/N = 10), i.e. limit of determination, are also summarized in Table 4. The LODs of the 14 PAHs range between 0.10 and 4.6 pg mL^{-1} with a UV detector. This method is at least 4300 times more sensitive than the reversed-phase LC-UV method [1] (LOD = 0.02–1.05 μg mL^{-1}), also 10 times better than the HPLC-fluorescence detection [3] (LOD = 1.0–150 ng L^{-1}), and is comparable to the GC–FID method [10] (LOD = 0.3–3 pg g^{-1}).

Table 5
Summarized linear-regression coefficients (R^2) data for the 14 PAHs within the working sample concentration and sample volume ranges

PAHs	Concentration range *1 (0–100 ng mL^{-1})		Sample volume range *2 (0–500 μL)	
	Peak area	Peak height	Peak area	Peak height
NAPH	0.9073	0.9604	0.9186	0.9080
ACY	0.9635	0.9790	0.9034	0.9176
ACE	0.9979	0.9939	0.9173	0.9212
FLU	0.9934	0.9788	0.9524	0.9242
PHEN	0.9926	0.9955	0.9333	0.9276
ANTH	0.9762	0.9426	0.9748	0.9585
FLT	0.9917	0.9918	0.9882	0.9903
PYR	0.9699	0.9890	0.9890	0.9909
BaA	0.9698	0.9890	0.9953	0.9978
BkF	0.9812	0.9495	0.9871	0.9602
BaP	0.9456	0.9893	0.9928	0.9935
DiahA	0.9420	0.9468	0.9114	0.9683
BghiP	0.9083	0.9145	0.9895	0.9895
INPY	0.9002	0.9010	0.9308	0.9345

Operating conditions as in Fig. 7. *1 = Sample volume: 200 μL. *2 = Sample concentration: 20 ng mL^{-1}.

On the other hand, the LOQs obtained for all the tested PAHS are between 0.32 and 15 pg mL^{-1} and this method is sensitive enough for the determination of PAHs in soil samples as their concentrations are normally in the sub μg mL^{-1} to ng mL^{-1} order.

3.6. Linearity

Table 5 gives the summarized linear-regression coefficients (R^2) data for the 14 PAHs within the working sample concentration and sample volume ranges. The peak signals were linear to the PAHs concentration up to 100 μg mL^{-1} with the R^2 ranges between 0.901–0.996 and 0.900–0.998 for the peak height and peak area, respectively. The relationship between signal intensity and enrichment volume was also investigated. When PAHs concentration of 20 μg mL^{-1} was used, the peak signals were linear to the enrichment volume up to 500 μL with R^2 between

Table 4
Repeatability of retention time and peak signals together with LODs and LOQs

PAHs	R.S.D. (%, $n = 7$)			LOD	LOQ
	Retention time	Peak area	Peak height	(S/N = 3) (pg mL^{-1})	(S/N = 10) (pg mL^{-1})
NAPH	1.69	8.60	5.15	1.4	4.7
ACY	1.65	9.33	7.00	3.9	13.1
ACE	1.45	8.50	6.58	4.6	15.3
FLU	2.23	7.93	6.42	0.33	1.1
PHEN	0.96	3.83	6.51	0.15	0.50
ANTH	1.42	4.50	4.68	0.10	0.32
FLT	0.85	9.69	9.89	0.36	1.2
PYR	1.66	7.41	9.90	0.56	1.9
BaA	1.17	9.61	7.30	0.56	1.9
BkF	1.00	9.71	7.57	0.87	2.9
BaP	0.98	9.75	8.51	1.1	3.7
DiahA	0.86	8.87	7.92	2.2	7.2
BghiP	0.95	8.11	9.42	2.9	9.8
INPY	1.13	9.68	9.12	3.0	10.0

Operating conditions as in Fig. 7.

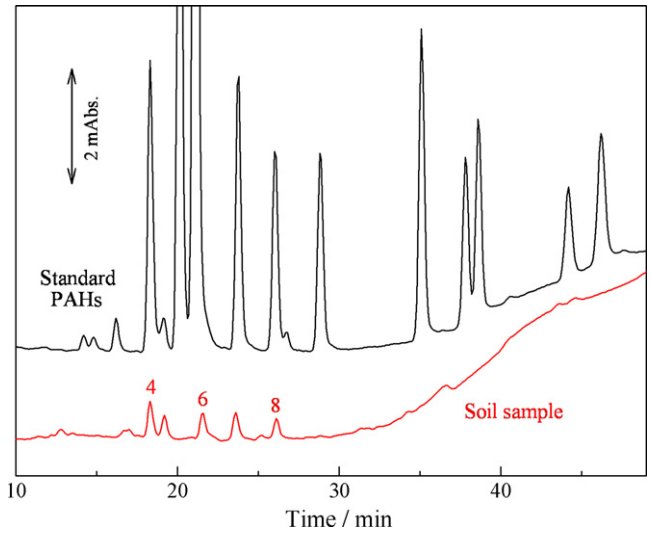

Fig. 9. Gradient elution of PAHs in a soil sample (lower trace). Operating conditions as in Fig. 7, except for the sample. Sample: 0.2 mL of extracted soil sample.

0.908–0.998 and 0.903–0.995 for the peak height and peak area, respectively. These results are relatively satisfactory as far as the determination of PAHs is concerned and they could be improved by using a longer micro precolumn for the enrichment, i.e. to increase the amount of stationary phase as the sorbents.

3.7. Determination of PAHs in soil sample

The on-line sample enrichment unit using a monolithic precolumn (10 mm × 0.10 mm I.D.) was applied to the determination of trace PAHs contained in soil sample. Fig. 9 demonstrates the chromatogram for the enriched soil sample, i.e. 200 μL or equivalent to 1000-fold enrichment. It can be seen that five obvious peaks were detected and the retention times of three of these peaks for the soil sample are the same as those for the standard sample, i.e. FLU, ANTH and PYR. The concentrations of FLU, ANTH and PYR in the soil sample were determined to be 0.1, 0.02 and 0.1 μg g^{-1}, respectively. In addition, in order to improve the precision of the determination of PAHs in the soil of a certain area, a more thorough sampling method should be practiced, and other extraction methods should also be carried out for cross-checking purposes.

4. Conclusion

PAHs are mostly found in soils or sediments than in water or atmosphere. These carcinogens are normally present in trace level and their determination is difficult by using conventional HPLC systems without enrichment procedure. We managed to utilize three kinds of materials, i.e. C30 particles, monolithic silica C18 stationary phase and quartz wool coated with C30, as the novel sorbing media of PAHs for the on-line enrichment of aqueous PAHs in microcolumn LC. This on-line enrichment unit coupled with microcolumn LC has shown to have achieved better sensitivity than many established analytical methods. With the diversification of the present method, i.e. to enlarge its ability and broaden its applications to determine not only PAHs but also other trace pollutants present in environment samples, will surely improve the use and popularity of microcolumn LC in the near future.

Acknowledgement

This research was financially supported by the Sasakawa Scientific Research Grant from The Japan Science Society.

References

[1] F. Sun, D. Littlejohn, M.D. Gibson, Anal. Chim. Acta 364 (1998) 1.
[2] S. Reindl, F. Höfler, Anal. Chem. 66 (1994) 1808.
[3] V. Pino, J.H. Ayala, A.M. Afonso, V. González, J. Chromatogr. A 949 (2002) 291.
[4] F. Busetti, A. Heitz, M. Cuomo, S. Badoer, P. Traverso, J. Chromatogr. A 1102 (2006) 104.
[5] P.R. Kootstra, M.H.C. Straub, G.H. Stil, E.G. van der Velde, W. Hesselink, C.C.J. Land, J. Chromatogr. A 697 (1995) 123.
[6] M. Charalabaki, E. Psillakis, D. Mantzavinos, N. Kalogerakis, Chemosphere 60 (2005) 690.
[7] V. Yusà, G. Quintas, O. Pardo, A. Pastor, M. de la Guardia, Talanta 69 (2006) 807.
[8] M.-X. Xie, F. Xie, Z.-W. Deng, G.-S. Zhuang, Talanta 60 (2003) 1245.
[9] Z.D. Parrish, M.K. Banks, A.P. Schwab, Environ. Pollut. 137 (2005) 187.
[10] A.R. Ghiasvand, S. Hosseinzadeh, J. Pawliszyn, J. Chromatogr. A 1124 (2006) 35.
[11] T. Takeuchi, Anal. Bioanal. Chem. 375 (2003) 26.
[12] T. Takeuchi, Chromatography 26 (2005) 7.
[13] L.W. Lim, T. Miwa, T. Takeuchi, Anal. Sci. 17 (Suppl. 2001) (2001) i887.
[14] L.W. Lim, J.-Y. Jin, T. Takeuchi, Anal. Sci. 19 (2003) 447.
[15] L.W. Lim, K. Hirose, S. Tatsumi, H. Uzu, M. Mizukami, T. Takeuchi, J. Chromatogr. A 1033 (2004) 205.
[16] L.W. Lim, T. Takeuchi, J. Chromatogr. A 1106 (2006) 139.
[17] T. Takeuchi, D. Ishii, J. Chromatogr. 213 (1981) 25.
[18] T. Takeuchi, S. Tatsumi, S. Masuoka, K. Hirose, H. Uzu, J.-Y. Jin, C. Fujimoto, K. Ohta,.K.-P. Lee, J.-J. Ryoo, S.-H. Choi, J. Chromatogr. A 1021 (2003) 55.
[19] A.P. Schwab, J. Su, S. Wetzel, S. Pekarek, M.K. Banks, Environ. Sci. Technol. 33 (1999) 1940.

Available online at www.sciencedirect.com
ScienceDirect
Talanta 72 (2007) 1599
Talanta
www.elsevier.com/locate/talanta

Preface

The rising environmental problems call for analysts paying much more effort to investigate the origins, physiological effects, transfer laws of pollutants, and so forth. In these fields, the research and development of analytical methodology, including the determination of the elements their species and organics as well as biomolecules in the environment, are much more important. Owing to the activities of development and the hope of developing countries to enter world markets by exporting their agricultural or manufactured products, the needs to monitor the environment in developing countries, and the necessities for reliable and trustworthy testing results, are very crucial. In such cases, it is very important to collaborate with analytical chemists in developing countries. The China–Japan–Korea (CJK) Symposium on Environmental Analytical Chemistry, dating back from 2002 in Beijing, is trying to supply such a platform for the analytical chemists in China, Japan and Korea to build their capacity as staff members and managers of analytical laboratories.

With the exchange in 2002 between the GC discussion group of Japan and the Research Center for Eco-Environmental Science (RCEES), the Chinese Academy of Sciences (CAS, Beijing, China), and the construction of the GC research group of Korea in 2003 in Korea (Seoul, 2003), this CJK symposium had successfully started in Beijing (2004) and proceeded in Tokyo (2005) with fruitful success for the Chinese, Japanese and Korean environmental analysts. Two special devoted to the 2002 China–Japan Symposium on Environmental Analytical Chemistry and 2005 CJK symposium have been published in the Chinese Journal of Environmental Chemistry (2003) and Talanta (2006), respectively.

Followed by the previous yearly symposium, the 2006 CJK symposium was held in Chongqing, China. Professor Dr. Jin-Ming Lin of Tsinghua University and RCEES, Professor Dr. Cheng Zhi Huang of Southwest University (Chongqing, China), and Dr. Tsuneaki Maeda in National Institute of Advanced Industrial Science and Technology (Japan) co-organized this symposium under the direction of Professor Xiaoquan Shan of RCEES. The symposium had 3 plenary lectures, 17 invited speakers, 41 oral and 40 poster presentations involving the area of basic studies of air and water, new techniques, monitoring, sensor, and instrumental hyphenations. Dr. Takahisa Tsugoshi was awarded as an Outstanding Young Analyst. Prof. Jianhua Wang and Prof. Zhengyu Lin obtained the best poster awards. Twenty-two papers from the symposium were selected for this special issue and we are sorry to say that many other excellent manuscripts were not accepted due to the limitation of the number of pages available for the special issue.

Acknowledgements

We are grateful to the authors who submitted manuscripts for this special issue, and to the many reviewers to maintain the high quality of the papers. The Organizing Committee of the 2006 China–Japan–Korea Symposium on Environmental Analytical Chemistry wishes to thank the grant supports of the National Nature Science Foundation of China, the Japanese Society for Analytical Chemistry, the Chinese Academy of Sciences and the Shimadzu Beijing Office, which made this symposium and special issue a success.

Guest Editor
Jin-Ming Lin*
Department of Chemistry, Tsinghua University, Beijing 100084, China

Guest Editor
Tsuneaki Maeda
National Institute of Advanced Industrial Sciences and Technology, Ibaraki 305-8563, Japan

* Corresponding author. Tel.: +86 10 62792343; fax: +86 10 62792343.
E-mail address: jmlin@mail.tsinghua.edu.cn (J.-M. Lin)

Available online 23 May 2007

doi:10.1016/j.talanta.2007.05.013

Available online at www.sciencedirect.com
ScienceDirect
Talanta 72 (2007) 1681–1686
Talanta
www.elsevier.com/locate/talanta

Study on the electrochemiluminescent behavior of menadione sodium bisulfite in presence of luminol

Zhenyu Lin [a,b], Jinhua Chen [a,b], Guonan Chen [a,b,*]

[a] *Ministry of Education Key Laboratory of Analysis and Detection Technology for Food Safety, Fuzhou University, China*
[b] *Department of Chemistry, Fuzhou University, Fuzhou, Fujian 350002, China*

Received 17 December 2006; received in revised form 1 March 2007; accepted 12 March 2007
Available online 25 March 2007

Abstract

Menadione sodium bisulfite (MSB) is a stable water-soluble derivative of Vitamin K_3, which is found to be able to enhance the ECL of luminol at potential of 0.88 V in phosphate buffer solution. The conditions for the enhanced ECL, such as the selection of the type of buffer solution, applied potential mode, scanning rate, the effect of pH and concentration of luminol have been investigated in detail in this paper. Under the optimum conditions, the enhanced ECL intensity is linear with the concentration of MSB over a wide range, the detection limit for MSB is 3.0×10^{-7} mol/L. The proposed method has been applied to determine the MSB in the commercial injection samples. A possible mechanism for the enhanced ECL of luminol by MSB has also been proposed.

Keywords: Menadione sodium bisulfite; Electrochemiluminescence; Luminol

1. Introduction

Vitamin K_3 (2-methyl-1,4-naphthoquinone, or menadione, VK_3) is a synthetic quinone derivative of naphthalene and is highly unstable. It is a fat-soluble vitamin precursor, which can be converted into menaquinone in the liver. It has been shown to have an anticancer activity and anticoagulation function. In a series of in vitro or in vivo animal studies, VK_3 showed significant antineoplastic activities against both malignant and a variety of human tumor cells [1]. Menadione sodium bisulfite (MSB) is a water-soluble derivative of menadione and is relatively stable. Numerous methods for the determination of MSB have been published [1–14], such as spectrophotometry [1], polarography [5], fluorometry [6] and stripping voltammetry [7,8]. Liquid chromatography with different detection systems has also been used, such as HPLC methods with ultraviolet (UV) [1] and fluorescence [9] detection using reversed-phase columns with post column derivatization have been developed for animal feeds and premixes [10]. Recently, chemiluminescent (CL) detection methods has been developed [11–13]. The most notable characteristics of CL methods are higher sensitivity and large scale of dynamic concentration range.

Electrochemiluminescence (ECL) was developed based on CL, in which an appropriate voltage is applied to an electrode to produce the light emission, which has the advantage of high sensitivity, high selectivity, well reproducibility and can be controlled easily. ECL has been proved to be useful for analytical applications [15–24]. Till now, no attention has been paid to use ECL method for determination of MSB. It has been found that MSB would enhance the ECL of luminol in neutral or alkaline phosphate buffer solution. The aim of the present study is to investigate the behavior of this ECL system and to develop a sensitive ECL method for determination of MSB. The possible mechanism of this ECL system has also been investigated and proposed.

2. Experimental

2.1. Chemicals and solution

All chemicals except Menasione sodium bisulfite injection were of analytical-reagent grade, and the ultra-pure water obtained from a Milli-Q system was used throughout.

* Corresponding author at: Department of Chemistry, Fuzhou University, Fuzhou, Fujian 350002, China. Tel.: +86 591 87893315; fax: +86 591 83713866.
E-mail address: gnchen@fzu.edu.cn (G. Chen).

0039-9140/$ – see front matter © 2007 Elsevier B.V. All rights reserved.
doi:10.1016/j.talanta.2007.03.038

MSB and luminol were obtained from Sigma Chemical Co. (USA) and used without further purification. Menadione sodium bisulfite injection was made by Pharmaceucical Co. Ltd. of Wuxi, China. The concentration of stock solution of MSB is 1.5 mmol/L and stored in dark under 4 °C. A luminol stock standard solution (1.0 mmol/L) was prepared by dissolving 17.72 mg luminol (Sigma Chemical Co., USA) in 100 mL water. Working standard solutions were prepared daily from the stock standard solution by appropriate dilution with the buffer.

2.2. Apparatus

ECL intensity versus potential was measured by a system made in our laboratory, which consists of a BPCL Ultra-Weak Chemiluminescence Analyzer (the applied voltage to the PMT is −850 V) controlled by a personal computer with BPCL program (Institute of Biophysics, Chinese Academy of Sciences) in conjunction with a CH Instruments model 660a electrochemical analyzer (Shanghai Chenghua instrument Co., China). The electrochemical analyzer was used for controlling waveforms and potentials. A block diagram of this system is shown in Fig. 1.

A conventional three-electrode system was used for the electrochemical measurement, including a glassy carbon electrode (GCE) (diameter 3 mm) as the working electrode, a platinum wire as the counter electrode and Ag/AgCl (sat. KCl) as the reference electrode. A commercial 5 mL cylindroid glass cell was used as ECL cell, and it was placed directly in the front of the photomultiplier tube. The working electrode was pretreated before use by polishing their surfaces with aqueous slurries alumina powders (average particle diameters: 1.0 μm and 0.3 μm α-Al_2O_3) on a polishing microcloth and rinsed with water to give a smooth electrode surface.

2.3. Procedure for ECL measurement

The working electrode was carefully polished and sonicated in ethanol and water successively. The ECL cell was washed with 0.2 mol/L nitric acid and water before use. The required volume of sample solution or MSB standared solution and 0.1 mL of 1.0 mmol/L luminol were added to 10 mL volumetic flask and diluted with buffer solution to the required volume. 3 mL mixture solution was transferred to the ECL cell. Potential was applied to the working electrode and the ECL signal was recorded simultaneously.

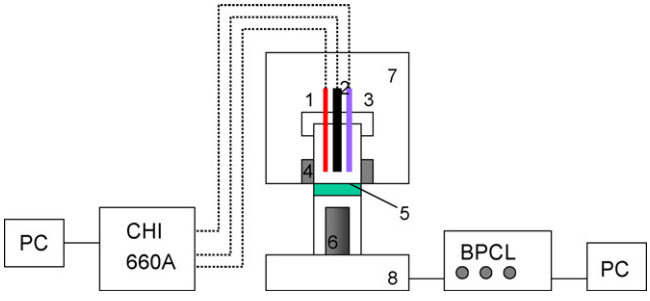

Fig. 1. Experimental setup for ECL. (1) Counter electrode; (2) working electrode; (3) reference electrode; (4) jacket for localization; (5) quartz window; (6) photomultiplier tube; (7) detection chamber; (8) base frame; BPCL: CL detector; CHI: CH Instruments model 660a electrochemical.

3. Results and discussion

3.1. ECL behavior of MSB in the presence of luminol

Our preliminary experiments showed that MSB did not give ECL at glass carbon electrode (GCE) in the absence of luminol, but it could enhance the ECL of luminol at GCE at 0.880 V, and the enhanced ECL intensity was dependent on the chemical and other factors, such as the scan rate, the type of buffer solution, pH of media solution and the concentration of luminol. The ECL intensity of the system increased with the increasing of the concentration of MSB in a certain of range. Fig. 2 shows the ECL behavior of MSB/luminol system under different MSB concentration. So the quantitative analysis of MSB can be carried out based on the enhancement of the ECL intensity.

3.2. Selection of electrochemical parameters

The cyclic voltammetry (CV), linear sweep voltammetry (LSV), square wave voltammetry (SWV) and differential pulse voltammetry (DPV) were selected to examine the effect of applied potential waveform on the ECL signal of luminol/MSB system. The potential was scanned in the range of 0.4–1.2 V. The results showed that the ECL signals were not stable when DPV and SWV scan modes were used, but the ECL signals were found to be very stable and reproducible when CV and LSV were used. Therefore, in the present work, LSV was selected for the subsequent studies.

Under the mode of LSV, the effect of scan rate on the ECL of luminol/MSB system has been examined and the result was

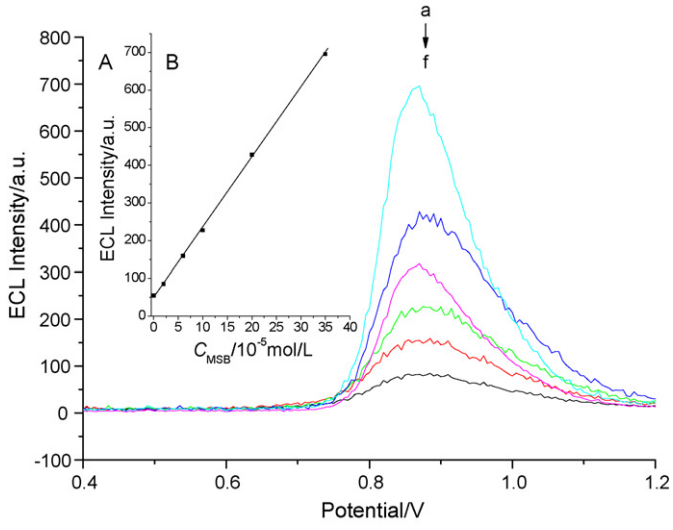

Fig. 2. (A) ECL of MSB/luminol under different MSB concentration in PBS buffer solution (0.2 mol/L, pH 7.0). (B) The correction line between the ECL intensity and the concentration of MSB. (a) 3.5×10^{-5}; (b) 2.0×10^{-5}; (c) 1.0×10^{-5}; (d) 6.0×10^{-6}; (e) 2.0×10^{-6} of mol/L; (f) blank; luminol: 1.5×10^{-5} mol/L; scan rate: 50 mV/s.

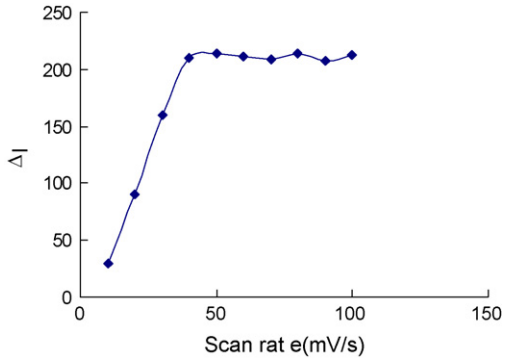

Fig. 3. Effect of the scanning rate on the enhanced ECL intensity (ΔI) of MSB in PBS buffer solution (pH 7.0). Luminol: 1.5×10^{-5} mol/L; MSB: 1.0×10^{-5} mol/L.

shown in Fig. 3. It can be known from Fig. 3 that ΔI is increased with the increasing of scan rate below 40 mV/s, then ΔI reaches the maximum and constant, so 50 mV/s was selected as the scan rate for the subsequent studies.

3.3. Selection of chemical reaction conditions

It is well known that medium plays an important role in ECL reaction. The ECL of luminol/MSB system in different buffer media (pH 7.0), such as Britton–Robinson buffer solution (BR), phosphate buffer solution (PBS), H_3BO_3–NaOH buffer solution (BS) were investigated in detail. The experimental results shown that in BR buffer solution, the ECL signals were not stable. Although the ECL signals were stable both in PBS and BS buffer solution, a higher enhanced ECL intensity could be obtained in PBS buffer solution, so the PBS buffer solution was selected subsequently.

pH of the solution can also affect on ECL of luminol greatly, luminol will give ECL in neutral or alkali solution, and with increasing of pH, the ECL intensity of luminol will be increased too. In PBS buffer solution, the effects of MSB on the enhancement of ECL of luminol have been examined under different pH, the results are shown in Fig. 4. When the pH of buffer solution is 5.0, luminol will not give light emission, so there was no ECL signal in the luminol/MSB system. When pH was in the range of 6.0–7.0, there was an ECL signal at about 0.88 V, and the ECL intensity at pH 7.0 is stronger a little bit than that at pH 6.0. This ECL peak is affected by MSB, since if there is no MSB, there is no ECL too. When the pH was changed to pH 8.0, except the peak appeared at 0.88 V, another shoulder peak appeared at 0.54 V, and the peak at 0.88 V was become much higher. If the solution does not contain MSB, luminol also give an signal at 0.54 V in PBS (pH 8.0), so the shoulder peaks maybe come from luminol itself in the alkaline solution. This peak has been confirmed to be due to the reaction between the production of the reduced dissolved oxygen and luminol in solution [25]. If the pH is higher than 10.0 (not shown in Fig. 4), the chemiluminescent of this system is very strong, which will interfere the measurement of ECL signals. Considering the interference of the chemiluminescent, pH 7.0 was selected as the optimum pH for subsequent experiments.

In pH 7.0 PBS buffer solution, luminol would not give any ECL signal in the concentration of 1.0×10^{-6} mol/L and below, however, with the increasing of the concentration of luminol, the ECL of luminol was enhanced by MSB. The effect of luminol concentration on the enhanced ECL intensity has been investigated when MSB is 3.0×10^{-5} mol/L, and the results are shown in Fig. 5. Fig. 5 indicates that ΔI is increased with the concentration of luminol in the range of 1.0×10^{-6} to 1.4×10^{-5} mol/L, after 1.4×10^{-5} mol/L, ΔI reaches maximum and constant. Therefore, 1.5×10^{-5} mol/L of luminol was used for subsequent experiments.

3.4. Interferences

In order to apply the proposed method to determine MSB in pharmaceutical formulations samples, the interference of some possible co-existing ions was examined. A foreign ion was considered not to interfere if it caused a relative error <5% during the measurement of 2.0×10^{-5} mol/L MSB solution. It was found that 1000 times Na^+, K^+, NO_3^-, Cl^-, 100 times glucose, Mg^{2+} and Ca^{2+} have no interference with the determination of MSB.

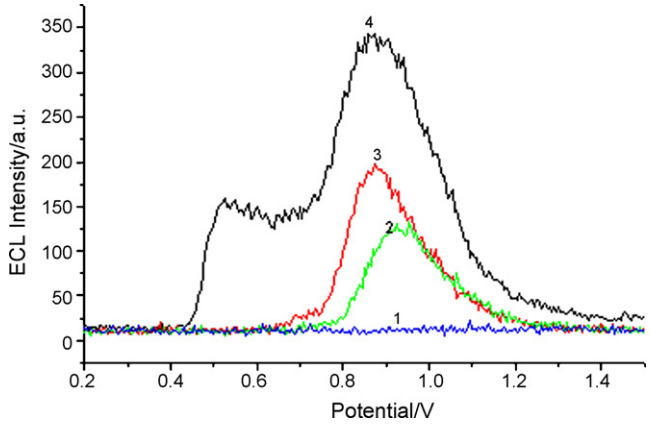

Fig. 4. Effect of pH on the ECL of luminol/MSB system in PBS buffer solution. Scan rate: 50 mV/s. 1: pH 5.0; 2: pH 6.0; 3: pH 7.0; 4: pH 8.0. Luminol: 1.5×10^{-5} mol/L; MSB: 1.0×10^{-5} mol/L; scan rate: 50 mV/s.

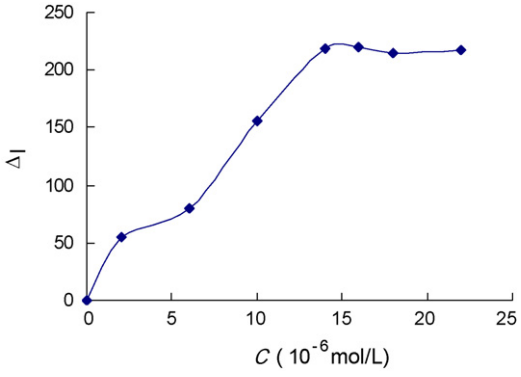

Fig. 5. Effect of the concentration of luminol on the enhanced ECL intensity (ΔI) of MSB in PBS buffer solution (0.2 mol/L, pH 7.0). MSB: 1.0×10^{-5} mol/L; scan rate: 50 mV/s.

3.5. Linear response range and detection limit

Under the optimum conditions, the enhanced ECL intensity was linear with the concentration of MSB in the range of 6.0×10^{-7} to 7.0×10^{-5} mol/L. The regression equation was

$$\Delta I = 7.5 + 184C \times 10^{-5}\ \text{mol/L}, \quad R = 0.9986$$

where C is the concentration of MSB. The relative standard deviation for 6.0×10^{-6} mol/L MSB was 2.9% ($n = 8$). The detection limit (defined as the concentration that could be detected at the signal-to-noise ratio of 3) was 2.0×10^{-7} mol/L.

3.6. Analytical application

The optimized procedure was applied for the assay of MSB in the commercial injection samples. The measurement procedure was the same as the measurement of standard MSB solution. The samples were diluted appropriately with the PBS buffer solution before measurement. The determination results are shown in Table 1. The values obtained by the calibration method, as well as the standard addition method, were in excellent agreement with the reference value. The relative standard deviation of the same sample (labeled amount 4.0 mg/mL) for 8 measurements is 3.1%.

3.7. Possible mechanism

In order to explain the reason for the enhancement of the ECL of luminol by MSB, LSV mode has been applied to study the electrochemical behaviors of luminol, MSB, luminol/MSB systems in pH 7.0 buffer solution (see Fig. 6). From the figure we knew that MSB has no oxidation wave in the studied potential range (Fig. 6a), luminol has a oxidation wave at about 0.5 V (Fig. 6b), but when the MSB is added to the luminol solution, another oxidation wave appears at about 0.7 V (Fig. 6c), this oxidation wave maybe come from the oxidation of H_2O_2, since there has a oxidation wave at about 0.7 V in luminol/H_2O_2 system (Fig. 6d).

Bubbled the high pure Ar gas into the solution for 10 min to wipe off the dissolved oxygen in the solution, and Ar gas flow was maintained during the experiment. It was found that at pH 6.0 or 7.0, there was no ECL signal to be found, which indicated that the enhancement ECL of luminol was related closely to the dissolved oxygen.

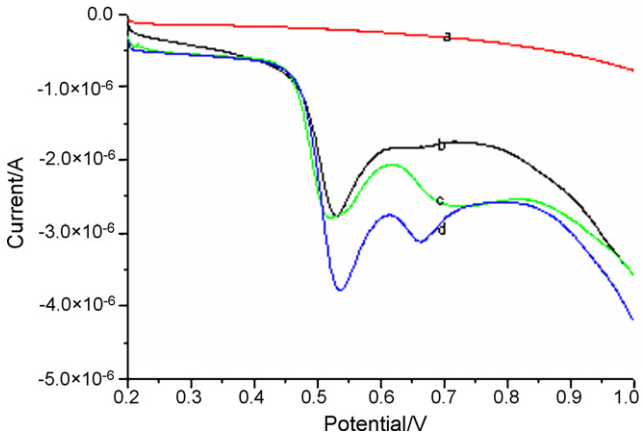

Fig. 6. The LSV behavior of (a) 1.0×10^{-5} mol/L MSB; (b) 1.5×10^{-5} mol/L luminol; (c) 1.5×10^{-5} mol/L luminol + 1.0×10^{-5} mol/L MSB; (d) 1.5×10^{-5} mol/L luminol + 1.0×10^{-6} mol/L H_2O_2. Scan rate 50 mV/s; 0.2 mol/L pH 7.0 PBS solution.

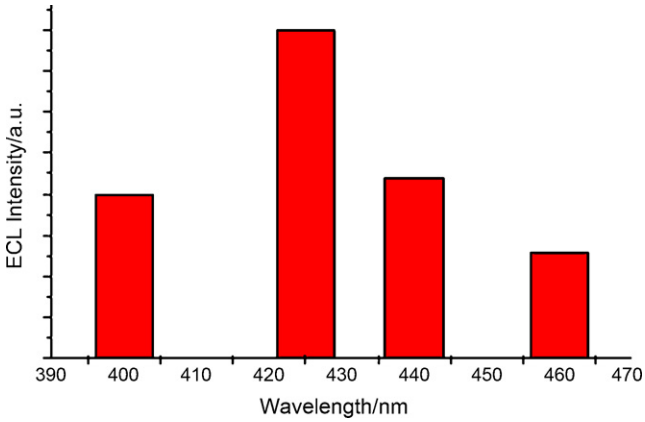

Fig. 7. ECL spectrum of luminol/MSB system in PBS buffer solution (pH 7.0).

The ECL emission spectrum was examined under the air-saturated conditions and was obtained by using a series of filters. The maximum emission of the ECL peak is shown in Fig. 7. It can be known from Fig. 7 that the maximum emission wavelength is 425 nm, which is corresponding to the light emission of 3-aminophthalate. Therefore, it can be concluded that the ECL signals are initiated by ECL reaction of luminol [13].

Table 1
Analytical results for determination of MSB in injection

Samples	Labeled amount (mg/mL)	Amount found[a] (mg/mL)		Added amount (mg/mL)	Founded amount (mg/mL)	Recovery (%)
		D	R			
1	4.00	3.96	3.97	2.00	1.96	98.0
2	4.00	3.98	4.01	3.00	2.98	99.3
3	4.00	3.95	3.98	4.00	3.95	98.8

[a] Average of five determinations. D: proposed ECL methods; R: reported methods [27].

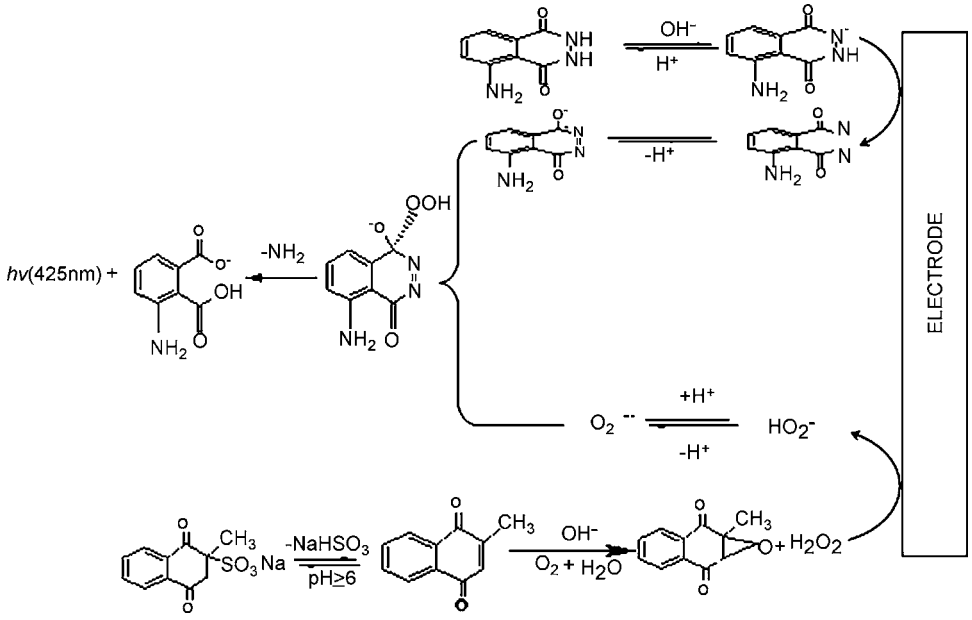

Fig. 8. The proposed mechanism for the ECL reaction of luminol/MSB system.

It has been reported that there is an equilibrium reaction as follows [2]:

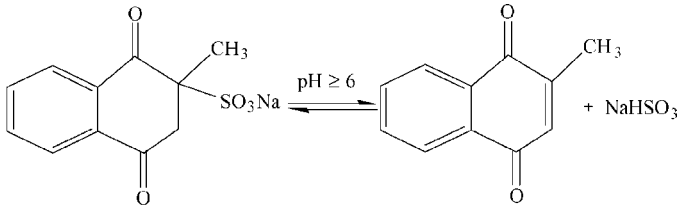

(1)

In neutral and weakly alkaline solution, a oxidation can occur by reaction with oxygen [26]:

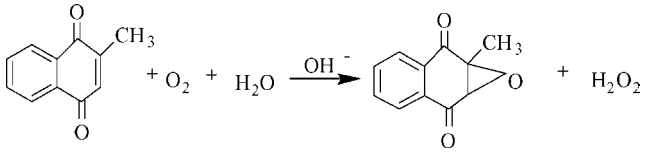

(2)

And it is well known that the present of H_2O_2 can enhance the ECL intensity of luminol [28]. So the present of MSB can enhance the ECL intensity of luminol. The mechanism of luminol/MSB system is shown in Fig. 8.

4. Conclusions

MSB has been found to be able to enhance the ECL of luminol at a glassy carbon electrode in phosphate buffer solution, based on which a novel ECL method for determination of MSB was developed. Compared with the previous methods for the determination of MSB, the method in this paper is simple, rapid and convenient and can also be well applied for analysis of pharmaceutical sample. The preliminary experiments revealed that the dissolved oxygen was a key factor in this ECL system, in which the dissolved oxygen oxidized VK_3 first to produce the hydrogen peroxide, which would enhance the ECL of luminol on the glassy carbon electrode at 0.88 V.

Acknowledgements

This project was supported by the National Nature Sciences Funding of China (20575011), the Science Foundation of State Education Department (JA00145) and the International Corporation Program of Science and Technology Department of Fujian Province, China (2004I015).

References

[1] O.Y.P. Hu, C.Y. Wu, W.K. Chan, F.Y.H. Wu, J. Chromatogr. B 666 (1995) 299–305.
[2] Q.H. He, Z.X. Wang, X.X. Cao, H.W. Chen, Y.F. Ke, Anal. Sci. 17 (2001) 1209–1212.
[3] Z.M. Liu, T. Li, J. Li, E.K. Wang, Anal. Chim. Acta 338 (1997) 57–62.
[4] X.Q. Guo, Y.B. Zhao, J.G. Xu, Anal. Chim. Acta 343 (1997) 109–116.
[5] H. Zou, Z.B. Yuan, Chinese J. Anal. Lab. 16 (1997) 5–9.
[6] J.J. Berzas Nevado, J.A. Murillo Pulgarin, M.A. Gomez Laguna, Analyst 123 (1998) 287–290.
[7] L. Wang, C. Ma, X. Zhang, Y. Xu, Microchem. J. 50 (1994) 101–105.
[8] J.C. Vire, N.A. Ei Malli, G.J. Patriarche, G.D. Christian, Talanta 35 (1988) 100–997.
[9] S.M. Billedeau, J. Chromatogr. 472 (1989) 371–379.
[10] A.J. Speek, J. Schrijver, W.H.P. Schreurs, J. Chromatogr. 301 (1984) 441–447.
[11] Y.M. Hung, Z.Q. Chen, Z.J. Zhang, Anal. Sci. 15 (1999) 1227–1230.
[12] P.R. Tomas, M.L. Carmen, V. Tmas, J. Martin, Analyst 124 (1999) 197–201.
[13] B.X. Li, X.Y. Zhang, C.X. Zhang, Anal. Chim. Acta 575 (2006) 212–216.
[14] I.G. Torro, J.V. Garcia Mateo, J. Martinez Calatayud, Analyst 122 (1997) 139–142.
[15] R.G. Gerardi, N.W. Barnett, S.W. Lewis, Anal. Chim. Acta 378 (1999) 1–41.
[16] M.M. Richter, Chem. Rev. 104 (2004) 3003–3036.
[17] K.A. Fähnrich, Talanta 54 (2001) 531–559.

[18] B. Tamamushi, H. Akiyama, Trans. Faraday Soc. 35 (1939) 491–494.
[19] K.D. Legg, D.M. Hercules, J. Am. Chem. Soc. 91 (1969) 1902–1907.
[20] J. Wang, G.N. Chen, J.L. Huang, Analyst 130 (2005) 71–75.
[21] Y.Y. Su, J. Wang, G.N. Chen, Talanta 65 (2005) 531–536.
[22] X.P. Wu, G.N. Chen, Talanta 65 (2005) 1279–1285.
[23] G.N. Chen, Y.W. Chi, X.P. Wu, J.P. Duan, N.B. Li, Anal. Chem. 75 (2003) 6602–6607.
[24] Y.W. Chi, J.P. Duan, Z.F. Zhao, H.Q. Chen, G.N. Chen, Electroanalysis 15 (2003) 208–218.
[25] H. Cui, Y. Xu, Z.F. Zhang, Anal. Chem. 76 (2004) 4002–4010.
[26] J.C. Vire, G.J. Patriarche, G.D. Christian, Anal. Chem. 51 (1979) 752–757.
[27] H. Zhou, Z.B. Yuan, Chinese J. Anal. Lab. 16 (1997) 5–9.
[28] C.S. Ouyang, C.M. Wang, Electroanal. Chem. 474 (1999) 82–88.

Available online at www.sciencedirect.com
ScienceDirect
Talanta 72 (2007) 1644–1649
Talanta
www.elsevier.com/locate/talanta

Determination of polybrominated diphenyl ethers in freshwater fishes from a river polluted by e-wastes

Qian Luo [a], Minghung Wong [b,**], Zongwei Cai [a,*]

[a] *Department of Chemistry, Hong Kong Baptist University, Kowloon Tong, Hong Kong SAR, China*
[b] *Croucher Institute for Environmental Sciences and Department of Biology, Hong Kong Baptist University, Kowloon Tong, Hong Kong SAR, China*

Received 2 November 2006; received in revised form 12 February 2007; accepted 3 March 2007
Available online 15 March 2007

Abstract

Analytical method using mass spectrometric techniques was applied for the determination of polybrominated diphenyl ethers (PBDEs) in freshwater fishes. Fish samples collected from Nanyang River contaminated by the recycling electron-wastes (e-wastes) materials were prepared by using Soxhlet extraction and multiple-step column chromatographic clean-up. PBDEs were determined by gas chromatography (GC) coupled with ion trap mass spectrometry (for mono- to hepta-BDEs) and quadrupole mass spectrometry (for BDE-209). The method performance was evaluated with the recovery of ^{13}C-labeled internal standards and with the analysis of certified reference biota. The obtained recoveries ranged from 75 to 125% with a relative standard deviation of lower than 10% for 16 PBDE congeners. The total PBDE (ΣPBDE) concentrations in fishes showed the following trend: grass carp < mud carp < crucian carp < silver carp < carp. ΣPBDE concentrations in the abdomen, back and tail muscles of carp ranged from 766, 458 and 530 ng/g w.w., and 53, 52, 45 ng/g w.w. in grass carp, respectively. The ΣPBDE concentrations in abdomen muscles were no significantly higher than in back and tail muscles in carp, crucian carp, grass carp and mud carp. PBDE congener concentrations in muscles correlated well with their lipid content. BDE-47 and BDE-28 were the most abundant congeners followed by BDE-17, BDE-15, BDE-66, BDE-154 and BDE-153 in fishes collected from Guiyu.

Keywords: PBDEs; Freshwater fishes; e-waste; GC/MS; GC/MS/MS

1. Introduction

Polybrominated diphenyl ethers (PBDEs) are used as flame retardant additives in a variety of products such as electrical appliances, textiles, building materials, carpets and vehicles, and they more likely leach out and transfer into the environment and biota [1,2]. The use of PBDEs has significantly increased with commercial products almost doubling between 1992 and 2001[3]. There are three commercial products, commonly referred to as penta-BDE, octa-BDE, and deca-BDE, e.g., penta-BDE is itself a mixture of related substances, which contain four to six atoms of bromine per molecule, octa-BDE contain six to eight and deca-BDE with 97% of BDE-209 and 3% ninth-BDE. For PBDEs, each is with varying degrees of bromination, different physicochemical properties, and contains a limited number of congeners (PBDEs named after like as PCB in the IUPAC numbering scheme).

PBDEs are hydrophobic with the log K_{ow} ranging from 5.0 to 8.3, semivolatile and fairly nonvolatile [4,5]. Tetra- and penta-substituted PBDEs have been shown to be more persistent, lipophilic and bioaccumulating than octa- or deca-BDE [6]. Penta- and octa-BDE were banned period from 2004 to 2006 in the US [7]. Aquatic toxicity and bioaccumulation potential of PBDEs decrease with increasing bromination, therefore, the studies showed that deca-BDE was not acutely toxic or mutagenic, and was not a developmental or reproductive toxicant for rat [8] at concentrations below its solubility limit. Several of these PBDE congener and metabolites are suspected of disrupting the endocrine system [9,10]. They are potent compounds with respect to thyroid function [11]. The photolysis and pyrolysis [12] degradation of PBDE may lead to the for-

* Corresponding author. Tel.: +852 34117070; fax: +852 34117348.
** Corresponding author.
E-mail addresses: mhwong@hkbu.edu.hk (M. Wong), zwcai@hkbu.edu.hk (Z. Cai).

0039-9140/$ – see front matter © 2007 Elsevier B.V. All rights reserved.
doi:10.1016/j.talanta.2007.03.012

mation of lower brominated with higher toxic products and other persistent organic pollutants such as PBDDs and PBDFs [13].

However, studies have indicated that current PBDEs levels could adversely affect sensitive human populations, such as young children, indigenous peoples and fish consumers [14]. One important transport pathway by which humans and other upper trophic level species can be adsorbed PBDEs is through the consumption of contaminated fish. PBDEs are an emerging contaminant that appears to ubiquitous in the environment and magnify in fish mussels [15]. PBDEs have been demonstrated global contaminants with their presence in the blubber of marine mammals collected from Arctic Ocean [16]. The chemicals were detected in a pike fish (*Esox lucius*) from the Viskan River in Sweden [17] and found in fresh water and marine fish from Europe, Canada and US [14,18,19]. PBDEs were also found in all the mussel samples that indicate widespread contamination in the coastal waters of Asia countries [12,20].

Gas chromatography (GC) has become the standard analytical method for PBDEs separation due to its high resolution [5,21,22]. The most widely used detection technique for the PBDEs determination is mass spectrometry operated either in electron capture negative ionization (ECNI) or electron ionization (EI) mode. Occasionally, electron capture detector (ECD) has been used for specific applications. The two mass spectrometric ionization modes are subjected to different types of interferences. EI-MS was affected by interferences from chlorinated compounds existed in the sample matrices. The negative ion chemical ionization (NICI-MS) may be interfered from various brominated interferences. The major advantage of using EI-MS is to allow the application of ^{13}C-labeled internal standards for a more precise determination. The isotope dilution mass spectrometry technique is often not possible for the ECNI-MS, because generally only the Br ions ($m/z = 79$ and 81) are monitored.

Electron-waste (e-waste) includes end-of-life electronic products such as computers, printers, photocopy machines, television sets and mobile phones. Obsolete electronic products generated from developed countries are being exported into developing countries such as China. Peoples of Guiyu (Guangdong province) have engaged in the recycling business of e-waste since 1995. Uncontrolled dismantling, acid treatment and open burning have resulted in rather high concentrations of PBDEs and other POPs in sediment, river, fish and human. However, there is little information of PBDEs in fresh fishes collected from river polluted by recycled electronic and electrical waste.

This study aims to apply gas chromatography/mass spectrometry (GC/MS) and gas chromatography/tandem mass spectrometry (GC/MS/MS) methods for analyzing PBDEs in fish samples collected from river polluted by the e-waste disposal and burned residues, and to focus on the determination of PBDE congener concentrations and distributions. The results obtained provide valuable information on the adverse environmental and health effects of PBDEs derived from uncontrolled recycling of e-wastes.

2. Experimental

2.1. Materials

2.1.1. Chemicals and reagents

The solvents including dichloromethane, hexane and acetone were purchased from Tedia Company Inc. (Fairfield, OH, USA) and nonane from Fluka (Milwaukee, USA) in pesticide grade. Granular anhydrous sodium sulfate were purchased from Tedia (Fairfield, USA), silica gel 60 (0.063–0.200 mm) from Merck (Whitehouse Station, USA), acid alumina (Brockmann I, Standard Grade:150 mesh, Aldrich Chemical Co., Milwaukee, USA), copper powder (UniChem, Surrey, UK) and concentrated sulfuric acid (BDH Laboratory Supplies, Dorset, UK) were analytical grade. Certified reference material WMF-01 (reference fish tissue for organic contaminant analysis) was also obtained from Wellington Laboratories.

PBDE standard solutions were purchased from Wellington Laboratories (Ontario, Canada). A calibration solution BDE-CVS-E (five ampoules in one kit) contained 20 PBDE congeners (BDE-3, 7, 15, 17, 28, 47, 66, 71, 77, 85, 99, 100, 119, 126, 138, 153, 154, 183and 209). A native PBDE standard mix contained BDE-MXD (BDE-17, 47, 66, 100, 153, 183 and 209) and ^{13}C-labeled PBDE mix (MBDE-MXC) (^{13}C-labeled BDE-15, 28, 47, 99, 153, 154 and 183) and ^{13}C- BDE209 were used to optimize extraction and cleanup procedure for good recovery and sensitivity.

2.2. Sample preparation

Fish samples of crucian carp, grass carp, silver carp, mud carp and carp (total 15 fishes) were collected from a specific area in Nanyang River (N: 23.3208; E: 116.369) in 2005 where the largest open e-waste burning site is located. A large quantity of printed circuit boards, chipping and plastics were burned at the e-waste recycling site. Many burned parts and unknown e-waste residues have been dumped in the vicinity of the river.

Fish samples were wrapped in aluminum foil and transported to the laboratory with ice bag and hermetical cold box. Fishes were weighted and measured for the length. All fishes were divided into abdomen, back and tail muscle without skin. The same position muscles were mixed uniformly, wrapped in foil and stored at −20 °C. After being freeze-dried, each dried fish muscle was homogenized in a stainless steel blender. Lipid and moisture contents in tissues were determined gravimetrically [23]. Lipid contents in abdomen, back and tail muscle were 9.7%, 9.5% and 8.1% for grass carp, 12.5%, 7.2% and 7.6% for mud carp, 5.6%, 7.5% and 7.7% for cap, 11.7%, 8.8% and 7.8% for crucian carp, and 16.8%, 8.96% and 9.0% for silver carp. Moisture content was similar for all of freshwater fishes and ranged from 77 to 81%.

2.3. Extraction and clean up

About 1–5 g of dried fish muscles were mixed with 4 g of anhydrous sodium sulfate that was cleaned with DCM and activated at 140 °C for 24 h in advance. After spiked with 10 to

Table 1
Optimized GC/ion trap MS parameters for analyzing mono- to hepta-BDEs

Group	RT	^{12}C		^{13}C		REV	q
		Parent ion	Fragment ion	Parent ion	Fragment ion		
Mono	6.00–8.20	248	141 169	260	153 181	2	0.45
Di	8.20–10.50	327.9	167.9 218.9	339.9	179.9 231.0–233.0	1.5	0.3
Tri	10.50–13.00	405.8	245.8–247.8	417.8	257.8–259.8	2	0.45
Tetra	13.00–16.00	485.7	323.7–325.7	497.8	335.8–339.8	2.5	0.45
Penta	16.00–19.50	565.6	405.6–407.8	577.6	418.0–420.0	3	0.25
Hexa	19.50–22.50	643.5	481.7–485.7	655.6	493.6–495.6	3.5	0.3
Hepta	22.50–26.0	721.4	561.6–563.6	733.5	573.5–575.6	2.5	0.225

REV: resonant excitation voltage.

50 ng MBDE-MXC (^{13}C-labeled PBDEs) standard, the samples were extracted with 80 mL of DCM/acetone (1/1, v/v) for 12 h in Soxhlet extraction system. The muscle sample extracts were concentrated with a rotary evaporator and transferred to a glass bottle with 6 ml of hexane. The extracts were then treated with concentrated sulfuric acid to remove the bulk of lipids. Further, cleanup was done on a column containing 2 g anhydrous sodium sulfate, 1 g of silica gel impregnated with sulfuric acid (44%), 3 g 30% acid silica gel and 1 g active silica gel with the order from top to bottom. *n*-Hexane (30 ml) was use for elution. The eluted solution was loaded on to a column containing 2 g anhydrous sodium sulfate and 4 g acid alumina. The column was eluted with 30 ml *n*-hexane/DCM (7:3) that was collected and concentrated under gentle nitrogen evaporation apparatus at room temperature. The sample was reconstituted in 50 μl nonane containing ^{13}C-labeled BDE-139 at 100 pg/μl.

2.4. GC/MS and GC/MS/MS analyses

GC/MS/MS analysis was performed on a Trace GC/PolarisQ ion trap mass spectrometer (Thermo Quest, Austin, TX, USA). A DB-5 ms capillary column (30 m × 0.25 mm I.D., 0.25 μm film thickness) was used for the determination of congeners from mono- to hepta-BDEs. The temperature program was set from 110 °C (held for 1 min) to 180 °C (held for 1 min) at 8 °C/min, then from 180 to 240 °C (held for 5 min) at 2 °C/min, and then from 240 to 265 °C (held for 6 min) at 2 °C/min. Splitless injection mode was set for 0.5 min. The GC injector temperature was maintained at 250–280 °C. The temperatures of the MS ion source and transfer line were kept at 250 °C and 280 °C, respectively. Sample extract or standard solution (1 μl) was manually injected with a solvent delay set at 6.0 min. The mass spectrometer was operated with electron impact ionization (EI) mode and electron energy of 70 eV. Ions peaks ($[M]^+$ or $[M-Br_2]^+$) were selected. Under the GC/MS/MS conditions, the molecular ions ($[M]^+$ or $[M+2]^+$) and fragment ions resulting from the loss of Br_2 (i.e., $[M-Br_2+2]^+$ or $[M-Br_2+4]^+$) were selected as the precursor ions for tandem mass spectrometric analysis (see Table 1). The quantitative ions were selected based on the criteria of peak intensity and ion specificity as well as potential interference from other compounds. The instrumental parameters such as "q" value, resonant excitation voltage (REV), excitation time (ET) and isolation time (IT) [24] were optimized.

A short DB-5ms column (15 m × 0.25 mm I.D., 0.10 μm film thickness) was used for the determination of BDE-209, with the temperature program from 150 °C (held for 1 min) to 300 °C (held for 18 min) at 30 °C/min. The GC/MS analysis was performed on Agilent 6890 gas chromatograph connected to a 5975 Network mass spectrometer (Agilent Technologies, Madrid, Spain) with EI (70 eV) and selected ion monitoring (SIM) of fragment ions of *m/z* 231.8, *m/z* 398.6, *m/z* 400.5 and *m/z* 799.3.

2.5. Quality assurance and quality control

The extraction recoveries were assessed for the surrogate standards added to the samples prior to extraction. Mass labeled (MBDE-MXC: 8 ^{13}C—labeled BDEs at 10 ng and ^{13}C-BDE-209 at 20 ng) were used as internal standards for PBDEs, and the $^{13}C_{12}$-BDE-139 as recovery standard. Calibration solutions BDE-CVS-E was used in constructing the calibration curve. A native PBDE standard BDE-MXD were added to control samples (fish from MaiPo marsh pound in Hong Kong) and used for QA/QC tests.

The recovery test was undertaken for target concentrations ranging from 50 to 5000 ng/ml in the final extract for different PBDE congener, because this range is representative of congener levels previously reported in fish samples [14]. The spiking solution was added to the homogenized muscles sample prior to extraction. Recoveries of control sample ranged from 87 to

Table 2
Analytical results for certified reference material of "Freeze-Dried" fish tissue (WMF-01)

Congener	Certified reference material (pg/g)	Experimental result (pg/g)
BDE-28	3124 ± 290	2816 ± 231
BDE-47	123200 ± 24800	103892 ± 12800
BDE-99	37500 ± 4220	32382 ± 4040
BDE-100	35870 ± 14500	59505 ± 1358
BDE-153	17040 ± 8000	19928 ± 1692
BDE-154	19790 ± 2880	20394 ± 3452
BDE-183	532 ± 400	1224 ± 56

103%. The recovery rates of all fish samples ranged from 78 to 113%. The analytical method validated in our study was used to quantify PBDEs in certified reference materials (WMF-01) (Table 2). To determine the limits of detections (LOD) for the target analytes, control samples were spiked with PBDE standards at five levels (1.0 and 1000 ppb) (R^2: 0. 9991–1) and were subjected to the same extraction and cleanup steps described above.

Quantification was based on isotope dilution method and the presence of two confirming ions at the area ratios within 10% variation. Retention time shifts in the chromatogram were corrected using the isotope internal standards and injection standard was based on an agreement within <0.2 min of the expected retention time.

3. Results and discussion

3.1. Mass spectrometry analysis

Potential interferences may present in instrumental analysis although sample extract was prepared by multiple-step column clean-up procedure. Particular concerns have been addressed to

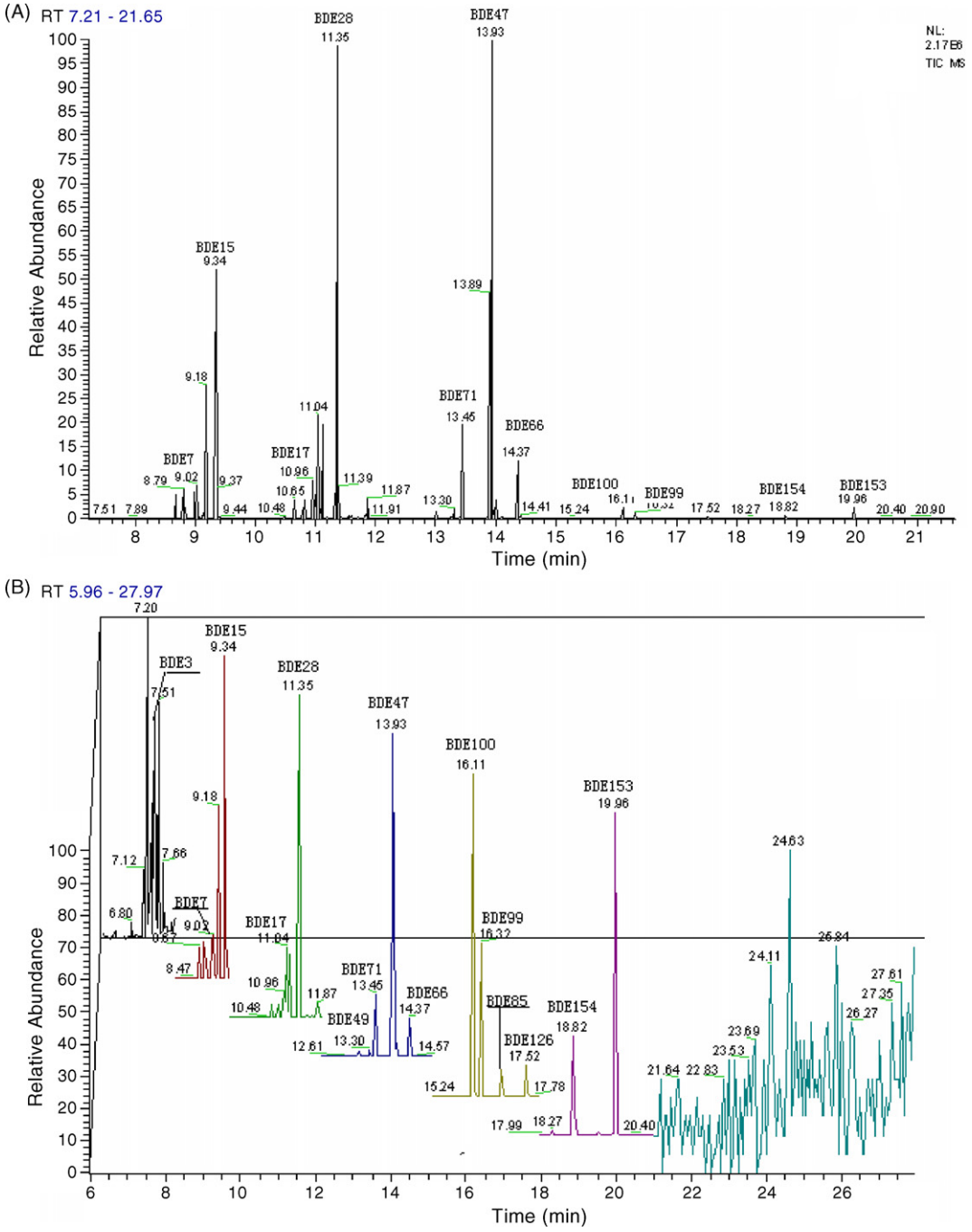

Fig. 1. Total ion chromatogram (A) and extracted ion chromatograms (B) from the GC–ion trap MS analysis of the fish sample-carp in Nanyang River.

co-elution of BDE-47 ($[M-Br_2]^+$: m/z 325.7) and PCB-180 ($[M-Cl_2+2]^+$: m/z 324.8), BDE-100 and PCB-194, BDE-154 and PBB-153, as well as the co-elution of BDE-153 and tetrabromobisphenol-A (TBBP-A) on a 30 m DB-5 column because PBB-153 and TBBP-A have be detected in the American marine fish and population [25–27]. In the ion trap MS analysis, most PBDEs tend to loss of Br_2 (similar to PCBs that loss Cl_2) excepted that some congeners loss COBr. Interestingly, all of the exceptions occur for the ortho-substitued congeners. The most predominant and characteristic ion clusters for each of the congeners were selected for the MS/MS windows (Table 1). For mono-PBDE through tri-PBDE, the M^+ ions were selected. For the rest of the homologue groups (tetra- through hepta-PBDE), $M-Br_2^+$ ions were selected. Fig. 1 showed fish sample TIC (A) and extracted ion chromatograms (B). Calibration linear range obtained with the developed sample preparation procedure and with the optimized GC/MS/MS and GC/MS parameters were from 0.01 to 100 and 1 to 1000 ng/g w.w., respectively. Limitation of detection of mono to hepta-BDE was 0.01 ng/g w.w. and of BDE-209 was 1 ng/g w.w. when ratio of signal to noise was 3.

3.2. PBDE congener concentrations and distributions in fish

Total PBDE congener concentrations (ΣPBDEs) in the fishes were grass carp < mud carp < cruciam carp < silver carp < carp (Table 3). ΣPBDEs of abdomen in grass carp (53 ng/g w.w. or 585 ng/g lipid weight (l.w.)) and mud carp (96 ng/g w.w. or 766 ng/g l.w.) were about 10–20 times lower than those in crucian carp, silver carp and carp (570–766 ng/g w.w. or 3659–4919 ng/g l.w.). Relatively low accumulations of PBDEs were routinely observed in grass carp in comparison to other fishes with 1–2 orders. Different fish species demonstrate different metabolic capacities. Some of this difference may be due to dietary difference, however, the magnitude of the difference may suggest a higher metabolic activity in crucian carp, silver carp and carp.

PBDEs levels in carp from Guiyu were much higher than those reported in other countries. Analytical methods with EI-MS for low brominated congeners and ECNI for BDE-209 were applied to detect the total PBDEs at 18 ng/g w.w. in carp collected from the polluted area of Des Plaines River in Flanders, Belgium [28] and at 65 ng/g w.w. from river near manufacturing facility [29]. PBDEs were found 11.4 ng/g w.w. by using GC/halogen-selective electrolytic conductivity detection in carp (Cyprinus carpio) in Hyco River in Virginia, USA [30]. Furthermore, the GC/ECD analytical results showed that ΣPBDE levels in crucian carp, silver carp and carp from Nanyang River were higher than those observed in edible fish (118 and 197 ng/g w.w.) from downstream of rivers in North East UK located near to a BFR manufacturing plant [31].

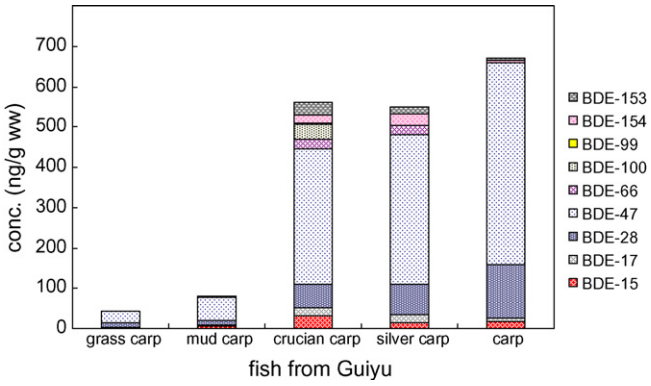

Fig. 2. PBDE congener concentration and pattern in fishes collected from Nanyang River, Guiyu.

Fig. 2 showed that BDE-47, 28, 15, 17, 154 and 153 were the mainly congeners detected in the fish muscles. BDE-47 was the most predominant congener with its concentration ratio in the total PBDEs ranging from 53% in grass carp to 65.2% in carp. Subsequently, BDE-28 that was higher than penta-, hexa and hepta-BDE ranged from 10% in mud carp and crucian carp, 12% in silver carp, 17.4% in carp and to 20% in grass carp. BDE-66 was found in grass carp, crucian carp and silver carp. BDE100 and BDE-99 were detected at the lowest concentration or not detected in fishes (except for crucian carp). BDE-183 and BDE-209 were not found in carp, silver carp, grass carp and mud carp. Various fish species may have different

Table 3
PBDE congener concentrations and pattern distribution in abdomen, back and tail muscles in fish collected from Nanyang River, Guiyu (unit: ng/g w.w.)

Congener	Grass carp			Mud carp			Crucian carp			Silver carp			Carp		
	A	B	T	A	B	T	A	B	T	A	B	T	A	B	T
BDE-15	1.9	2.1	1.8	4.6	2.2	3.2	30.42	1.4	1.8	14.5	2.2	3.2	16.0	5.0	5.5
BDE-17	2.2	2.3	2.1	4.1	2.1	2.8	19.99	2.3	4.2	18.6	2.6	3.9	9.2	9.4	10.9
BDE-28	10.4	10.4	8.9	10.2	6.1	8.3	58.89	9.3	12.1	74.8	10.6	16.3	133.1	68.1	78.9
BDE-47	28.1	27.0	23.5	58.1	28.8	37.0	335.54	45.6	56.2	372.2	54.5	84.9	499.4	309.5	359.6
BDE-66	1.0	1.0	0.8	0.0	0.0	0.0	25.62	2.5	1.9	22.5	2.8	4.4	0.0	0.0	0.0
BDE-100	0.2	0.2	0.2	0.0	0.0	0.0	37.34	4.3	5.1	0.0	0.4	0.7	0.6	0.4	0.0
BDE-99	0.0	0.0	0.0	0.5	0.2	0.3	1.88	0.2	0.3	0.0	0.0	0.0	0.0	0.0	0.0
BDE-154	0.4	0.4	0.4	1.9	0.9	1.1	19.90	3.2	1.5	29.2	5.0	7.9	7.7	5.0	5.6
BDE-153	0.2	0.1	0.1	2.4	0.4	1.4	32.82	2.1	2.9	18.4	2.7	4.4	4.9	3.2	3.4
Total (wet weight)	53.1	52.1	45.2	96.0	48.0	63.4	570	70.9	86.0	614.9	89.8	140.0	765.9	458.1	530.1
Total (lipid weight)	585	551	561	766	666	740	4271	940	1118	3659	1002	1553	4919	6377	5810

A: abdomen muscle; B: back muscle; T: tail muscle.

adsorption for PBDE congeners but tend to adsorb low brominated diphynel ethers. The other reason of detecting higher levels of low brominated PBDEs in the fish tissue samples may be because high brominated diphynel ethers were metabolized in the fish muscles.

The concentration of PBDEs in abdomen, back and tail muscle was related with lipid contents with linear regression. The correlation coefficiency ranged from 0.9839 to 0.9999 in carp, grass carp, crucian carp, mud carp and silver carp. The result indicates PBDEs are more accumulated in muscle with higher lipid content fish and muscle in a fish. River largely polluted by e-waste recycling materials where are a little fish can be found.

4. Conclusion

Isotope dilution GC/MS and GC/MS/MS were applied for the determination of PBDEs in fish muscle tissues. The obtained results indicated that levels of ΣPBDEs (especially low bromo-BDE) in the fish collected from a river closed to the e-waste sites in Guiyu were higher than those reported from other locations in the world, probably due to pollution of river water and sediment by uncontrolled dismantling, open burning, and dumping of e-waste in the environment. The tissues with high lipid content had higher concentrations of PBDE in many fish species.

Acknowledgements

Financial support from the Group Research, Central Allocation (HKBU 1/03C) of Research Grants Council of the University Grants Committee, Hong Kong is gratefully acknowledged.

References

[1] G.A. Stern, M.G. Ikonomou, Organohalogen Compd. 47 (2000) 81.
[2] B. Strandberg, N.G. Dodder, I. Basu, R.A. Hites, Environ. Sci. Technol. 35 (2001) 1078.
[3] Bromine Science Environmental Forum (BSEF). Major Brominated Flame Retardants Volume Estimates; Brussels, Belgium, 2003.
[4] K. Hartonen, S. Bowadt, S.B. Hawthorne, M.L. Riekkola, J. Chromatogr. A 774 (1997) 229.
[5] A. Covaci, J. de Boer, J.J. Ryan, S. Voorspoels, P. Schepens, Anal. Chem. 74 (2002) 790.
[6] J. de Boer, K. de Boer, J.P. Boon, in: J. Paasivirta (Ed.), The Handbook of Environmental Chemistry, vol.3, Springer-Verlag, Berlin, 2000, p. 61.
[7] BSEF (2006) BFR-Related Legislation in the United States. http://www.bsef.com/regulation/regulator_ov_usa/index.php?/regulationregulator_ov_usaregulator_ov_usa.php.
[8] M.L. Hardy, Chemosphere 46 (2002) 757.
[9] K. Hooper, T. McDonald, Environ. Health Perspect. 108 (2000) 5.
[10] J. Legler, A. Brouwer, Environ. Int. 29 (2003) 879.
[11] T. Zhou, M.M. Taylor, M.J. DeVito, K.M. Crofton, Toxicol. Sci. 66 (2002) 105.
[12] N. Kajiwara, S. Kamikawa, K. Ramu, D. Ueno, T.K. Yamada, A. Subramanian, P.K. Lam, T.A. Jefferson, M. Prudente, K.H. Chung, S. Tanabe, Chemosphere 64 (2006) 287.
[13] H. Nobuyasu, O. Tsuyoshi, G. Keerthi, F. Jerzy, Y. Nobuyoshi, Organohalogen Compd. 66 (2004) 207.
[14] C.A. de Wit, Chemosphere 46 (2002) 583.
[15] R.A. Hites, Environ. Sci. Technol. 38 (2004) 945.
[16] O. Andersson, G. Blomkvist, Chemosphere 10 (1981) 1051.
[17] B. Jansson, L. Asplund, M. Olsson, Chemosphere 16 (1987) 2343.
[18] R.J. Law, M. Alaee, C.R. Allchin, J.P. Boon, M. Lebeuf, P. Lepom, G.A. Stern, Environ. Int. 29 (2003) 757.
[19] A. Holden, Organohalogen Compd. 61 (2003) 255.
[20] D. Ueno, N. Kajiwara, H. Tanaka, A. Subramanian, G. Fillmann, P.K. Lam, G.J. Zheng, M. Muchitar, H. Razak, M. Prudente, K.H. Chung, S. Tanabe, Environ. Sci. Technol. 38 (2004) 2312.
[21] W. Vetter, Anal. Chem. 73 (2001) 4951.
[22] J. Björklund, P. Tollbäck, C. Östman, J. Mass Spectrom. 38 (2003) 394.
[23] A. Hara, M.S. Radin, Anal. Biochem. 90 (1978) 420.
[24] D. Wang, Z. Cai, G. Jiang, M.H. Wong, W.K. Wong, Rapid Commun. Mass Spectrom. 19 (2005) 83.
[25] A. Sjodin, D.G. Patterson Jr., A. Bergman, Environ. Sci. Technol. 35 (2001) 3830.
[26] C. Thomsen, L.S. Haug, H. Leknes, E. Lundanes, G. Becher, G. Lindstrom, Chemosphere 46 (2002) 641.
[27] L.Y. Zhu, R.A. Hites, Environ. Sci. Technol. 38 (2004) 2779.
[28] A. Covaci, L. Bervoets, P. Hoff, S. Voorspoels, J. Voets, K. Van Campenhout, P. Schepens, R. Blust, J. Environ. Monit. 7 (2005) 132.
[29] N.G. Dodder, B. Strandberg, R.A. Hites, Environ. Sci. Technol. 36 (2002) 146.
[30] R.C. Hale, M.J. La Guardia, E.P. Harvey, T.M. Mainor, W.H. Duff, M.O. Gaylor, Environ. Sci. Technol. 35 (2001) 4585.
[31] C.R. Allchin, R.J. Law, S. Morris, Environ. Pollut. 105 (1999) 197.

Available online at www.sciencedirect.com
ScienceDirect
Talanta 72 (2007) 1659–1666
Talanta
www.elsevier.com/locate/talanta

Development of soft plasma ionization (SPI) source for analysis of organic compounds

Hyunkook Park [a,*], Ickhee Lee [b], Kyu Seong Choi [b], Kazuaki Wagatsuma [a], Sang Chun Lee [b]

[a] *Institute for Materials Research, Tohoku University, Katahira 2-1-1, Sendai 980-8577, Japan*
[b] *Department of Chemistry, Kyungnam University, 449 Wolyoung-dong, Masan, Republic of Korea*

Received 30 October 2006; received in revised form 17 April 2007; accepted 1 May 2007
Available online 17 May 2007

Abstract

We present a newly designed soft plasma ionization (SPI) source developed for mass spectrometric study of organic compounds in this study. The SPI cell having a relatively small size consists of a hollow anode and a hollow mesh cathode. The voltage–current characteristic depending on the pressure was investigated, indicating that it has similar characteristics to conventional hollow cathode glow discharges. To investigate the emission characteristics of the SPI source, some molecular band emission spectra (N_2, N_2^+ and OH^+) were measured by using argon and helium discharge gases. The SPI source was installed to a commercially used quadrupole mass analyzer for analyzing organic compounds. To demonstrate the SPI source, the mass spectra of some organic compounds (methylene chloride, toluene, benzene, cyclohexane and chloroform) were measured. The organic compounds were ionized with good stability in the plasma, and the fragmentation depended on the applied current. When helium and argon gases were used as the discharge gas, the helium plasma was more suitable for SPI-MS rather than argon because the argon plasma not only suffers from spectral interference but also has lower sensitivity.

Keywords: Soft plasma ionization; Glow discharge process; Molecular emission spectrum; Plasma source mass spectrometry; Organic mass spectrometry

1. Introduction

In plasma source mass spectrometry, inductively coupled plasma (ICP), laser induced or ablation plasma (LIP), spark/ark plasma, microwave induced plasma (MIP) and glow discharge plasma (GDP) have been used as an ionization source. They have favorable features for inorganic mass spectrometry because inorganic samples are easily atomized and ionized due to their high plasma temperature. However, to apply the plasmas sources in organic mass spectrometry, they must be operated at much lower temperatures. When the plasma is classified according to their temperature, ICP and LIP belong to a high temperature plasma (or hot plasma, >10,000 K). On the other hand, GDP belongs to a low temperature plasma (or cold plasma, 4000–5000 K) because low-energy electrons are used in the ionization process [1].

Since glow discharge plasma (GDP) ionization sources have numerous unique advantages which include low power consumption, low cost of the device and the simplicity in the operation compared to other plasma sources [2], they have been combined with various mass spectrometers such as quadrupole, ion trap and time of flight mass spectrometers [3–5]. In addition, because the glow discharge is operated at reduced pressure (a few Torr), the background spectrum is very simple and the polyatomic interference which usually appears in ICP-MS can be removed [6]. For this reason, some glow discharge users attempted to apply the GDMS for organic compounds; however, since they were employed only at lower current conditions for decreasing the plasma temperature, clear fragment patterns could not be obtained in their mass spectra. They only gave a fragment pattern like as the electron impact ionization (EI) [7–9]. A softly ionized plasma developed in this study was designed so that the current can be adjusted over much wider range (a few mA to a hundred mA), to control the amount of energetic gas atoms and metastable atoms in the plasma effectively.

In this study, a new soft plasma device was designed and constructed on the basis of the glow discharge processes, and the principle of the plasma generation process was also introduced.

* Corresponding author.
E-mail address: parking8@imr.tohoku.ac.jp (H. Park).

0039-9140/$ – see front matter © 2007 Elsevier B.V. All rights reserved.
doi:10.1016/j.talanta.2007.05.004

The discharge parameters (voltage, current and pressure) were measured to compare with those in a conventional GDP. Emission band spectra of several molecule species in the discharge chamber were measured, and dependence of their emission intensities on the discharge current as well as the kind of discharge gases was investigated. To demonstrate a mass spectrometric application of the SPI source, it was equipped with a commercial quadrupole mass analyzer. The mass spectra of some organic compounds such as methylene chloride, toluene, cyclohexane, benzene and chloroform were measured by using this SPI-MS system. To evaluate the performance of the SPI source as an ionization source for organic compounds, variations of fragment patterns were investigated when the discharge parameters such as voltage, current, kind and pressure of the plasma gas were varied.

2. Experimental

2.1. Design of SPI cell

The developed soft plasma ionization chamber has a rectangular shape in dimension of 50 mm × 50 mm × 110 mm, which is similar in size to the cell employed in our previous study [10]. The chamber contains a cylindrical hollow SPI cell. Fig. 1 shows a detailed drawing of the developed SPI cell. Since the SPI source is operated under relatively low vacuum conditions, we need not take account of the material of the cell for a strict vacuum sealing. Therefore, in order to decrease the weight of the cell, the discharge chamber is made of aluminum instead of stainless steel. For electrical insulation of the discharge system, a Teflon tube is used instead of machinable ceramic. The discharge chamber is sealed up with O-rings. The anode is made of a copper tube, and copper gauze in 20 meshes is used as the cathode. The dimension of the anode and the mesh cathode is 16 and 12 mm in the inner diameter, and 35 and 60 mm in the length, respectively. The temperature of the SPI source was not so elevated, so Teflon could be used as the insulator. The anode is located inside the Teflon tube. To produce having low-energy

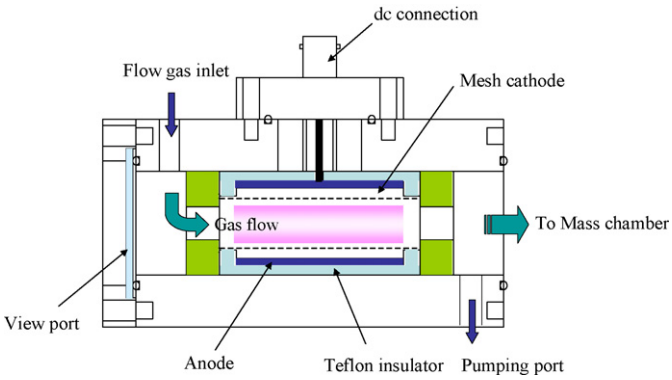

Fig. 1. A schematic diagram of SPI source cell.

electrons, the distance between the cathode and the anode was adjusted as near as possible (ca. 2 mm).

2.2. Construction of SPI-MS

A commercial quadrupole mass analyzer (RGA-300, Stanford Research System) was employed. As shown in Fig. 2, a home-made interfacing part composed with a sampler cone and a skimmer cone was designed for differential pumping and effective ion transmission. In the interface between the SPI cell and the mass chamber, the skimmer having a hole of 0.95 mm in diameter (Nickel alloyed stainless steel, SUS-45C) and the sampler (inner diameter of 0.25 mm, home-made) were installed. The pressure of the SPI source, the interface part and the mass chamber were maintained at a few hundred mTorr, 1×10^{-3}, and 1×10^{-6} Torr, respectively, by using a turbo molecular pump (Alcatel, ATP 100) backed by a mechanical pump system.

2.3. Experimental setup

Fig. 3 shows a schematic diagram of the experimental setup for studying the emission characteristics of the SPI source. In this study, argon (UHP grade, 99.9999%) or helium (UHP

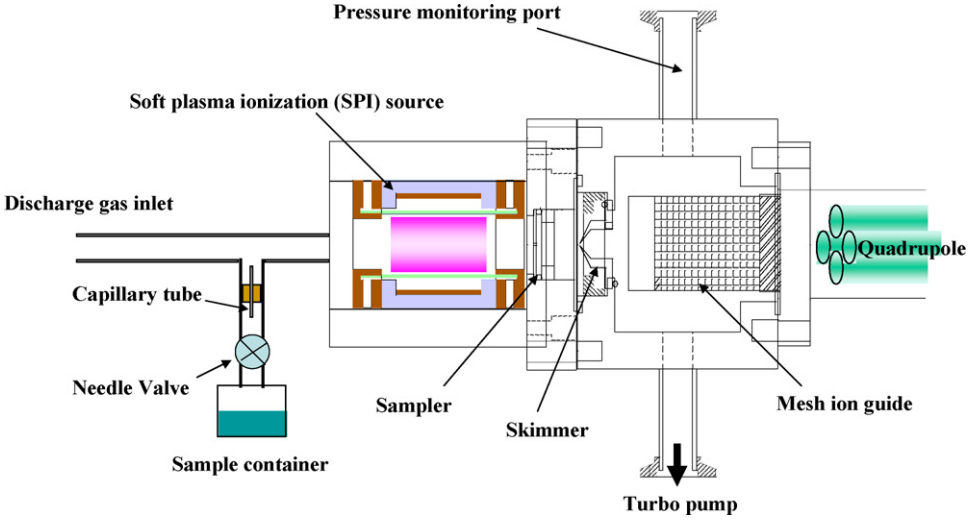

Fig. 2. A schematic diagram of SPI-MS.

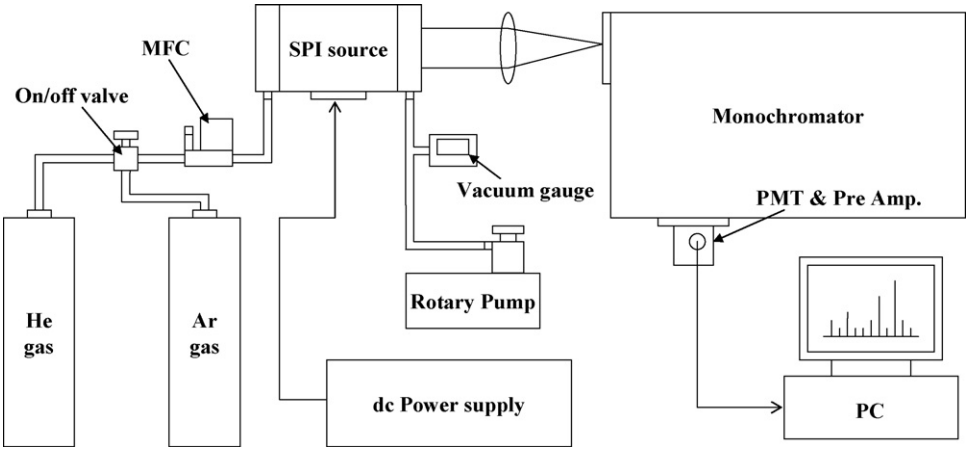

Fig. 3. A schematic diagram of the experimental setup for emission characteristics of SPI source.

grade, 99.9995%) was used as a discharge gas, the gas flow was controlled independently by using an on–off valve which is connected to a T-type Swage-lock. A 1/4-in. Teflon tube was used for transport of the discharge gas, and swage-lock fittings were used for the entire vacuum tight. A mass flow controller (MKS 1179A) was used for control of the gas amount, and a vacuum gauge (Granville-Phillips, Convectron gauge) located between the vacuum port and a rotary pump (Alcatel, 2021SD) was used for monitoring the pressure of the SPI cell. A plasma was generated by applying a dc voltage between the anode and the mesh cathode, and then emission signals were dispersed by using a monochromator (McPherson, 207). The emission signal was detected and amplified by a photo multiplier tube (Hamamatsu, R955) and a pre-amplifier (NF electronics, LI-76), and then recorded on a personal computer via an A/D converter. The apparatus and the experimental conditions are summarized in Table 1.

2.4. Liquid phase sample introduction

As shown in Fig. 2, organic samples were stored in a sample container which was located between a flow gas tube and the SPI cell, and a needle valve controlled the amount of the organic sample introduced. Table 2 indicates the experimental parameters for SPI-MS including the pressure of SPI source, the discharge voltage and current and so on.

In general, it is difficult for liquid phase samples to be introduced into the mass chamber. The main problem was that enough flow rates of liquid samples are not achieved easily because the high vacuum condition must be maintained. If we assume that about 1 ml/min of water is introduced to a vacuum chamber of 10^{-6} or 10^{-7} Torr, the liquid flow must produces a gas flow rate of more than 1000 ml/min [6]. To reduce the effect, a capillary tube of about 0.5 mm in diameter needs to be inserted between the gas flow tube and the sample container. The sample vapor was introduced to the SPI cell along with the flow of a discharge gas.

Organic samples prepared for this study are as follows: toluene (J.T. Baker, 99.7%), methylene chloride (J.T. Baker, 99.8%), cyclohexane (Wako, 96%), benzene (Wako, 99.7%),

Table 1
Instrumentation for constructing SPI-MS

Soft plasma ionization source	Home-made
Hollow anode	16 mm in inner diameter
Mesh cathode	12 mm in inner diameter
Electrode distance	2.0 mm
Spectrometer	Model 207 (McPherson)
Grating	Concave, 1200 g/mm
Focal length	0.67 m
dc power supply	Model PS310 (Korea Switching)
Voltage employed	10–500 V
Current employed	20–120 mA
Mass spectrometer	RGA-300 (Stanford Research System)
Detector	Faraday-cup & Channel Electron multiplier
Mass filter type	Quadrupole
Mass range	1–300 amu
Resolution	Better than 0.5 amu (10% peak height)
dc power supply	Model PS-310 (Korea Switching)
Turbo molecular pump	ATP 100C (Alcatel)
Rotary vane pump	Model 2021SD (Alcatel)
Vacuum gauge	122B Baratron type (MKS)
	TC-1A Thermocouple type (Varian)
	423-IMAG cold cathode type (Alcatel)
Mass flow controller	Model 1179A (MKS)
Gases	Ultra high grade (99.9999%) argon
	Ultra high grade (99.9995%) helium

Table 2
Typical working conditions for SPI-MS

SPI source	
Discharge voltage	300–500 V
Discharge current	5–40 mA
Interface part	
Skimmer voltage	0 to −100 V
Ion guide voltage	−10 to −150 V
Focus plate voltage	−50 to −200 V
Mass spectrometer	
CEM voltage	−1.5 to 2.0 kV
Pressure	
SPI source part	800–900 mTorr
Interface part	1.0×10^{-3} Torr
Mass spectrometer part	1.0×10^{-6} Torr

and chloroform (Mallinckrodt, 99.9%). The sample compounds were employed without any purification.

3. Results and discussion

3.1. Principle of soft plasma ionization source

The principle of soft plasma ionization is based on the following idea regarding the glow discharge process; the major ionization can be caused not by fast electron collisions but by gentle collisions with gas species such as metastable atoms. In order to obtain lots of such gas spices and simultaneously to reduce high energy electrons, we employ a specified design cell having a narrow distance of two electrodes (2 mm).

Fig. 4 shows a cross-section of the SPI cell and the principle of soft plasma ionization. The discharge cell comprises an outer hollow anode and a coaxially arranged inner cathode made of a mesh copper material. When a discharge gas flows between two electrodes and a voltage is applied to the electrodes, electrons having high energy (primary or fast electrons), which has the energy corresponding to the voltage difference between two electrodes, are moved from the mesh cathode to the anode. Some high energy electrons collide with the discharge gas. Their collisions can produce various atomic and ionic gas species (electron impact process). The positive ionic species produced by electron impact are principally accelerated towards the cathode. Because the cathode is made of the mesh material, the gas ionic species and neutralized gas species, having kinetic and/or internal energies, pass through the mesh cathode and come out in the central portion of the electrode ((b) region in Fig. 4). The region is filled with energetic plasma gas species, so that they collide with each other. These collision processes can produce low-energy electrons (ultimate or slow electrons). There are three kinds of electrons which are known as a primary, secondary, and ultimate electron in the glow discharge plasma, the densities of the electrons have been reported to be 5×10^6, 5×10^7, and 4×10^9 [11], respectively, therefore meaning that the ultimate electrons occupy the largest part in the plasma. The plasma created in the SPI source is roughly divided into two parts, the outer region ((a) region in Fig. 4) consists of primary and secondary electrons, and the inner region ((b) region in Fig. 4) consists of ultimate electrons and the energetic species of the discharge gas. For this reason, only the low-energy electrons and atomic and ionic gas species remain in the inner region of the plasma. Therefore, if an organic sample is introduced to the inner region of the plasma, it can be ionized softly because the sample molecules collide mainly with the energetic gas species such as Penning ionization.

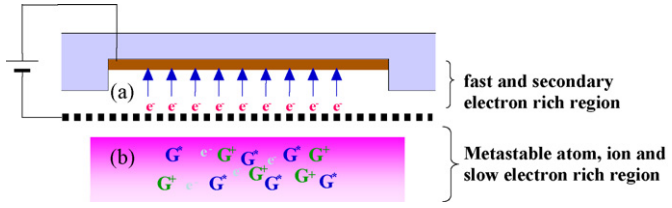

Fig. 4. Principle of soft plasma ionization.

The main ionization processes within the SPI source are as follows:

- Electron impact ionization (process in the outer region)

$$A + e^-(\text{primary electron}) \rightarrow A^+ + 2e^-(\text{secondary electrons}) \quad (1)$$

- Penning ionization (process in the inner region)

$$A + G^m \rightarrow A^+ + G + e^-(\text{ultimate electron}) \quad (2)$$

where G and G^m are the ground and the metastable state of plasma gas, and A and A^+ are the atom and the ion of sample molecules.

3.2. Emission characteristics of SPI source

In glow discharge process, the discharge voltage, the current and the pressure are very important parameters. When the SPI source is discharged using argon gas, the variation of the voltage and the current as a function of the pressure is shown in Fig. 5. The pressure was changed from 1 to 4 Torr.

The current increased linearly with increasing the voltage as shown in Fig. 5. Such voltage–current characteristics mean that the plasma is in an abnormal glow in the glow discharge process. And also, it has similar characteristic to a conventional hollow cathode glow discharge since the current is drastically varied (20–120 mA) with a little increase in the voltage (350–500 V), which is the most different characteristics from the Grimm style discharge.

In the Grimm style glow discharge, both the voltage and the current are reduced along with increasing the gas pressure and the characteristics are changed logarithmically. On the other hand, such variations in the voltage and current in the Grimm source were found also in the SPI source, but the variation curves were changed linearly from 1 to 4 Torr.

Fig. 6 shows background emission spectra in the range from 320 to 440 nm in the argon and the helium plasmas, respec-

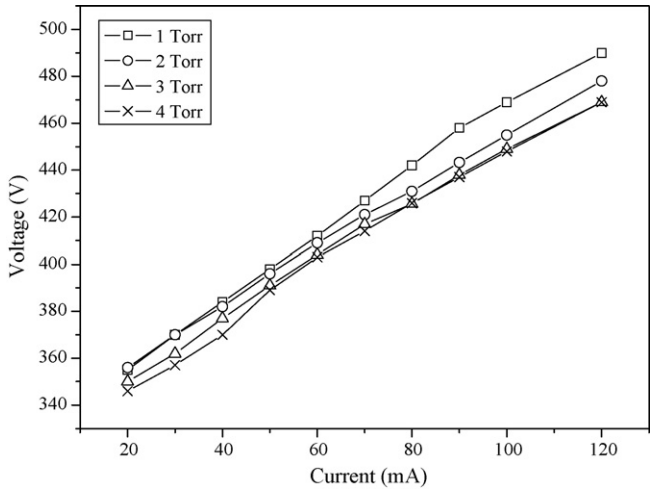

Fig. 5. Voltage and current characteristics of the SPI source as a function of gas.

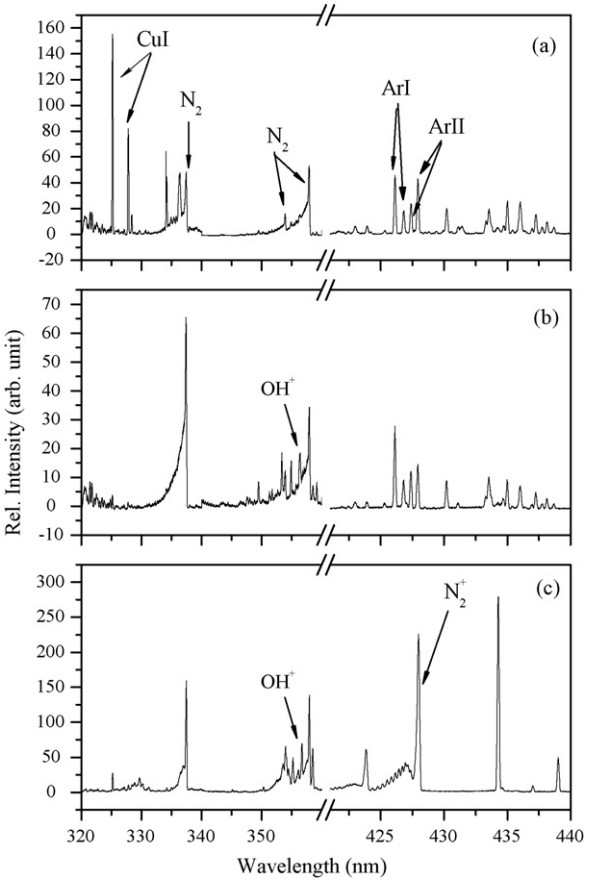

Fig. 6. Background emission spectra in the range from 320 to 440 nm. The discharge conditions were as follows: (a) 420 V/50 mA (2 Torr of Ar gas); (b) 300 V/10 mA (2 Torr of Ar gas); (c) 330 V/10 mA (1 Torr of He gas).

tively. The discharge conditions were 420 V/50 mA (Fig. 6a) and 300 V/10 mA (Fig. 6b) at 2-Torr argon gas, and 330 V/10 mA (Fig. 6c) at 1-Torr helium gas. A band head at 337.1 nm is identified to nitrogen molecule (N_2, $C^3\prod \rightarrow B^3\prod$, 2nd positive system). In GD-OES, air gas always flows into the discharge chamber from the surrounding atmosphere because the chamber is evacuated at low vacuum conditions (a few Torr). Therefore, N_2 or OH spectra derived from small amounts of air and water vapor always appear. However, they have a little influence on the routine analysis, if the discharge voltage or current increase slightly, because the signals are relatively reduced and kept almost constant as the background. As shown in Fig. 6, the intensity of nitrogen seems to have higher intensity at the discharge of 10 mA in argon as well as the helium discharges, but if the current increase to 50 mA, the intensity was relatively decreased. When a copper mesh was used as the cathode, no resonance lines appeared at lower current (see Fig. 6b); however, they were observed at 324.7 and 327.4 nm, as shown in Fig. 6a. This effect indicates that the sputtering of the copper cathode occur in the current range over 50 mA, so that the SPI have to be operated under lower current condition enough to ionize molecule species.

The molecular band spectrum of OH^+ ($^3\prod \rightarrow {}^3\sum$) is shown at 356.5 nm in both gas discharges. N_2 molecular band spectra (2nd positive system) at 353.7 and 357.7 nm are also observed. Their intensities were higher under the helium discharge than the argon.

In the background emission spectra in the range from 420 to 440 nm (the right part of Fig. 6), a band head at 427.8 nm is identified to nitrogen molecular ion (N_2^+, $B^2\sum_U{}^+ \rightarrow X^2\sum_g{}^+$, 1st negative system). The emission line was observed only in the helium discharge; on the other hand, the nitrogen molecular ion line was not observed in the argon discharge (Fig. 6a and b). Emission lines of argon atom (ArI 425.9 nm and ArI 426.6 nm) and ion (ArII 427.2 nm and ArII 427.7 nm) were observed in both the currents, and only the intensities of atomic species were elevated with increasing the discharge current.

It is considered from these results that helium gas can be more effective rather than argon as the discharge gas in the soft plasma ionization system.

3.3. Characteristics of SPI-MS: variations of fragmentation pattern with discharge current

The mass spectra of toluene and methylene chloride obtained by using SPI-MS were shown in Figs. 7 and 8. The fragmentation pattern was investigated when the discharge current was changed with the other discharge conditions of the SPI source fixed.

Fig. 7 shows mass spectra of toluene (C_7H_8) when the discharge current varied from 10 to 20 mA (320–370 V). Fig. 7a

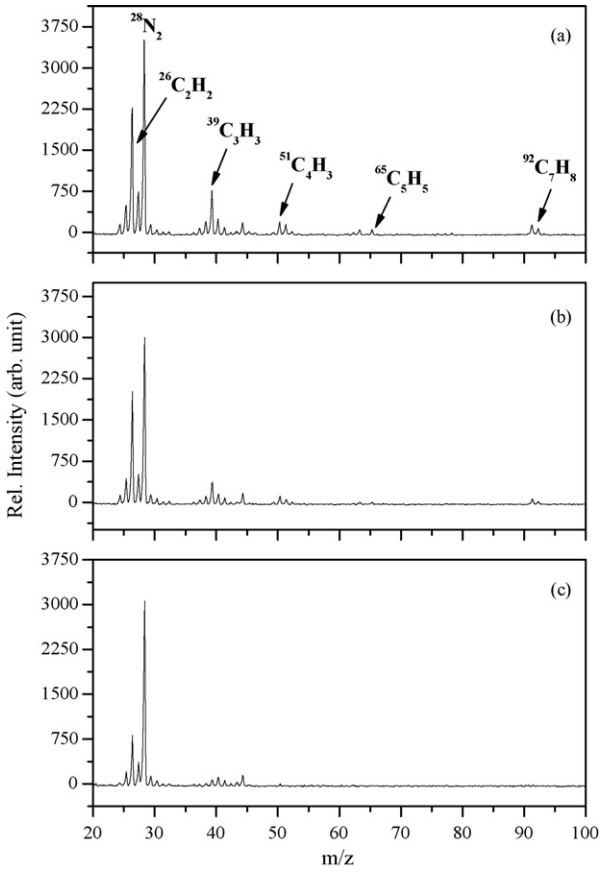

Fig. 7. Mass spectra of toluene (C_7H_8). The discharge current was (a) 320 V/10 mA, (b) 340 V/15 mA, or (c) 375 V/20 mA, and the other conditions were constant.

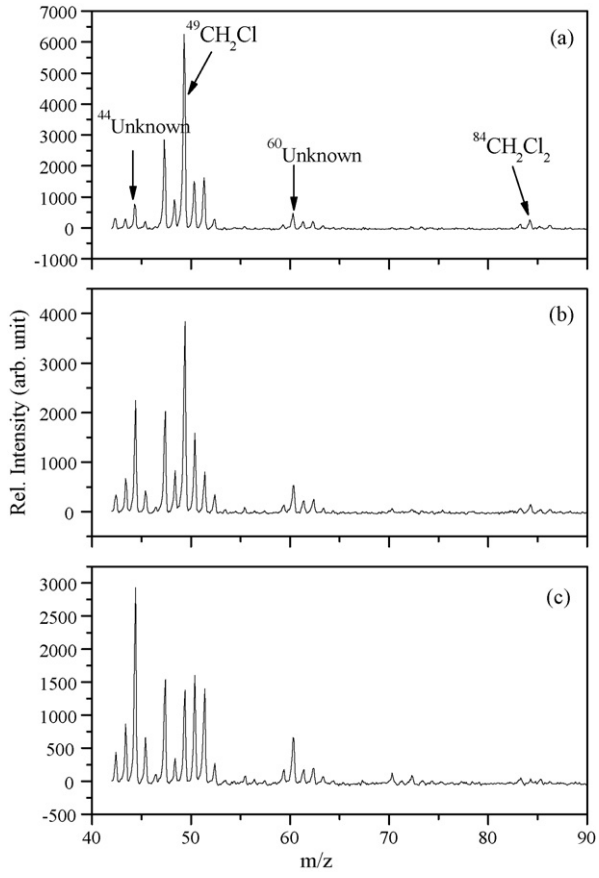

Fig. 8. Mass spectra of methylene chloride (CH_2Cl_2). The discharge current was (a) 350 V/15 mA, (b) 400 V/25 mA, or (c) 485 V/40 mA, and the other conditions were constant.

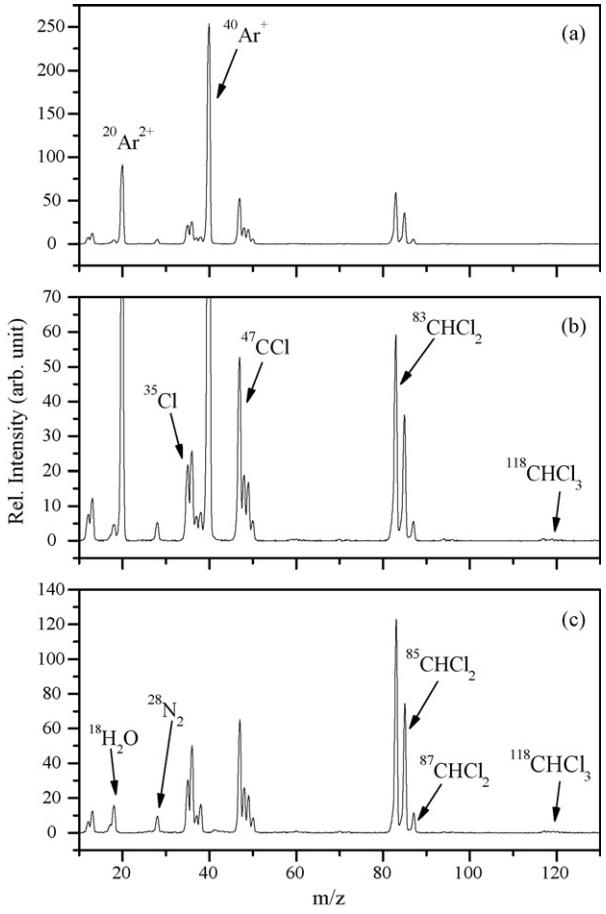

Fig. 9. Mass spectra of chloroform ($CHCl_3$). The discharge gas and conditions were as follows: (a) 460 V/11 mA (2.6 Torr of Ar) and (c) 400 V/10 mA (2.5 Torr of He), and (b) is three-times expanded in the intensity scale of the data (a).

shows a fragmentation pattern at discharge current of 10 mA. It was shown that the fragmentation pattern was almost the same as the reported data of the electron impact (EI) ionization [12], although the relative intensity of each peak was different from that of EI. As the current was increased, however, the intensities of the peaks of molecular ions and other fragment peaks were reduced (Fig. 7b). When the current increased up to 20 mA, the peaks of molecular ions and the peaks having higher masses disappeared, and only the fragment peaks of $^{26}C_2H_2$ and $^{39}C_3H_3$ remained. Furthermore, one could find that only the fragment peaks of toluene were much more decreased, but the peak intensity of $^{28}N_2$ is kept almost constant. It is known that, when the energy of electrons colliding with sample molecules decreases down to 70–35 eV, the peak intensity of the molecular ions increases; at the same time, the intensities of the fragment ions decrease. As mentioned above, we can expect that a little increase of the voltage with drastic variation of the current in the SPI source results in an increase of the number of electrons, with their energies unchanged. It is thus considered that variations of the current in the SPI source hardly affect the fragment pattern.

Fig. 8 shows mass spectra of methylene chloride (CH_2Cl_2) which were obtained by varying the current from 15 to 40 mA. As similar to the result of toluene (Fig. 7), the intensity of the molecular ion ($^{84}CH_2Cl_2$) decreased with increasing the current, and the intensity of the $^{49}CH_2Cl$ having the highest mass abundance among the fragments was also reduced. On the other hand, the intensities at the *m/z* 44 and 66 which was not found in the reference data of EI mass spectra increased with increasing the current. Since the mass chamber was kept at a pressure of 1×10^{-5} Torr, small amounts of H_2O and N_2 molecules could leak into the chamber. It is therefore expected that the fragment at 44 in *m/z* is identified to $^{44}C_2H_4O$, $^{44}C_3H_8$, $^{44}CO_2$, or $^{44}N_2O$, the position of 60 in *m/z* is $^{60}C_3H_8O$, $^{60}C_2H_8N_2$, $^{60}C_2H_4O_2$, $^{60}C_2HCl$, or $^{60}CH_4N_2O$. Though the origin of molecules in 44 and 66 *m/z* could not be determined definitely, it could be confirmed that the intensities of them increased by fragmentation of the molecular ion ($^{84}CH_2Cl_2$) and the main peak ($^{49}CH_2Cl$).

3.4. Characteristics of SPI-MS: variations of mass spectrum with discharge gases

Mass spectra of some organic compounds were investigated when changing the discharge gas. High purity (99.9999%) argon and helium gases were used as the discharge gas in this study. For comparison with the EI mass spectrum, the discharge current was adjusted to get similar spectrum patterns to the EI ionization source.

Fig. 9 shows mass spectra of chloroform ($CHCl_3$) when argon (Fig. 9a and b) or helium (Fig. 9c) was used as the discharge gas.

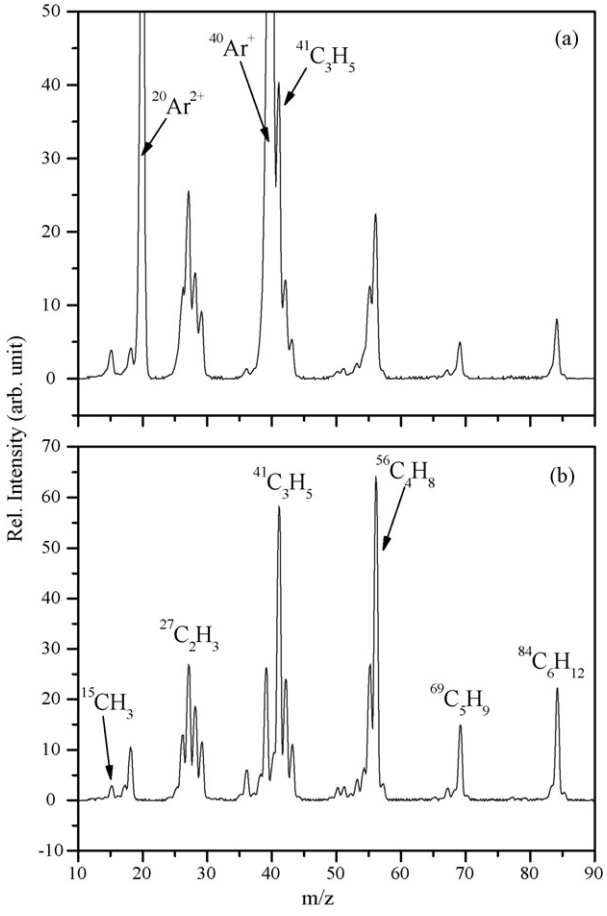

Fig. 10. Mass spectra of cyclohexane (C_6H_{12}). The discharge gas and conditions were as follows: (a) 340 V/10 mA (2.3 Torr of Ar) and (b) 435 V/10 mA (4.9 Torr of He).

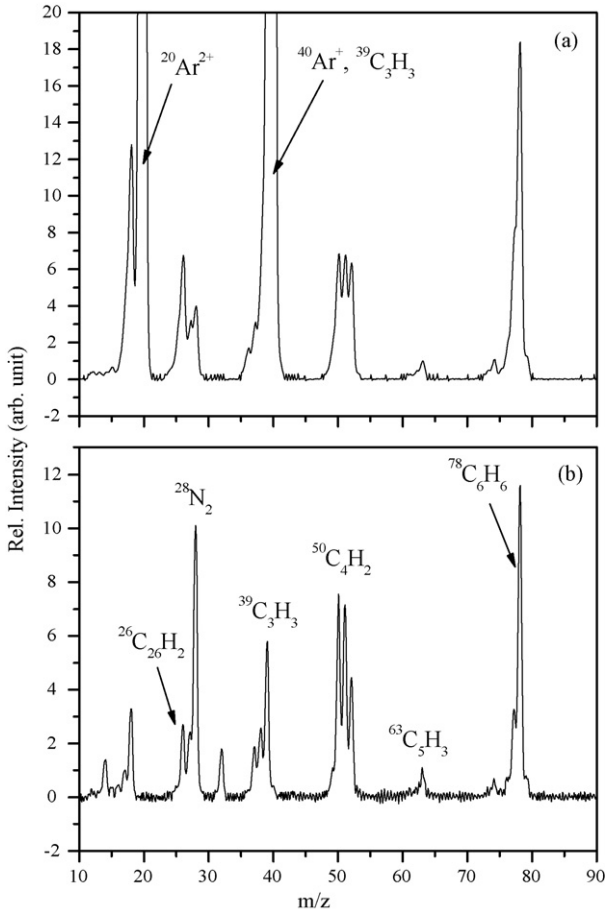

Fig. 11. Mass spectra of benzene (C_6H_6). The discharge gas and conditions were as follows: (a) 340 V/13 mA (2.6 Torr of Ar) and (b) 320 V/5 mA (2.0 Torr of He).

As shown in Fig. 9a, argon ion peaks ($^{40}Ar^+$, $^{20}Ar^{2+}$) may cause spectral interference in the argon discharge plasma since their intensities are much larger than the sample ions.

Fig. 9b shows a three-times expanded spectrum in the intensity scale, and the entire fragment of chloroform was measured well in the mass range not overlapping with argon ions. When helium was used as the discharge gas, it was found that the relative intensities of all the mass peaks were higher than those in the argon plasma (see Fig. 9c). In this case, the mass spectra could be analyzed more easily because the helium plasma yielded no spectral interference observed in the argon plasma where discharge conditions were employed at 460 V/11 mA, and in the helium discharge of 400 V/10 mA the spectrum pattern were in good agreement with EI mass spectra reported [12].

Mass spectra of cyclohexane (C_6H_{12}) and benzene (C_6H_6) were shown in Figs. 10 and 11, respectively. In the same manner of Fig. 9, argon (Figs. 10a and 11a) or helium (Figs. 10b and 11b) was used as the discharge gas, and the discharges were controlled as follows: 340 V/10 mA in argon discharge and 435 V/10 mA in helium discharge in case of cyclohexane, and 340 V/13 mA in argon discharge and 320 V/5 mA in helium discharge in case of benzene. The spectral interference clearly appeared ($^{40}Ar^+$ and $^{41}C_3H_5$ in Fig. 10a, $^{40}Ar^+$ and $^{39}C_3H_3$ in Fig. 11a) in both the mass spectra observed in the argon discharge. When helium was used as the discharge gas, fragments of the molecular ions were very clearly assigned, and the mass spectra patterns well agreed with the published data of the EI spectra.

In these results, the helium glow discharges are more suitable for ionization of organic compounds in SPI-MS since the argon discharges in some cases lead to spectral interference, and in addition the spectra provide faint intensities.

4. Conclusion

In this study, a glow discharge plasma designed under a new principle was produced by using a set of the anode and the mesh cathode. Because the design is based upon a conventional hollow cathode glow discharge, the voltage–current characteristics were similar each other. When the current of 50 mA was applied, molecular band spectra were observed, and in the helium discharge much more various spectra of molecules can be excited with higher sensitivity than in the argon discharge. It is expected that the helium discharge is more useful for ionization of molecular species, and the SPI source can be used as an ionization source for organic compounds.

The soft plasma ionization (SPI) source was successfully combined with a quadrupole mass analyzer. The mass spectra of some organic compounds were investigated with varying the dis-

charge current. Helium gas was more suitable for ionization of organic compounds in SPI-MS because the argon discharge gave strong molecular peaks ($^{40}Ar^{+}$, $^{20}Ar^{2+}$) which might cause to spectral interference and the analyte peaks have lower sensitivity. As our further study, the analytical performance of SPI-MS such as linearity, precision, reproducibility, sensitivity will be investigated. Since the SPI source can be used as an ionization of gaseous samples as well as solid samples, we consider that SPI-MS can be applied for various kinds of environmental analytical works.

References

[1] R.K. Marcus, J.A.C. Broekaert, Glow Discharge Plasmas in Analytical Spectroscopy, John Wiley and Sons, Chichester, 2003.
[2] D.P. Myers, M.J. Heints, P.P. Mahoney, G. Li, G.M. Hieftje, Appl. Spectrosc. 48 (1994) 1337.
[3] Y.X. Su, Z. Zhou, P.Y. Yang, X.R. Wang, B.L. Hung, Spectrochim. Acta, Part B 52 (1997) 633.
[4] C.M. Barshick, J.R. Eyler, J. Am. Soc. Mass Spectrom. 4 (1993) 387.
[5] J.L. Stephenson Jr., S.A. Mcluckey, Int. J. Mass Spectrom. Ion Processes 162 (1997) 89.
[6] J. Abian, J. Mass Spectrom. 34 (1999) 157.
[7] J.P. Guzowski Jr., J.A.C. Broekaert, S.J. Ray, G.M. Hieftje, JAAS 14 (1999) 1121.
[8] J.P. Guzowski Jr., G.M. Hieftje, JAAS 15 (2000) 27.
[9] M.A. Dempster, R.K. Marcus, JAAS 15 (2000) 43.
[10] K. Song, H. Cha, H. Park, S.C. Lee, Microchem. J. 70 (2001) 285.
[11] B.N. Chapman, Glow Discharge Process, John Wiley and Sons, New York, 1980.
[12] NIST/EPA/NIH Mass Spectral Database, U.S. Department of Commerce, 1992.

Available online at www.sciencedirect.com
ScienceDirect
Talanta 72 (2007) 1625–1629
Talanta
www.elsevier.com/locate/talanta

Determination of iodide in seawater using C30 column modified with polyoxyethylene oleyl ether in ion chromatography

Li Rong *, Lee Wah Lim, Toyohide Takeuchi

Department of Chemistry, Faculty of Engineering, Gifu University, 1-1 Yanagido, Gifu 501-1193, Japan

Received 9 November 2006; received in revised form 7 March 2007; accepted 12 March 2007
Available online 19 March 2007

Abstract

An ion chromatographic method for rapid and direct determination of iodide in seawater samples is reported. Separation was achieved using a laboratory-made C30 packed column (100 mm × 0.32 mm i.d.) modified with polyoxyethylene oleyl ether, with an aqueous solution of 300 mM sodium chloride as eluent and using UV detection at 220 nm. Samples containing iodate, nitrate, iodide and thiocyanate were eluted within 8 min, and the relative standard deviations of the retention time, peak area and peak height were all smaller than 4.19% for all of the analyte anions. Effects of eluent composition on retention behavior of inorganic anions have been investigated. Both cation and anion of the eluent affected the retention time of analytes. When inorganic eluents, such as ammonium chloride, ammonium sulfate, lithium chloride, sodium chloride, sodium sulfate, magnesium chloride and magnesium sulfate were used, the retention time of analytes increased with increasing eluent concentration. The limit of detection of iodide was 19 $\mu g\,l^{-1}$ (S/N = 3), while the limit of quantitation was 66 $\mu g\,l^{-1}$ (S/N = 10). The present method was successfully applied to the rapid and direct determination of iodide in seawater samples.

Keywords: Ion chromatography; Polyoxyethylene oleyl ether stationary phase; C30 modified stationary phase; Iodide; Seawater

1. Introduction

Iodine is one of the most abundant and biologically essential minor elements in seawater, where it exists mainly as iodide and iodate [1–4] along with a small fraction of organic iodine compounds [5]. Iodide, a thermodynamically unstable species in the oceans, is produced by biologically mediated reduction of iodate, also favorable under reducing conditions [6,7]. In addition, determination of iodide and iodate in environmental samples attracts more attention because iodine may play a role in taste and odor problems [8]. In fact, the concentrations of iodine and iodide are usually very low in seawater except coast, estuary and bay water [9], where the pollution due to human activities is unavoidable. In some seawater samples, the concentrations of iodide were determined to be 48–60 $\mu g\,l^{-1}$ [10]. Thus, the distribution of iodide gives clues for understanding the marine chemistry, and the determination of iodine in seawater has long been an essential task in marine chemistry.

Up to now, a number of analytical methods, such as inductively coupled plasma mass spectrometry (ICPMS) [11], radiochemical neutron activation analysis [9,12,13] and capillary electrophoresis [14–16] have been proposed for the direct determination of trace iodide in seawater. ICPMS and radiochemical neutron activation analysis for the determination of iodide can achieve the required sensitivity and accuracy. However, some means of preliminary separation are required and none of the two techniques are easily accessible due to the high level of specialization needed and high cost of the instrument and maintenance [17]. Capillary electrophoresis is a powerful tool for the determination of iodide, but its concentration sensitivity is not enough to apply to less concentrated samples [14].

Two factors are essential in order to attain good sensitivity: (1) separation of iodide from an excess of anions in seawater and (2) highly sensitive detection of iodide. Recently, attention has been paid to ion chromatography (IC) as a simple method for determination of trace iodide in seawater [4,10,18–21]. But, IC method for iodide analysis at trace levels in seawater faces the difficulty of ion separation in high matrix concentrations of chloride and sulfate from the much smaller iodide peak [4,22], thus, some IC methods use the addition of sodium chloride to

* Corresponding author. Tel.: +81 58 293 2815; fax: +81 58 230 1893.
E-mail address: kathyrong@gmail.com (L. Rong).

0039-9140/$ – see front matter © 2007 Elsevier B.V. All rights reserved.
doi:10.1016/j.talanta.2007.03.017

the mobile phase to remove interferences by the variability in the composition of inorganic matrix ions. In our previous studies [23,24], it was showed that 300 mM sodium sulfate in the presence of 50 mM sodium chloride was effective for the separation of iodide in seawater, due to faster elution of an excess of matrix anions in seawater and slow elution of iodide with hydrophobicity on modified C30 columns. However, these dynamically modified columns could be used for only ca. 2 weeks, because the modifier was gradually flushed away by eluent during the experiment.

In the present study, we tried to develop a new stationary phase for simple and direct determination of iodide in seawater using a laboratory-made C30 packed stationary phase modified with polyoxyethylene oleyl ether (POEOE). Due to an extra hydrophobic oleyl bond, POEOE is more hydrophobic than PEG and it was expected POEOE has a stronger hydrophobic interaction with C30, which could lead to longer stability. For better resolution, the modification conditions of POEOE onto hydrophobic C30 stationary phases as well as the eluent conditions are examined in this paper. It should be noted that the determination of iodide in seawater sample will be successful when the eluent containing high concentration of chloride can be used as the eluent.

2. Experimental

2.1. Apparatus

A μIC system was comprised from an MF-2 Micro Feeder (Azumadenkikogyo, Tokyo, Japan) equipped with an MS-GAN 050 gas-tight syringe (0.5 ml; Ito, Fuji, Japan) as a pump, a model 7520 injector with an injection volume of 0.2 μl (Rheodyne, Cotati, CA, USA), a 100 mm × 0.32 mm i.d. microcolumn and a UV-2070 plus UV–vis detector (Jasco, Tokyo, Japan). The flow-rate of the pump was kept at 2.1 μl min^{-1} and the UV detector was operated at 220 nm. The data were acquired by a Chromatopac C-R7Ae plus data processor (Shimadzu, Kyoto, Japan).

2.2. Reagents

The reagents employed were of guaranteed reagent grade and were obtained from Nacalai Tesque (Kyoto, Japan), unless otherwise noted. POEOE was obtained from Wako Chemical. Purified water was produced in the laboratory by using a GS-590 water distillation system (Advantec, Tokyo, Japan). All solutions used in this study were prepared using the purified water and filtered through a 0.45 μm membrane filter and stored at 4 °C in a refrigerator before use.

2.3. Column preparation

On the basis of our previous work [23], poly(ethylene glycol) (PEG) can be fixed on appropriate hydrophobic adsorbents, such as C30. Since C30 is comparatively hydrophobic, it is expected that PEG adsorbed on the C30 stationary phase is more stable, and C30 stationary phases possess another advantage that the retention time of analytes is stable even when aqueous solution, such as pure water is used as the eluent. This is because, aqueous eluent is not excluded from mesopores of C30 packing materials during the operation [25].

Fused-silica capillary was packed with 5 μm C30 (Nomura Chemical, Seto, Japan) by using a slurry packing method as previously reported [26], and then conditioned with purified water. An aqueous solution containing POEOE was then passed into the fused-silica capillary at a flow-rate of 2.1 μl min^{-1} for ca. 2 h, followed by washing with purified water for ca. 30 min to remove the remaining POEOE until the baseline was stabilized. The concentration of POEOE dissolved in water as the modification solution was examined. The column was operated at room temperature (ca. 25 °C).

3. Results and discussion

3.1. Effect of modification conditions

UV-absorbing anions, such as iodate, nitrate, iodide and thiocyanate were chosen as the test analytes for this study, and 100 mM sodium sulfate was chosen as the mobile phase. To begin with, effect of concentration of POEOE was examined. Fig. 1 shows the separation of authentic mixture of UV-absorbing anions on the laboratory-made C30 packed column modified with different concentration of POEOE aqueous solution. Iodide ion was completely separated from the anions IO_3^-, NO_3^- and SCN^-, and the elution order of anions, $IO_3^- < NO_3^- < I^- < SCN^-$, was the same as that observed in common ion chromatography. The retention time decreased with increasing POEOE concentration up to 10% (w/v). Higher concentration of POEOE was not tried because of its higher viscosity.

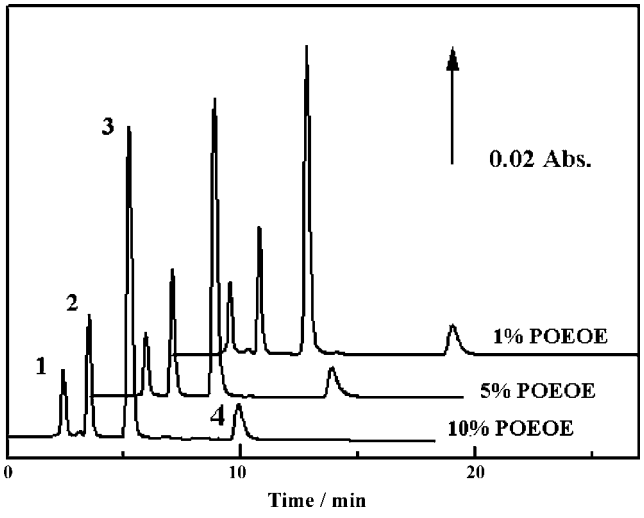

Fig. 1. Separation of authentic mixture of UV-absorbing anions on the laboratory-made C30 packed column (100 mm × 0.32 mm i.d.) modified with POEOE aqueous solution. Column: C30 modified with 1, 5 and 10% POEOE; eluent: 100 mM sodium sulfate; wavelength: 220 nm; flow-rate: 2.1 μl min^{-1}; injection volume: 0.2 μl; peaks: 1 iodate, 2 nitrate, 3 iodide and 4 thiocyanate; analyte concentration: 0.2 mM each.

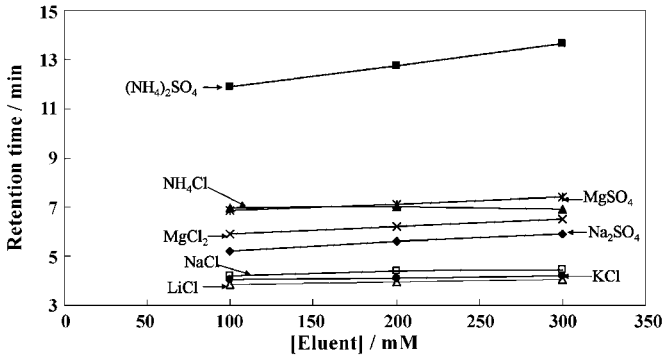

Fig. 2. Retention time of iodide as a function of the eluent concentration. Column: laboratory-made C30 packed column (100 mm × 0.32 mm i.d.) modified with 10% POEOE; eluent: ammonium chloride, ammonium sulfate, lithium chloride, sodium chloride, sodium sulfate, magnesium chloride or magnesium sulfate, as indicated; flow-rate: 2.1 μl min^{-1}; injection volume: 0.2 μl; analyte: 0.2 mM sodium iodide; wavelength of UV detection: 220 nm.

Since the C30 column modified with 10% POEOE provided the best separation result, C30 columns were modified with 10% POEOE in the following experiments. In the case of iodide, the wavelength is also important. The UV spectrum of iodide indicates two main absorption peaks at 194 and 226 nm. Since nitrate and iodate were found to have maximum absorption peaks at 210 nm [17,10], and considering thiocyanate ion, the wavelength of 220 nm was chosen for the measurement of iodide. Actually, larger signal intensities were obtained at 220 nm for iodide compared to the detection at 210 nm.

3.2. Optimization of eluent for anion separation

In IC, retention and selectivity vary as the extent of the interaction between the eluent ion and the stationary phase. Eluent concentration is one of the most important parameters affecting the retention [27]. Fig. 2 shows the retention behavior of iodide on the laboratory-made C30 packed column modified with 10% POEOE using different eluents. It can be seen that both cation and anion of the eluent affect the retention time of iodide. When inorganic eluents, such as ammonium chloride, ammonium sulfate, lithium chloride, sodium chloride, sodium sulfate, magnesium chloride and magnesium sulfate were used, the retention time of iodide increased with increasing eluent concentration.

The retention time of iodide depends on the combination of the eluent anion and eluent cation. Sulfate and chloride as the eluent anion had a tendency to achieve longer retention time for iodide in this order when ammonium and sodium were chosen as the eluent cations. The elution order of iodide coincides with the order of the hydration strength of anion, e.g., sulfate > chloride. In other words, the larger the hydration strength of the counter anion, the larger is the retention time. On the contrary, sodium eluent cation provided smaller retention times than ammonium eluent cation when sulfate and chloride were chosen as the counter eluent anions. The retention time of iodide when magnesium was chosen as the eluent cation, was between the retention times when ammonium and sodium were chosen as the eluent cations. It should be noted that the hydration strength of the above cations is sodium > ammonium > magnesium. It can be concluded that the strongly hydrated eluent cation provides smaller retention time, and unexpected result in the case of magnesium is because of its different charge.

In Hofmeister series, SO_4^{2-} and Cl^- are known as salting-out, water-structure-maker or cosmotropic ions; they compete for water at various interfaces, leading to dehydration of the stationary phase [28,29]. This in turn means that the C30 modified stationary phase becomes more hydrophobic with increasing salt concentration. In addition, since SO_4^{2-} has much more salting-out ability than Cl^- [26], there was a marked increase in retention of analytes when SO_4^{2-} was used as the eluent anion compared with the case for Cl^-. On the other hand, since eluent anions generally give stronger Hofmeister effects than eluent cations, slight difference of retention time of iodide was observed for lithium chloride, sodium chloride and potassium chloride.

According to Fig. 2, ammonium sulfate gives larger retention time. Although, ammonium sulfate is expected to achieve better resolution, according to the separation results of analyte anions using these different eluents, 300 mM sodium chloride provided the best resolution, so 300 mM sodium chloride was selected as the eluent to determine iodide ion in seawater.

From the above studies, the final experimental conditions were separation column, C30 modified with 10% POEOE; eluent, 300 mM sodium chloride; flow-rate, 2.1 μl min^{-1}; and wavelength, 220 nm. Fig. 3 demonstrates the separation of four UV-absorbing anions. It can be seen that iodide is eluted in ca. 4.5 min and well separated from nitrate and thiocyanate.

The repeatability of the retention time, peak area and peak height was examined under the conditions in Fig. 3, for six successive chromatographic runs. The results are given in Table 1. From the table, it can be seen that the relative standard deviations (R.S.D.s, for six successive chromatographic runs) of the retention time, peak area and peak height were all smaller than 4.19%

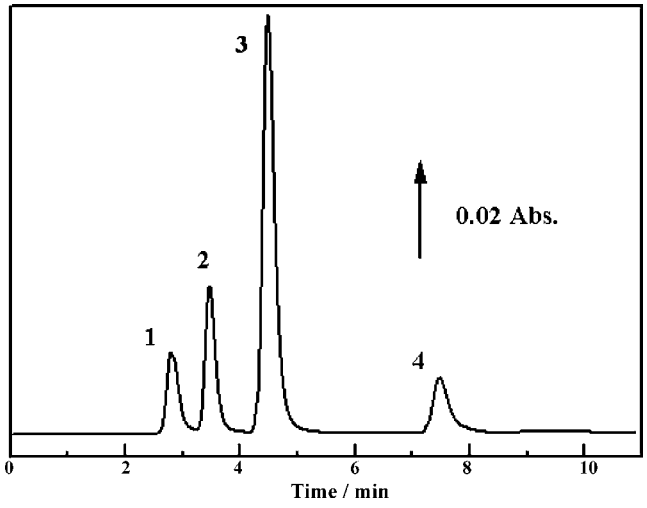

Fig. 3. Separation of authentic mixture of UV-absorbing anions on the laboratory-made C30 packed column (100 mm × 0.32 mm i.d.) modified with 10% POEOE aqueous solution. Eluent: 300 mM sodium chloride; peaks: 1 iodate, 2 nitrate, 3 iodide and 4 thiocyanate; analyte concentration: 0.2 mM each. Other operating conditions as in Fig. 2.

Table 1
Repeatability for test analyte anions

	R.S.D. (%, $n=6$)		
	Retention time	Peak area	Peak height
IO_3^-	1.68	3.67	1.34
NO_3^-	1.73	3.41	1.81
I^-	1.66	4.19	1.05
SCN^-	1.40	3.31	1.02

Column: laboratory-made C30 packed column (100 mm × 0.32 mm i.d.) modified with 10% POEOE aqueous solution; analyte: iodate, nitrate, iodide and thiocyanate; analyte concentration: 0.2 mM each. Other operating conditions as in Fig. 3.

for all of the analyte anions. These values show comparatively satisfactory repeatability of the present method.

In addition, the modified column could be used for about 1 month (8 h day^{-1}). Spent columns can easily be regenerated by passing 50% aqueous acetonitrile solution, followed by passing POEOE solution.

3.3. Validation and application

To illustrate an application of the developed method, seawater samples collected from Izu (Shizuoka, Japan) and Waikiki (Honolulu, HI, USA) were used for the determination of iodide. These seawater samples were applied to the determination within a few days after the sampling. After filtration through a 0.45-μm membrane filter, the samples were stored at 4 °C in a refrigerator and directly subjected to ion chromatographic analysis. Under the conditions in Fig. 3, a peak due to iodide was actually observed for the seawater sample, as demonstrated in Fig. 4. Despite the fact that the seawater samples contained molar concentration of chloride and sulfate which were greatly in excess of the eluent concentration of chloride, the retention of these analyte ions was very small and have no interference on the determination of iodide ion and a large peak preceding the iodide peak is thought to be due to the matrix ion effect.

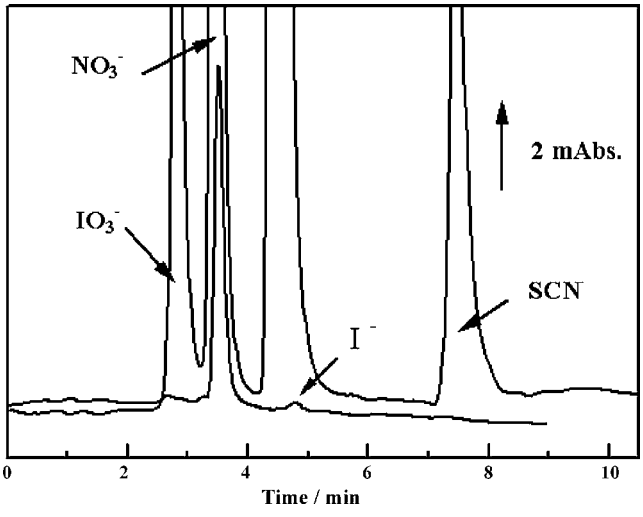

Fig. 4. Separation of authentic mixture of UV-absorbing and iodide in seawater sample using 300 mM sodium chloride. Upper trace: 0.2 mM each of iodate, nitrate, iodide and thiocyanate and lower trace: 0.2 μl seawater. Operating conditions as in Fig. 3.

Table 2
Iodide concentration and recovery in seawater samples

Seawater sample	Iodide (μg l^{-1})	Recovery (%)
Izu	~69	101.2
Waikiki	~102	99.6

Operating conditions as in Fig. 3.

Iodide contained in the seawater sample was determined to be 69 and 102 μg l^{-1} for Izu and Waikiki seawater, respectively, by using a standard addition method. The recoveries of added iodide's peak were 101.2 and 99.6% for these spiked seawater samples, as shown in Table 2. In addition, nitrate in seawater could not be determined because, bromide and nitrate eluted close and could not be separated.

Under the optimized operating conditions in Fig. 3, the limit of detection of iodide was 19 μg l^{-1} (calculated from a signal-to-noise ratio of 3) and the limit of quantitation of iodide was 66 μg l^{-1} (calculated from a signal-to-noise ratio of 10). Peak height (H) was linear with the concentration (c) in the range of 66 μg l^{-1} to 25 mg l^{-1} and calibration equation for peak height by IC was $H = 361.87c + 0.0055$, while the regression coefficient (r^2) was 0.9998.

3.4. Conclusion

A simple, rapid and direct ion chromatographic method has been described for the determination of anions within 8 min, using laboratory-made C30 packed column (100 mm × 0.32 mm i.d.) modified with 10% POEOE aqueous solution. Since, when 300 mM sodium chloride was used as the eluent, there was no interference of matrix ions on the determination of iodide ion in seawater, it was presumed that determination of iodide ion in seawater samples using this proposed IC system was possible. Further improvement of the limit of detection will be necessary for the determination of lower concentration of iodide in seawater due to the fact that iodide concentration decreases steeply with an increase in depth. In addition, further research utilizing the oleyl bond on this dynamically modified stationary phase is in view.

References

[1] E. Nakayama, T. Kimoto, S. Okazaki, Anal. Chem. 57 (1985) 1157.
[2] G.T.F. Wong, Rev. Aquat. Sci. 4 (1991) 45.
[3] C.B. Swartz, W.J. Ullman, Anal. Chem. 60 (1988) 1721.
[4] K. Ito, Anal. Chem. 69 (1997) 3628.
[5] V.W. Truesdale, Mar. Chem. 3 (1975) 111.
[6] M.L.A.M. Campos, Mar. Chem. 57 (1997) 107.
[7] A.M. Farrenkopf, M.E. Dollhopy, S. NiChadhain, G.W. Luther, K.H. Nealson, Mar. Chem. 57 (1997) 347.
[8] B. López-Ruiz, J. Chromatogr. A 881 (2000) 607.
[9] X. Hou, H. Dahlgaard, B. Rietz, U. Jacobsen, S.P. Nielsen, A. Aarkrog, Anal. Chem. 71 (1999) 2745.
[10] C. Sankaran, V. Bhavaniamma, K. Satrugnan, Mikrochim. Acta 128 (1998) 75.
[11] M. Haldimann, B. Zimmerli, C. Als, H. Gerber, Clin. Chem. 44 (1998) 817.

[12] X.L. Hou, H. Dahlgaard, B. Rietz, U. Jacobsen, S.P. Nielsen, J. Radioanal. Nucl. Chem. 244 (2000) 87.
[13] J.R.W. Woittiez, H.A. Van der Sloot, G.D. Wals, B.J.T. Nieuwendijk, J. Zonderhuis, Mar. Chem. 34 (1991) 247.
[14] K. Ito, T. Ichihara, H. Zhuo, K. Kumamoto, A.R. Timerbaev, T. Hirokawa, Anal. Chim. Acta 497 (2003) 67.
[15] T. Hirokawa, T. Ichihara, K. Ito, A.R. Timerbaev, Electrophoresis 24 (2003) 2328.
[16] K. Yokota, K. Fukushi, N. Ishio, N. Sasayama, Y. Nakayama, S. Takeda, S. Wakida, Electrophoresis 24 (2003) 2244.
[17] H.-B. Li, F. Chen, X.-R. Xu, J. Chromatogr. A 918 (2001) 335.
[18] W.Z. Hu, P.-J. Yang, K. Hasebe, P.R. Haddad, K. Tanaka, J. Chromatogr. A 956 (2002) 103.
[19] K. Ito, T. Hirokawa, Anal. Sci. 17 (2001) 579.
[20] W.Z. Hu, K. Hasebe, K. Tanaka, P.R. Haddad, J. Chromatogr. A 850 (1999) 161.
[21] W.Z. Hu, P.R. Haddad, K. Hasebe, K. Tanaka, P. Tong, Anal. Chem. 71 (1999) 1617.
[22] K. Ito, J. Chromatogr. A 830 (1999) 211.
[23] L. Rong, T. Takeuchi, J. Chromatogr. A 1042 (2004) 131.
[24] L. Rong, L.W. Lim, T. Takeuchi, Chromatographia 61 (2005) 371.
[25] N. Nagae, T. Enami, S. Doshi, LCGC 20 (2002) 964.
[26] T. Takeuchi, D. Ishii, J. Chromatogr. 213 (1981) 25.
[27] Safni, T. Takeuchi, J. Chromatogr. A 850 (1999) 65.
[28] F. Hofmeister, Arch. Exp. Pathol. Pharmakol. (Leipzig) 24 (1888) 247.
[29] E. Leontidis, Curr. Opin. Colloid Int. Sci. 7 (2002) 81.

Available online at www.sciencedirect.com
ScienceDirect
Talanta 72 (2007) 1609–1617
Talanta
www.elsevier.com/locate/talanta

Sequential-injection on-line preconcentration using chitosan resin functionalized with 2-amino-5-hydroxy benzoic acid for the determination of trace elements in environmental water samples by inductively coupled plasma-atomic emission spectrometry

Akhmad Sabarudin [a], Narong Lenghor [a], Mitsuko Oshima [a], Lukman Hakim [a], Toshio Takayanagi [a], Yun-Hua Gao [b], Shoji Motomizu [a,*]

[a] *Department of Chemistry, Faculty of Science, Okayama University, Tsushimanaka 3-1-1, Okayama City 700-8530, Japan*
[b] *Technical Institute of Physics and Chemistry, Chinese Academy of Sciences (CAS), Add. No. 2 Beiyitiao Zhongguancun, Beijing 100080, China*

Received 30 October 2006; received in revised form 8 January 2007; accepted 9 January 2007
Available online 18 January 2007

Abstract

A new chelating resin using chitosan as a base material was synthesized. Functional moiety of 2-amino-5-hydroxy benzoic acid (AHBA) was chemically bonded to the amino group of cross-linked chitosan (CCTS) through the arm of chloromethyloxirane (CCTS-AHBA resin). Several elements, such as Ag, Be, Cd, Co, Cu, Ni, Pb, U, V, and rare earth elements (REEs), could be adsorbed on the resin. To use the resin for on-line pretreatment, the resin was packed in a mini-column and installed into a sequential-injection/automated pretreatment system (Auto-Pret System) coupled with inductively coupled plasma-atomic emission spectrometry (ICP-AES). The sequential-injection/automated pretreatment system was a laboratory-assembled, and the program was written using Visual Basic software. This system can provide easy operation procedures, less reagent consumption, as well as less waste production.

Experimental variables considered as effective factors in the improvement sensitivity, such as an eluent concentration, a sample and an eluent flow rate, pH of samples, and air-sandwiched eluent were carefully optimized. The proposed system provides excellent on-line collection efficiency, as well as high concentration factors of analytes in water samples, which results in highly sensitive detection of ultra-trace and trace analysis. Under the optimal conditions, the detection limits of 24 elements examined are in the range from ppt to sub-ppb levels. The proposed method was validated by using the standard reference material of a river water, SLRS-4, and the applicability was further demonstrated to the on-line collection/concentration of trace elements, such as Ag, Be, Cd, Co, Cu, Ni, Pb, U, V, and REEs in water samples.

Keywords: Sequential-injection; On-line preconcentration; Trace elements; ICP-AES; Chitosan resin

1. Introduction

Chelating resins are often used for the preconcentration, separation, and recovery of metal in analytical chemistry. The development of novel chelating resins for solid phase extraction (SPE) is very opportune because of its reliability, excellent metal loading capacity, and adsorption ability [1]. Pretreatment of aqueous samples with chelating resin as SPE can provide several advantages: high enrichment/collection factors, better removal of interferent ions, high performance and rate of reaction process, and the possibility of the combination with several detections methods [2]. Chelating resins can be synthesized by chemically immobilizing appropriate chelating agents on polymeric supports. Polystyrene functionalized with 2,5-dimercapto-1,3,4-thiodiazole [3], dithiocarbamate [4], maleic acid [5], 2-(α-hydroxymethyl) benzimidazole [6], bis(2-benzimidazolylmethyl)amine [7], 2-napthol-3,6-disulfonic acid [8], glucosamine [9] have been reported so far for the adsorption of several metal ions. Commercially available resins of Amberlite series have been widely used as a polymeric support for designing chelating resins. Amberlite XAD-2 functionalized with pyrochatechol [10], chromotropic acid [11], and

* Corresponding author. Tel.: +81 86 251 7846; fax: +81 86 251 7846.
E-mail address: motomizu@cc.okayama-u.ac.jp (S. Motomizu).

0039-9140/$ – see front matter © 2007 Elsevier B.V. All rights reserved.
doi:10.1016/j.talanta.2007.01.024

o-aminophenol [12] were applied as a collector for Cu, Co, Cd, Ni, and Zn. Ambelite XAD-4 functionalized with bicine [13], and *o*-vanillinsemicarbazone [14] has been used for preconcentration and separation of rare earth elements (REEs), U, and Th, whereas Amberlite XAD-4 possessing salen moiety [15] was applied to the separation and determination of Cu, Pb, and Bi. Amberlite XAD-16 resins modified with phosphonic acid derivatives [16–18] have reported as a selective collector for U, Th, and La. Epoxy-polyamide chelating resins have been applied to the preconcentration and separation of trace Ga, In, Bi, V, Cr, and Ti [19], as well as the collection/concentration of trace noble metals [20].

Chitosan, one of the most abundant biomass, has been found to be an excellent base material compared to other natural polymers, activated sludge, synthetic polymer, etc. The use of chitosan as solid support for an ion exchange and a chelating resin is increasing due to its advantages, such as easy derivatization of its amino groups and more hydrophilic than such synthetic base materials as polystyrene-divinylbenzene, polyethylene, and polyurethane [21–22]. These advantages provide fast reaction rate, as well as fast in sorption kinetics of analyte species. However, chitosan can easily dissolve in acidic solutions due to the protonation of its amino groups. Therefore, cross-linking agents such as ethyleneglycoldiglycidylether (EGDE) and glutaraldehyde [23–24] were used for improving its chemical stability and mechanical strength. By using the cross-linked chitosan (CCTS) as a polymeric support, chitosan-based chelating resins possessing such moieties as iminodiacetate [22], leucine [25], serine [26], imino di(methyl phosphonic acid) [27], *N*-methyl-D-glucamine [28], and 3,4-diaminobenzoic acid [29] were synthesized for the collection/concentration of trace elements.

Several chelating resins mentioned above can provide several advantages for the improving sensitivity and selectivity in trace metal analysis. However, the operations are usually very tedious because it is performed manually in batch method. Stringent control of the laboratory environment is also required to avoid sample contamination when trace and ultra-trace detection levels are attempted. Such situations can be overcome by utilizing on-line preconcentration procedures using functionalized solid materials coupled with flow-based (FB)-spectroscopic detection system [1,30–37]. By employing an on-line system, such general drawbacks of batchwise preconcentration procedures were mostly eliminated. In addition, the reagent consumption is reduced to a few percent of the usual manner, and the requirements on the laboratory environment for trace analysis are much less stringent.

A sequential-injection analysis (SIA) comes next to the continous-flow analysis concept. SIA is very useful for improving tedious and time-consuming pretreatment of samples prior to the measurement, because it is more robust and versatile, and is characterized by the use of discrete volumes and variable-flow conditions throughout the analytical cycle [38]. A sequential-injection/ICP-MS method in combination with on-line solvent extraction for the determination of lead was reported by Wang and Hansen [39]. Although the method is very sensitive, the use of organic solvent, methyl isobutyl keton (MIBK), could not be avoided. Sequential-injection/anodic stripping voltammetry [40–41] allows simultaneous determination of Pb, Cu, Cd, and Zn. However, because of the detection limits are several 10 ppb levels, it could not be applied to the determination of trace elements in natural water samples.

In this work, the chitosan resin cross-linked with EGDE (CCTS) was chemically modified by combining hydroxyl group of 2-amino-5-hydroxy benzoic acid (AHBA) moiety to the amino group of chitosan through the arm of chloromethyloxirane (CCTS-AHBA resin). Then, the resin was packed in a mini-column, which was utilized as an on-line preconcentration device. The mini-column was installed into the laboratory-assembled sequential-injection/automated pretreatment system (Auto-Pret System) coupled with inductively coupled plasma-atomic emission spectrometry (ICP-AES) for the collection/concentration and determination of Ag, Be, Cd, Co, Cu, Ni, Pb, U, V, and REEs in water samples. Experimental variables considered as effective factors for improving detection sensitivity, such as an eluent concentration, a flow rate of eluent, a sample flow rate, pH of samples, and air-sandwiched eluent, were carefully optimized. The proposed system can provide excellent on-line collection efficiency, less reagent consumption compared to conventional flow-based method, and high sensitivity (several ppt level LOD of some analytes), as well as excellent separation efficiency of the analytes from commonly existing matrices in water samples.

2. Experimental

2.1. Apparatus

An ICP-AES system (Vista Pro, Seiko Instruments, Chiba, Japan) was used for the measurement of Ag, Be, Cd, Co, Cu, Ni, Pb, U, V, and REEs. The operating conditions of ICP-AES were summarized in Table 1. The ICP-AES was coupled with a laboratory-assembled Auto-Pret System, which consists of a syringe pump (SP: Cavro, San Jose, CA, USA) with volumes of 2.5 ml, a 6-port selection valve (SL: Hamilton, Reno, NV, USA), and a 6-way switching valve (SV: Hamilton, Reno). The pump, valves, as well as ICP-AES, were fully controlled by a computer. The program for Auto-Pret System was written using Visual Basic software. The manifold of the Auto-Pret System

Table 1
Operating conditions of ICP-AES

Spectrometer	VISTA PRO
Plasma conditions	
RF power	40 MHz, 1.2 kW
Plasma gas flow rate (l min^{-1})	Ar 15.0
Auxiliary gas flow rate (l min^{-1})	Ar 1.50
Nebulizer gas flow rate (l min^{-1})	Ar 0.75
Spray chamber	Glass cyclonic spray chamber
Nebulizer	K-style concentric glass nebulizer
Torch	One-piece low flow extended torch in the axial view mode
Data acquision	
Measurement mode	Time scan mode

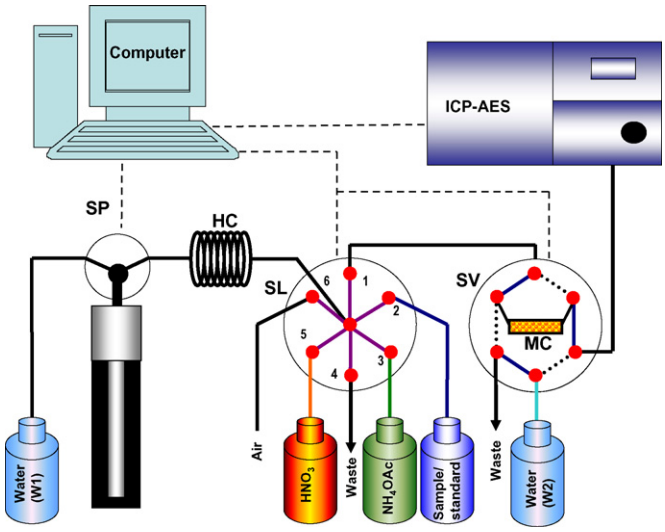

Fig. 1. Laboratory-assembled sequential-injection automated pretreatment system (Auto-Pret System) for on-line preconcentration and determination of trace elements (at inject position). SP, syringe pump; SL, selection valve; SV, switching valve; MC, mini-column (40 mm × 2 mm i.d.) packed with CCTS-AHBA resin; HC, holding coil.

used in this work was shown in Fig. 1. The PTFE tubing (0.8 mm i.d.) was used for assembling all flow lines except for a holding coil (2 mm i.d.). In the proposed system, only water flows continuously by using peristaltic pump fixed in ICP-AES, whereas the consumption of other reagents depends on the optimized volumes, which result in much less reagent consumption compared to conventional batchwise method.

The laboratory-made mini-column was prepared from PTFE tubing with the volume of about 0.13 ml (2 mm i.d. × 4 cm length), which corresponds to about 26 mg of CCTS-AHBA resin. This column was equipped with the plugs of quartz wool at both ends of the tubing to keep CCTS-AHBA resin in the column.

An automated titration system, Model AT-510 (Kyoto Electronics Manufacturing Co., Kyoto, Japan), was used for the acid-base titration for the estimation of the pKa values of CCTS-AHBA resin synthesized. Infrared spectra (4000–400 cm^{-1}) were taken by KBr pellet method using a FT/IR-4100 spectrometer (JASCO Co., Tokyo, Japan).

2.2. Reagents and solutions

Flake-type chitosan and 2-amino-5-hydroxy benzoic acid were purchased from Tokyo Kasei Co. Ltd. (Tokyo, Japan). Chitosan flakes were ground to fine pieces and sieved to obtain chitosan particles of 100–300 μm. All other reagents used for the synthesis of CCTS-AHBA resin were of analytical reagent grade.

The standard reference material of river water (SLRS-4) was issued by National Research Council Canada (NRCC).

Working solutions of multi-element standard solutions were prepared by diluting several kinds of a single element standard solution for atomic absorption spectrometry (1000 ppm, Wako Pure Chemicals, Osaka, Japan) and a multi-element standard solution for ICP-MS; XSTC-13 and XSTC-1 (10 ppm, Spex CertiPrep Inc., NJ, USA), and by mixing them together. The XSTC-13 contains 31 elements of Th, Ag, Al, As, Ba, Be, Bi, Ca, Cd, Co, Cr, Cs, Cu, Fe, Ga, In, K, Li, Mg, Mn, Na, Ni, Pb, Rb, Se, Sr, TL, V, Zn, U, and Hg, whereas XSTC-1 contains 16 elements of Ce, Dy, Er, Eu, Gd, Ho, La, Lu, Nd, Pr, Sm, Sc, Tb, Tm, Yb, and Y. The mixed standard solutions were then adjusted to desired concentration and pH before introducing to Auto-Pret System.

Acetic acid (minimum 96%) and ammonia water (29%) used for the preparation of ammonium acetate solution were of an electronic industrial reagent grade (Kanto Chemicals, Tokyo, Japan). The solutions were used for adjusting pH from 3 to 9. Diluted nitric acid (ultrapure grade, 60%, density 1.38 g ml^{-1}, Kanto Chemicals) was used for adjusting pH 1–2 of samples. Ultrapure water (18.3 MΩ cm^{-1} resistivity) prepared by an Elix 3/Milli-Q Element system (Nihon Millipore, Tokyo, Japan) was used throughout.

2.3. Preparation of CCTS-AHBA resin

The CCTS-AHBA resin was synthesized through three steps. In the first step, the cross-linked chitosan with the arm of chloromethyloxirane was synthesized in a similar manner as in the previous works [25–28]. In the second step, the amino group of 2-amino-5-hydroxy benzoic acid moiety was protected by treating 10 g of AHBA with 20 g of benzaldehyde in 20 ml of methanol: the mixture was stirred for 12 h at room temperature. Then, the CCTS with the arm of chloromethyloxirane (5 g) and the AHBA protected-amino group were suspended in dioxane (100 ml), and to this suspension, 2 M NaOH (40 ml) was added. The mixture was refluxed for 3 h in order to couple hydroxy phenolic group of AHBA with chloro terminal of the arm of CCTS. In the last step, the protection group (benzaldehyde), which was condensed with amino groups of AHBA, was removed by stirring the product in 100 ml of 0.5 M HCl for 12 h at room temperature: this procedure was repeated two times. Then, the product (CCTS-AHBA) was filtered on the glass filter and washed with methanol and water. The synthesis scheme of this resin was shown in Fig. 2. Before being packed in mini-column as on-line preoncentration device, the CCTS-AHBA resin was cleaned up by stirring at low speed for 3 h in 2 M nitric acid followed by washing with ultrapure water.

2.4. Operating procedures for on-line collection/concentration of trace elements

The whole procedure run through four steps, during which the carrier (ultrapure water) is pumped continuously into the ICP-AES by a peristaltic pump fixed in the ICP-AES system.

Step 1. Column conditioning: in this step, SV is in load position, and SP is set up to aspirate 1000 μl (at flow rate of 100 μl s^{-1}) of 0.5 M ammonium acetate buffer (NH_4OAc, pH 7) into HC via the port 3 of SL, which

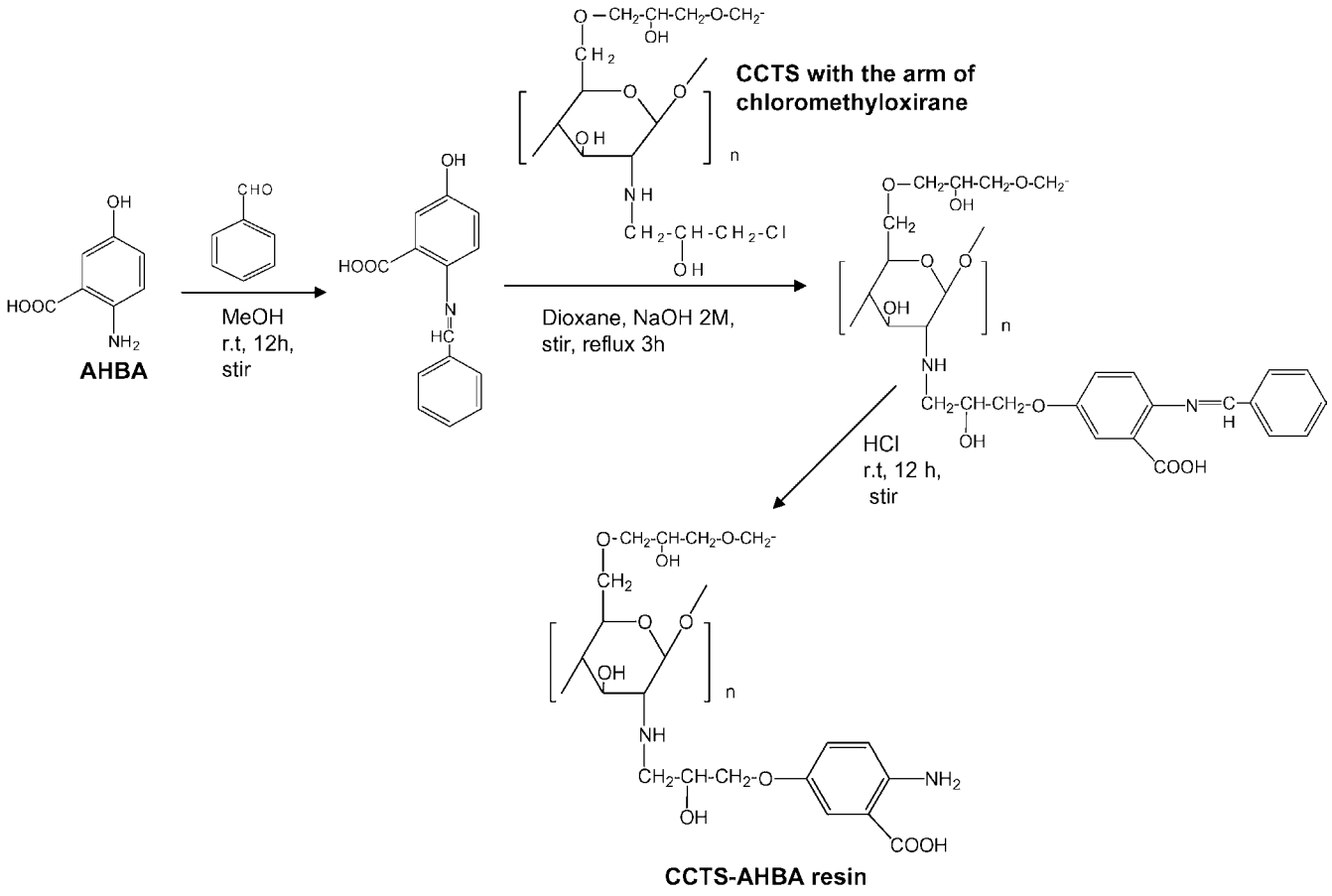

Fig. 2. Synthesis scheme of CCTS-AHBA resin. CCTS, cross-linked chitosan; AHBA, 2-amino-5-hydroxy benzoic acid; CCTS-AHBA, cross-linked chitosan possessing 2-amino-5-hydroxy benzoic acid moiety.

is then dispensed through the port 1 at the flow rate of 40 μl s^{-1} for conditioning the column.

Step 2. Collection and preconcentration: SV is in load position, and SP is set to aspirate 2500 μl of the samples into HC via the port 2 of SL (at the flow rate of 100 μl s^{-1}), followed by flowing it into the column via the port 1 (at the flow rate of 30 μl s^{-1}) for the collection and preconcentration of trace elements, as well as the removal of the matrices. This step was repeated two times to introduce total sample volume of 5 ml.

Step 3. Washing: after sample is loaded to the column, 500 μl of the ultrapure water (W_1) is aspirated into the syringe (at the flow rate of 200 μl s^{-1}), and then dispensed to wash the column via the port 1 of SL (at the flow rate of 40 μl s^{-1}), while SV is still in load position.

Step 4. Elution and measurement: in this step, the air-sandwiched eluent was used. The SP is set to aspirate air (40 μl, flow rate: 40 μl s^{-1}), eluent (2 M HNO_3; 250 μl, flow rate: 100 μl s^{-1}), air (40 μl, flow rate: 40 μl s^{-1}) into HC via the port 5, port 6, and port 5 of SL, respectively, followed by aspirating ultrapure water (W_1) into the syringe (at the flow rate of 200 μl s^{-1}) to fill the syringe up to 2500 μl. Then, SL is switched to the port 1, while SV is switched to the inject position, as shown in Fig. 1. Afterwards, the zones in the holding coil, which consists the zone of 40 μl air-250 μl eluent-40 μl air (in the front side) and the zone of 2170 μl ultrapure water (in the back side), are dispensed to elute the collected trace elements on the CCTS-AHBA column (at the flow rate of 30 μl s^{-1}), followed by their measurement with ICP-AES. Peak height was used as an analytical signal for the preparation of a calibration graph, as well as analytes measurement.

3. Results and discussion

3.1. Characteristics of CCTS-AHBA resin

The IR spectrum of CCTS-AHBA resin, in comparison with the one of cross-linked chitosan, depicted several bands at 1646.93, 1575.80, and 1384.66 cm^{-1}, which are attributed to C=C stretching of benzene, C=O of carboxylate group, and C–N stretching of aromatic amino group, respectively. These bands showed the existence of AHBA moiety attached to CCTS in the synthesized resin.

Fig. 3 shows the results of an acid-base titration for the synthesized CCTS-AHBA resin in an acidic solution with a 0.10 M NaOH solution as a titrant. There are three pKa values, which can be expected from the chemical structure of the CCTS-AHBA resin. The pKa value comes from –COOH and $–NH_2$ group of AHBA moiety, and –NH- group of CCTS. For the estimation of pKa of this resin, the pKa values of 2-amino benzoic acid,

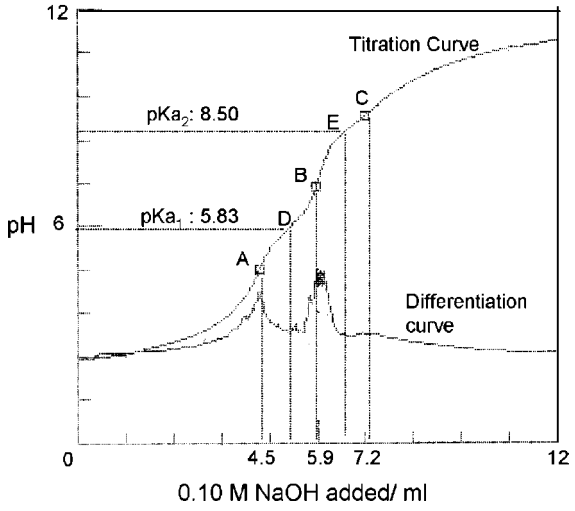

Fig. 3. Acid-base titration curve of the CCTS-AHBA resin. A sample solution for the titration contains 1 ml of the CCTS-AHBA resin (wet volume, 0.18 dry weight), 3 ml of 0.1 M HCl and 27 ml of the ultrapure water. (A) The inflection point of HCl and –COOH group of the resin; (B and C) the inflection point of $-NH_2$ and –NH- group of CCTS-AHBA resin; and (D and E) the half point of the equivalent points.

which are attributed to –COOH (pKa: 2.11) and $-NH_2$ (pKa: 4.95) group can be referred [42]. As shown in Fig. 3, there are two pKa values of 5.83 and 8.50, were clearly observed from the titration curve. The pKa of 5.83 in the resin is attributed to the $-NH_2$ group of the moiety, whereas the pKa of 8.50 is due to the –NH- group of cross-linked chitosan. The pKa value of –COOH group of AHBA moiety cannot be observed from the titration curve because the neutralization reaction of –COOH group overlapped with the neutralization of HCl. In this experiment, 3 ml of 0.10 M HCl in 30 ml water was added to the resin-suspended solution before titration. Therefore, the pH of HCl solution is about 2, whereas –COOH group of AHBA is seemed to be about 2.11 of pKa. When the sample is titrated, the amount of H^+ from HCl and H^+ from –COOH group cannot be separated.

At the first end point (A), the volume of 0.10 M NaOH required to neutralize total acid of HCl and –COOH was 4.5 ml. The volume, 4.5 ml of NaOH, can be attributed to the neutralization of HCl (3.0 ml of NaOH), and the neutralization of –COOH group (1.5 ml of NaOH). The most important value is the volume of NaOH required to neutralize $-NH_2$ group of AHBA, should be the same amount as that used to neutralize –COOH group. From the second end point (B), 1.4 ml of NaOH is needed to neutralize $-NH_2$ group: it means that the moles of –COOH and $-NH_2$ present in the synthesized resin are almost equal with each other. Similarly, the volume of NaOH required to neutralizing –NH- group of CCTS was about 1.3 ml (third end point, C). This result indicates that the amounts of AHBA moiety attached to cross-linked chitosan can be estimated to be 0.8 mmol g^{-1} resin.

3.2. Adsorption behavior of metal ions on the CCTS-AHBA resin

The adsorption behavior of 60 elements on the CCTS-AHBA resin was examined in a similar manner as in the previous works [25–29]. Fig. 4 shows the results obtained for the adsorption/recovery of 5 ppb of the 60 elements in the pH ranges from 1 to 9. The CCTS-AHBA resin can adsorb almost completely V, Cu, and U from acidic to alkaline pH regions. Other elements, such as Be, Co, Ni, Ag, Cd, Pb, and REEs (Y, La, Ce, Pr, Nd, Sm, Eu, Gd, Tb, Dy, Ho, Er, Tm, Yb, Lu) are adsorbed on the resin at around neutral to alkaline regions. Vanadium as an oxoanion can be adsorbed on the resin through an ion exchange mechanism, whereas other elements may adsorb on the resin through a chelating mechanism.

In our previous reports [22–23,43], it was found that the cross-linked chitosan itself could adsorb Cu, V, Ni, and Ag. Accordingly, the AHBA moiety attached to CCTS is seemed to possess excellent adsorption ability for Be, Co, Cd, Pb, U, and REEs. In our previous work [29], the chitosan resin functionalized with 3,4-diamino benzoic acid (CCTS-DBA resin) had poor adsorption capacities for REEs, however, the present resin (CCTS-AHBA) had excellent enrichment efficiency for REEs. Possibly, in the CCTS-AHBA resin, REEs can form six-membered ring chelate, which is more stable than five-membered ring chelate as in the CCTS-DBA resin. This is why the enrichment of REEs can be strongly improved when a –COOH group was added as in the CCTS-AHBA resin.

3.3. Optimization of Auto-Pret System

3.3.1. Factors affecting the collection/preconcentration of analytes

Several factors affecting the collection/preconcentration of analytes, involving sample pH and sample loading flow rate, were examined. Among these factors, the pH of sample solutions is seemed to be the most important parameter for the effective collection and preconcentration of analytes.

The effect of sample pH on the recovery of 60 elements was examined in the pH ranges from 1 to 9 as shown in Section 3.2. For further experiment, pH 7 was selected because it allows simultaneous determination of 24 elements, such as Be, Cd, Co, Cu, Ni, Pb, V, Ag, U, Y, La, Ce, Pr, Nd, Sm, Eu, Gd, Tb, Dy, Ho, Er, Tm, Yb, and Lu. The resin was packed in a mini-column (4 cm × 2 mm i.d.) and installed into Auto-Pret System coupled with ICP-AES, which can provides automated on-line preconcentration and determination of trace elements.

Faster flow rate of sample loading and higher adsorption efficiency of analytes are desired in the preconcentration experiments because these conditions can give a higher preconcentration factor in a shorter time. However, the kinetics of the adsorption may limit the flow rate, at which the sample can be dispensed through the column. Therefore, in the present study the effect of sample flow rate was examined in the ranges of 10–50 μl s^{-1}. The peak height tends to decrease with an increase in sample flow rate for REEs, whereas no significant decrease of the peak heights for Be, Cd, Co, Cu, Ni, Pb, V, Ag, and U up to the flow rate of 30 μl s^{-1}. Even the flow rate of 10 μl s^{-1} resulted in highest intensity for almost all analytes, however, it cannot be recommended because of the time-consuming analysis. As a

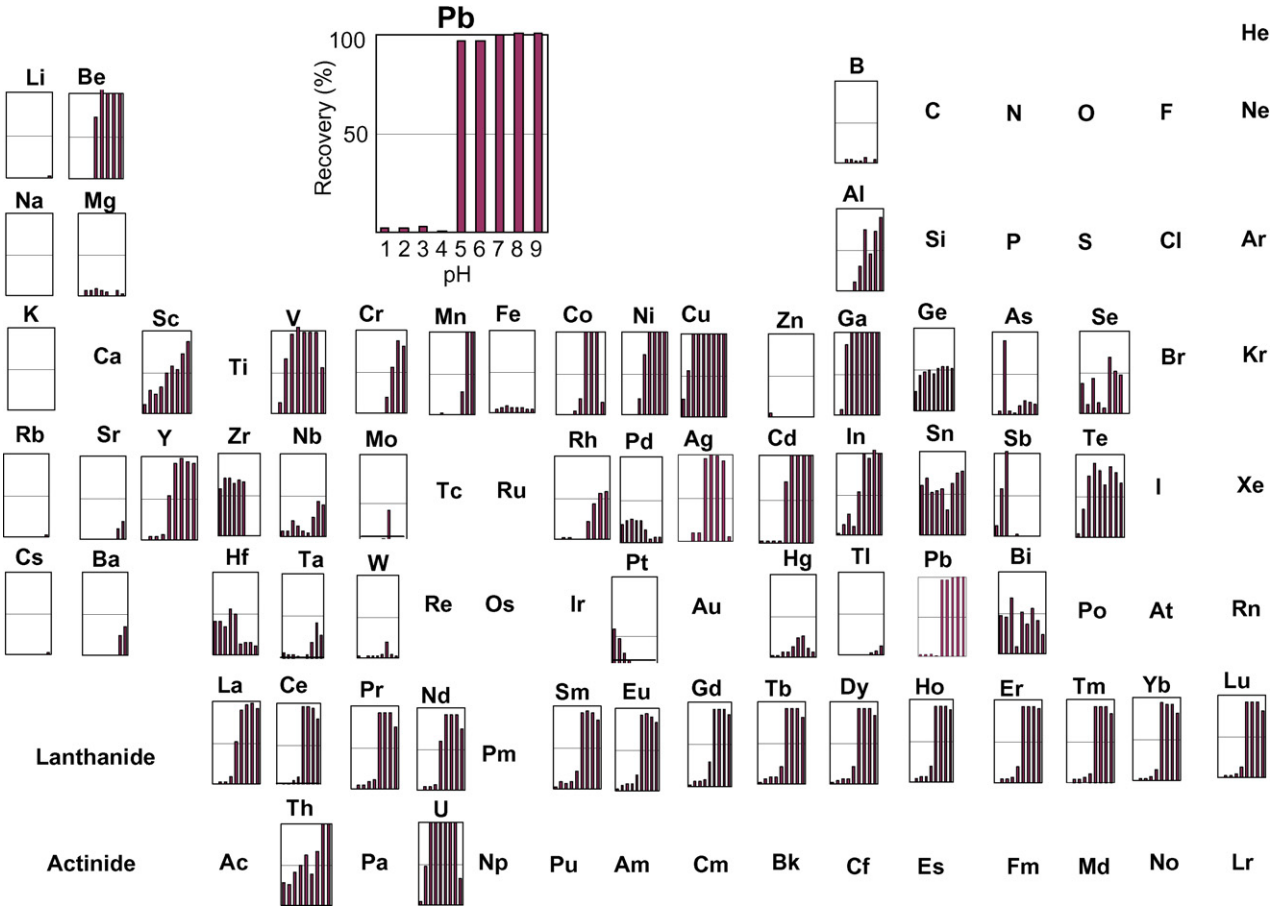

Fig. 4. Adsorption behavior of trace elements at various pHs with CCTS-AHBA resin. Concentration of each element in the samples: 5 ppb; eluent: 2 M HNO_3.

compromise of the sensitivity and the analysis time, a sample flow rate of 30 μl s^{-1} was selected as an optimum condition.

3.3.2. *Factor affecting the elution of the analytes*

Nitric acid (HNO_3) was used as an eluent for the present study. Several factors affecting the elution efficiency of analytes, such as an eluent concentration, an eluent volume, an eluent flow rate, and air-sandwiched eluent method were studied.

The concentration of HNO_3 for the elution of analytes collected on the column was examined in the ranges of 0.5–3.0 M. It was found that 0.5 M HNO_3 was not effective to elute analytes from the column, which gave the lowest peak height for all analytes examined. Some elements, such as Cu, Co, and Pb, could be eluted completely with 1 M HNO_3. However, most of the elements gave the highest peak height when these were eluted with 2 M HNO_3. Similar results were found when 3 M HNO_3 was used. From these results, a 2 M HNO_3 was chosen as an optimal eluent concentration.

The volume of eluent (2 M HNO_3) was examined from 0.05 to 2 ml to ascertain the complete elution of the analytes and the highest peak height. The peak height of the collected elements increases with increasing eluent volume up to 0.2 ml, though some elements, such as La, Co, and Be can be eluted completely using 0.1 ml of 2 M HNO_3. When the volume of the eluent was varied from 0.2 to 2 ml, the peak height of analytes did not show any significant differences. In the procedure required for the preconcentration of analytes, the volume of the eluent is seemed to be as low as possible to obtain the highest enrichment factor. Therefore, the eluent volume of 0.25 ml of 2 M HNO_3 was selected for further experiments.

The effect of the flow rate of eluent (2 HNO_3) was examined from 10 to 50 μl s^{-1}. It was found that the flow rate slower than 20 μl s^{-1} resulted in the lowest sensitivity due to the largest dispersion of the eluate during their transportation to ICP-AES. However, when the flow rate is faster than 30 μl s^{-1}, the peak height tends to decrease. The highest intensity was found in the ranges of 20–30 μl s^{-1}. Considering the analysis time, the eluent flow rate of 30 μl s^{-1} was selected as an optimal condition.

The optimized parameters of the Auto-Pret System were summarized in Table 2. Under the optimal conditions, the

Table 2
Optimized conditions for on-line preconcentration using Auto-Pret System

Parameter	Range examined	Selected
pH of sample	pH 1–9	pH 7
Sample loading flow rate	10–50 μl s^{-1}	30 μl s^{-1}
Eluent concentration	0.5–3 M HNO_3	2 M
Eluent volume (2 M HNO_3)	0.05–2 ml	0.25 ml
Eluent flow rate (2 M HNO_3)	10–50 μl s^{-1}	30 μl s^{-1}
Volume of air-sandwiched	0–70 μl	40 μl

analysis time of one sample was about 6 min using 5 ml of sample.

3.4. Analytical properties of merits

In order to evaluate the performance of the proposed method, the enrichment factor, collection efficiency, and detection limits obtained by using on-line preconcentration sequential-injection system were studied. The effect of matrices commonly exist in water sample (Na, Ca, Mg, and K) was also examined. This was followed by an assessment of the accuracy and reproducibility.

The enrichment factor and collection efficiency were investigated under optimal conditions. The enrichment factor was calculated by comparing the peak height obtained using the Auto-Pret System with those obtained by directly introducing the samples (5 ml), and collection efficiency was calculated by comparing peak area of flow signals of each analyte obtained with and without column preconcentration device as shown in Table 3.

The effect of river water matrices (Na: 20 ppm, K: 10 ppm, Mg: 15 ppm, Ca: 20 ppm) were examined by comparing the peak height of 1 ppb of each analyte in the presence and absence of the matrices. The results showed that no significant difference in the peak intensity between sample with and without the addition of the matrices. Such results demonstrated that the column packed with CCTS-AHBA resin was efficient for retaining the analytes and effectively removing them from potential interfering matrices. In addition, the column containing CCTS-AHBA resin can be used at least for 4 months.

Table 3
Enrichment factor and collection efficiency of trace elements obtained using Auto-Pret System

Elements	Enrichment factor	Collection efficiency (%)
Ag (I)	26.7	89.0
Be (II)	20.7	80.9
Cd (II)	21.6	88.6
Ce (III)	25.1	80.3
Co (II)	33.0	96.3
Cu (II)	36.2	94.1
Dy (III)	28.3	89.8
Er (III)	31.6	80.5
Eu (III)	24.5	86.3
Gd (III)	25.7	80.2
Ho (III)	27.6	86.5
La (III)	21.1	80.6
Lu (III)	30.8	99.3
Nd (III)	29.4	80.1
Ni (II)	22.6	94.2
Pb (II)	23.7	94.1
Pr (III)	30.1	85.7
Sm (III)	26.4	85.2
Tb (III)	27.5	84.2
Tm (III)	27.6	106.8
U (VI)	20.2	105.2
V (IV, V)	20.7	91.1
Y (III)	26.8	96.6
Yb (III)	27.7	106.5

Sample: 5 ml of 5 ppb each element. Other conditions for on-line preconcentration system are the same as shown in Table 2.

Table 4
Calibration graphs and limit of detection obtained by the Auto-Pret System

Elements	Range (ppb)	Equation	Correlation coefficient	LOD (ppb)
Ag (I)	0.01–5	$Y = 2593.1X + 91.0$	0.9961	0.006
Be (II)	0.005–5	$Y = 315713X - 14.9$	0.9974	0.001
Cd (II)	0.01–5	$Y = 1726.7X + 7.8$	0.9981	0.006
Ce (III)	0.5–5	$Y = 577.7X - 5.5$	0.9910	0.22
Co (II)	0.05–5	$Y = 1044.8X + 6.8$	0.9967	0.023
Cu (II)	0.01–5	$Y = 1832.7X + 8.7$	0.9994	0.006
Dy (III)	0.05–5	$Y = 2845.8X + 3.9$	0.9952	0.009
Er (III)	0.05–5	$Y = 2553.9X + 3.2$	0.9963	0.018
Eu (III)	0.01–5	$Y = 14462.0X + 3.9$	0.9980	0.008
Gd (III)	0.01–5	$Y = 2457.0X + 6.2$	0.9980	0.007
Ho (III)	0.01–5	$Y = 1484.2X + 8.1$	0.9932	0.005
La (III)	0.01–5	$Y = 3358.5X + 4.1$	0.9958	0.006
Lu (III)	0.01–5	$Y = 9564.2X + 4.3$	0.9965	0.004
Nd (III)	0.05–5	$Y = 368.8X + 0.9$	0.9948	0.020
Ni (II)	0.05–5	$Y = 391.8X + 7.5$	0.9962	0.028
Pb (II)	0.05–5	$Y = 162.1X + 4.2$	0.9961	0.022
Pr (III)	0.05–5	$Y = 477.2X + 7.5$	0.9978	0.015
Sm (III)	0.01–5	$Y = 1475.8X - 5.9$	0.9954	0.008
Tb (III)	0.05–5	$Y = 1830.1X + 10.9$	0.9963	0.018
Tm (III)	0.005–5	$Y = 7055.1X + 8.3$	0.9986	0.002
U (VI)	1–5	$Y = 240.1X + 19.9$	0.9939	0.93
V (IV, V)	0.01–5	$Y = 1043.4X + 10.5$	0.9951	0.007
Y (III)	0.005–5	$Y = 8232.3X + 7.9$	0.9983	0.002
Yb (III)	0.005–5	$Y = 32800.0X + 15.5$	0.9970	0.001

The calibration graphs for Be, Tm, Y, and Yb could be constructed at several ppt levels, whereas other elements, such as Ag, Cd, Co, Cu, Dy, Er, Eu, Gd, Ho, La, Lu, Nd, Ni, Pb, Pr, Sm, Tb, and V, were constructed at several 10 ppt levels. The detection limits (LOD) of analytes examined were determined by the signal to noise ratio (S/N = 3). As shown in Table 4, ppt to sub-ppb levels of LOD could be achieved. The relative standard deviations ($n = 6$) of analytes examined at a 1 ppb level were in the ranges of 0.2–1.2%, which means that the proposed method is superior in reproducibility.

The accuracy of the proposed method was evaluated by analyzing the standard reference material of river water (SLRS-4). The results were summarized in Table 5. Uranium could not be detected, because its concentration was lower than LOD. Larger volume of sample can be used to improve the LOD of uranium although such procedure can increase the analysis time substantially. The results obtained by the proposed method are in good agreement with the certified values.

3.5. Application to real river water samples

The applicability and robustness of the proposed method were demonstrated by determining trace elements in environmental river water samples. The analytical results were shown in Table 5. Most of the elements examined by the proposed method could be determined using 5 ml of the sample solutions. Cadmium could be detected clearly when 10 ml of the sample solution was used. However, it is very difficult to detect uranium because of LOD limitation and the poor sensitivity of ICP-AES for uranium.

Table 5
Analytical results of trace elements in river water samples and standard reference material

Element	Found (ppb)			Certified value of SLRS-4 (ppb)
	River water A[a]	River water B[b]	SLRS-4[c]	
Ag (I)	0.023 ± 0.002	0.025 ± 0.001	0.035 ± 0.004	
Be (II)	0.004 ± 0.000	0.008 ± 0.001	0.009 ± 0.001	0.007 ± 0.002
Cd (II)	0.008 ± 0.05[d]	0.004 ± 0.000[d]	0.013 ± 0.002	0.012 ± 0.002
Ce (III)	1.29 ± 0.01	0.95 ± 0.06	0.36 ± 0.01	
Co (II)	0.14 ± 0.01	0.12 ± 0.02	0.036 ± 0.005	0.033 ± 0.006
Cu (II)	0.57 ± 0.03	0.82 ± 0.01	1.85 ± 0.04	1.81 ± 0.08
Dy (III)	0.075 ± 0.004	0.070 ± 0.001	0.020 ± 0.003	
Er (III)	0.12 ± 0.02	0.15 ± 0.02	0.014 ± 0.006[d]	
Eu (III)	0.070 ± 0.000	0.059 ± 0.005	0.008 ± 0.000[d]	
Gd (III)	0.078 ± 0.004	0.029 ± 0.005	0.036 ± 0.005	
Ho (III)	0.041 ± 0.002	0.039 ± 0.000	0.005 ± 0.000[d]	
La (III)	0.12 ± 0.01	0.38 ± 0.04	0.032 ± 0.003	
Lu (III)	0.012 ± 0.000	0.015 ± 0.001	0.002 ± 0.000[d]	
Nd (III)	0.27 ± 0.03	0.29 ± 0.02	0.27 ± 0.01	
Ni (II)	0.41 ± 0.02	0.82 ± 0.02	0.62 ± 0.02	0.67 ± 0.08
Pb (II)	0.069 ± 0.003	0.073 ± 0.005	0.091 ± 0.003	0.086 ± 0.007
Pr (III)	0.066 ± 0.004	0.059 ± 0.008	0.072 ± 0.004	
Sm (III)	0.061 ± 0.002	0.042 ± 0.003	0.057 ± 0.003	
Tb (III)	0.049 ± 0.008	0.041 ± 0.001	0.005 ± 0.001[e]	
Tm (III)	0.017 ± 0.002	0.022 ± 0.005	0.002 ± 0.000[d]	
U (VI)	≪LOD	≪LOD	≪LOD	0.050 ± 0.003
V (IV, V)	0.45 ± 0.01	0.77 ± 0.03	0.36 ± 0.03	0.32 ± 0.03
Y (III)	0.037 ± 0.006	0.036 ± 0.002	0.15 ± 0.02	
Yb (III)	0.014 ± 0.000	0.018 ± 0.000	0.010 ± 0.001	

[a] River water sample was sampled at Asahi River, Okayama City.
[b] River water sample was sampled at Zasu River, Okayama City.
[c] Standard reference material of river water.
[d] Volume of sample: 10 ml.
[e] Volume of sample: 15 ml; volume of samples for other elements were 5 ml; all conditions are similar as shown in Table 2.

4. Conclusion

The cross-linked chitosan functionalized with 2-amino-5-hydroxy benzoic acid moiety (CCTS-AHBA resin) facilitates the determination of 24 trace elements with excellent collection efficiency, high enrichment factor, and effective matrix separation.

The proposed method, in which CCTS-AHBA resin was packed in a mini-column and utilized as an on-line pre-concentration device coupled with a laboratory-assembled sequential-injection/automated pretreatment system and ICP-AES, provides excellent detection limit, and it can be used as a versatile technique for the determination of trace elements in river waters with satisfied results. Easy operation could be attributed to the Auto-Pret System equipped with a laboratory-written software.

Acknowledgement

The present work was partially supported by the Grant-in-Aid for Scientific Research (B) No. 16350044 from Japan Society for Promotion of Science (JSPS).

References

[1] V.A. Lemos, E.M. Gama, A.S. Lima, Microchim. Acta 153 (2006) 179.
[2] D. Bilba, D. Bejan, L. Tofan, Croat. Chem. Acta 71 (1998) 155.
[3] R. Qu, C. Sun, C. Ji, C. Wang, Z. Zhao, D. Yu, Polym. Eng. Sci. 45 (2005) 1515.
[4] P.K. Roy, A.S. Rawat, P.K. Rai, Talanta 59 (2003) 239.
[5] P.K. Roy, A.S. Rawat, V. Choudhary, P.K. Rai, J. Appl. Polym. Sci. 59 (2003) 239.
[6] M.R. Maurya, S. Sikarwar, T. Joseph, P. Manikandan, S.B. Halligudi, React. Funct. Polym. 63 (2005) 71.
[7] S. Pramanik, P.K. Dhara, P. Chattopadhyay, Talanta 63 (2004) 485.
[8] B.C. Mondal, D. Das, A.K. Das, Talanta 56 (2002) 145.
[9] C. Sun, R. Qu, C. Wang, C. Ji, G. Cheng, J. Appl. Polym. Sci. 95 (2005) 890.
[10] P.K. Tewari, A.K. Singh, Talanta 53 (2001) 823.
[11] P.K. Tewari, A.K. Singh, Analyst 124 (1999) 1847.
[12] M. Kumar, D.P.S. Rathore, A.K. Singh, Talanta 51 (2000) 1187.
[13] K. Dev, R. Pathak, G.N. Rao, Talanta 48 (1999) 579.
[14] V.K. Jain, A. Handa, S.S. Sait, P. Shrivastav, Y.K. Agrawal, Anal. Chim. Acta 429 (2001) 237.
[15] Y.S. Kim, G. In, C.W. Han, J.M. Choi, Microchem. J. 80 (2005) 151.
[16] D. Prabhakaran, M.S. Subramanian, Anal. Bioanal. Chem. 379 (2004) 519.
[17] M.A. Maheswari, M.S. Subramanian, Talanta 64 (2004) 202.
[18] M.A. Maheswari, M.S. Subramanian, React. Funct. Polym. 62 (2005) 105.
[19] D. Yang, X. Chang, Y. Liu, S. Wang, J. Appl. Polym. Sci. 97 (2005) 2330.
[20] D. Yang, X. Chang, Y. Liu, S. Wang, Microchim. Acta 147 (2004) 219.
[21] K. Oshita, M. Oshima, Y.H. Gao, K.H. Lee, S. Motomizu, Anal. Sci. 18 (2002) 1121.
[22] Y.H. Gao, K. Oshita, K.H. Lee, M. Oshima, S. Motomizu, Analyst 127 (2002) 1713.
[23] K. Oshita, Y.H. Gao, M. Oshima, S. Motomizu, Anal. Sci. (Suppl.) 17 (2001) a317.
[24] T.Y. Hsien, G.L. Rorrer, Ind. Eng. Chem. Res. 36 (1997) 3631–3638.
[25] K. Oshita, J. Xu, Y.H. Gao, K.H. Lee, M. Oshima, S. Motomizu, Bull. Chem. Soc. Jpn. 76 (2003) 1555.

[26] K. Oshita, M. Oshima, Y. Gao, K.H. Lee, S. Motomizu, Anal. Chim. Acta 480 (2003) 239.
[27] S. Yamakawa, K. Oshita, A. Sabarudin, M. Oshima, S. Motomizu, Bunseki Kagaku 53 (2004) 1039.
[28] A. Sabarudin, K. Oshita, M. Oshima, S. Motomizu, Talanta 66 (2005) 136.
[29] A. Sabarudin, K. Oshita, M. Oshima, S. Motomizu, Anal. Chim. Acta 542 (2005) 207.
[30] S. Hirata, T. Kajiya, N. Takano, M. Aihara, K. Honda, O. Shikino, E. Nakayama, Anal. Chim. Acta 499 (2003) 157.
[31] T. Kajiya, M. Aihara, S. Hirata, Spectrochim. Acta Part B 59 (2004) 543.
[32] A.O. Martins, E.D. Silva, E. Carasek, N.S. Gonçalves, M.C.M. Laranjeira, V.T. Fávere, Anal. Chim. Acta 521 (2004) 157.
[33] C.R.T. Tarley, S.L.C. Ferreira, M.A.Z. Arruda, Microchem. J. 77 (2004) 163.
[34] E.L. Silva, D. Budziak, E. Carasek, Anal. Lett. 37 (2004) 1909.
[35] V.A. Lemos, J.S. Santos, P.X. Baliza, Sep. Sci. Technol. 39 (2004) 3317.
[36] Z.H. Wang, Z.P. Zhang, Z.P. Wang, L.W. Liu, X.P. Yan, Anal. Chim. Acta 514 (2004) 151.
[37] V.A. Lemos, D.G. da Silva, A.L. de Carvalho, D.A. Santana, G.S. Novaes, A.S. dos Passos, Microchem. J. 84 (2006) 14.
[38] J. Ruzicka, M.D. Marshall, Anal. Chim. Acta 237 (1990) 329.
[39] J. Wang, E.H. Hansen, J. Anal. At. Spectrom. 17 (2002) 1284.
[40] S. Suteerapatarapon, J. Jakmunee, Y. Vaneesorn, K. Grudpan, Talanta 58 (2002) 1235.
[41] A. Economou, A. Voulgaropoulos, J. Autom. Methods Manage. Chem. 25 (2003) 133.
[42] D.R. Lide, Handbook of Chemistry and Physics, 81st ed., CRC Press, New York, 2000, pp. 8–51.
[43] Y. Gao, K.H. Lee, M. Oshima, S. Motomizu, Anal. Sci. 16 (2000) 1303.

Available online at www.sciencedirect.com
ScienceDirect
Talanta 72 (2007) 1637–1643
Talanta
www.elsevier.com/locate/talanta

Dual low thermal mass gas chromatography–mass spectrometry for fast dual-column separation of pesticides in complex sample

Kikuo Sasamoto, Nobuo Ochiai *, Hirooki Kanda

GERSTEL K.K., 2-13-18 Nakane, Meguro-ku, Tokyo 152-0031, Japan

Received 30 October 2006; received in revised form 11 March 2007; accepted 13 March 2007
Available online 20 March 2007

Abstract

A method is described for fast dual-column separation of pesticides by use of dual low thermal mass gas chromatography–mass spectrometry (dual LTM-GC–MS) with different temperature programming. The method can provide two total ion chromatograms with different separation on DB-5 and DB-17 in a single run, which allows improved identification capability, even with short analysis time (<17 min). Also simultaneous detection with MS and elemental selective detector, e.g. pulsed flame photometric detection (PFPD) was evaluated for fast dual-column separation of 82 pesticide mixtures including 27 phosphorus pesticides. Dual LTM-GC–MS/PFPD was applied to analysis of pesticides in a brewed green tea sample with dual stir bar sorptive extraction method (dual SBSE).

Keywords: Fast dual-column separation; Low thermal mass GC (LTM-GC); Mass spectrometry; Simultaneous detection; Fast GC–MS

1. Introduction

The determination of pesticide residues in environmental samples, e.g. water and soil, and agricultural products has been a major subject for many years because of their potential risk for human health, persistence and tendency to bio-accumulate. Japan, e.g., has introduced positive list system for agricultural chemical residues such as pesticide residues in foods [1]. The system prohibits the distribution of foods that are containing pesticides above a certain level. About 700 pesticides have to be analyzed with maximum residue limit (MRL) or 10 $\mu g\,kg^{-1}$ as uniform limit if there is no MRL. Under these situations, multiresidues, high sensitivity, high efficient and high sample throughput methods are needed to improve analytical quality and laboratories efficiency.

Mass spectrometry (MS) is universal detection method that has identification capability with mass spectral information, and high selectivity with extracted ion trace. Thus, GC–MS is the most often used for quantitative and confirmatory analysis of GC-amenable pesticides [2]. Although MS detection has high identification capability and high selectivity, it is easily reduced by the co-elution of matrices and analytes even with extracted ion traces.

Dual-column separation with different stationary phase combination is informative and effective for the complex sample matrix. Kinton et al. reported analysis of blood alcohol using dual-column separation and flame ionization detections [3]. Pagliuca et al. reported residue analysis of organophosphorus pesticides in animal matrices by dual-column separation and nitrogen phosphorus detections [4]. Generally, dual-column separation is performed with typical GC detectors except MS. Matsuda et al. reported analysis of pesticide with dual-column separation and MS detection [5]. Their system consisted of a single GC with two inlets, dual-column and a single MS. With this system, two analyses should be performed for one sample. Also selection of GC column for dual-column separation might be limited because dual-column has to be placed in a single GC oven.

Fast GC–MS has been recognized as a potential tool for pesticide multiresidues analysis, which can provide high sample throughput and laboratory efficiency [6,7]. Recently, several fast GC systems with direct resistive heating as a principle have become commercially available in which a capillary column is inserted into a resistively heated metal tube or enclosed in resistively heated toroid-formed assembly. The latter is called low thermal mass (LTM) GC [8]. An LTM-GC system can pro-

* Corresponding author. Tel.: +81 3 5731 5321; fax: +81 3 5731 5322.
E-mail address: nobuo_ochiai@gerstel.co.jp (N. Ochiai).

0039-9140/$ – see front matter © 2007 Elsevier B.V. All rights reserved.
doi:10.1016/j.talanta.2007.03.020

vide fast temperature programming rates combined with rapid cool-down and short equilibration times for shortest possible analytical cycle times. Using LTM-GC system, one can achieve maximal heating rate of 30 °C s^{-1} and cool-down time of less than one minute (e.g. from 280 to 40 °C) [8]. An LTM-GC system consists of a specially constructed oven door for a GC that has built-in electronics and slots for inserting from one column module to four column modules. This structure allows flexible column configuration and independent temperature programming of column modules.

The aim of this work was to develop new and fast method of dual-column separation based on LTM-GC–MS consisting of one injector and two column modules (dual LTM-GC–MS), for analysis of pesticide in the complex sample. Also elemental selective detector, e.g. pulsed flame photometric detector (PFPD) was coupled to dual LTM-GC–MS for simultaneous detection in dual-column separation.

2. Experimental

2.1. Material

Standard solutions of pesticides mixtures at 10 μg mL^{-1} each in acetone were purchased from Kanto Kagaku (Tokyo, Japan). Some pesticides in stock solutions are composed of several isomers. For these compounds, concentration (10 μg mL^{-1}) is sum of concentration of individual isomers. Stock standard solutions were then mixed and diluted with acetone to prepare test mixture. The stock standard solutions were kept at −20 °C. Acetone and methanol, pesticide residues grade, were purchased from Kanto Kagaku. Sodium chloride (NaCl), reagent grade, was also purchased from Kanto Kagaku and baked at 350 °C for several hours before use. A green tea sample was obtained from local store in Tokyo Japan.

2.2. Instrumentation

The dual LTM-GC–MS/PFPD analysis was performed with a Gerstel MPS 2 auto-sampler and a Gerstel CIS 4 programmed temperature vaporization (PTV) inlet with dual-column interface and a Gerstel MACH LTM-GC system (Gerstel GmbH, Mulheim an der Ruhr, Germany), and Model5380 PFPD with phosphorus mode (OI Analytical, College Station, TX, USA) installed on an Agilent 6890N gas chromatograph with an Agilent 5975 mass-selective detector (Agilent Technologies, Palo Alto, CA, USA). A MACH LTM-GC system consists of two wide format column modules (5 in.), LTM-heated transfer lines, cooling fans, temperature controller, power supply, and a specially constructed door. The separations were performed on a DB-5 fused silica capillary column (10 m × 0.18 mm i.d., 0.18 μm film thickness, Agilent Technologies) and a DB-17 fused silica capillary column (10 m × 0.18 mm i.d., 0.18 μm film thickness, Agilent Technologies) which were coiled and packed together with heating wire, sensor, and ceramic fibers in MACH column modules separately (long-end format, 5 in. module). The columns were connected to a PTV inlet with a dual-column interface (Gerstel) and a cross piece splitter (Gerstel) for MS and PFPD. A deactivated fused silica capillaries were connected between the splitter and MS, PFPD, respectively. The schematic flow diagram was illustrated in Fig. 1. For thermal desorption, a Gerstel TDU thermal-desorption unit (Gerstel) was used with the CIS PTV inlet.

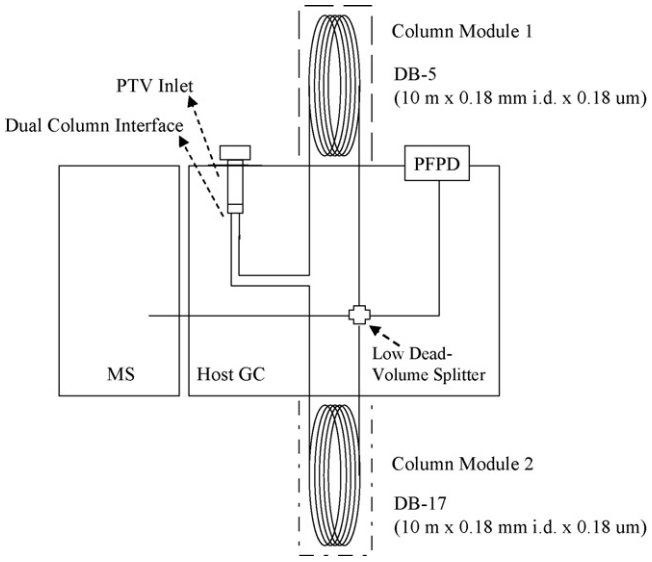

Fig. 1. Schematic diagram for Dual LTM GC–MS/PFPD.

2.3. Dual LTM-GC–PFPD/MS

A PTV was programmed from 10 to 300 °C (held for 5 min) at 720 °C min^{-1}. Quartz wool packed liner was used in a PTV injector. Injection was performed in splitless mode and a split valve was closed for 2 min. The column temperature for a DB-5 was programmed from 40 (held for 2 min) at 75 °C min^{-1} to 300 °C (held for 11 min) and one for a DB-17 was programmed from 40 °C (held for 10 min) at 75 °C min^{-1} to 300 °C (held for 3 min). Helium was used as carrier gas. Host GC oven and MS interface were kept at a constant temperature of 250 °C. The mass spectrometer was operated in scan mode using electron-impact ionization (electron-accelerating voltage: 70 V). Scan range was set from *m/z* 58 to 510 and sampling rate of zero, resulting in scan rate of 10.83 scan s^{-1}. PFPD temperature was set by 280 °C and its acquisition rate was set by 4 Hz.

2.4. Dual SBSE–TD–dual LTM-GC–PFPD/MS for green tea sample

Stir bars coated with 24 μL of PDMS (Twister) were obtained from Gerstel. For SBSE, 20 mL headspace vial with screw cap containing PTFE-coated silicone septa were used. SBSE was performed by use of a multiple position magnetic stirrer.

Extraction of brewed green tea sample was performed according to dual SBSE method [9] as follows; brewed green tea sample was prepared by suspending green tea (1.25 g) in 200 mL of boiling water for 5 min and centrifuged for 5 min at 3000 rpm. Twenty milliliters of sample were transferred to two 20 mL headspace vials and 30% NaCl was added to one of the sam-

ple. SBSE was simultaneously performed at room temperature (24 °C) for 60 min while stirring at 1500 rpm. After extraction, stir bar was dipped briefly in Milli-Q water, dried with a lint-free tissue, and placed in a glass liner of a thermal desorption system. The glass liner was then placed in thermal desorption unit. Stir bars were thermally desorbed with programming a TDU from 40 °C (held for 0.5 min) to 280 °C (held for 5 min) at 720 °C min^{-1}. Desorbed compounds were cryo-focused in a PTV at −100 °C for subsequent GC–MS analysis. Quartz wool packed liner was used in a PTV injector. After desorption, a PTV was programmed from −100 to 280 °C (held for 5 min) at 720 °C min^{-1} to inject trapped compounds on to the analytical columns.

3. Results and discussion

3.1. Dual LTM-GC–MS/PFPD

On dual LTM-GC–MS/PFPD, both carrier gas flow for a DB-5 and a DB-17 are combined at the splitter, but only controlled by a head pressure and its flow rates depend on both column temperatures. After simultaneous injection onto both columns (Fig. 1), DB-5 separation was first carried out while DB-17 was kept at initial temperature of 40 °C, to focus half of analytes on the top of the column. Initial temperature of DB-5 was also set by 40 °C to keep a split ratio to 1:1. After DB-5 separation, DB-17 separation was subsequently performed. This procedure allows dual-column separation in a single run with the shortest analysis time because no sample injection, cool-down time and equilibrium time are needed for second separation on DB-17. In addition, dual-column separation in a single run provides easy handling for data analysis because two total ion chromatograms with different separation on DB-5 and DB-17 are stored as a single total ion chromatogram.

A column outlet flow rate was calculated by using the Agilent column calculator software based on following equation. The software can be downloaded at Agilent web site (http://www.chem.agilent.com/cag/servsup/usersoft/files/GCFC.htm):

$$F = \left[\frac{60\pi r^4}{16\eta L}\right]\left[\frac{p_i^2 - p_o^2}{p_o}\right]\left[\frac{p_o}{p_{ref}}\right]\left[\frac{T_{ref}}{T}\right]$$

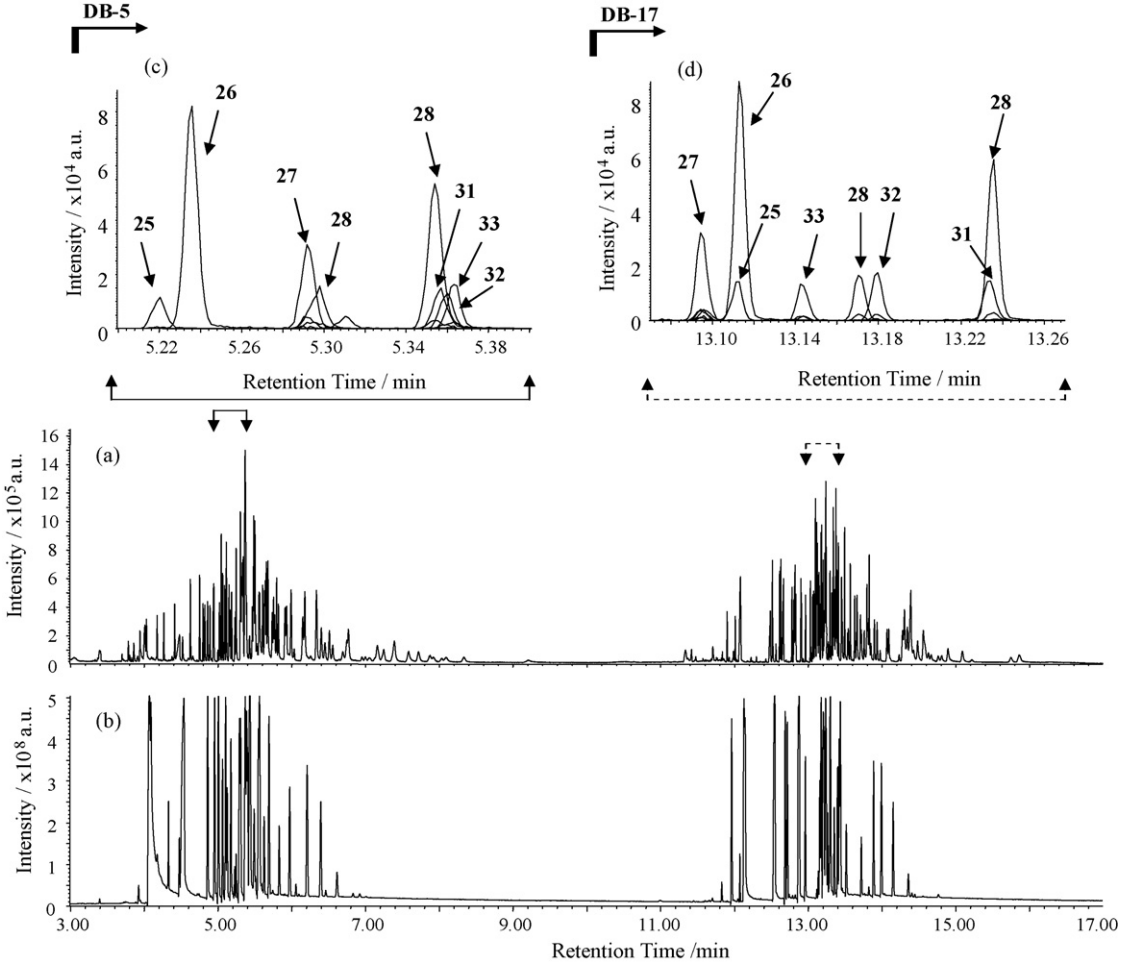

Fig. 2. Total ion chromatogram, some representative mass chromatograms and PFPD chromatogram obtained by Dual LTM-GC–PFPD/MS of 82 pesticides at 5 ng each. (a) Total ion chromatogram; (b) PFPD chromatogram; (c) some representative mass chromatograms on DB-5; (d) some representative mass chromatograms on DB-17—25: parathion-methyl (*m/z* 263), 26: tolclofos-methyl (*m/z* 265), 27: pirimiphos-methyl (*m/z* 290), 28: fenitrothion (*m/z* 277), 30: fenthion (*m/z* 278), 31: dimethylvinphos (*m/z* 297), 32: chloropyrifos (*m/z* 314) and 33: parathion (*m/z* 291).

Table 1
Pesticides studied, selected ions for quantification, retention time and repeatability obtained for dual LTM-GC–MS/PFPD analysis

No.	Compounds	*m/z*[a]	DB-5				DB-17			
			Retention time[b]		Peak area	r^2 (0.25–5.0 ng)[c]	Retention time[b]		Peak area	r^2 (0.25–5.0 ng)[c]
			Average (min)	R.S.D. (%)	R.S.D. (%)[b]		Average (min)	R.S.D. (%)	R.S.D. (%)[b]	
OCPs										
1	α-BHC	217	4.93	0.13	3.37	0.9990	12.78	0.00	3.31	0.9998
2	β-BHC	217	5.01	0.13	2.99	0.9985	12.91	0.00	3.92	0.9987
3	γ-BHC (lindane)	217	5.04	0.13	4.28	0.9997	12.96	0.00	3.68	0.9955
4	δ-BHC	217	5.11	0.10	3.14	0.9997	13.06	0.00	3.75	0.9995
5	*p,p*-DDE	246	5.65	0.18	3.42	0.9995	13.41	0.00	3.31	0.9993
6	Chlorobenzilate	251	5.74	0.11	3.70	0.9995	13.49	0.00	3.57	0.9985
7	*p,p*-DDD	235	5.78	0.11	3.02	0.9989	13.57	0.00	2.69	0.9996
Carbamate pesticides										
8	Isoprocarb	121	4.62	0.11	3.84	0.9976	12.51	0.04	2.99	0.9993
9	Fenobucarb	121	4.75	0.14	3.67	0.9994	12.61	0.00	2.41	0.9997
10	Chlorpropham	213	4.82	0.14	3.69	0.9992	12.63	0.00	2.87	0.9991
11	Bendiocarb	166	4.85	0.13	3.64	0.9992	12.83	0.00	2.85	0.9972
12	Pirimicarb	238	5.14	0.12	2.79	0.9996	13.03	0.00	2.63	0.9990
13	Ethiofencarb	107	5.16	0.12	3.85	0.9974	13.09	0.00	3.87	0.9985
14	Diethofencarb	267	5.24	0.15	3.18	0.9994	13.11	0.03	3.90	0.9994
15	Methiocarb	168	5.30	0.09	3.62	0.9963	13.20	0.00	2.76	0.9981
16	Esprocarb	222	5.31	0.12	2.03	0.9993	13.10	0.00	3.50	0.9986
17	Thiobencarb	100	5.33	0.12	3.00	0.9996	13.17	0.00	2.15	0.9980
OPPs										
18	Dichlorvos	185	4.03	0.18	4.26	0.9970	11.90	0.00	2.71	0.9986
19	Ethoprophos	158	4.79	0.14	4.80	0.9968	12.63	0.00	4.05	0.9999
20	Cadusafos	159	4.89	0.13	3.38	0.9993	12.65	0.04	4.33	0.9981
21	Thiometon	246	4.94	0.00	4.85	0.9947	12.81	0.04	4.36	0.9962
22	Terbufos	231	5.04	0.14	3.17	0.9995	12.80	0.04	4.08	0.9989
23	Diazinon	304	5.06	0.13	3.70	0.9999	12.82	0.00	2.84	0.9997
24	Etrimfos	292	5.11	0.13	4.24	0.9990	12.90	0.00	3.57	0.9993
25	Parathion-methyl	263	5.22	0.12	4.28	0.9982	13.11	0.03	3.89	0.9990
26	Tolclofos-methyl	265	5.24	0.15	3.26	0.9989	13.11	0.04	3.26	0.9993
27	Pirimiphos-methyl	290	5.29	0.12	3.23	0.9995	13.10	0.03	4.20	0.9993
28	Fenitrothion	277	5.30	0.12	3.93	0.9998	13.17	0.00	4.38	0.9986
29	Malathion	173	5.32	0.12	3.63	0.9977	13.15	0.00	4.19	0.9987
30	Fenthion	278	5.36	0.17	2.75	0.9992	13.24	0.03	3.07	0.9990
31	Dimethylvinphos	297	5.36	0.09	4.04	0.9991	13.23	0.04	3.88	0.9965
32	Chlorpyrifos	314	5.36	0.12	2.92	0.9986	13.14	0.04	3.87	0.9997
33	Parathion	291	5.37	0.17	4.24	0.9979	13.18	0.00	3.81	0.9984
34	Isofenphos oxon	229	5.37	0.12	4.19	0.9988	13.18	0.00	2.63	0.9975
35	*E,Z*-Chlorofenvinphos	323	5.48	0.14	3.34	0.9994	13.29	0.00	2.77	0.9987
36	Isofenphos	255	5.48	0.17	3.07	0.9995	13.24	0.00	3.66	0.9991
37	Quinalphos	298	5.49	0.11	3.63	0.9986	13.34	0.00	3.20	0.9994
38	Phenthoate	274	5.49	0.11	3.73	0.9985	13.36	0.00	3.31	0.9990
39	Prothiofos	309	5.62	0.11	3.55	0.9997	13.37	0.04	2.26	0.9994
40	Fensulfothion	293	5.76	0.16	4.68	0.9970	13.66	0.00	4.39	0.9980
41	Edifenphos	310	5.90	0.17	3.47	0.9986	13.82	0.04	2.98	0.9984
42	EPN	157	6.13	0.25	4.71	0.9979	13.93	0.00	4.17	0.9979
43	Phosalone	182	6.31	0.24	3.36	0.9978	14.09	0.04	3.68	0.9975
44	Pyraclofos	360	6.53	0.30	4.05	0.9958	14.29	0.04	3.01	0.9966
Pyrethroid pesticides										
45	Tefluthrin	197	5.08	0.13	3.58	0.9991	12.66	0.06	2.23	0.9987
46	Cyhalothrin 1,2	181	6.31	0.28	4.66	0.9990	13.81	0.04	3.22	0.9985
47	Acrinathrin	181	6.42	0.33	2.61	0.9969	13.84	0.04	4.09	0.9986
48	Permrthrin 1,2	183	6.71	0.34	3.12	0.9996	14.26	0.04	3.47	0.9990
49	Cyfluthrin 1,2,3,4	226	6.96	0.65	2.48	0.9907	14.39	0.13	2.73	0.9964
50	Halfenprox	263	7.11	0.42	3.07	0.9978	14.47	0.04	4.45	0.9964
51	Cypermethrin 1,2,3,4	181	7.18	0.47	3.90	0.9971	14.62	0.06	3.17	0.9989
52	Flucythrinate 1,2	199	7.19	0.53	3.91	0.9970	14.57	0.08	4.17	0.9965
53	Fenvalerate 1,2	167	7.65	0.61	2.87	0.9964	15.08	0.09	2.96	0.9964
54	Fluvalinate 1,2	250	7.85	0.65	3.34	0.9950	15.79	0.07	3.31	0.9980
55	Deltamethrin	253	8.25	0.68	4.06	0.9996[d]	15.73	0.10	3.65	0.9988[d]

Table 1 (*Continued*)

No.	Compounds	*m/z*[a]	DB-5				DB-17			
			Retention time[b]		Peak area	r^2 (0.25–5.0 ng)[c]	Retention time[b]		Peak area	r^2 (0.25–5.0 ng)[c]
			Average (min)	R.S.D. (%)	R.S.D. (%)[b]		Average (min)	R.S.D. (%)	R.S.D. (%)[b]	
Other pesticides										
56	EPTC	128	4.26	0.16	3.13	0.9984	12.01	0.00	3.13	0.9996
57	Butylate	217	4.41	0.00	3.00	0.9992	12.09	0.05	3.75	0.9978
58	Benfuresate	163	5.18	0.10	3.09	0.9993	13.07	0.04	3.26	0.9991
59	Metolachlor	238	5.36	0.13	3.51	0.9994	13.12	0.04	3.98	0.9988
60	Pendimethalin	252	5.37	0.17	4.36	0.9986	13.22	0.00	3.10	0.9990
61	*Z*-Pyrifenox	262	5.47	0.09	3.98	0.9991	13.32	0.00	2.61	0.9988
62	Chinomethionate	234	5.55	0.11	2.66	0.9992	13.45	0.00	2.60	0.9990
63	*E*-Pyrifenox	262	5.55	0.12	4.52	0.9990	13.38	0.04	3.92	0.9980
64	Flutolanil	323	5.60	0.18	2.94	0.9991	13.39	0.00	3.43	0.9993
65	Pretilachlor	238	5.63	0.11	4.05	0.9990	13.34	0.00	3.40	0.9991
66	Mycrobutanil	179	5.66	0.11	4.19	0.9994	13.49	0.00	4.42	0.9997
67	Flusilazole	233	5.67	0.17	4.75	0.9993	13.45	0.00	3.17	0.9988
68	Cyproconazole	222	5.73	0.18	4.46	0.9996	13.54	0.00	3.46	0.9979
69	Mepronil	119	5.81	0.17	3.29	0.9992	13.63	0.04	2.99	0.9992
70	Propiconazole 1,2	173	5.91	0.28	3.82	0.9990	13.66	0.00	4.09	0.9989
71	Thenylchlor	288	5.98	0.16	2.62	0.9994	13.82	0.03	2.44	0.9989
72	Tebconazole	250	5.98	0.17	3.18	0.9996	13.70	0.04	4.40	0.9983
73	Tebufenpyrad	318	6.16	0.26	4.48	0.9993	13.79	0.03	2.47	0.9992
74	Pyriproxyfen	136	6.31	0.24	2.91	0.9989	13.06	0.04	1.97	0.9985
75	Mefenacet	192	6.37	0.28	2.27	0.9971	14.38	0.05	2.98	0.9982
76	Fenarimol	251	6.48	0.27	4.79	0.9989	14.30	0.05	3.39	0.9982
77	Bitertanol 1,2	170	6.65	0.39	2.91	0.9971	14.27	0.04	2.79	0.9924
78	Pyridaben	364	6.73	0.37	2.45	0.9994	14.33	0.04	3.07	0.9982
79	Silafluofen	286	7.33	0.52	2.10	0.9984	14.55	0.07	2.86	0.9980
80	Pyrimidifen	184	7.52	0.54	4.18	0.9970	14.88	0.06	2.55	0.9970
81	Difenoconazole 1,2	323	8.02	0.65	4.73	0.9970	15.84	0.11	2.93	0.9962
82	Imibenconazole	125	9.10	0.80	3.61	0.9942[d]	12.83	0.12	4.66	0.9866[d]

[a] Selected ion for repeatability and linearity.
[b] Reproducibility was calculated at 5.0 ng ($n = 6$).
[c] Linear range of calibration curve
[d] Linear range was 0.50–5.0 ng.

where F is outlet flow (mL min^{-1} at T_{ref} and p_{ref}), r the column inner radius (cm), L the column length (cm), p_i the inlet pressure (absolute, dynes cm^{-1}), p_o the outlet pressure (absolute, dynes cm^{-1}), p_{ref} the reference pressure, typically 1 atm, T the column (oven) temperature (K), T_{ref} the reference temperature, typically 298 K and η is the carrier gas viscosity at column temperature (poise).

The splitter and transfer lines from the splitter to the MS and the PFPD are placed in a host GC oven. The host GC oven is kept at a constant temperature during analysis on LTM-GC. When it was kept at 250 °C at a constant and split ratio to a MS and a PFPD was set by 1:1, delay time, which were time difference between one from a splitter to a MS and one from a splitter to a PFPD, was minimized with a deactivated fused silica capillary with 600 mm long, 0.15 mm i.d. for connecting between a splitter and MS, and 450 mm long, 0.25 mm i.d. for connecting between a splitter and a PFPD. With this condition, pressure of the splitter was 5.3 kPa and carrier gas flow to both detectors was 1.23 mL min^{-1} each. To obtain constant and minimum delay time during an analysis, one should keep carrier gas flow which provides to the splitter, 2.46 mL min^{-1} at a constant. Therefore the head pressure program was set as follow; 146 kPa (held for 2 min) at 8.4 kPa min^{-1} to 175 kPa (held for 4.5 min) and then at 20 kPa min^{-1} to 244 kPa (held for 4.5 min). Total carrier gas flow rate (sum of carrier gas flow rates of DB-5 and DB-17) was 2.46 mL min^{-1} at the splitter and the split ratio for a PFPD and a MS was 1:1.

3.2. System performance

We evaluated repeatability of retention time and peak area for 82 pesticides at 5.0 ng and linearity at five concentration levels between 0.25 and 5.0 ng on both columns. One micro-liter of the standard solution was injected into the PTV injector. Fig. 2(a) shows a total ion chromatogram of 82 pesticides at 5.0 ng and Fig. 2(b) shows a PFPD chromatogram of the 27 phosphorus pesticides at 5.0 ng. Fig. 2(c) and (d) shows some representative mass chromatograms. Table 1 shows repeatability for retention time, peak area and linearity on both columns by dual LTM-GC–MS/PFPD for 82 pesticides. Analysis time of dual LTM-GC–MS/PFPD detection was less than 17 min. For 82 pesticides, good repeatability was achieved with relative standard deviation (R.S.D., $n = 6$) in the range of 0.00–0.80% for retention time and 2.03–4.85% for peak area on DB-5, 0.00–0.12% for retention

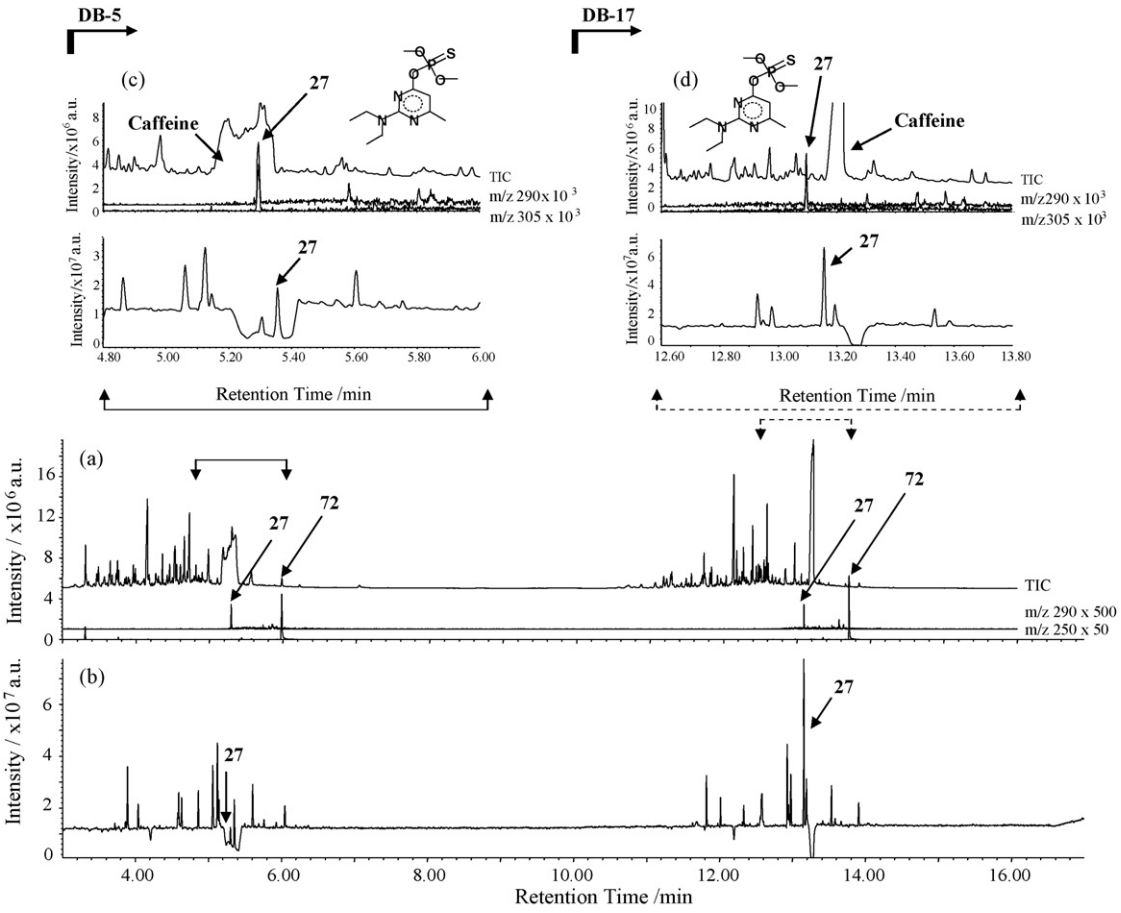

Fig. 3. Total ion chromatogram, representative mass chromatograms and PFPD chromatogram obtained by dual SBSE–TD–dual LTM-GC–MS/PFPD of a brewed green tea. (a) Total ion chromatogram and representative mass chromatograms; (b) PFPD chromatogram; (c) representative mass chromatograms and PFPD chromatogram on DB-5; (d) representative mass chromatograms and PFPD chromatogram on DB-17—27: pirimiphos-methyl (*m/z* 290) and 72: tebuconazole (*m/z* 250).

time and 1.97–4.66% for peak area on DB-17, respectively. Also good linearity was achieved with a correlation coefficient (r^2) in the range of 0.9907–0.9999 on DB-5 and 0.9866–0.9999 on DB-17.

Elution order of most of the analytes on DB-5 and DB-17 was much different from each other. For example, although primiphos-methyl (no. 10 on Fig. 2(c)) and fenitrothion (no. 11 on Fig. 2(c)) were co-eluted on DB-5, they were completely separated on DB-17 (Fig. 2(d)). On the other hand, parathion-methyl (no. 8 on Fig. 2(c)) and tolclofos-methyl (no. 9 on Fig. 2(c)) were co-eluted on DB-17 (Fig. 2(d)), they were completely separated on DB-5. Moreover, fenthion (No. 13 on Fig. 2(c)), dimethylvinphos (no. 14 on Fig. 2(c)), chloropyrifos (no. 15 on Fig. 2(c)) and parathion (no. 16 on Fig. 2(c)) were co-eluted on DB-5, chloropyrifos and parathion were completely separated, however fenitrothion and dimethylvinphos (no. 14 on Fig. 2(c)) were still co-eluted on DB-17 (Fig. 2(d)).

Retention times of phosphorus pesticides detected with MS were very slimier to those of PFPD. The delay times were in the range of 0.055–0.089 min with an average of 0.062 min on DB-5 and in the range of 0.048–0.075 min with an average of 0.061 min on DB-17, respectively. Thus, PFPD can serve as reasonable marker of phosphorus pesticides for fast identification in a total ion chromatogram.

3.3. Application

Dual LTM-GC–MS/PFPD was applied to screening of pesticide residues in a brewed green tea sample. Extraction of a brewed green tea sample was performed according to dual SBSE method [7]. Fig. 3(a) shows a total ion chromatogram and Fig. 3(b) shows a PFPD chromatograms of a brewed green tea sample. Tebuconazole was easily detected and identified with MS in the total ion chromatogram. Although pirimiphos-methyl was completely buried in the complex matrix, pirimiphos-methyl was pinpointed with PFPD and was easily identified with MS. The determination was done by use of standard addition calibration method for peak area of selected ion (*m/z* 250 for tebuconazole, *m/z* 290 for pirimiphos-methyl, respectively). Standard solution was fortified at 25, 50, 100 and 150 pg mL^{-1} in brewed green tea sample. For tebuconazole, five times fold dilution was needed. Then TD–dual LTM-GC–PFPD/MS was followed by dual SBSE method. Determination results were 510 pg mL^{-1} (R.S.D.: 7.2, $n = 5$)

on DB-5 and 550 pg mL^{-1} (R.S.D.: 7.0%, $n=5$) on DB-17 for tebuconazole, 22 pg mL^{-1} (R.S.D.: 9.3%, $n=5$) on DB-5 and 21 pg mL^{-1} (R.S.D.: 8.5%, $n=5$) on DB-17 for pirimiphos-methyl, respectively. Correlation coefficient (r^2) of the standard addition curves were 0.9966 on DB-5 and 0.9960 on DB-17 for tebuconazole, 0.9847 on DB-5 and 0.9992 on DB-17 for pirimiphos-methyl, respectively. Results on both columns were quite similar to each other with an acceptable precision. Also linearities on both columns were quite similar to each other for tebuconazole. For pirimiphos-methyl, however, linearity on DB-17 was better than those on DB-5, because pirimiphos-methyl was separated from huge matrix such as caffeine on DB-17.

4. Conclusion

A method was described for fast dual-column separation of pesticides in the complex sample. The method consisted of dual LTM-GC–MS, which allows fast dual-column separation with independent temperature programming. Also simultaneous detection with the MS and the PFPD was evaluated for fast identification of phosphorus containing pesticides. The method provides remarkable precision for various classes of 82 pesticides and rapid analysis resulting in high sample throughput. Moreover, the method was successfully applied to determination of pg mL^{-1} levels of pesticides in a brewed green tea sample with dual SBSE method.

Acknowledgements

The authors thank Toshio Teranishi of Kinryo Electric and Takashi Yamagami of Nishikawa Keisoku for their support. Our colleagues, Chiaki Nagamori, Teruyo Ieda of GERSTEL K.K. are also thanked for their contribution.

References

[1] Positive List System for Agricultural Chemical Residues in Foods, Ministry of Health, Labour and Welfare, Japan, http://www.mhlw.go.jp/english/topics/foodsafety/positivelist060228/index.html.
[2] Analytical Methods for Residual Compositional Substances of Agricultural Chemicals, Feed Additives, and Veterinary Drugs in Food, Ministry of Health, Labour and Welfare, Japan, http://www.mhlw.go.jp/english/topics/foodsafety/positivelist060228/index.html.
[3] V.R. Kinton, E.A. Pfannkoch, J.A. Whitecavage, GERSTEL AppNote 1/2005, 2005.
[4] G. Pagliuca, T. Gazzotti, E. Zironi, P. Sticca, J. Chromatogr. A 1071 (2005) 67.
[5] K. Matsuda, H. Miyakawa, H. Tanaka, K. Nakagawa, Abstracts Presented at the 90th Symposium on the Food Hygienics Society of Japan, Omiya, Japan, The Food Hygienics Society of Japan, 2005, p. 21 (in Japanese).
[6] K. Mastovska, S.J. Lehotay, J. Chromatogr. A 1000 (2003) 153.
[7] M. Kirchner, E. Matisova, S. Hrouzkova, J.D. Zeeuw, J. Chromatogr. A 1090 (2005) 126.
[8] J.C. Luong, R.L. Gras, H.J. Cortes, R.M. Mustacich, Abstracts of 27th ISCC, Riva der Garda, Italy, I.O.P.M.S., Kortrijk, Belgium, 2004, CD-ROM paper PL11.
[9] N. Ochiai, K. Sasamoto, H. Kanda, S. Nakamura, J. Chromatogr. A 1130 (2006) 83.

Available online at www.sciencedirect.com
ScienceDirect
Talanta 72 (2007) 1698–1703
Talanta
www.elsevier.com/locate/talanta

Detection of ferulic acid based on the plasmon resonance light scattering of silver nanoparticles

Hui Ying Wang, Yuan Fang Li, Cheng Zhi Huang *

Laboratory of Molecular Chemistry and Chemical Biology, Chongqing Municipal Key Laboratory of Luminescence and Real-Time Analysis, College of Chemistry and Chemical Engineering, Southwest University, Chongqing 400715, China

Received 25 December 2006; received in revised form 8 February 2007; accepted 11 February 2007
Available online 23 February 2007

Abstract

In this contribution, a plasmon resonance light scattering (PRLS) detection method of ferulic acid (FA) is proposed based on the formation of silver nanoparticles (NPs). It was found that, FA acted as a reducing agent in alkaline medium and could be oxidized by $AgNO_3$, resulting in the formation of silver NPs. The formed silver NPs, which were identified by measuring the plasmon resonance absorption spectra, PRLS spectra and transmission electron microscopy (TEM) image, display characteristic plasmon resonance optical absorption and PRLS band in the visible region. It was found that the PRLS intensity, which could be easily measured using a common spectrofluorometer, was in proportion to the concentration of FA over the range from 0.2 to 2.0 $\mu mol\,l^{-1}$ with the corresponding limits of determination (3σ) of 15.2 $nmol\,l^{-1}$. With that, ferulate sodium injection samples have been detected with R.S.D. lower than 3.0% and recoveries over the range of 101.2–104.5%. On the other hand, the present reaction maybe provides the basis of an environmentally friendly approach for the synthesization of silver NPs.

Keywords: Ferulic acid (FA); Silver nanoparticles (NPs); Plasmon resonance light scattering (PRLS)

1. Introduction

Metal nanoparticles have received considerable interests in recent years for their unusual optical and electrical properties. They have dramatically found the applications in the fields of detection of metal ions [1], DNA hybridization [2–4], optical sensors [5,6], immunoassay [7,8], aptamer-protein assay [9,10]. Among the conspicuous properties, the most interesting one but absent in the bulk metals is the plasmon resonance absorption and plasmon resonance light scattering (PRLS) which result from coherent oscillation of the conduction electrons.

When a particle is exposed to an electromagnetic wave, the electrons in the particle oscillate at the same frequency as the incident wave. According to electromagnetic theory, the oscillating electron radiates electromagnetic radiation with the same frequency as the oscillating electron. It is the secondary radiation that constitutes the scattered light, which depends on the size, composition, shape, homogeneity of the nanoparticles, and refractive index of the medium [11]. Thus, the nanoparticles absorb light very strongly in the visible region and display strong colors. So to date, most of the reported applications of metal nanoparticles involve in the plasmon resonance absorption and the yielding visual sensing. What's more, gold NPs, for the more brilliant color than silver NPs, are often used for colorimetric assay [5,13]. On the other hand, the PRLS property of the nanoparticles, a much more useful and simpler property, has been ill explored with regard to sensing, which might be more sensitive than that based on the plasmon resonance absorption of nanoparticles [11], and limited reports have been obtained for the PRLS properties of metal nanoparticles [14,15].

For different physicochemical properties of gold and silver nanoparticles, silver NPs may have more wide applications than the gold in some fields, such as in the fields of surface enhanced Raman scattering [16,17]. Previous studies mainly focused on developing different methods for synthesization of silver NPs, and limited reports can be found on the emphasis of the optical applications as that of gold NPs. Coupled with the properties and the research status of the metal nanoparticles, we have carried on the research on the PRLS properties of silver NPs [18]. We believe that the colloid nanoparticles maybe have the poten-

* Corresponding author. Tel.: +86 23 68254659; fax: +86 23 68866796.
E-mail address: chengzhi@swu.edu.cn (C.Z. Huang).

0039-9140/$ – see front matter © 2007 Published by Elsevier B.V.
doi:10.1016/j.talanta.2007.02.028

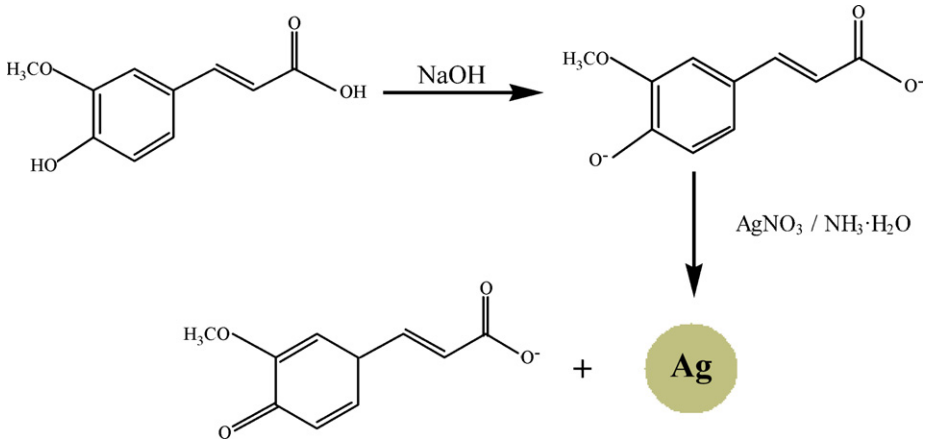

Fig. 1. The molecular structure of FA and the chart of the reaction mechanism between FA and $AgNO_3$.

tial to offer new analytical approaches based on their PRLS properties.

Ferulic acid (FA, 4-hydroxy,3-methoxycinnamic acid, its molecular structure is displayed in Fig. 1) is an effective component of medicine herbs, such as Angelica sinensis and Lignsticum Chuanxiong. FA is a phenolic acid and generally serves pharmacological functions such as anticoagulant, antioxidant, antimicrobial, anti-inflammatory, anti-arrhythmic and so on [19,20]. It also possesses the function of sanitarian care. Due to its pharmacological importance, developing simple and accurate detection methods of FA is desired. To date, reported methods involved UV–vis spectrophotometry [21], high performance liquid chromatography [22–24], micellar electrokinetic chromatography [25], capillary electrophoresis [26], electroanalysis [27,28], chemiluminescence [29], and so on. However, most of above methods are less sensitive, time-consuming or using expensive apparatus.

In this contribution, we propose a sensitive and simple method to detect FA based on the formation of silver NPs by measuring the PRLS signals of silver NPs with a common spectrofluorometer.

2. Experimental

2.1. Apparatus

The plasmon resonance light scattering (PRLS) spectra and intensity were measured with a F-4500 spectrofluorometer (Hitachi, Tokyo, Japan). The plasmon resonance optical absorption was performed on a U-3010 spectrophotometer (Hitachi, Tokyo, Japan). A TecNai-10 electron microscope (FEI, USA) was used to measure the transmission electron microscopy (TEM) images of silver NPs. A vortex mixer QL-901 (Haimen, China) was used to blend the solution.

2.2. Reagents

Ferulic acid was commercially purchased from the National Institute for the Control of Pharmaceutical and Biological Products (Beijing, China) and used without further purification. 1.0×10^{-4} mol l^{-1} of the stock solution was prepared by dissolving the standard in distilled water. Ferulate sodium injection (Chongqing yaoyou Co., Ltd., Chongqing, China) was dissolved in distilled water. 0.1 mol l^{-1} stock solution of $AgNO_3$ was prepared by dissolving solid $AgNO_3$ in distilled water and the working solution was obtained by diluting the stock solution to 1.0×10^{-3} mol l^{-1} with water. 0.1 mol l^{-1} NaOH, 0.25 mol l^{-1} $NH_3{\cdot}H_2O$ were used. All the reagents employed in this work were of analytical grade without further purification. Water used throughout was doubly distilled.

2.3. Procedures

In a 10-ml test tube were added 2.5 ml of 1.0×10^{-3} mol l^{-1} $AgNO_3$, 10 μl of 0.1 mol l^{-1} NaOH and 60 μl of 0.25 mol l^{-1} $NH_3{\cdot}H_2O$, the mixture was mixed thoroughly, and then FA solution was added into the mixture. At last, the mixture was diluted to 5.0 ml with the doubly distilled water, and blended thoroughly again. Thirty minutes later, the plasmon resonance absorption and light scattering spectra were recorded against the reagent blank solution treated in the same way without the ferulic acid.

The plasmon resonance scattering spectrum was obtained by scanning simultaneously the excitation and emission monochromators of the F-4500 spectrofluorometer from 350 to 700 nm (namely, $\Delta\lambda = 0$ nm), and all the PRLS measurements were made with 5.0 nm slit-width of the excitation and the emission of the spectrofluorometer and the PMT voltage 400 V.

3. Results and discussion

3.1. The spectral features of the redox reactions between FA and $AgNO_3$

The absorption features of the redox reaction system were displayed in Fig. 2. It was found that the absorption of FA in the alkaline medium is very low over the range from 370 to 500 nm. While $AgNO_3$ was added, the mixture presents slight yellowish 30 min later and a new absorption peak appeared at nearby 430 nm, which should be ascribed to the plasmon resonance absorption of silver NPs [11,30], indicative of silver NPs.

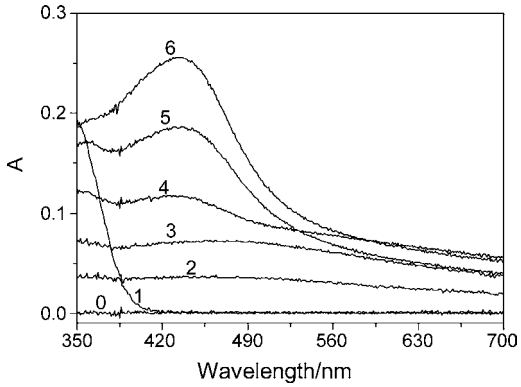

Fig. 2. The plasmon absorption of silver NPs resulting from the redox reaction between FA and $AgNO_3$ in alkaline medium. Concentrations: $AgNO_3$, 5.0×10^{-4} mol l^{-1}; NaOH, 2.0×10^{-4} mol l^{-1}; $NH_3{\cdot}H_2O$, 3.0×10^{-3} mol l^{-1}; FA (from curves 0 to 6, μmol l^{-1}), 0, 3.6 (without $AgNO_3$), 0.6, 1.2, 1.8, 2.6 and 3.6.

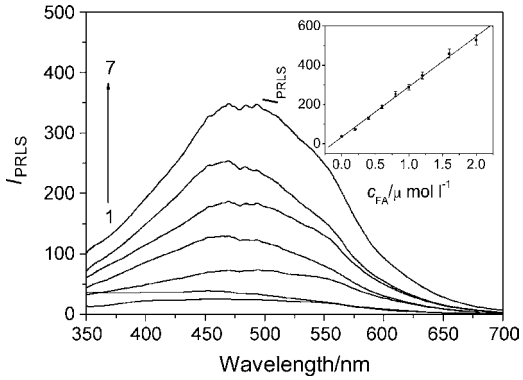

Fig. 4. The PRLS spectra of silver NPs resulting from the reaction of $AgNO_3$ and FA. Concentrations: $AgNO_3$, 5.0×10^{-4} mol l^{-1}; NaOH, 2.0×10^{-4} mol l^{-1}; $NH_3{\cdot}H_2O$, 3.0×10^{-3} mol l^{-1}; FA (from curves 1 to 7, μmol l^{-1}), 1.2 (without $AgNO_3$), 0, 0.2, 0.4, 0.6, 0.8 and 1.2. The inset is the calibration curve of the FA under optimal conditions. Linear regression equation (c, μmol l^{-1}), $\Delta I = -5.4 + 258.0c$ over the range of 0.2–2.0 μmol l^{-1} with the correlation coefficient 0.9978 and limits of determination (3σ) 15.2 nmol l^{-1}.

The generation of silver NPs proceeded without the addition of silver NPs seeds. The formation of silver NPs can also be identified by the TEM image showed in Fig. 3. In contrast, no silver NPs formed within 30 min in a control experiment in the absence of FA, that is, the presence of FA is essential for the formation of silver NPs. From Fig. 2 we could see that with the increase of the concentration of FA, the absorption characteristic to plasmon resonance absorption of the silver NPs was intensified.

From the spectra of the plasmon resonance absorption, we can find that the shape of the spectra remains nearly symmetric and no significant changes display, indicating that the formed silver nanoparticles are nearly homogeneous, which can be identified by the TEM image. The average dimensions are about 28–33 nm (Fig. 3A and B). When the concentration of FA is relatively low, the formed silver NPs are nearly monodisperse and keep dispersion in the solution. While in the higher concentration of FA, the formed silver NPs begin to get larger and give a trend to be aggregated (Fig. 3C).

Fig. 4 shows the PRLS spectra of the redox reaction between FA and $AgNO_3$ detected with a common spectrofluorometer. We can see that the PRLS peak located at around 470 nm, which belongs to the plasmon absorption region of 370–500 nm, so the light scattering of the silver NPs is ascribed to the resonance light scattering and the signals we measured herein are truly the PRLS ones. Considering the relationship between the absorption and light scattering spectra of the silver NPs, we think that the PRLS spectra can also demonstrate the formation of silver NPs from another point of view, and the process of formed silver NPs is correlative to the presence of FA. Fig. 4 indicates that the PRLS intensity of FA or the $AgNO_3$ blank solution alone was quite weak. After reacting with $AgNO_3$, however, the silver NPs were formed in the mixture, the RPLS intensity gets enhanced and increases with increasing the FA concentration. So we can construct a quantitative analytical method for the detection of FA.

3.2. Optimal conditions of the reaction

In this reaction system, $AgNO_3$ serves as an oxidant. Its concentration in the solution is important, and it is not better for more $AgNO_3$ were used in the reaction, that is, there is an optimal concentration in the reaction solution. Thus we first investigated the dependence of PRLS intensity on the concentration of $AgNO_3$. Fig. 5 displays the PRLS intensity got enhanced with the increase of $AgNO_3$ concentration, the strong PRLS signals could be obtained when 2.5 ml 1.0×10^{-3} mol l^{-1} $AgNO_3$ was used, and then declined gradually.

We tried the reaction under neutral or acidic pH conditions, but we failed to obtain silver NPs. Motivated by the "silver mirror" reaction and Ref. [31], with some modifications

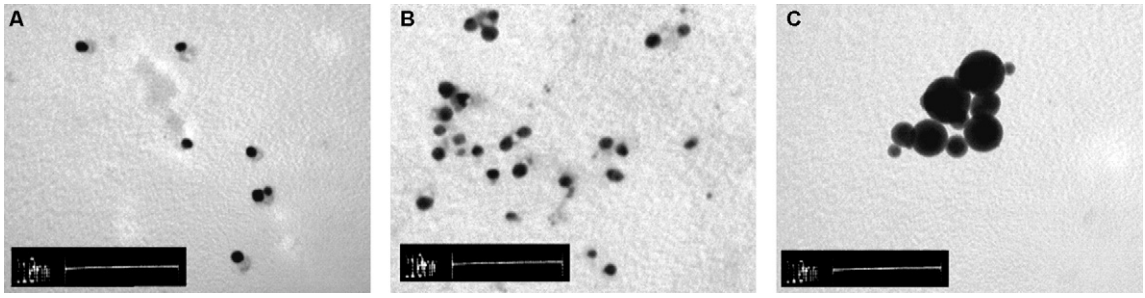

Fig. 3. TEM images of silver NPs resulting from the reaction of FA and $AgNO_3$. Concentrations: $AgNO_3$, 5.0×10^{-4} mol l^{-1}; NaOH, 2.0×10^{-4} mol l^{-1}; $NH_3{\cdot}H_2O$, 3.0×10^{-3} mol l^{-1}; FA, 0.8, 1.8, 6.0 μmol l^{-1}.

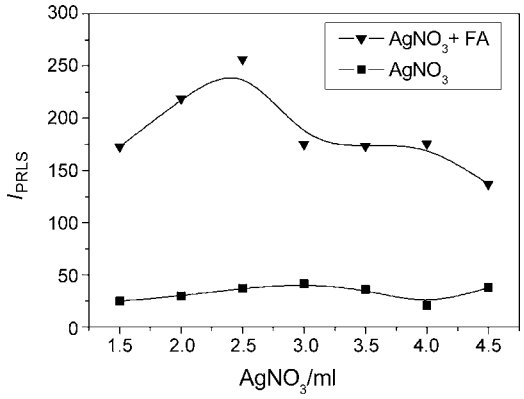

Fig. 5. Dependence of the PRLS intensity on the concentrations of $AgNO_3$. Concentrations: NaOH, 2.0×10^{-4} mol l^{-1}; $NH_3{\cdot}H_2O$, 3.0×10^{-3} mol l^{-1}; FA, 0.8 μmol l^{-1}.

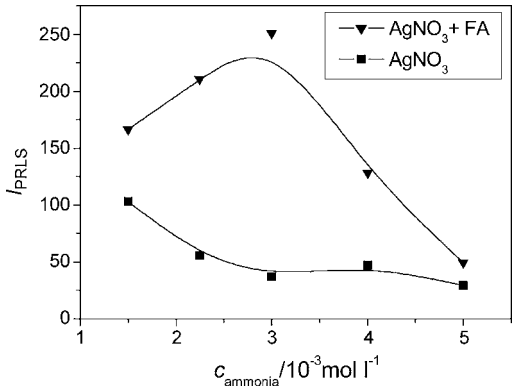

Fig. 7. Dependence of the PRLS intensity on the concentrations of ammonia. Concentrations: $AgNO_3$, 5.0×10^{-4} mol l^{-1}; NaOH, 2.0×10^{-4} mol l^{-1}; FA, 0.8 μmol l^{-1}.

we added NaOH coupled with ammonia into the mixture in order to provide enough alkalinity. Fig. 6 shows the effect of NaOH concentration on the PRLS intensity, we can see that the PRLS intensity was intensified with increasing the concentration of NaOH until 2.0×10^{-4} mol l^{-1}, the PRLS signals got to the strongest, and then decreased quickly. So at last NaOH 2.0×10^{-4} mol l^{-1} was used. The problem is that NaOH alone would make silver cation deposit, weakening the capacity of oxidation. In this case, ammonia is needed. The ammonia concentration on the PRLS intensity was investigated. As Fig. 7 shows, with ammonia increasing, the PRLS intensity gets increased at first until it is up to 3.0×10^{-3} mol l^{-1} and then declines evidently.

3.3. Mechanism of the redox reaction

The principle of the method is to detect the PRLS intensity of silver NPs resulting from deoxidized by FA in alkaline medium (Fig. 1). As Fig. 1 shows, FA, with a phenol group in its molecular structure, can be oxidized under certain conditions. Studies [31–33] have shown that compounds with the phenol hydroxyl groups in their molecular structures possessed some reducing power and could be oxidized under certain conditions, and then they were oxidized into corresponding quinone structure. In the present reaction of FA and $AgNO_3$, $AgNO_3$ oxidized the phenol acid in alkaline medium. The carboxylic and phenol groups are firstly ionized, but the former cannot be oxidized under the present conditions and the phenol is converted into a phenate ion, which become more reducible. So we can deduce that $AgNO_3$ oxidizes the phenate ion in the presence of ammonia. As we know, under the conditions silver ions can complex with ammonia, but there is an equilibrium in solution between the $[Ag(NH_3)_2]^+$ and Ag^+ ($[Ag(NH_3)_2]^+ \leftrightarrow Ag^+ + 2NH_3$), so it is deduced that at last FA was oxidized by Ag^+, and converted to corresponding quinone structure, at the same time Ag^+ was deoxidized into silver NPs leading to the strong PRLS signals. So it is the phenol group that is oxidized in company with the formation of silver NPs.

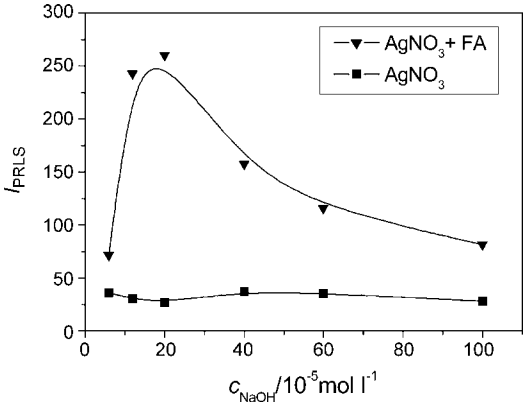

Fig. 6. Dependence of the PRLS intensity on the concentrations of NaOH. Concentrations: $AgNO_3$, 5.0×10^{-4} mol l^{-1}; $NH_3{\cdot}H_2O$, 3.0×10^{-3} mol l^{-1}; FA, 0.8 μmol l^{-1}.

Table 1
Interference of coexisting foreign substances

Foreign substances	Concentration (μmol l^{-1})	Change in I (%)
Na^+, Cl^-	15.0	1.21
K^+, Cl^-	15.0	1.43
Ba^{2+}, Cl^-	10.0	4.02
Mg^{2+}, F^-	10.0	3.53
Cu^{2+}, $SO_4{}^{2-}$	8.0	−5.80
Al^{3+}, Cl^-	10.0	1.79
L-Phenylalanine	10.0	−6.68
Glutamic acid	8.0	2.61
Glucose	10.0	−6.69
CTMAB	8.0	9.34
Fe^{3+}, Cl^-	2.0	3.54
Vitamin C	1.0	3.79
Ni^{2+}, Cl^-	10.0	6.24
Pb^{2+}, $NO_3{}^-$	4.0	1.62
Cd^{2+}, $NO_3{}^-$	6.0	5.60
SDS	2.0	5.42
Glycine	8.0	2.46
Urea	10.0	−7.31
Lactose	10.0	2.21
OP	0.004[a]	5.16

[a] %; Concentrations: $AgNO_3$, 5.0×10^{-4} mol l^{-1}; NaOH, 2.0×10^{-4} mol l^{-1}; $NH_3{\cdot}H_2O$, 3.0×10^{-3} mol l^{-1}; FA, 1.0×10^{-6} mol l^{-1}.

Table 2
Determination of FA in real samples ($n = 5$)

Sample	Found (μM)	Added (μM)	Total found (μM)	Recovery (%)	R.S.D. (%)
1	0.662	0.400	1.069	101.2	3.0
2	0.762	0.600	1.389	104.5	2.7
3	0.598	0.800	1.420	102.8	2.6

All the values were the average of five measurements obtained using FA as standard. The FA sample was prepared by dissolving with water as work solution. Concentrations: $AgNO_3$, 5.0×10^{-4} mol l^{-1}; NaOH, 2.0×10^{-4} mol l^{-1}; $NH_3{\cdot}H_2O$, 3.0×10^{-3} mol l^{-1}.

3.4. Interference of the coexisting foreign substances

In order to evaluate the present method, the influences of foreign coexisting substances such as metal ions, amino acids, glucide, surfactants were tested. The results are presented in Table 1. Of these tested substances, Na^+, K^+, Ba^{2+}, Al^{3+}, Mg^{2+}, glucide, L-phenylalanine, glutamic acid, glycine and urea could be allowed to be high concentration given the tolerance level of 10%. Heavy metal ions including Fe^{3+}, Cu^{2+}, Cd^{2+}, Ni^{2+}, Pb^{2+}, on the other hand, could be allowed lower possibly for these metal ions can complex with the ammonia and then affect the detection. Vitamin C with strong reducibility may be oxidized by $AgNO_3$ at the conditions and produce silver NPs interfering the determination. So maybe the substances with more reducible ability than FA or the heavy metal ions strongly complex with ammonia interfere the detection to some extent.

3.5. Analytical performance

According to the above general procedures, under the optimal conditions, the dependence of PRLS intensity on the concentration of FA was determined (the inset in Fig. 4). All the PRLS intensities were obtained at 469.4 nm. The analytical parameters of this method show that there is a good linear relationship between the PRLS intensities and the concentrations of FA over the range from 0.2 to 2.0 μmol l^{-1}, and the linear regression equation is $\Delta I = -5.4 + 258.0c$ (c, μmol l^{-1}) with the correlation coefficient 0.9978. The limits of determination (3σ, LOD) 15.2 nmol l^{-1}, showing the present method is very sensitive for the detection of FA.

In order to test the reliability of the present method, we determined the Ferulate sodium injection by dissolving them in distilled water without further purification under the optimal conditions according to the general procedures. The results are listed in Table 2. As Table 2 shows that the detection values for the Ferulate sodium injection are identical to the expected, and the R.S.D. values lower than 3.0% and the recoveries over the range of 101.2–104.5% are acceptable.

4. Conclusions

In this contribution, we have proposed an approach for the detection of FA by detecting the PRLS intensity of formed silver NPs with a common spectrofluorometer. FA served as a reducing agent and could be oxidized by $AgNO_3$ in alkaline medium, at the same time $AgNO_3$ was deoxidized, and then produced silver NPs. The approach is simple and convenient which avoid the pretreatment and separation of the drugs. The detection of samples shows that the method is sensitive and reliable. In the future, when the conditions are under control, this method may also be a valuable basis for development of drugs detection and exploits the applications of silver NPs on optical properties. In addition, the present reaction maybe provides an environmentally friendly approach for the synthesization of silver NPs.

Acknowledgments

All authors herein are grateful to the supports from the National Natural Science Foundation of China (NSFC, No: 30570465, 20425517) and the Ministry of Science and Technology of the People's Republic of China (2006CB933100).

References

[1] S.-Y. Lin, S.-W. Liu, C.-M. Lin, C.-H. Chen, Anal. Chem. 74 (2002) 330.
[2] J.J. Storhoff, R. Elghanian, R.C. Mucic, C.A. Mirkin, R.L. Letsinger, J. Am. Chem. Soc. 120 (1998) 1959.
[3] K. Sato, K. Hosokawa, M. Maeda, J. Am. Chem. Soc. 125 (2003) 8102.
[4] B.-A. Du, Z.-P. Li, C.-H. Liu, Angew. Chem. Int. Ed. 45 (2006) 8022.
[5] R. Elghanian, J.J. Storhoff, R.C. Mucic, R.L. Letsinger, C.A. Mirkin, Science 277 (1997) 1078.
[6] J.W. Liu, Y. Lu, Anal. Chem. 76 (2004) 1627.
[7] S.-B. Zhang, Z.-S. Wu, M.-M. Guo, G.-L. Shen, R.-Q. Yu, Talanta 71 (2007) 1530.
[8] L.A. Lion, M.D. Musick, M.J. Natan, Anal. Chem. 70 (1998) 5177.
[9] V. Pavlov, Y. Xiao, B. Shlyahovsky, I. Willner, J. Am. Chem. Soc. 126 (2004) 11768.
[10] C.-C. Huang, Y.-F. Huang, Z.H. Cao, W.G. Tan, H.-T. Chang, Anal. Chem. 77 (2005) 5735.
[11] J. Yguerabide, E.E. Yguerabide, Anal. Biochem. 262 (1998) 137.
[13] M.S. Han, A.K.R. Lytton-Jean, C.A. Mirkin, J. Am. Chem. Soc. 128 (2006) 4954.
[14] K. Aslan, J.R. Lakowicz, C.D. Geddes, Anal. Chem. 77 (2005) 2007.
[15] D. Roll, J. Malicka, I. Gryczynski, Z. Gryczynski, J.R. Lakowicz, Anal. Chem. 75 (2003) 3440.
[16] C.E. Talley, L. Jusinski, C.W. Hollars, S.M. Lane, T. Huser, Anal. Chem. 76 (2004) 7064.
[17] S.M. Nie, S.R. Emory, Science 275 (1997) 1102.
[18] L.P. Wu, Y.F. Li, C.Z. Huang, Q. Zhang, Anal. Chem. 78 (2006) 5570.
[19] W.X. Fang, C.S. Song, L.X. Zhou, Chinese Traditional Medicine Pharmacology, People's Medical Publishing House, Beijing, China, 1998.
[20] S.Y. Ou, H.Y. Bao, Z.D. Lan, J. Chin, Med. Mater. 24 (2001) 220.
[21] N. Cui, J.H. Qian, Y.Q. Qian, Y.F. Tang, Lishizhen Med. Mater. Med. Res. 11 (2000) 32.
[22] X.P. Li, J. Yu, J.Y. Luo, H.S. Li, F.J. Han, X.G. Chen, Z.D. Hu, Chem. Pharm. Bull. 52 (2004) 1251.
[23] Y. Li, K. Bi, Biomed. Chromatogr. 17 (2003) 543.
[24] G.-H. Lu, K. Chan, K. Leung, C.-L. Chan, Z.-Z. Zhao, Z.-H. Jiang, J. Chromatogr. A 1086 (2005) 209.
[25] T. Guo, Y. Sun, Y. Sui, F.M. Li, Anal. Bioanal. Chem. 375 (2003) 840.

[26] S.G. Ji, Y.F. Chai, Y.T. Wu, X.P. Yin, D.S. Liang, Z.-X. Xu, X. Li, Biomed. Chromatogr. 13 (1999) 333.
[27] Z. Ai, F. Liao, L. Zhu, D.C. Cai, Appl. Chem. Chin. 123 (2006) 566.
[28] W. Cao, Z.R. Suo, J.R. Song, J.B. Zheng, J. Chin. Univ. 26 (2005) 1424.
[29] L.N. Li, N.B. Li, H.Q. Luo, Anal. Sci. 21 (2005) 963.
[30] J. Yguerabide, E.E. Yguerabide, Anal. Biochem. 262 (1998) 157.
[31] P.R. Selvakannan, A. Swami, D. Srisathiyanarayanan, P.S. Shirude, R. Pasricha, A.B. Mandale, M. Sastry, Langmuir 20 (2004) 7825.
[32] M. Scampicchio, J. Wang, A.J. Blasco, A.S. Arribas, S. Mannino, A. Escarpa, Anal. Chem. 78 (2006) 2060.
[33] R. Baron, M. Zayats, I. Willner, Anal. Chem. 77 (2005) 1566.

Available online at www.sciencedirect.com
ScienceDirect
Talanta 72 (2007) 1655–1658
Talanta
www.elsevier.com/locate/talanta

Simplification of determination method for standard materials using post-column reaction GC/FID

Takuro Watanabe [a,*], Kenji Kato [a], Nobuhiro Matsumoto [a], Tsuneaki Maeda [b]

[a] *Organic Standards Section 1, Organic Analytical Chemistry Division, National Metrology Institute of Japan (NMIJ), National Institute of Advanced Industrial Science and Technology (AIST), AIST Tsukuba Central 3-10, 1-1-1 Umezono, Tsukuba, Ibaraki 305-8563, Japan*
[b] *National Metrology Institute of Japan (NMIJ), National Institute of Advanced Industrial Science and Technology (AIST), AIST Tsukuba Central 5-2, 1-1-1 Higashi, Tsukuba, Ibaraki 305-8565, Japan*

Received 30 October 2006; received in revised form 16 March 2007; accepted 18 March 2007
Available online 24 March 2007

Abstract

For the simple and fast preparation of highly reliable standard materials, a post-column reaction GC/FID system was developed and evaluated on the mixture of oxygen-containing organic compounds. The oxygen-containing organic compounds mixing solution were determined with the post-column reaction GC/FID system using *n*-dodecane as an internal calibration standard. Required value of relative expanded uncertainty as an original source of SI-traceable standard materials was within 1% and it aimed at this value as accuracy of the quantitative analysis. The results showed good agreement between the prepared concentrations and analytical values using post-column reaction GC/FID system. These results indicated that the post-column reaction GC/FID system would be used for getting SI-traceable values.

Keywords: GC/FID; Post-column reaction; Standard material; Oxygen-containing organic compound

1. Introduction

The requirement for the calibration of an analytical instrument using highly reliable standards, e.g. SI-traceable standard materials, is increasing in recent years. Generally, the SI-traceable standard materials are prepared by gravimetric mixing purity known raw materials which is traceable to SI. However, it is very difficult to prepare the SI-traceable standard materials. There are three points of the difficulty. First point is the determination of the purity of raw material. If we can find all impurity in the raw material and have an appropriate method for the quantification, we can use subtracting method [1]. Freezing point depressing method, which is one of the primary methods for the measurements [2] can determine the purity of the raw material directly. However the unit of this purity is molar fraction, $\mathrm{mol\,mol^{-1}}$, it is necessary to convert unit from the $\mathrm{mol\,mol^{-1}}$ into a mass fraction ($\mathrm{kg\,kg^{-1}}$) prior to the preparation of the mixture. The information of the impurity in the raw materials should be available. The second one is the preparation of the mixture using gravimetry. The gravimetry is very precise measurement method for the stable materials. An error in weighing must be minimized during the preparation, and special care has to be exercised to prevent the mixture from contamination and vaporization. The third one is the chemical reactions after the preparation or storage. In such case, gravimetry is not precise method.

In order to avoid these three difficult points, a new method for the evaluation of standard materials was developed and evaluated using a post-column reaction GC/FID system [3]. The target compounds in a sample were separated by GC, oxidized at first furnace, then reduced into methane by chemical reactions, and then detected as methane by FID. It was shown that the hydrocarbons as target compounds were quantitatively detected as methane. We selected the oxygen-containing organic compounds as target compounds because of the following three reasons. Firstly, the relative response of these compounds on FID was strongly affected by the functional groups [4–10] and it changed by the operational conditions of the FID. The secondly, purities of these compounds were difficult to determine. The thirdly, it is easy to contaminate water in the oxygen-containing

* Corresponding author. Tel.: +81 29 861 6851; fax: +81 29 861 6854.
E-mail address: watanabe-takuro@aist.go.jp (T. Watanabe).

0039-9140/$ – see front matter © 2007 Elsevier B.V. All rights reserved.
doi:10.1016/j.talanta.2007.03.032

organic compounds at a calibration standard preparation process.

Relative expanded uncertainty [11] of the preparation for standard materials with the gravimetric method is generally below 0.1%. However, measurements with analytical instruments are required in order to check this preparation accuracy. The uncertainty of measurement should be added to the uncertainty of the preparation. Therefore, desired value of relative expanded uncertainty as an original source of SI-traceable standard materials is 1%, and the value was targeted as the measurement accuracy of the post-column reaction GC/FID system.

2. Experimental

2.1. Instrument

A schematic diagram of the instrument was shown in Fig. 1. The system was simplified from previous one [3]. The bypass valve for the oxidation micro-reactor was removed, a heated transfer line was added and the end of the capillary column was inserted almost directly into the oxidation catalyst. The oxidation catalyst was changed from palladium-asbestos to palladium wool (Tanaka Kikinzoku Kogyo K.K., Tokyo, Japan) for safety. The operating conditions of the post-column reaction GC/FID system is summarized in Table 1.

2.2. Chemicals

Methyl benzoate, 2-octanone, *n*-dodecane, and acetone were purchased from Wako Pure Chemical Industries Ltd. (Osaka, Japan). Ethyl phenyl ether and *n*-octanol were purchased from Tokyo Chemical Industry Co., Ltd. (Tokyo, Japan). Purities of all chemicals were analyzed and specified by ourselves, and summarized in Table 2. *n*-Dodecane was selected as an internal standard.

2.3. Preparation of high precision sample solutions of an oxygen-containing organic compound, n-dodecane, and acetone using gravimetric method

A 30-mL vial was equipped with a crimp-top Mininert valve (Valco Instruments Co. Inc., Houston, TX, USA). An oxygen-containing organic compound was added to the vial using a syringe, and then *n*-dodecane was added. After the addition, the mixture was diluted with acetone, and this mixture was used as a parent solution. A portion of the parent solution was added to the other 30-mL vial equipped the crimp-top Mininert valve, and then the parent solution was further diluted with acetone. This final solution was used as the sample. Prepared sample solutions were summarized in Table 3.

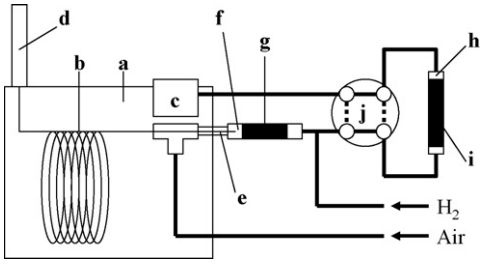

Fig. 1. Schematic diagram of the post-column reaction GC/FID. (a) gas chromatograph; (b) capillary column; (c) detector (FID); (d) automatic injector and cool on-column injector; (e) transfer line; (f) micro-reactor for oxidation; (g) oxidation catalyst; (h) micro-reactor for reduction; (i) reduction catalyst; (j) bypass valve (four-port valve) for the micro-reactor (h).

Table 1
Operating condition of the post-column reaction GC/FID system

Condition of the GC/FID	
Gas chromatograph	Agilent 6890
Injection method	On-column injection with automatic liquid sampler
Sample volume	0.1 μL
Column	SOLGEL-WAX (60 m × 0.25 mm i.d., 0.25 μm thickness)
Column flow	He: 3.0 mL min^{-1}
Oven temperature	An initial hold of 2 min at 35 °C, 5 °C/min until 165 °C, 15 °C/min until 225 °C, and then hold 4 min at 225 °C
Fuel gas[a]	H_2: 40 mL min^{-1}; air: 450 mL min^{-1}
Makeup gas	He: 40 mL min^{-1}
FID temperature	250 °C
Condition of the post-column reaction system	
Oxidizing reagent	Air: 1 mL min^{-1}
Oxidation catalyst	Palladium wool
Oxidizing temperature	390 °C
Reducing reagent	H_2: 5 mL min^{-1}
Reduction catalyst	Nickel catalyst for methanizer
Reducing temperature	390 °C
Transfer line temperature	250 °C

[a] These values include the volume of added oxidizing/reducing reagent.

Table 2
Chemical purities

Compounds	Purities (%)
Methyl benzoate	99.86
2-Octanone	98.55
Ethyl phenyl ether	99.26
n-Octanol	99.81
n-Dodecane	99.83
Acetone	99.95

3. Results and discussion

3.1. Performance check of oxidation process

The efficiency of the oxidation reaction in the instrument was evaluated for *n*-dodecane, methyl benzoate, *n*-octanol, ethyl phenyl ether, and 2-octanone. In this experiment, the second micro-reactor is bypassed, and then all components are converted to CO_2 and introduced into the FID. There appeared no peaks as FID has no response to CO_2. All compounds' peaks did not appear, so the oxidation reaction was carried out perfectly.

Table 3
Prepared sample solutions

Sample	Oxygen-containing organic compound	Concentration (μmol mol^{-1}) (mean ± expanded uncertainty, $k=2$)	
		Oxygen-containing organic compound	*n*-Dodecane
1	Methyl benzoate	112.47 ± 0.19	72.89 ± 0.13
2	*n*-Octanol	363.85 ± 0.26	248.89 ± 0.20
3	Ethyl phenyl ether	279.56 ± 0.29	190.85 ± 0.20
4	2-Octanone	273.49 ± 0.27	184.69 ± 0.19

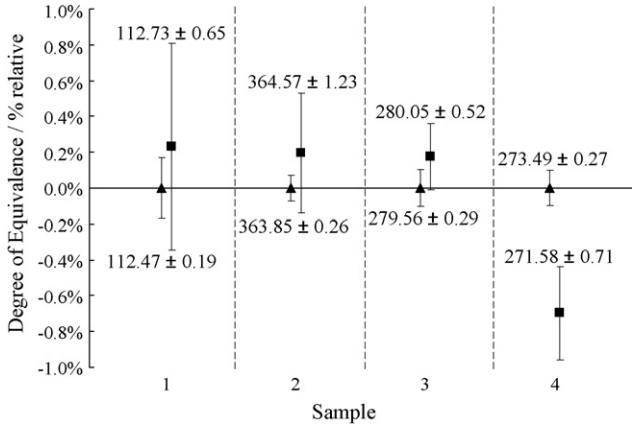

Fig. 2. Comparison of the reference values of target compounds' concentrations in sample solution with the results obtained by the post-column reaction GC/FID. Units of the values (mean ± expanded uncertainty, $k=2$, $n=5$) of the reference and the result were μmol mol^{-1}. (▲) Reference value of each target compounds; (■) obtained result.

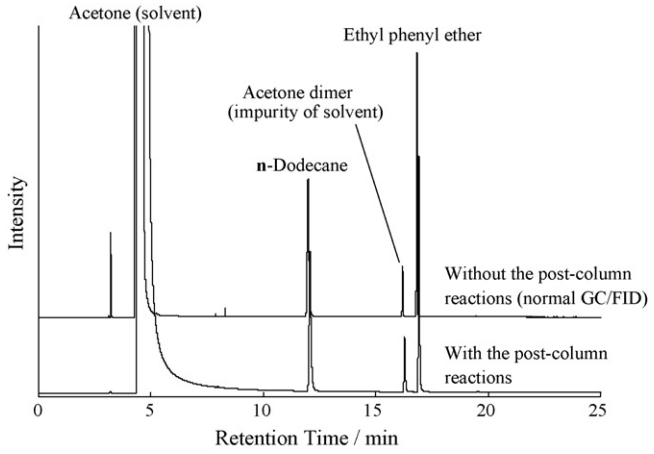

Fig. 3. Chromatograms of the sample solution **3** with and without the post-column reactions. The scale of these chromatograms was identical. Both chromatograms were shifted for clarity.

3.2. Application to the oxygen-containing organic compounds

Quantitative analysis of the oxygen-containing organic compounds in sample solutions was carried out with the post-column reaction GC/FID system. Sample solutions **1**, **2**, **3**, and **4**, which contained oxygen-containing organic compounds and *n*-dodecane as an internal standard were used. The analyte concentrations and their combined uncertainty were calculated with the equations in the previous report [3]. Five measurements for each sample solutions were performed, and the obtained results are summarized in Fig. 2. The vertical axis of the figure represents the relative difference in the experimental values to the reference values. Chromatograms of the sample solution **3** with and without the post-column reactions were shown in Fig. 3. The peak shape and the retention time of all peaks in the two chromatograms practically agreed. It showed the micro-reactors worked well. The results on the relative responses of the oxygen-containing organic compounds to *n*-dodecane were summarized in Table 4. The uncertainties of the measurements were almost the same whether there is used the post-column reaction system or not. The analytical results, except for that of 2-octanone, were in good agreement with the prepared values. The result for 2-octanone was slightly lower than the prepared values. It was estimated that both of 2-octanone and acetone as solvent are ketones and the aldol reaction [12] was occurred a little bit during preparation and storage. Thus, the value of true concentration of 2-octanone in the sample solution **4** was lower than the reference value. The true concentration of calibration standards may change during preparation and storage, but generally it is difficult to estimate the amount of change. In the post-column reaction GC/FID system, the amount can be estimated. The relative response factor of the oxygen-containing organic compounds and *n*-dodecane showed same value by the post-column reaction GC/FID system. These results had shown

Table 4
Relative response on FID for target hydrocarbons to the reference compounds per carbon atom with/without using the post-column reactors

Compounds		Sample	Relative response for the target compound to the reference compound per carbon atom ($n=5$, mean ± expanded uncertainty, $k=2$)	
Target	Reference		Without	With
Methyl benzoate	*n*-Dodecane	**1**	0.848 ± 0.007	1.002 ± 0.006
n-Octanol	*n*-Dodecane	**2**	0.929 ± 0.002	1.002 ± 0.003
Ethyl phenyl ether	*n*-Dodecane	**3**	0.892 ± 0.002	1.002 ± 0.002
2-Octanone	*n*-Dodecane	**4**	0.894 ± 0.002	0.993 ± 0.003

that the post-column reaction GC/FID system can be employed in order to determine precisely the compounds which contain only carbon, hydrogen, and oxygen atoms using any of hydrocarbons and oxygen-containing organic compound as a calibration standard. In other words, the post-column reaction GC/FID system is acceptable to use as a primary ratio method [2]. These results also indicate that it is possible to revaluation the prepared standard materials without using a specific calibration material. Furthermore, if the precise mixing ratio of the raw material is known, the purity of the raw material can be estimated.

4. Conclusion

The post-column reaction GC/FID system still needs one stable standard material. We achieved simplification of the preparation of the SI-traceable standard materials. The advantages of the post-column reaction GC/FID system are the followings; first, evaluation of SI-traceable concentration of a prepared sample can be carried out at any time without using a specific calibration standard. Secondly, determination of the specific value of SI-traceable standard materials is possible even if the purity of the raw materials could not be determined.

Using the post-column reaction GC/FID system, it is possible to prepare precise standard materials more simply and quickly using the system even without knowing purity of raw material. Further, it could also be applicable to unstable materials. The result on the comparison of the SI-traceable certified material and this method will be reported on the next paper.

References

[1] ISO 6142, Gas Analysis – Preparation of Calibration Gas Mixtures – Gravimetric Method, International Organization for Standards, Geneva, 2001.
[2] M.J.T. Milton, T.J. Quinn, Metrologia 38 (2001) 289.
[3] T. Watanabe, K. Kato, N. Matsumoto, T. Maeda, Chromatography 27 (2006) 49.
[4] J.C. Sternberg, W.S. Gallaway, D.T.L. Jones, in: N. Brenner, J.E. Callen, M.D. Weiss (Eds.), Gas Chromatography, Academic Press, New York, 1962, pp. 231–267.
[5] G. Perkins Jr., G.M. Rouayheb, L.D. Lively, W.C. Hamilton, in: N. Brenner, J.E. Callen, M.D. Weiss (Eds.), Gas Chromatography, Academic Press, New York, 1962, pp. 269–285.
[6] G. Perkins Jr., R.E. Laramy, L.D. Lively, Anal. Chem. 35 (1963) 360.
[7] R.G. Ackman, J. Gas Chromatogr. 2 (1964) 173.
[8] H.Y. Tong, F.W. Karasek, Anal. Chem. 56 (1984) 2124.
[9] J.T. Scanlon, D.E. Willis, J. Chromatogr. Sci. 23 (1985) 333.
[10] A.D. Jorgensen, K.C. Picel, V.C. Stamoudis, Anal. Chem. 62 (1990) 683.
[11] BIPM, IEC, IFCC, IUPAC ISO, IUPAP, OIML, Guide to the Expression of Uncertainty in Measurement, 1st ed., International Organization for Standards, Geneva, 1995.
[12] R. Mahrwald (Ed.), Modern Aldol Reactions, vols. 1 and 2, Wiley–VCH Verlag GmbH & Co. KGaA, Weinheim, 2004.

Available online at www.sciencedirect.com
ScienceDirect
Talanta 72 (2007) 1693–1697
Talanta
www.elsevier.com/locate/talanta

Multifunctional nanoparticles possessing magnetic, long-lived fluorescence and bio-affinity properties for time-resolved fluorescence cell imaging

Jing Wu [a], Zhiqiang Ye [a], Guilan Wang [b], Jingli Yuan [a,b,*]

[a] *Department of Analytical Chemistry, Dalian Institute of Chemical Physics, Chinese Academy of Sciences, Dalian 116023, PR China*
[b] *State Key Laboratory of Fine Chemicals, Department of Chemistry, Dalian University of Technology, Dalian 116012, PR China*

Received 20 November 2006; received in revised form 3 March 2007; accepted 12 March 2007
Available online 20 March 2007

Abstract

Multifunctional nanoparticles possessing magnetic, long-lived fluorescence and bio-affinity properties have been prepared by copolymerization of a conjugate of (3-aminopropyl)triethoxysilane bound to a fluorescent Eu^{3+} complex, 4,4′-bis(1″,1″,1″-trifluoro- 2″,4″-butanedion-4″-yl)chlorosulfo-*o*-terphenyl-Eu^{3+} (APS-BTBCT-Eu^{3+}), free (3-aminopropyl)triethoxysilane (APS) and tetraethyl orthosilicate (TEOS) in the presence of poly(vinylpyrrolidone) (PVP) stabilized magnetic Fe_3O_4 nanoparticles (∼10 nm) with aqueous ammonia in ethanol. The nanoparticles were characterized by transmission electron microscopy (TEM), spectrofluorometry and vibrating sample magnetometry methods. The direct-introduced amino groups on the nanoparticle's surface by using free APS in nanoparticle preparation facilitated the surface modification and bioconjugation of the nanoparticles. The nanoparticle-labeled transferrin was prepared and used for staining the cultured Hela cells. A time-resolved fluorescence imaging technique that can fully eliminate the fast-decaying background noises was developed and used for the fluorescence imaging detection of the cells. A distinct image with the high ratio of signal to noise (S/N) was obtained.

Keywords: Europium; Biolabeling; Cell imaging; Nanoparticle; Time-resolved fluorescence

1. Introduction

Magnetic ferrite nanoparticles have been widely used in analytical biochemistry, medicine and biotechnology recently [1–8]. These super-paramagnetic nanoparticles can be attracted by a magnetic field but retain no residual magnetism after the field is removed. Therefore, suspended super-paramagnetic nanoparticles tagged to the biomaterials of interest can be easily separated from a matrix by using a magnetic field without agglomeration after removal of the field.

Transmission electron microscopy and magnetic resonance imaging have been used to study magnetic nanoparticles incorporated into cells. However, they are not convenient for in situ monitoring, thus a sensitive and simple technique for in situ monitoring of the nanoparticles in living cells is desirable. In the past few years, fluorescence labeling and imaging techniques for living cells using fluorescent nanoparticles, such as semiconductor nanoparticles (quantum dots) [9,10] and silica-based fluorescent nanoparticles [11,12], have been developed. Compared to conventional organic fluorescence probes, advantages of the nanometer-sized fluorescence probes mainly include their higher photostability and stronger fluorescence. The main problem in cell imaging using the fluorescent nanoprobes is that the fluorescence signal is easily affected by the background noises caused by the cells, matrix and the non-specific scattering lights. The high signal to noise (S/N) ratio is difficult to be obtained.

Time-resolved fluorescence bioassays using lanthanide complexes as probes have been widely used for highly sensitive detections of various biomolecules [13–15]. This technique is also a very useful tool for fluorescence bioimaging detections [16,17] since the fast-decaying background fluorescence from biosample, matrices, scattering lights and the optical components can be easily suppressed. However, lanthanide complex-based fluorescence probes have the drawbacks of

* Corresponding author at: Department of Analytical Chemistry, Dalian Institute of Chemical Physics, Chinese Academy of Sciences, Dalian 116023, PR China. Tel.: +86 411 84379660; fax: +86 411 84379660.
E-mail address: jingliyuan@yahoo.com.cn (J. Yuan).

0039-9140/$ – see front matter © 2007 Elsevier B.V. All rights reserved.
doi:10.1016/j.talanta.2007.03.018

smaller fluorescence quantum yield and weaker photostability, which have limited their application for the fluorescence imaging detection that needs a long-time continuous excitation. Recently we have developed several kinds of fluorescent lanthanide complex-doped silica nanoparticles that can be used for biolabeling and time-resolved fluorescence bioassays [18–20]. It has been demonstrated that the fluorescence intensity and photostability can be effectively improved by using these nanoprobes instead of lanthanide complex-based probes. In addition, the silica shell of the nanoparticles provided good biocompatibility for avoiding the potential toxic effects of the precursor on cells [21,22].

In this work, multifunctional nanoparticles possessing magnetic, long-lived fluorescence and bio-affinity properties were prepared and used for time-resolved fluorescence cell imaging detection. The magnetic-fluorescent nanoparticles prepared by the copolymerization of APS-BTBCT-Eu^{3+}, free APS and TEOS in the presence of poly(vinylpyrrolidone) (PVP) stabilized magnetic Fe_3O_4 nanoparticles (~10 nm) are highly stable without dye leaking during the washing, biolabeling and bioassay processes since the Eu^{3+} complex molecules are covalently bound to silicon atoms in the nanoparticles, and can be directly conjugated to biomoleculues by using their surface free amino groups [23]. To confirm their usefulness for bioimaging detection, the nanoparticle-labeled transferrin was prepared and used for staining the cultured Hela cells. A time-resolved fluorescence imaging technique that allows only the long-lived fluorescence signal to be imaged was developed for the fluorescence imaging detection of the stained cells.

2. Experimental

2.1. Materials and instrumentation

The BTBCT-Eu^{3+} complex was synthesized according to a previously reported method [24]. TEOS and APS were purchased from Acros Organics. PVP with an average mass of 58000 g/mol was purchased from Sigma. HeLa cells were purchased from Dalian Medical University. The APS-BTBCT-Eu^{3+} conjugate (containing free APS) was prepared by the reaction of 3-aminopropyltriethoxysilane (10 μl) and BTBCT-Eu^{3+} (1.5 mg) in 1.0 ml of absolute ethanol for 30 min before use [23]. Super-paramagnetic Fe_3O_4 nanoparticles (~10 nm in diameter) were synthesized by using a reported method [25] with a slight modification. A typical synthesis procedure is described as follows. A 50 ml portion of 2-pyrrolidone solution containing 5 mmol $Fe(acac)_3$ was purged with argon to remove oxygen and then heated to 250 °C. After being refluxed for 12 min, the reaction system was cooled to room temperature. The target Fe_3O_4 nanoparticles were obtained as a dark black-brown precipitate by adding methanol into the solution, which was washed with acetone for several times and then dried. Unless otherwise stated, all chemical materials were purchased from commercial sources and used without further purification.

All normal fluorescence imaging and time-resolved fluorescence imaging measurements were carried out on a laboratory-use fluorescence microscope [26]. The microscope-equipped 100 W mercury lamp, UV-2A fluorescence filters (excitation filter, 330–380 nm; dichroic mirror, 400 nm; emission filter, >420 nm) and color CCD camera system were used for the normal fluorescence imaging measurement with a exposure time of 2 s. The microscope-equipped 30 W xenon flashlamp, UV-2A fluorescence filters, and time-gated digital black-and-white CCD camera system, were used for the time-resolved fluorescence imaging measurement with the conditions of delay time, 100 μs; gate time, 1 ms; lamp pulse width, 10 μs; and exposure time, 120 s. The shape and size of the nanoparticles were measured on a JEOL model JEM-2000EX transmission electron microscope (TEM). Fluorescence spectra and emission lifetime were measured on a Perkin-Elmer LS 50B spectrofluorometer. The magnetic properties of the nanoparticles were measured on a JDM-13 vibrating sample magnetometer.

2.2. Preparation of the multifunctional nanoparticles

The 0.65 g of PVP was dissolved in 20 ml of water by ultrasonication for 15 min. Subsequently the PVP solution was mixed with 5 mg of the Fe_3O_4 nanoparticles under stirring. After the reaction mixture was stirred for 24 h at room temperature, the PVP-stabilized Fe_3O_4 nanoparticles were separated by adding acetone and centrifuging. The nanoparticles were suspended in 5 ml of absolute enthanol again, and then a mixture of 20 μl TEOS and 200 μl ethanol solution containing APS-BTBCT-Eu^{3+} and free APS was added. The polymerization reaction was initiated by adding 0.8 ml of aqueous ammonia (30% by NH_3). After stirring for 16 h, the grey nanoparticles were obtained by centrifuging, and washing with ethanol and water for several times. The obtained nanoparticles were dried in desiccator for the following use.

2.3. Preparation of the nanoparticle-labeled transferrin

To 1.0 ml of 0.1 M phosphate buffer of pH 7.1 containing 10 mg of bovine serum albumin (BSA) were added 2.0 mg of the nanoparticles and 0.1 ml of 1% glutaraldehyde with stirring. After stirring for 22 h at room temperature, the nanoparticles were centrifuged and washed with the phosphate buffer. The nanoparticles were added to 1.0 ml of the phosphate buffer containing 1.0 mg of transferrin, then 0.1 ml of 1% glutaraldehyde was added. After stirring for 22 h at room temperature, 1.0 mg of $NaBH_4$ was added, and the solution was incubated for 2 h at room temperature. The nanoparticle-labeled transferrin was centrifuged, washed three times with the phosphate buffer, and stored at 4 °C before use.

2.4. Cell imaging

Hela cells were cultured in a 25 cm^2 glass culture vial in the nutrition solution 1640 [RPMI-1640 medium (Sigma–Aldrich, Inc.) supplemented with 10% fetal bovine serum (Corning Inc., USA), 1% penicillin and 1% streptomycin (Invitrogen Co. USA)] at 37 °C in a 5% CO_2–95% air incubator. When the amount of the cells reached to ~10^5 cells/vial, the culture medium was removed, and the mixture of 0.2 ml of the

nanoparticle-labeled transferrin in PBS buffer (2 mg/ml) and 2.0 ml of the nutrition solution 1640 was added to the culture vial. After incubating for 20 h at 37 °C in 5% CO_2–95% air incubator, the culture vial was washed 16 times by PBS buffer, and then subjected to the fluorescence imaging detection.

3. Results and discussion

3.1. Preparation of the nanoparticles

Fig. 1A shows the TEM image of super-paramagnetic Fe_3O_4 nanoparticles (∼10 nm in diameter) synthesized by the thermal decomposition of $Fe(acac)_3$ in 2-pyrrolidone [25]. These nanoparticles were confirmed to be soluble in water and 2-pyrrolidone. To obtain the Fe_3O_4 and Eu^{3+} complex co-doped silica nanoparticles, we tested several literature methods, such as Stöber [27] and water-in-oil microemulsion [18–20] methods. However, these methods were found not to be applicable to the preparation because some free Fe_3O_4 nanoparticles are still present in the products.

The PVP method has been demonstrated to be a good method to prepare silica-coated colloidal particles [28]. Herein we employed a modified PVP method to prepare the Fe_3O_4 and Eu^{3+} complex co-doped silica nanoparticles by the copolymerization of APS-BTBCT-Eu^{3+}, TEOS and free APS in the presence of the PVP-stabilized Fe_3O_4 nanoparticles. The nanoparticles were prepared in two steps. At first, the PVP-stabilized Fe_3O_4 nanoparticles were prepared by adsorbing PVP onto the surface of Fe_3O_4 nanoparticles, which made the Fe_3O_4 surface highly affinitive to silica [28]. After the PVP-stabilized Fe_3O_4 nanoparticles were transferred into ethanol, the fluorescent silica-coated Fe_3O_4 nanoparticles were prepared by the copolymerization of APS-BTBCT-Eu^{3+}, TEOS and free APS on the Fe_3O_4 surface using aqueous ammonia as a catalyst. By this way, the magnetic-fluorescent nanoparticles having Fe_3O_4 core and Eu^{3+} complex bound silica shell were obtained. Since the fluorescent Eu^{3+} complex molecules were covalently bound to silicon atoms in silica shell of the nanoparticles, the dye leaking problem in biolabeling and bioassay processes using the luminophore-doped silica nanoparticle probes can be effectively resolved [23]. Furthermore, the direct-introduced amino groups on the nanoparticle's surface by using free APS in nanoparticle preparation facilitated the biolabeling process of the nanoparticles. As shown in Fig. 1B, the magnetic-fluorescent nanoparticles prepared by this method are ∼55 nm in diameter, with a standard deviation of around 20%. The dark dots embedded inside the silica network that can be observed on the TEM image show that the magnetic Fe_3O_4 particles have been completely coated by the silica shell (no free Fe_3O_4 particles were observed). Although some agglomerations of the nanoparticles, which causes irregularity of the shape and size of the nanoparticles, can also be observed from Fig. 1B, it was found that these agglomerations had not obvious effect on protein labeling and fluorescence staining applications of the nanoparticles since the agglomeration is not serious.

3.2. Characterization of the nanoparticles

Time-resolved fluorescence spectra of pure BTBCT-Eu^{3+} complex, the magnetic-fluorescent nanoparticles and the BSA-coated magnetic-fluorescent nanoparticles in 0.05 M Tris–HCl buffer of pH 7.8 containing 0.05% Triton X-100 are shown in Fig. 2. The Eu^{3+} complex and the BSA-coated and uncoated nanoparticles show the same excitation and emission maximum wavelengths at 334 and 611 nm, respectively. This phenomenon indicates that the fluorescence properties of the Eu^{3+} complex are not distinctly influenced by silica network and surface conjugated BSA molecules. The fluorescence lifetimes of the BSA-coated and uncoated nanoparticles in aqueous solution were measured to be 0.398 and 0.347 ms, respectively. These results show that the nanoparticles have an enough long fluorescence lifetime for time-resolved fluorescence bioimaging measurement. The increase in fluorescence lifetime (∼0.05 ms) of the nanoparticles after BSA coating also indicates that the surface conjugated BSA molecules can further decrease the effect of water molecules on the fluorescence lifetime of the Eu^{3+}

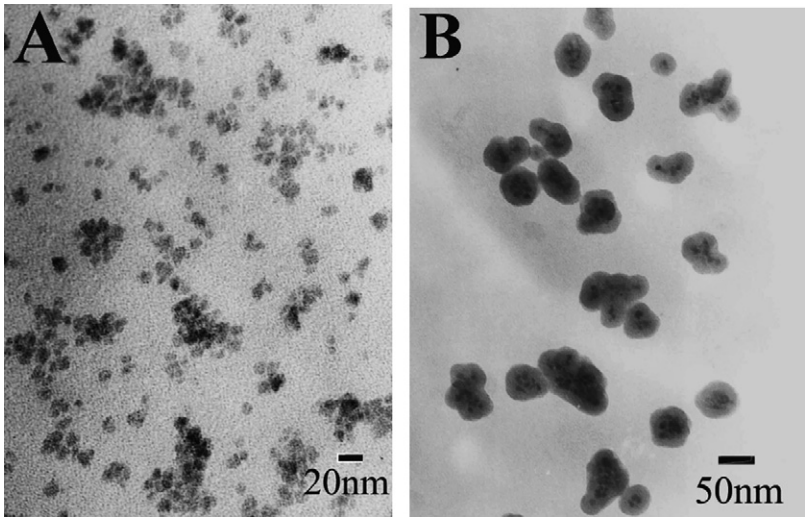

Fig. 1. TEM images of the Fe_3O_4 nanoparticles (A) and the magnetic-fluorescent nanoparticles (B).

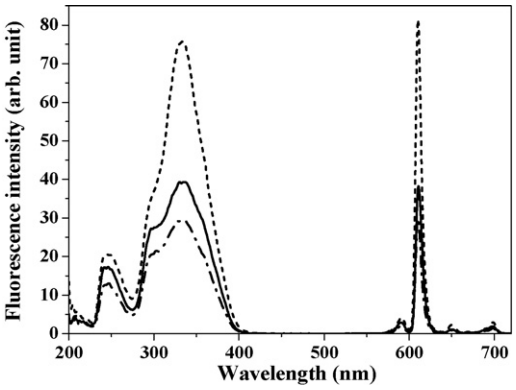

Fig. 2. Time-resolved fluorescence excitation and emission spectra of pure BTBCT-Eu^{3+} complex (180 nM, dash lines), the magnetic-fluorescent nanoparticles (~130 mg/l, solid lines) and the BSA-coated magnetic-fluorescent nanoparticles (~130 mg/l, dash dot lines) in 0.05 M Tris–HCl buffer of pH 7.8 containing 0.05% Triton X-100. The conditions of delay time, 0.2 ms; gate time, 0.4 ms; cycle time, 20 ms; excitation slit, 10 nm, and emission slit, 5 nm, were used for the measurements.

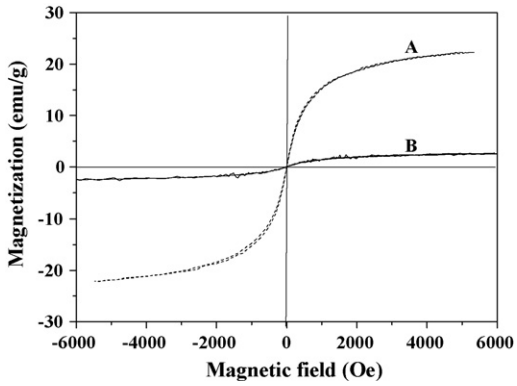

Fig. 3. Room-temperature magnetization curves of the Fe_3O_4 nanoparticles (A) and the magnetic-fluorescent nanoparticles (B).

complex in silica network, which is favorable for time-resolved fluorescence measurement application of the nanoparticles.

The magnetic properties of free Fe_3O_4 nanoparticles and the magnetic-fluorescent nanoparticles were investigated with a vibrating sample magnetometer. Fig. 3 shows the room-temperature magnetization of as-prepared magnetite nanoparticles. Both the Fe_3O_4 nanoparticles and the magnetic-fluorescent nanoparticles exhibit the super-paramagnetic characteristics. The saturation magnetization of the magnetic-fluorescent nanoparticles is 2.5 emu/g, which is much lower than that of the Fe_3O_4 nanoparticles (26 emu/g), probably because of the thick shells coated on magnetic nanoparticles. Nonetheless, the magnetization value is enough for common bio-separation [5].

3.3. Biolabeling and fluorescence cell imaging

Due to the presence of surface amino groups, the magnetic-fluorescent nanoparticles can be directly conjugated to proteins. However, it was found that the nanoparticle-labeled transferrin prepared by direct conjugation method had only lower activity for the transferrin–transferrin receptor interaction on the cell surface. The reason might be due to the effect of steric hindrance between the rigid nanoparticle and the cell surface since the labeled transferrin is tightly fixed on the surface of the nanoparticle. In previous reports [18–20,23], we had established an effective method for biolabeling of silica-based nanoparticles, in which the amino groups on the nanoparticle's surface were conjugated to BSA to form a layer of BSA on the nanoparticle's surface, and then the BSA-coated nanoparticles were used for binding to transferrin by coupling the amino groups of BSA and transferrin with glutaraldehyde. Because there is a flexible BSA 'bridge' between the nanoparticle and transferrin in this case, the steric hindrance between the nanoparticle and the cell surface is decreased, and thus the transferrin–transferrin receptor interaction on the cell surface can occur. By using this method, the nanoparticle-labeled transferrin was prepared and used for the staining and fluorescence imaging of living Hela cells.

It is known that transferrin can react with transferrin receptor on the surface of HeLa cells to form a reversible but tight complex. At first, we tested the interaction of free fluorescent nanoparticles (transferrin unconjugated) and HeLa cells to confirm the non-specific adsorption of the nanoparticles on HeLa cells. After free fluorescent nanoparticles were incubated with HeLa cells, no nanoparticles were observed inside the cells by the detections of fluorescence microscopy and time-resolved fluorescence microscopy. This result shows that the

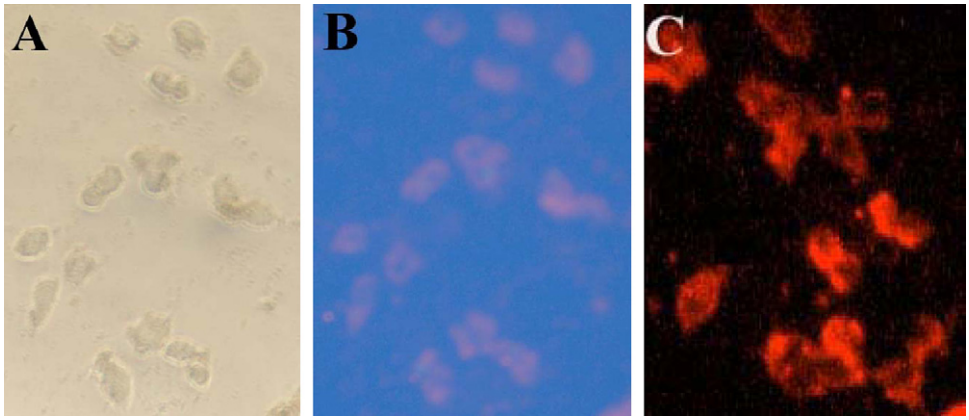

Fig. 4. Bright-field (A), fluorescence (B) and time-resolved fluorescence (C) images of the HeLa cells stained by the nanoparticle-labeled transferrin. The time-resolved fluorescence image (C) is shown in pseudo-color (wavelength of 615 nm) treated by a SimplePCI software [26].

non-specific adsorption of the nanoparticles is negligible. When the nanoparticle-labeled transferrin was incubated with HeLa cells, accompanying the transferrin–transferrin receptor interaction on the cell surface, the receptor-mediated endocytosis occurred, and thus the nanoparticles were transported into the cells [29]. Fig. 4 shows the bright-field, fluorescence and time-resolved fluorescence images of the HeLa cells that have been incubated with the nanoparticle-labeled transferrin. It is clear that the nanoparticle-labeled transferrin is still active and can be recognized by the receptors of the Hela cells, and fluorescent nanoparticles do not distinctly interfere with the ligand-receptor binding and endocytosis (because the pathways of the excitation lights and imaging fields of two CCD systems for fluorescence and time-resolved fluorescence images are different, the imaging field of Fig. 4C is different from 4A and 4B). The S/N ratio of the time-resolved fluorescence image is ∼4 times higher than that of fluorescence image, which reveals the usefulness of time-resolved fluorescence imaging technique to eliminate the interference of cellular autofluorescence and background fluorescence of matrix.

4. Conclusion

Multifunctional nanoparticles possessing magnetic, long-lived fluorescence and bio-affinity properties have been prepared, characterized, and used for time-resolved fluorescence cell imaging. The fluorescence imaging results of Hela cells using the nanoparticle-labeled transferrin demonstrated that time-resolved fluorescence imaging technique is favorably useful to eliminate the background noises caused by cells and matrix. As a biolabeling material, the new nanoparticles have the advantages of high hydrophilicity and biocompatibility, strong fluorescence with long lifetime, direct availability for biolabeling, and a potential utility for bio-separation. These properties of the silica-based magnetic-fluorescent nanoparticles lead to application advantages in biological labeling and detection, cell separation, and drug and gene delivery over conventional probes.

Acknowledgement

The present work was supported by the National Natural Science Foundation of China (No. 20575069).

References

[1] Y.-W. Jun, Y.-M. Huh, J.-S. Choi, J.-H. Lee, H.-T. Song, S. Kim, S. Yoon, K.-S. Kim, J.-S. Shin, J.-S. Suh, J. Cheon, J. Am. Chem. Soc. 127 (2005) 5732.
[2] Y.-S. Lin, P.-J. Tsai, M.-F. Weng, Y.-C. Chen, Anal. Chem. 77 (2005) 1753.
[3] J. Lai, K.V.P.M. Shafi, A. Ulman, K. Loos, R. Popovitz-Biro, Y. Lee, T. Vogt, C. Estournes, J. Am. Chem. Soc. 127 (2005) 5730.
[4] H.-H. Yang, S.-Q. Zhang, X.-L. Chen, Z.-X. Zhuang, J.-G. Xu, X.-R. Wang, Anal. Chem. 76 (2004) 1316.
[5] H. Lu, G. Yi, S. Zhao, D. Chen, L.-H. Guo, J. Cheng, J. Mater. Chem. 14 (2004) 1336.
[6] H. Gu, P.-L. Ho, K.W.T. Tsang, L. Wang, B. Xu, J. Am. Chem. Soc. 125 (2003) 15702.
[7] D. Wang, J. He, N. Rosenzweig, Z. Rosenzweig, Nano Lett. 4 (2004) 409.
[8] I. Willner, E. Katz, Angew. Chem. Int. Ed. 42 (2003) 4576.
[9] M. Bruchez Jr., M. Moronne, P. Gin, S. Weiss, A.P. Alivisatos, Science 281 (1998) 2013.
[10] W.C.W. Chan, S. Nie, Science 281 (1998) 2016.
[11] H. Ow, D.R. Larson, M. Srivastava, B.A. Baird, W.W. Webb, U. Wiesner, Nano Lett. 5 (2005) 113.
[12] S. Santra, P. Zhang, K. Wang, R. Tapec, W. Tan, Anal. Chem. 73 (2001) 4988.
[13] G. Wang, J. Yuan, X. Hai, K. Matsumoto, Talanta 70 (2006) 133.
[14] B. Song, G. Wang, J. Yuan, Talanta 72 (2007) 231.
[15] J. Yuan, G. Wang, TrAC-Trends Anal. Chem. 25 (2006) 490.
[16] A. Bjartell, S. Laine, K. Pettersson, E. Nilsson, T. Lövgren, H. Lilja, Histochem. J. 31 (1999) 45.
[17] R. Connally, D. Veal, J. Piper, Microsc. Res. Tech. 64 (2004) 312.
[18] Z. Ye, M. Tan, G. Wang, J. Yuan, Anal. Chem. 76 (2004) 513.
[19] M. Tan, Z. Ye, G. Wang, J. Yuan, Chem. Mater. 16 (2004) 2494.
[20] Z. Ye, M. Tan, G. Wang, J. Yuan, Talanta 65 (2005) 206.
[21] Y. Lu, Y. Yin, B.T. Mayers, Y. Xia, Nano Lett. 2 (2002) 183.
[22] M.A. Correa-Duarte, M. Giersig, N.A. Kotov, L.M. Liz-Marzán, Langmuir 14 (1998) 6430.
[23] M. Tan, G. Wang, X. Hai, Z. Ye, J. Yuan, J. Mater. Chem. 14 (2004) 2896.
[24] F.-B. Wu, C. Zhang, Anal. Biochem. 311 (2002) 57.
[25] Z. Li, H. Chen, H. Bao, M. Gao, Chem. Mater. 16 (2004) 1391.
[26] B. Song, G. Wang, M. Tan, J. Yuan, J. Am. Chem. Soc. 128 (2006) 13442.
[27] W. Stöber, A. Fink, E. Bohn, J. Colloid Interface Sci. 26 (1968) 62.
[28] C. Graf, D.L.J. Vossen, A. Imhof, A. Blaaderen, Langmuir 19 (2003) 6693.
[29] E. Smythe, G. Warren, Eur. J. Biochem. 202 (1991) 689.

Available online at www.sciencedirect.com
ScienceDirect
Talanta 72 (2007) 1650–1654
Talanta
www.elsevier.com/locate/talanta

Triclosan determination in water related to wastewater treatment

Jian-Lin Wu [a], Ng Pak Lam [a], Dieter Martens [b], Antonius Kettrup [b], Zongwei Cai [a,*]

[a] *Department of Chemistry, Hong Kong Baptist University, Kowloon Tong, Kowloon, Hong Kong SAR, China*
[b] *Institute of Ecological Chemistry and Environmental Analysis, National Research Center for Environment and Health, Ingolstädter Landstreet 1, D-85764 Neuherberg, Germany*

Available online 23 March 2007

Abstract

Triclosan in the waste, river and sea water samples collected in Hong Kong was analyzed by using gas chromatography–ion trap mass spectrometry method. $^{13}C_{12}$-triclosan was used as internal standard for the quantitative analysis. Water samples were prepared and cleaned-up by using a C_{18} solid-phase extraction cartridge. The recoveries of triclosan in spiked coastal water at three different concentrations ranged from 83 to 110%. The method detection limit was 0.25 ng/L for triclosan in 1-L water and the relative standard deviations and relative error were less than 11.0 and 12.3%, respectively ($n = 3$). The method was successfully applied to analyze water samples collected from rivers, coastal water bodies and wastewater treatment plants at ng/L levels.

Keywords: Triclosan; Wastewater; Coastal water; River water; Gas chromatography–ion trap mass spectrometry

1. Introduction

Triclosan, 5-chloro-2-(2,4-dichlorophenoxy)phenol (CAS reg. no. 3380-34-5), is an active ingredient in many household disinfectants and has been extensively used in improving environmental hygiene [1]. The chemical can be found as an antiseptic component in medical products such as hand disinfecting soaps, medical skin creams, dental products and many household cleansers. Triclosan has been found as a contaminant of rivers and lakes [2]. In Europe, about 350 tonnes of triclosan are produced annually for commercial applications [3]. Triclosan is a relatively stable, lipophilic compound. Its environmental occurrence has been reported, and the compound has been detected in coastal water [4]. As a consumer product ingredient, the majority of triclosan enters sewer systems and is transported to wastewater sewage treatment plants. It has been reported that large number of household cleaning agents contained triclosan were used in Hong Kong in 2003 due to the outbreak of the severe respiratory syndrome (SARS) [5]. Triclosan has been detected in sewage sludge, discharge effluent, receiving surface waters and sediments [1,4]. This compound has also been found in rivers, lakes and the open sea at ng/L levels [6–8]. The toxicity of triclosan on human had been investigated for many years. The adverse effects include mild itching and allergic redness on sensitive skins. Thus, triclosan is generally regarded as a low toxicity chemical [9,10].

Attention has been drawn to triclosan and its degradation products recently due to their chemical structural similarity with highly toxic contaminants, such as dioxins. Recent studies suggested that triclosan can be undergone cyclization to form 2,8-dichlorodibenzo-*p*-dioxin (2,8-DCDD) in aqueous solution under UV irradiation [2,11]. Triclosan can also easily be chlorinated by sodium hypochlorite solution to produce chlorinated derivatives, which can be converted to chlorinated dioxins upon heating and UV irradiation [12]. Furthermore, 2,4-dichlorophenol and 2,4,6-trichlorophenol have been detected as the degradation products of triclosan in water with the presence of low concentrations of free chlorine or in chloraminated waters [13,14]. Therefore, it is necessary to develop sensitive and selective analytical method for triclosan in order to support investigations its environmental fate. This paper reports method development and application of the isotope dilution GC–MS/MS

* Corresponding author. Tel.: +852 34117070; fax: +852 34117348.
E-mail address: zwcai@hkbu.edu.hk (Z. Cai).

0039-9140/$ – see front matter © 2007 Elsevier B.V. All rights reserved.
doi:10.1016/j.talanta.2007.03.024

technique for the analysis of triclaosan in environmental waters.

2. Experimental

2.1. Reagents and chemicals

Triclosan and $^{13}C_{12}$-labeled triclosan were purchased from Wellington Laboratories (Ontario, Canada). ABSOLV or HPLC grade of organic solvents of hexane, ethyl acetate, *n*-hexane, nonane, acetone, acetic anhydride and methanol were obtained from Riedel-de Haen® (Hanover, Germany). Stock solution was prepared by dissolving 1.0 mg of triclosan in 1.0 mL of ethyl acetate. Calibration standard solutions containing the analytes and internal standard were prepared by diluting the stock solution. Anhydrous sodium sulfate and 0.1% (v/v) formic acid were analytical grade. All standard solutions were kept under 4 °C in a refrigerator. Milli-Q water was used as clean water and produced by using a Milli-Q® Ultrapure Water Purification Academic System from Millipore (Billerica, USA).

Sea water samples were collected from Tai Po Harbour and Victoria Harbour. River water was collected from rivers in the vicinity of Fo Tan industrial and Sha Tin residential areas in Hong Kong as well as the Pearl River (Guangzhou, China). The wastewater samples were collected from Sha Tin Sewage Treatment Work, Kwun Tong Preliminary Treatment Plant and Stonecutters Island Chemical Treatment Place from June 2005 to March 2006 (Table 1).

Table 1
Sample collection sites and concentration of triclosan in different sites

Site	Time of water sample collection	Concentration[a] (ng/L)
Sea water		
Tai Po Harbour	June 2005	16.2 ± 1.3
Victoria Harbour	December 2005	99.3 ± 10.6
Victoria Harbour	March 2006	31.9 ± 2.1
River water		
Fo Tan industrial area	September 2005	37.6 ± 3.8
Sha Tin residential area	September 2005	26.0 ± 1.9
Pearl River	September 2005	31.6 ± 4.1
Wastewater		
Sha Tin[b]		
Raw water	September 2005	142.0 ± 16.5
Primary treatment	September 2005	170.2 ± 18.3
Secondary treatment	September 2005	22.5 ± 1.4
Kwun Tong[c]		
Raw water	September 2005	213.8 ± 20.6
Primary treatment	September 2005	177.3 ± 21.5
Stonecutters Island[d]		
Raw water	September 2005	213.4 ± 23.9
Primary treatment	September 2005	151.2 ± 12.4

[a] Averaged ± standard deviation ($n = 3$).
[b] From Sewage Treatment Work in Sha Tin.
[c] From preliminary treatment plant in Kwun Tong.
[d] From chemical treatment place in Stonecutters Island.

2.2. Water sample pre-treatment

Prior to the sample collection, amber glass bottles were pre-cleaned sequentially with detergent water, tap water, distilled water, methanol, ethyl acetate, methanol and distilled water. Three bottles of 2-L water samples were collected from each of sampling sites. After the samples were collected, the water samples were acidified with concentrated phosphoric acid to pH 2, covered with caps lined with Teflon and placed in an ice-filling cooler. The samples were then immediately delivered to the analytical laboratory and stored at 4 °C in a refrigerator until sample analysis.

Solid-phase extraction (SPE) was used for water sample extraction and clean-up. Interferences in the water matrices were removed by using an activated Florisil SPE column. Prior to the SPE extraction, the cartridge was pre-washed and conditioned by 5 mL of ethyl acetate, methanol and Milli-Q water, sequentially. One liter water sample was filtered, spiked with 40 ng of internal standard ($^{13}C_{12}$-labeled triclosan) and then passed through the cartridge with a flow rate of approximately 3 mL/min under a vacuum using water pump. The column was rinsed with 5 mL of 5% methanol in Milli-Q water to wash the interferences. The SPE cartridge was aspirated for about 15 min to remove water residue. Then the cartridge was eluted with 3 mL × 2 mL ethyl acetate at a slow rate of 1 mL/min, and the combined extracts were dried by adding 0.05 g of anhydrous sodium sulfate. The extract was then concentrated under gentle stream of nitrogen to dryness in water bath at 40 °C. The sample was reconstituted in 200 μL ethyl acetate.

2.3. GC–MS/MS analysis

Gas chromatography–ion trap mass spectrometry operated in MS/MS mode was employed for the analysis of triclosan. The MS/MS analysis was performed on Thermo Finnigan Trace GC system interfaced with a Polaris Q ion trap mass spectrometer. A DB-5MS GC column (30 m × 0.25 mm × 0.25 μm film thickness (5%-phenyl)-methylpolysiloxane) was used for the triclosan analysis. The GC injector inlet temperature was 260 °C. The GC temperature program was set as follows: initial temperature was 80 °C and held at 1 min, then increased at 20 °C/min to 280 °C where it was held for 6 min. The GC–MS transfer line and ion source temperatures were 300 and 265 °C, respectively. The carrier gas was helium with a constant flow rate of 1 mL/min. The sample injected volume was 1 μL in splitless mode. The mass spectrometer was operated in electron impact ionization (EI) mode with the ionization potential at 70 eV. A solvent delay of 4 min was set for each sample injection. The native triclosan with the molecular ion at *m/z* 288 and ^{13}C-triclosan at *m/z* 300 were eluted out of the GC column at the retention time of 10.2 min. The selected precursor ion of triclosan for the MS/MS analysis was *m/z* 218, and the selected product ion was *m/z* 155. To optimize the ion trap MS/MS performance, the following three major instrumental parameters were investigated in series: resonance excitation voltage, "*q*" value and excitation time.

3. Results and discussion

3.1. GC–MS/MS analysis of triclosan

Establishing the chromatographic retention time to select an appropriate precursor ion for the analyte was the initial step for developing a GC–MS/MS method. The GC–MS/MS analysis of triclosan standards in full-scan MS mode showed the molecular ion peaks of *m/z* 288 for the native triclosan and *m/z* 300 for the $^{13}C_{12}$-triclosan at time 10.2 min. The detection of triclosan and the established chromatographic retention time can be confirmed through the NIST EI-mass spectrum library search. The $[M-2Cl]^+$ ion resulted from the loss of two chlorines was the predominant ion peak in the full-scan mass spectrum with *m/z* 218 for the triclosan and *m/z* 230 for the $^{13}C_{12}$-triclosan. Thus, the ions at *m/z* 218 and 230 were chosen as the precursor ions for the second-stage mass spectrometric analysis. The MS/MS analyses of the precursor ions of triclosan and $^{13}C_{12}$-triclosan at *m/z* 218 and 230 showed the most abundant fragment ion peaks at *m/z* 155 and 166, respectively, which were therefore selected as the MS/MS quantitation ions (Fig. 1).

GC–MS/MS with ion trap mass spectrometry has become a popular analytical tool for the analysis of complicated matrices due to its high specificity. The identification of analytes is based on chromatographic retention time and specific fragmentations from the MS/MS analysis (Fig. 2). The optimization of GC–MS/MS parameters for triclosan analysis was achieved by monitoring the corresponding peak intensities of the selected

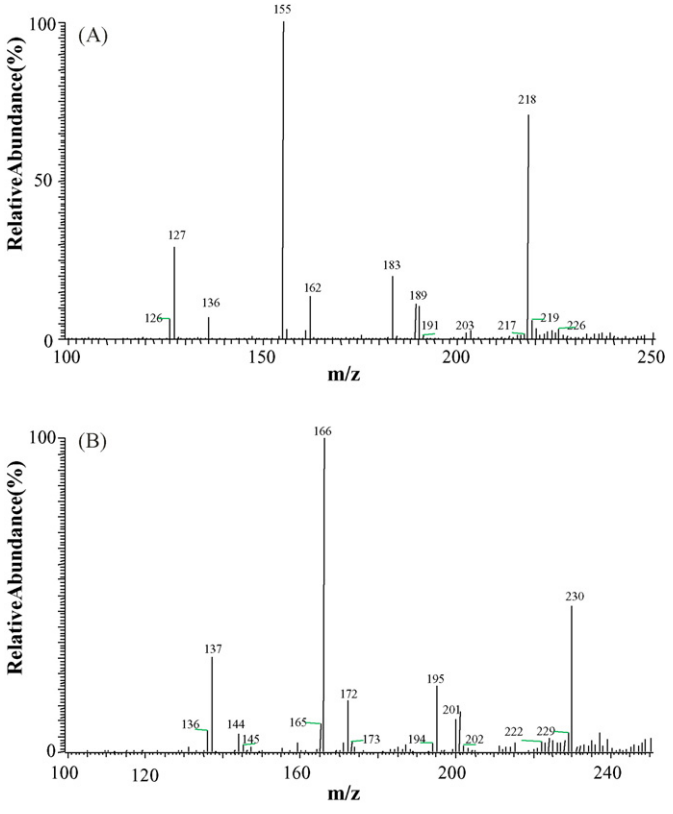

Fig. 1. MS/MS spectra of native triclosan (A) and $^{13}C_{12}$-triclosan (B).

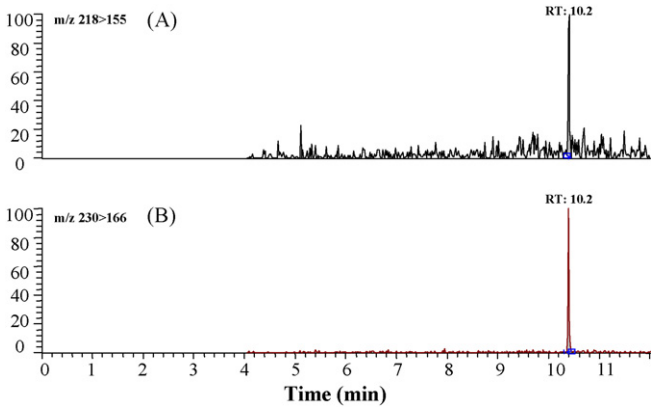

Fig. 2. MS/MS chromatograms of triclosan (A) and $^{13}C_{12}$-triclosan (B) with the quantitation ions at *m/z* 218 > 155 and 230 > 166, respectively, obtained from the analysis of the sea water sample collected from Tai Po Harbour on June 2005.

quantification ions. Three major parameters of MS/MS analysis, namely resonance excitation voltage (REV), "*q*" value and excitation time were optimized. The optimization concerned the determination under the best conditions to maximize the peak intensity of the selected quantitation ion of triclosan. The optimal values of REV, "*q*" value and excitation time were 0.75 V, 25 ms and 25 ms, respectively.

3.2. Recovery and detection limit

Extraction recoveries of triclosan were investigated by using 1-L coastal water spiked with 70, 120 and 200 ng of triclosan. Triplicated samples were extracted and analyzed for obtaining recovery data for each spiked level. Because the sea water matrices contained the targeted analyte, the recovery was therefore calculated upon the subtraction of the averaged level of triclosan in the coastal water. The triclosan extraction recovery from the sea water ranged from 83 to 110% (Table 2). Quantitative recovery of better than 85% was also achieved for other water matrices such as the river water and wastewater. The limit of detection was defined as the lowest sample amount giving an S/N ratio greater than 3. The procedure detection limit was 0.25 ng/L and therefore the limit of quantitation was 0.75 ng/L when the water sample volume was 1-L, which was well below the triclosan levels determined in the environmental water samples investigated in this study.

3.3. Method accuracy and precision

Results from the analysis of the spiked water samples containing triclosan at 70, 120 and 200 ng/L are reported in Table 2. The relative error and relative standard deviation data from the triplicated analyses of the three sets of samples were 10.6, −12.3 and −5.6%, as well as 1.2, 9.2 and 10.2%, respectively. The obtained results indicate that the isotope internal standard method provided satisfied accuracy and precision.

3.4. Determination of triclosan in environmental waters

The developed method with SPE extraction and GC–MS/MS analysis was applied for the analysis sea water, river water and

Table 2
Recovery, accuracy and precision from the solid-phase extraction with three different concentration of triclosan spiked

Compound	Concentration (ng/L)	Average recovery (%)	Accuracy and precision	
			Relative error (%)	R.S.D. (%) ($n = 3$)
Triclaosan	70	110	+10.6	1.2
	120	83	−12.3	9.2
	200	94	−5.6	10.2

wastewater samples. Sea water samples were collected from Victoria Harbour for the determination of triclosan because the harbour has accepted untreated and treated wastewater for many years. Sea water in the Tai Po harbour was also targeted because the harbour links directly to Sheng Man River that is used to collect wastewater. The selected two rivers located in Fo Tan and Sha Tin accept industrial and residential wastewaters, respectively. It was expected to compare the levels of triclosan in river water from the residential and industrial areas. Moreover, river water samples collected in two different seasons were analyzed to investigate the seasonal change of triclosan levels. Wastewater collected from three different sampling sites in the wastewater treatment plants were analyzed in order to investigate the removal of triclosan and potential formation of toxic degradation products during the water treatment. The first site was located at the entrance to target the raw wastewater. The second sampling point was selected for the water after the primary treatment. The third site was selected for the treated water effluent that would be emitted to the sea.

The GC–MS/MS chromatogram obtained from the analysis of the sea water sample collected from Tai Po Harbour on June 2005 is demonstrated in Fig. 2. The triclosan analytical results in the coastal, river and wastewaters are presented in Table 1. The data indicated that the triclosan level in sea water collected from Victoria Harbour were higher than that in samples collected from Tai Po Harbour, indicating that the Victoria Harbour was more contaminated with triclosan. The sea water samples collected from Victoria Harbor in December has an averaged triclosan level of 99.3 ng/L, which was three times higher than that in samples collected in March (31.9 ng/L). Lower level of triclosan in March samples might be explained from the water dilution in Victoria Harbour during the heavy raining season around March.

Triclosan was detected in the river closed to residential area at 37.6 ng/L, which was higher than that in river closed to industrial area. This might be due to the heavier usage of triclosan in residential household as commercial products for antibacterial mouth rinse and hand wash. The house hold wastewater was found to be discharged to the river in Sha Tin area. The triclosan level in the water samples from Pearl River which is about 150 km far away from Hong Kong was 38.8 ng/L.

Triclosan was detected in all wastewater samples with significant different levels at various sampling sites or different treatment stages. For the samples from the Sha Tin Sewage Treatment Work, Kwun Tong Preliminary Treatment Plant and Stonecutters Island Chemical Treatment Place, the detected triclosan levels ranged from 142.0 to 213.8 ng/L in raw water samples, from 151.2 to 177.3 ng/L in primary treated water samples and 25.5 ng/L in the secondary treatment water samples. It was surprised to observed higher levels of triclosan in the samples after the primary treatment than those in raw sewage samples in Sha Tin Sewage Treatment Work from the repeated sample collections and analyses. Since the primary treatment of the wastewater only involved the sedimentation process, the possible explanation of this observation could be that the wastewater had been concentrated at the second sampling collection site. The Sha Tin Wastewater Treatment Work had heavy working load, particularly for the secondary treatment. The wastewater after the first-stage treatment was kept for a while and thus the water could be concentrated. In secondary treatment, biodegradable organics and nutrients could be removed from the sewage by biological treatment through an activated sludge process. Wastewater after the first-stage treatment was passed to the aeration tanks for biological treatment. Air was supplied continuously into the aeration tanks for the growth and reproduction of microorganisms. The triclosan analytical results clearly indicated the efficiency of the biological treatment in reducing the triclosan levels.

Because the other two water treatment plants (Kwun Tong Preliminary Treatment Plan and Stonecutters Island Chemical Treatment Plant) only involved the first-stage of treatment, triclosan determination was performed on the raw wastewater and the samples after the first-stage treatment. Slightly decrease of triclosan levels was observed in the samples after the primary treatment, compared to those in raw water. This result was different from the data obtained for wastewater samples collected in the Sha Tin Sewage Treatment Work. The slight decrease of triclosan levels in samples from Kwun Tong Preliminary Treatment Plan and Stonecutters Island Chemical Treatment Plant might be due to the water dilution because the sediment filtered from the raw wastewater was washed with tap water.

The wastewater analytical results indicated that the biological treatment applied in the sewage treatment plant had the effect in removing triclosan from wastewater. However, the degradation products generated from triclosan during the treatment remained unknown. Because chlorophenols and dioxins had been reported as potential degradation products of triclosan, it is important to study the degradation mechanism and pathway of triclosan from the chemical and biological treatments of wastewater.

4. Conclusions

A method for the determination of triclosan in various environmental water samples was developed. The whole procedure combining SPE extraction and GC–MS/MS analysis provided good recoveries and sensitivity for the analysis of triclosan in coastal, river and wastewaters. The triclosan was detected at

concentrations of the low ng/L in all environmental water samples. GC–MS/MS method was proved to be a suitable approach for triclosan analysis in water, allowing the detection limits at low ng/L levels. Although triclosan can be removed extensively during wastewater treatment, investigation on its degradation products is needed.

References

[1] T. Okumura, Y. Nishikawa, Anal. Chim. Acta 325 (1996) 175–184.
[2] D.E. Latch, J.L. Packer, W.A. Arnold, K. McNeil, J. Photochem. Photobiol. A 158 (2003) 63–66.
[3] H. Singer, S. Muller, C. Tixier, L. Pillonel, Environ. Sci. Technol. 36 (2002) 4998–5004.
[4] W. Hua, E.R. Bennett, R.J. Letcher, Environ. Int. 31 (2005) 621–630.
[5] J.C. Yu, T.Y. Kwong, Q. Luo, Z. Cai, Chemosphere 65 (2006) 390–399.
[6] D.W. Kolpin, M. Skopec, M.T. Meyer, E.T. Furlong, S.D. Zaugg, Sci. Total Environ. 328 (2004) 119–130.
[7] P.M. Thomas, G.D. Foster, J. Environ. Sci. Health A 39 (8) (2004) 1969–1978.
[8] D.W. Kolpin, E.T. Furlong, M.T. Meyer, E.M. Thurman, S.D. Zaugg, L.B. Barber, H.T. Buxton, Environ. Sci. Technol. 36 (2002) 1202–1211.
[9] A. Lindström, I.J. Buerge, T. Poiger, P. Bergqvist, M.D. Müller, H. Buser, Environ. Sci. Technol. 36 (2002) 2322–2329.
[10] C. Tixier, H. Singer, S. Canonica, S. Müller, Environ. Sci. Technol. 36 (2002) 3482–3489.
[11] S.L. Murov, I. Carmichael, G.L. Hug, Handbook of Photochemistry, 2nd ed., Marcel Dekker Inc., New York, 1993.
[12] C. Nilsson, K. Andersson, C. Pappe, S. Westermark, J. Chromatogr. 96 (1974) 137–147.
[13] P. Canosa, S. Morales, I. Rodriguez, E. Rubi, R. Cela, M. Gomez, Anal. Bioanal. Chem. 383 (2005) 1119–1126.
[14] A.E. Greyshock, P.J. Vikesland, Environ. Sci. Technol. 40 (2006) 2615–2622.

Available online at www.sciencedirect.com
ScienceDirect
Talanta 72 (2007) 1710–1716
Talanta
www.elsevier.com/locate/talanta

Field speciation of chromium with a sequential injection lab-on-valve incorporating a bismuthate immobilized micro-column

Mei Yang [a,b], Jin-Xiang Li [b], Jian-Hua Wang [a,*]

[a] *Research Center for Analytical Sciences, Northeastern University, Box 332, Shenyang 110004, China*
[b] *Department of Chemistry, Liaoning Normal University, Dalian 116029, China*

Received 29 November 2006; received in revised form 9 January 2007; accepted 9 January 2007
Available online 19 January 2007

Abstract

A fully automated and portable analyzer for field speciation of inorganic chromium in wastewater was developed. The instrument consists of a micro-sequential injection lab-on-valve (LOV) system and a miniature USB2000 spectrophotometer. A multi-purpose flow cell was incorporated on one side of the main body of the LOV, which offers vast potentials and versatilities in its compatibility with various detection modes. On-line oxidation of trivalent chromium was performed on a bismuthate immobilized silica micro-column reactor integrated in the LOV. When determining Cr(VI), its chromogenic reaction with 1,5-diphenylcarbazide (DPC) was facilitated in the flow cell and the absorbance was monitored in situ at 548 nm via optical fibers. While for the quantification of total chromium, Cr(III) was oxidized on-line by aspirating sample solution through the oxidizing column reactor, followed by chromogenic reaction with DPC and the absorbance was monitored in the flow cell. With a sampling volume of 200 μl, the detection limits of 5.6 $\mu g\,l^{-1}$ for Cr(VI) and 6.8 $\mu g\,l^{-1}$ for total chromium were achieved along with a sampling frequency of 60 h^{-1}. A R.S.D. value of 2.0% was recorded at 32 $\mu g\,l^{-1}$ of Cr(VI). The practical applicability of the speciation analyzer was validated by analyzing Cr(VI) and total chromium contents in two certified reference materials. The feasibility of performing rapid field speciation of chromium in wastewater samples was also demonstrated.

Keywords: Sequential injection; Lab-on-valve; Chromium speciation; Sodium bismuthate immobilization; On-line oxidation of chromium

1. Introduction

It has been widely recognized that the impact of detrimental heavy metals on the ecological system, biological organisms as well as human health not only depends on the total amount of the element, but also most significantly, depends strongly on its chemical forms [1]. Therefore, appropriate speciation methods are highly demanded for the speciation of various metal species in biological and environmental samples.

Among the various analytical protocols devoted to metal speciation, the most attractive approaches are obviously the ones with an appropriate separation procedure coupled to spectrometry. HPLC and capillary electrophoresis have shown obvious advantages in metal speciation [2,3], attributed to their excellent separation capabilities. Their hyphenation to mass spectrometry provides most important speciation techniques, including the interface with ICPMS [4–6] and ESI-MS [7,8]. Electrothermal atomic absorption spectrometry (ETAAS) and atomic fluorescence spectrometry (AFS) are also frequently employed for this purpose [9,10]. These coupling procedures make it much easier to facilitate many of the sophisticated speciation tasks [11]. On the other hand, however, the use of these analytical techniques always require collection, pack up and transportation of samples, and during which process the conversions or alterations of the chemical forms of metals are frequently encountered, causing discrepancies between the analytical results and the real distributions of the species. At this juncture, field analysis is much more practical for metal speciation analysis. Therefore, the development of portable analytical instruments is one of the key issues.

Chromium is among the most important elements that frequently poses speciation tasks, and in most cases by using spectrophotometric detection, Cr(VI) is used for quantification, which always require the oxidation of Cr(III). Among the oxidation protocols, various homogeneous oxidizing reagents have been employed [12–15], but the requirement of an elevated

* Corresponding author. Tel.: +86 83688944; fax: +86 83676698.
E-mail address: jianhuajrz@mail.edu.cn (J.-H. Wang).

0039-9140/$ – see front matter © 2007 Elsevier B.V. All rights reserved.
doi:10.1016/j.talanta.2007.01.020

temperature and the peripheral facilities for temperature control makes it not feasible for field applications by flow through analytical systems. Attentions were thus directed to heterogeneous oxidizing reagents. Solid sodium bismuthate is a non-toxic oxidizing reagent with an oxidizing potential of $E^{\emptyset} > 1.8$ V in acidic medium. Although it can readily oxidize a large variety of organic and inorganic substances [16,17], it has been rather neglected in analytical chemistry field. The insolubility of sodium bismuthate provides a promising alternative for its immobilization and potential applications as an oxidizing agent in flow systems [18,19]. To the best of our knowledge, immobilized sodium bismuthate has not yet been applied for the on-line oxidation of chromium.

The development of sequential injection lab-on-valve (SI-LOV) system provides vast potentials for instrument miniaturization and on-line detection. It not only allows various experimental operations, but also facilitates in-valve homogenous and heterogeneous physical/chemical/bio-chemical reactions and real time detections. In addition to the downscaled fluidic manipulation and automatic operation, the LOV is ideal for on-line miniature sample treatment and field speciation analysis.

The aim of the present investigation is to develop a portable analyzer for fast field speciation of Cr(VI) and Cr(III). The entire system was miniaturized by employing a micro-SI-LOV in combination with a USB2000 spectrophotometer. A micro-column packed with sodium bismuthate immobilized silica beads was integrated into the SI-LOV system to facilitate on-line fast oxidation of chromium(III). The hexavalent chromium content in the original sample and the total chromium content after the oxidation of Cr(III) were quantified, respectively, based on the chromogenic reaction of Cr(VI) with 1,5-diphenylcarbazide (DPC). The chromogenic reaction was monitored with optical fibers in the flow cell of the LOV system, and the concentration of Cr(III) was thereafter derived by difference.

2. Experimental

2.1. Chemicals

All the reagents used were at least of analytical reagent grade, and de-ionized water (18 MΩ cm^{-1}) was used throughout. Glasswares were rinsed prior to use with 25% (v/v) nitric acid and afterward cleaned with ion-free water.

Cr(VI) and Cr(III) working standard solutions of various concentrations were prepared daily by stepwise dilution of the 1000 mg l^{-1} stock solutions with 0.5 mol l^{-1} phosphoric acid.

A 0.01 mol l^{-1} stock solution of 1,5-diphenylcarbazide (DPC) was prepared by dissolving appropriate amount of DPC (Di-san Chemicals Reagents Co., Shanghai) in 50 ml of acetone (Tianjin Kemiou Chemical Reagents Development Centre, China) and diluted with water to 100 ml. Working solutions of various concentrations were obtained by stepwise dilution of this stock solution with 0.6 mol l^{-1} H_2SO_4.

Other chemicals used were phosphoric acid (Shenyang Chemicals Reagents Co., Shenyang), sulfuric acid (Tianhe Chemicals Reagents Co., Tianjin).

Deionized water was used as carrier solution.

2.2. Bismuthate immobilization and preparation of the on-line column reactor

The immobilization of bismuthate and preparation of the on-line column reactor was performed as following: 5 g of silica gel beads (nominal bead size of ca. 80 mesh, Wu-si Chemicals Co., Shanghai) were treated in an oven at 1000 °C for 3 h, 1 g of sodium bismuthate (Merck) was afterwards added and the mixture was stirred for ca. 30 min, during which process the immobilization of sodium bismuthate was achieved. A micro-column was packed by using 50 mg of the obtained silica beads in a piece of PTFE tubing (2.0 mm i.d./3.2 mm o.d.) blocked at both ends with glass wool. The micro-column was then integrated into port 3 of the lab-on-valve unit. Before use, the column was conditioned thoroughly by pumping phosphoric acid (0.5 mol l^{-1}) and de-ionized water through it alternatively at a flow rate of 1.8 ml min^{-1} until the loosely adhered sodium bismuthate on silica surface was completely removed.

Based on the stoichiometry of the oxidizing reaction, the micro-column has a oxidation capacity of 0.1 mg of Cr(III) to Cr(VI), i.e., in the present case, it could be used for processing ca. 500 samples with a Cr(III) concentration of up to 1 mg l^{-1} and a sampling volume of 200 μl. For real-world samples, the lifetime of the column might be shortened because of the existence of other reducing components.

The performance of the column was checked alternatively by processing a certain amount of Cr(III) solution with a fixed concentration, and the absorbance resulted from the chromogenic reaction between Cr(VI) and DPC was recorded. Generally, the column was replaced whenever a significant drop of the absorbance was observed. Practically, however, a much easier way could be used to judge whether the column should be replaced. The color of a new column is brown, while it gradually turns to light when a number of samples have been processed, and it finally turned to white after excessive use, which revealed that most of the immobilized sodium bismuthate has been consumed, and the replacement of the column is required.

2.3. Configuration of the LOV unit

The LOV unit integrates all the necessary flow channels and sampling ports, in which various reagent-based assays can be performed. A demountable Z-type flow cell, with a volume of about 24 μl, is incorporated on one side of the LOV main body. The flow cell allows a series of miniaturized fluidic operations to be performed, including dispersion of fluidic zones. It can also be furnished with electrodes and fiber optic cables as well as other micro-sensors or probes, in order to facilitate various real-time monitoring of the reactions taking place inside the cell.

As compared with the previously described LOV units by integrating the flow cell into one of the six ports [20–24], the one presented herein accommodates the flow cell on one side of the main body. This configuration not only is much easier to fabricate, but also offers vast potentials and versatilities in its compatibility with a variety of detection modes, e.g., fluorescence, spectrophotometry and chemiluminescence [25]. In addition, electrochemistry and electrochemilumines-

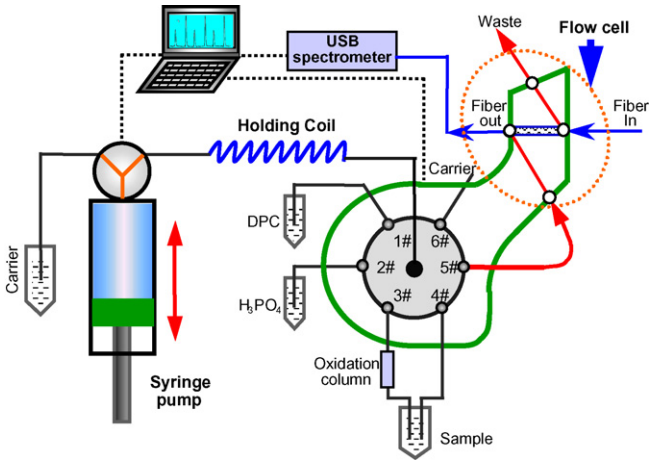

Fig. 1. Schematic set-up of the SI-LOV portable analyzer for chromium speciation.

cence detections could equally be facilitated. Furthermore, the present configuration allows the integration of an extra entity, e.g., a packed micro-column reactor, which facilitates various derivative reactions and post-column detections. While the pre-column or post-column derivatizations remain one of the most severe limitations for conventional sequential injection systems [26].

2.4. Description of the portable analyzer for chromium speciation

The miniaturized portable analyzer designed specifically for inorganic chromium speciation is illustrated in Fig. 1. A micro-SIA sequential injection system (FIAlab Instruments Inc., Bellevueo, WA, USA) equipped with a 2.5 ml syringe pump (Cavro, Sunnyvale, CA) was employed for fluidic delivery. A LOV unit mounted atop a six-port selection valve serves as the central part of the entire system. A micro-column packed with sodium bismuthate immobilized silica beads was integrated into port 3 of the lab-on-valve. The flow cell is incorporated on one side of the LOV unit and connected to port 5 of the main body. Both ends of the flow cell are furnished with 400 μm fiber optic cables, with one end communicating to an external light source, while the other end to a miniaturized USB2000 spectrophotometer (OceanOptics, Inc., Dunedin, FL, USA). The incident light from a tungsten halogen lamp (OceanOptics, Inc.,) was directed to the flow cell, while the transmitting light was directed to the USB2000 spectrophotometer for measuring the absorbance.

All the external channels were 0.8 mm i.d. PTFE tubing connected to the lab-on-valve unit with PEEK nuts/ferrules (Upchurch Scientific). The capacity of the holding coil was ca. 2.4 ml.

2.5. Operating procedure

An entire operating cycle includes three steps as described in the following sections.

2.5.1. The determination of Cr(VI)

The 800 μl of carrier was aspirated into the syringe, afterwards, 200 μl of sample and 200 μl of DPC solutions were aspirated sequentially into the holding coil via ports 4 and 1 of the LOV, at a same flow rate of 80 μl s^{-1}. Thereafter, the syringe pump was immediately set to dispense the stacked sample and DPC zones via port 5 at 80 μl s^{-1}. During the transportation process, the chromogenic reaction between Cr(VI) and the DPC solution was accomplished. The mixture was finally directed to the flow cell where the absorbance was monitored at 548 nm, and the concentration of the hexavalent chromium was derived.

2.5.2. On-line oxidation of Cr(III) and determination of the total chromium content

After 800 μl of carrier was aspirated as described above, 200 μl of sample was aspirated via port 3 of the LOV. A low flow rate of 15 μl s^{-1} was employed, in order to ensure the complete oxidation of the trivalent chromium into Cr(VI) while it flow through the oxidizing column in port 3. DPC (200 μl) solution was then aspirated at 80 μl s^{-1}. Thereafter, the syringe pump dispensed the stacked sample and DPC zones via port 5 and directed toward the flow cell, where the absorbance was monitored and the total amount of chromium was derived.

2.5.3. Refreshment of the micro-column

After trivalent chromium in the sample solution had been oxidized, 1000 μl of carrier and 800 μl of phosphoric acid (0.5 mol l^{-1}) were sequentially aspirated into the holding coil via ports 6 and 2, respectively, at 80 μl s^{-1}. The phosphoric acid zone was afterwards directed to flow through the port 3 at a flow rate of 20 μl s^{-1} for refreshing the micro-column, while the carrier was used to maintain the column in a neutral environment.

3. Results and discussion

3.1. Parameters affecting the performance of the oxidizing column reactor

The overall performance of the portable speciation analyzer depends strongly on the oxidation efficiency of the micro-column reactor. For a solid phase reactor, the bead size and bed height of packing materials directly influence the axial dispersion and thus the sensitivity and precision. When 40–60 mesh silica gel beads were employed, an increased axial dispersion was encountered, this resulted in a lower absorbance. In addition, the bismuthate was not uniformly immobilized on the surface of larger beads, caused a deterioration of the precision and the lifetime of the column. On the other hand, too small beads (150–200 mesh) cause excessive flow resistance in the column. The bed height of 10–60 mm at a fixed column diameter of 2.0 mm was also investigated. A slight decrease in the recorded absorbance was observed with the increase of the bed height, probably due to the axial dispersion. However, too short a bed height caused a decrease in the lifetime of the reactor. As a compromise, 60–80 mesh silica gel beads and 30 mm packing bed height was employed, yielding both a satisfactory oxidizing efficiency and an adequate lifetime of the column.

The amount of the immobilized sodium bismuthate on the surface of the silica beads was also studied by varying the mass ratio of bismuthate/silica within 1:1, 1:5 and 1:10. It indicated that both a better oxidizing efficiency and lifetime of the packed column was observed when a mass ratio of 1:5 for bismuthate/silica was employed for the immobilization process.

Quantitative oxidation of trivalent chromium is preferentially accomplished within a very short time period while the sample solution was aspirated by the syringe pump and flowing through the column reactor. The oxidation kinetics was therefore investigated by varying the contacting time of the sample solution with the oxidizing surface, which was readily realized by controlling flow rate for aspirating the sample solution through the column reactor. The results showed that an increment of the recorded absorbance was observed with the decrease of the flow rate, i.e., a longer contacting time resulted in a higher oxidizing efficiency of the trivalent chromium. Investigations revealed that quantitative oxidation of the trivalent chromium were accomplished by employing a flow rate of 15 μl s^{-1} to aspirate the sample solution flow through the column.

Sodium bismuthate has very strong oxidizing ability in acidic medium. In order to maintain its oxidizing capability and at the same time the stability of the packed column, an appropriate acid should be carefully chosen. The experiments indicated that acids with reducing or oxidizing nature could easily destruct the packed column or alter the chemical form of the analyte, thus HCl and HNO_3 were out of choice in this case. When H_3PO_4 and H_2SO_4 were used, a higher response and a longer lifetime of the column were achieved. Considering H_3PO_4 is a good masking reagent for Fe^{3+}, which might be a potential interference for the chromogenic reaction between Cr(VI) and DPC, it was therefore adopted in the present reaction system. A further investigation of the effect of H_3PO_4 concentration showed that the recorded signal increased with the increase of its concentration up to 0.5 mol l^{-1}, while afterwards a decline of the signal was observed along with a deterioration of the precision and the lifetime of the column. Thus, a 0.5 mol l^{-1} H_3PO_4 solution was selected for sample dilution.

3.2. Variables affecting the chromogenic reaction

For the present set-up of the portable lab-on-valve speciation analytical system, zone penetration or degree of the dispersion of the adjacent zones is the key factor governing the performance of the analyzer. The dispersion in the flow stream depends on various parameters, including the reaction time, the concentrations in the stacked zones, the zone volumes and the diameter of the flow channel.

The chromogenic reaction between Cr(VI) and DPC is quite fast, thus no incubation is required, and a maximum signal was achieved by employing a flow rate of 80 μl s^{-1}.

The chromogenic reaction between Cr(VI) and DPC is preferentially performed in a sulfuric acidic medium, it was thus employed in the present system without further investigation.

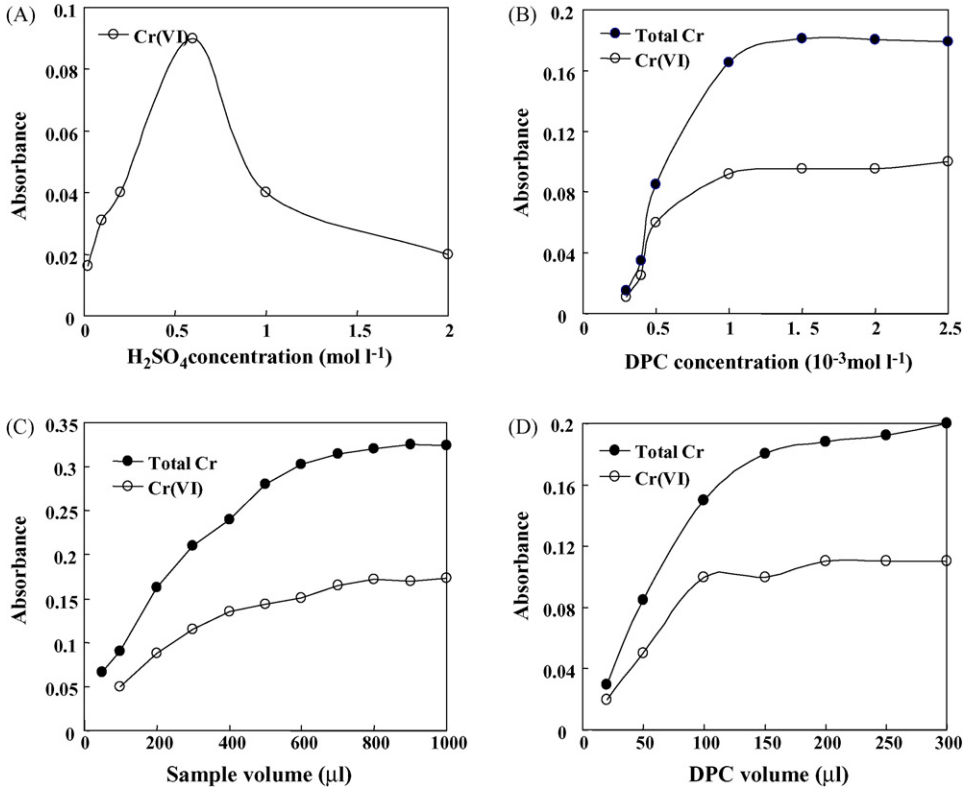

Fig. 2. The effects of chemical variables on the signal recorded by employing 256 μg l^{-1} Cr(VI) and Cr(III), with a fixed concentration of 0.5 mol l^{-1} H_3PO_4 for sample dilution, and a flow rate of 15 μl s^{-1} for aspirating sample solution through the oxidizing column. (A) DPC volume/concentration, 200 μl/2 × 10^{-3} mol l^{-1}; sample volume, 200 μl; (B) 0.6 mol l^{-1} H_2SO_4; sample and DPC volume, 200 μl; (C) 0.6 mol l^{-1} H_2SO_4; DPC volume/concentration, 200 μl/2 × 10^{-3} mol l^{-1}; (D) 0.6 mol l^{-1} H_2SO_4; DPC concentration, 2 × 10^{-3} mol l^{-1}; sample volume, 200 μl.

As illustrated in Fig. 2A that the absorbance increased substantially with the increase of H_2SO_4 concentration from 0.02 to 0.6 mol l^{-1}, while a further increase of the H_2SO_4 concentration beyond this range resulted in a decrease of the signal. Therefore, 0.6 mol l^{-1} H_2SO_4 was adopted for the dilution of DPC stock solution.

Fig. 2B illustrated the influence of the DPC concentration on the sensitivity for the determination of both Cr(VI) and total chromium. It can be seen that the absorbance increased steeply with the increase of DPC concentration up to 10^{-3} mol l^{-1}, while afterwards the increment was slowed down when further increasing its concentration. A DPC concentration of 2×10^{-3} mol l^{-1} was thus chosen for the ensuing experiments.

The investigations on the effects of the volumes of sample and DPC solutions indicated that an increase of the signal was recorded with the increase of the zone volumes within a certain range, as illustrated in Fig. 2C and D. This was readily attributed to the fact that the adjacent sample/reagent zones in the channel disperse into each other, and thus allowing the reaction to take place and give rise to the colored product. The amount of the product was increased with the increase of reagent/sample zone volume, thereby an increase of the absorbance was observed. On the other hand, within a certain time period, the penetration of the adjacent zones were limited, and thus an excessive increment of the zone volumes contribute virtually nothing to the dispersion and therefore no contribution to the amount of the formed product. Considering that excessive sample processing could potentially decrease the lifetime of the column and the sampling frequency, zone volumes of 200 μl for both sample and DPC were thus selected in the present system.The reaction temperature should be an important factor in the field determination because the present system involves redox reaction. At a lower temperature, the oxidation efficiency is consequently decreased which might pose further effects on the sensitivity. Practically, the absorbance of the system when employing standard and sample solutions was measured at identical temperatures. Therefore, the effect of the variation of temperature could be eliminated, although there might be a little deterioration in the sensitivity.

3.3. Interfering effects

In the present LOV speciation system, interferences might be categorized into two groups. The first group takes part in the competition with hexavalent chromium to form complexes with DPC, while another group tends to deteriorate the packed column reactor via either chemical reaction or physical adsorption on the surface of the column. In order to assess potential interferences, some frequently encountered species in water samples were investigated. At a chromium concentration level of 320 μg l^{-1} and within a ± 5% error range, the obtained tolerance molar ratios were summarized in Table 1. It is obvious that satisfactory tolerant limits for most of the tested species pose no interferences. Although the tolerant limits for Cd^{2+}, Al^{3+}, Co^{2+}, and Mn^{2+} were relatively low, their concentrations in common water samples or after appropriate dilution will not exceed the tolerant concentration listed herein. Therefore, the present procedure can be directly employed, and no further treatment or masking reagents are needed.

Table 1
The tolerance molar ratios of foreign species

Foreign species	Tolerance molar ratios[a]	
	Cr(VI)	Cr(III)
F^-, NO_3^-, SO_4^{2-}, NH_4^+, Na^+, K^+, Zn^{2+}	1000[b]	1000[b]
Cl^-	1000[b]	500
Cu^{2+}, Hg^{2+}	300	300
Al^{3+}	500[b]	100
Cd^{2+}	200	60
Ni^{2+}	500[b]	500[b]
Ca^{2+}	1000	300
Mg^{2+}	500[b]	300
Fe^{3+}	300	200
Co^{2+}	100	100
Mn^{2+}	200	40

[a] The maximum molar ratio of foreign species to chromium within an error range of ±5%.
[b] Higher concentrations were not investigated.

3.4. Analytical performance of the SI-LOV analyzer for chromium speciation

The performance data for the portable chromium speciation analyzer based on the sequential injection lab-on-valve format was summarized in Table 2, and the recorded peaks for three replicate determinations were illustrated in Fig. 3. It is obvious that although the detection limits of the present analyzer are not favorable for the speciation of very low concentrations of Cr(VI) and Cr(III), e.g., in seawater and municipal surface water, it works well for a variety of wastewater sam-

Table 2
Analytical performance of the field speciation analyzer for chromium

	Cr(VI)	Cr(III)	Total Cr
Linear calibration range	24–2000 μg l^{-1}	32–2000 μg l^{-1}	32–2000 μg l^{-1}
Regressive equation	$Y = 0.184X + 0.001$ ($R^2 = 0.9976$)	$Y = 0.146X + 0.006$ ($R^2 = 0.9966$)	$Y = 0.167X - 0.004$ ($R^2 = 0.9968$)
Oxidation efficiency	79.3%		
Sample consumption	200 μl		
Reagent consumption	200 μl		
Sampling frequency	60 h^{-1}		
Lifetime of the packed reactor	200–350 cycles		
Detection limit (3σ, $n = 11$)	5.6 μg l^{-1}	8.2 μg l^{-1}	6.8 μg l^{-1}
R.S.D. (32 μg l^{-1}, $n = 11$)	2.0%	3.2%	2.8%

Table 3
The speciation of chromium in various water samples ($\mu g\,l^{-1}$)

Samples	Certified values		Found values		Spiked		Recovery (%)	
	Cr(III)	Cr(VI)	Cr(III)	Cr(VI)	Cr(III)	Cr(VI)	Cr(III)	Cr(VI)
GSBZ 50027-94		121 ± 5		118 ± 6				
GSBZ 50009-88	490 ± 14[a]		499 ± 12					
Plate water 1			42 ± 3	Not found	48	48	98	101
Plate water 2			49 ± 1[b]	850 ± 30	20[b]	640	99	102
Tannery water			192 ± 4	52 ± 6	192	192	105	97

[a] Certified concentration of total chromium.
[b] $\mu g\,ml^{-1}$.

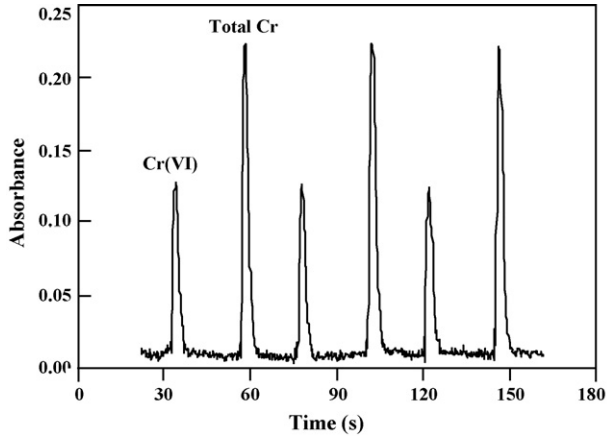

Fig. 3. The recorded response profiles for hexavalent chromium ($256\,\mu g\,l^{-1}$) and total chromium ($512\,\mu g\,l^{-1}$) at the optimal experimental conditions.

ples, i.e., tannery water, plate water etc. Considering that the aim of the present work is to develop a field speciation analyzer for emergent accident, where the concentration of the species of interest is usually high and variations of the concentration with time is one of the most critical issues. At this juncture, the present analyzer is most suitable in such cases, which provides vast potentials and versatilities for fast field speciation of chromium.

3.5. Applications of SI-LOV speciation analyzer

The practical applicability of the system was first validated by analyzing the Cr(VI) and total chromium contents in two certified reference materials, i.e., GSBZ 50027-94 and GSBZ 50009-88 (State Environmental Protection Administration of China). The data listed in Table 3 showed that agreements between the obtained results and the certified values were achieved for the contents of Cr(VI) in GSBZ 50027-94 and total chromium in GSBZ 50009-88. The speciation analyzer was also applied to the speciation of Cr(VI) and Cr(III) in industrial wastewater samples. The water samples were analyzed right after being filtered through a cellulose membrane of 0.45-μm pore size and appropriate dilution with $0.5\,mol\,l^{-1}$ H_3PO_4, in order to avoid alteration of the original distribution of the oxidation forms. The obtained results were summarized in Table 3.

4. Conclusions

This work demonstrated a portable analyzer for field speciation of inorganic chromium by employing a sequential injection lab-on-valve (SI-LOV) system. With the use of a micro-column reactor of bismuthate immobilized silica, the on-line quantitative oxidation of trivalent chromium was achieved in the LOV. Although the detection limits of the present analyzer might not be favorable for very low levels of chromium, it is quite sufficient for chromium in wastewaters, especially suitable for fast field speciation of chromium in water samples from accidental environmental pollution incidents. In addition, the miniaturized system and its portability show promising practicability. As a field speciation instrument, the entire system consists of a selection valve, a micro-syringe pump, a USB spectrophotometer integrated with a tungsten halogen lamp, which can easily be compacted into a box with size of 30 cm × 20 cm × 20 cm, and the entire system weighs about 2 kg. In addition, 10 ml of DPC solution, 100 ml of phosphoric acid ($0.5\,mol\,l^{-1}$) and 500 ml of deionized water as carrier solution should also be included.

Acknowledgements

The authors are indebted to the financial support from the National Natural Science Foundation of China (20575010), the key project for scientific research from the Ministry of Education (105056) and the SRFDP program (20050145026).

References

[1] B. Michalke, Ecotox. Environ. Saf. 56 (2003) 122.
[2] J. Szpunar, Analyst 125 (2000) 963.
[3] B. Michalke, Fresenius' J. Anal. Chem. 354 (1996) 557.
[4] S.C. Hight, J. Cheng, Anal. Chim. Acta 567 (2006) 160.
[5] V. Van Lierde, C.C. Chery, L. Moens, F. Vanhaecke, Electrophoresis 26 (2005) 1703.
[6] G. Alvarez-Llamas, M.R. de la Campa, A. Sanz-Medel, Anal. Chim. Acta 546 (2005) 236.
[7] O. Schramel, B. Michalke, A. Kettrup, Fresenius' J. Anal. Chem. 363 (1999) 452.
[8] A.L. Rosen, G.M. Hieftje, Spectrochim. Acta Part B 59 (2004) 135.
[9] X.-B. Long, M. Miró, E.H. Hansen, J. Anal. At. Spectrom. 20 (2005) 1203.
[10] X.-D. Tang, Z.-R. Xu, J.-H. Wang, Spectrochim. Acta Part B 60 (2005) 1580.
[11] M. Leermakers, W. Baeyens, M. De Gieter, B. Smedts, C. Meert, H.C. De Bisschop, R. Morabito, Ph. Quevauviller, Trend Anal. Chem. 25 (2006) 1.

[12] L.V. Mulaudzi, J.F. van Staden, R.I. Stefan, Anal. Chim. Acta 467 (2002) 51.
[13] Y. Sibel, R. Apak, Anal. Chim. Acta 505 (2004) 25.
[14] T. Adalet, A.R. Türker, Talanta 57 (2002) 1199.
[15] M.S. Tehrani, A.A. Ebrahimi, F. Rastegar, Ann. Chim. 94 (2004) 429.
[16] M. Postel, E. Duňach, Coord. Chem. Rev. 155 (1996) 127.
[17] K. Bimal, M.S. Banik, C.M. Venkatraman, F.B. Frederick, Tetrahedron Lett. 39 (1998) 7247.
[18] K. Kargosha, M. Noroozifar, Anal. Chim. Acta 413 (2000) 57.
[19] B.-X. Li, Z.-J. Zhang, L.-X. Zhao, C.-L. Xu, Anal. Chim. Acta 459 (2002) 19.
[20] C.-H. Wu, J. Ruzicka, Analyst 126 (2001) 1947.
[21] J.-H. Wang, E.H. Hansen, Anal. Chim. Acta 435 (2001) 331.
[22] Y. Chen, J. Ruzicka, Analyst 129 (2004) 597.
[23] X.-W. Chen, W.-X. Wang, J.-H. Wang, Analyst 130 (2005) 1240.
[24] T. Leelasattarathkul, S. Liawruangrath, M. Rayanakorn, W. Oungpipat, B. Liawruangrath, Talanta 70 (2006) 656.
[25] M. Yang, Y. Xu, J.-H. Wang, Anal. Chem. 78 (2006) 5900.
[26] M. Miró, E.H. Hansen, Trend Anal. Chem. 25 (2006) 267.

Available online at www.sciencedirect.com
ScienceDirect
Talanta 72 (2007) 1667–1674
Talanta
www.elsevier.com/locate/talanta

Investigation of the photocatalytic degradation of organochlorine pesticides on a nano-TiO_2 coated film

Binbin Yu [a], Jingbin Zeng [a], Lifen Gong [a,c], Maosheng Zhang [a], Limei Zhang [a], Xi Chen [a,b,*]

[a] *Department of Chemistry and the Key Laboratory of Analytical Sciences of the Ministry of Education, College of Chemistry and Chemical Engineering, Xiamen University, Xiamen 361005, China*
[b] *State Key Laboratory of Marine Environmental Science, Xiamen University, Xiamen 361005, China*
[c] *Department of Chemistry, Quanzhou Normal University, Quanzhou 362000, China*

Received 17 October 2006; received in revised form 27 February 2007; accepted 3 March 2007
Available online 15 March 2007

Abstract

The photocatalytic degradation of organochlorine pesticides including α-, β-, γ-, δ-hexachlorobenzene (BHC), dicofol and cypermethrin were carried out on a nano-TiO_2 coated films under UV irradiation in the air. The photocatalytic conditions, including the amount of TiO_2, irradiation time and the intensity of light were optimized. The pesticides were most effectively degraded under the condition of 2.24 mg/cm^2 on TiO_2 film and a 400 W UV irradiation of high-pressure mercury lamp with a wavelength of 365 nm. A typical organochlorine pesticide, 20 μg α-BHC, was dipped onto the TiO_2 film surface and degraded completely within 20 min. In addition, the photocatalytic degradation pathways on the nano-TiO_2 coated film were discussed.

Keywords: TiO_2; Photocatalytic degradation; Organochlorine pesticides; Nanocoated film

1. Introduction

Organochlorine pesticides, such as BHC, dicofol, cypermethrin, etc, are well known for their toxicity, widespread occurrence in the environment and especially their bioaccumulative abilities. Although the usage of these pesticides has been prohibited for 20 years, the original compounds as well as their degradation products have still been found in some foods and surface water [1–3]. There has been growing interest in developing efficient methods of degrading these pesticides including microbial degradation, mechanochemical destruction, thermal degradation and photocatalysis for their degradation mechanism studies or rapid analysis. Generally, in the microbial degradation [4], only a special kind of microorganism could be used to degrade an objective pesticide. In addition, the cultivation and purification of the microorganism were time-consuming, and it would take several days for the full degradation of the pesticides. In Hall et al.'s reported approach [5], an organochlorine pesticide, such as DDT, could be mechanochemically destroyed after a 12 h of milling with calcium oxide in the argon atmosphere, and then no volatile organic material was detected by a conventional GC/MS procedure. Photodegradation of polychlorinated debenzo-*p*-dioxine and dibenzofurans were carried out in aqueous solution and in organic solvents under the irradiation at 300 nm [6]. Although the above-mentioned methods were available to degrade organochlorine pesticides, they possessed some limitations such as time-consuming or high manipulation cost. Hence, the rapid, easy-to-operate, low cost degradation methods will be highlighted. During the past years, some considerations have been focused on the photocatalytic process based on anatase TiO_2 since it operates in ambient temperature and pressure with low energy photons ($\lambda < 388$ nm), requires no chemical reagents except oxygen in the ambient air and no expensive catalysts. TiO_2 has been predominantly used as a photocatalyst for the degradation of methoxychor and *p*,*p*′-DDT in aqueous suspension [2]. Liu et al. utilized TiO_2 nanoparticle to

* Corresponding author at: State Key Laboratory of Marine Environmental Science, Xiamen University, Xiamen 361005, China. Tel.: +86 592 2184530; fax: +86 592 2186401.
E-mail address: xichen@xmu.edu.cn (X. Chen).

0039-9140/$ – see front matter © 2007 Elsevier B.V. All rights reserved.
doi:10.1016/j.talanta.2007.03.013

transform chlorinated volatile organic compounds [7]. Recently, a TiO_2 film has been developed and applied to degrade polychlorinated debenzo-*p*-dioxine under UV irradiation [8]. Moreover, low-density polyethylene–TiO_2 nanocomposite film has usually been selected to degrade polyethylene [9].

In our laboratory, efforts have been made to develop a photocatalytic film based on the nano-TiO_2 coated on a glass side for higher degradation efficiency. This paper presents the study of photocatalytic degradation of organochlorine pesticides on a nano-TiO_2 coated film, which was prepared by immersing a glass slide into a nano-TiO_2 suspension. The photocatalytic efficiency of a few organochlorine pesticides degradation as a function of various experimental parameters was studied, and their photocatalytic mechanism on the nano-TiO_2 coated film were discussed. Compared with our previous work, the mode of nano-TiO_2 coated on a glass side showed higher degradation conversion of pesticides than aqueous suspension mode. Under the same condition, it costed 20 min to degrade dicofol for nano-TiO_2 coated film while 120 min were needed for aqueous suspension mode.

2. Experimental

2.1. Reagents and solutions

α-, β-, γ-, δ-BHC (95.5–100%), dicofol (97%) were obtained from Accustandard Co. Ltd. (USA). Cypermethrin were from Institute of Forensic Science Ministry of Public Security, P.R.C. (Beijing, China). Acetone and hexane were of pesticide residue grade and purchased from Tedia Co. Ltd. (USA). Stock solutions of BHC, dicofol and cypermethrin with 100 μg mL^{-1} were prepared and dissolved in acetone. TiO_2 nanoparticles from Degussa P25 (Haiyi Scientific Trading Co. Ltd., China) were 70% in anatase and 30% in rutile phases, and their primary particle diameters were in the range of 30–50 nm.

2.2. Apparatus

The photocatalytic degradation of organochlorine pesticides on the nano-TiO_2 coated film was performed under a 400 W mercury lamp irradiation with a typical wavelength of 365 nm. The distance between the lamp and the TiO_2 film was 20 cm. All the experiments were carried out at ambient pressure. A cooling system with flowing water was used to keep the reactor temperature at 20 ± 1 °C.

A Shimadazu GC-2010 gas chromatograph (GC) equipped with an electron capture detector (ECD) and a DB-5 column (30 m × 0.25 mm × 0.25 μm) was applied to detect the original and residual pesticides. The temperature program of the GC-ECD was selected as follows: 100–220 °C at 20 °C min^{-1}, 220–240 °C at 5 °C min^{-1}, 240–300 °C at 20 °C min^{-1} for BHC; 200–300 (10 min) °C at 10 °C min^{-1} for cypermethrin; 150 (1 min)–280 °C at 20 °C min^{-1}, 280–300 °C at 10 °C min^{-1} for dicofol. The temperature of ECD and injector was held at 300 and 280 °C, respectively. Each sample with 1 μL was repeatedly injected twice, and the data were collected and averaged.

An FT-IR spectrometer (Thermo Nicolet FT-IR 7400SX spectrometer) was applied to monitoring the spectral changes of the sample extracted from TiO_2 coated film before and after irradiation. A scanning electron microscope (LEO-1530, SEM) was used to observe the surface morphologies of TiO_2 coated film. The analysis of carbon or chlorine was implemented by the energy dispersive X-ray spectrometry (EDS) with the same equipment.

2.3. Preparation of nano-TiO_2 coated film

A nano-TiO_2 coated film was prepared by immersing a glass slide into a nano-TiO_2 suspension (0.5–2 wt.%) [8]. The slide was dried in the ambient air, and then immersed into the same nano-TiO_2 suspension twice. The 20 μg of each pesticide was pipetted on the TiO_2 film surface. The photocatalytic procedure was started as soon as the solvent in the pesticide sample was volatilized completely. For a full extraction of the residual pesticide, the TiO_2 coated film was immersed into a 3 mL acetone solvent for 30 min after irradiation. Also the photocatalytic procedure for each pesticide with different degradation time was held twice, and the data were collected and averaged.

2.4. Computational details

Full geometry optimizations of the hexachlorobenzene isomers and their chlorine-deleted derivatives were carried out by the B3LYP [10,11] method with 6–31G(d) basis set. Vibrational frequency analyses were employed to assess the nature of optimized structures. All calculations were performed using the Gaussian 03 program [12].

3. Results and discussion

3.1. Effect of nano-TiO_2 coating weight

The weight changes of the glass slides were compared before and after it was immersed into the different TiO_2 suspensions. The coating mass of nano-TiO_2 on the slide was measured and shown in Table 1. Obviously, a higher weight ratio of nano-TiO_2 suspension caused a more adsorption of nano-TiO_2 on the glass slide. Correspondingly, as shown in Fig. 1, the photocatalytic efficency generally increased with the usage of the more adsorption of nano-TiO_2 on the slide. Experimental results indicated that the film coated 2.24 mg cm^{-2} TiO_2, which prepared by immersed into the 2 wt.% nano-TiO_2 suspension, presented the highest photocatalytic conversion. However, the nano-TiO_2 coated film became unstable since the nano-TiO_2 could easily drop out of the film when the TiO_2 suspension such as 3 wt.% was selected, which decreased the degradation efficiency, reversely. In the

Table 1
Coating mass of TiO_2 on the film corresponding to its suspension

TiO_2 suspension (wt.%)	0.5	1	2	3
Coating mass (mg cm^{-2})	0.5	1.83	2.24	2.62

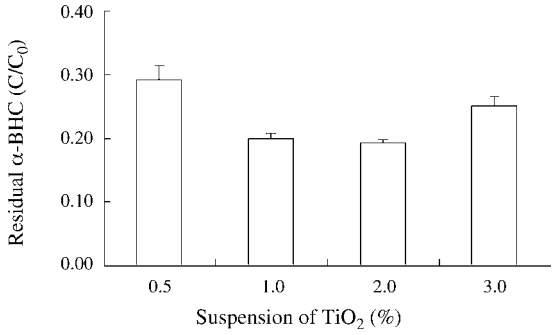

Fig. 1. Residual amount of α-BHC as a function of TiO_2 suspension. *Conditions*: Amount of α-BHC, 20 μg; irradiation time, 10 min.

preparation of nano-TiO_2 coated film, 2 wt.% TiO_2 suspension was selected.

3.2. Photocatalytic degradation of organochlorine pesticides

A series comparison of the direct photolytic and the photocatalytic degradation of organochlorine pesticides were performed under a UV irradiation using a 400 W mercury lamp. As shown in Fig. 2, C presented the content of residual pesticide and C_o was its original content. C/C_o was regarded as the degradation efficiency. Clearly, the whole photocatalytic degradation efficiency is much higher than that by the direct photolysis under the same conditions. After 10 min irradiation in the presence of TiO_2, only 32.0% α-BHC, 44.0% β-BHC, 0.2% γ-BHC, 9.0% δ-BHC, 31.0% dicofol and 0.4% cypermethrin remained, but for these organochlorine pesticides in the absence of nano-TiO_2, corresponding residual rates were found to be 100, 95.91, 19.10, 100, 100 and 26.13%, respectively. The results indicated that nano-TiO_2 evidently increased the degradation pesticides under the UV light irradiation.

The degradation efficiency of organochlorine pesticides was greatly affected by the UV irradiation time. The results as shown in Fig. 3 suggest that degradation degree quickly increases with the increase of the irradiation time. In addition, organochlorine pesticide with different chemical structure presents different conversion efficiency under the same conditions. Among the four isomers of BHC, which chemical structures are presented in Fig. 4, the C–Cl bond exhibits aaeeee, eeeeee, aaaeee or

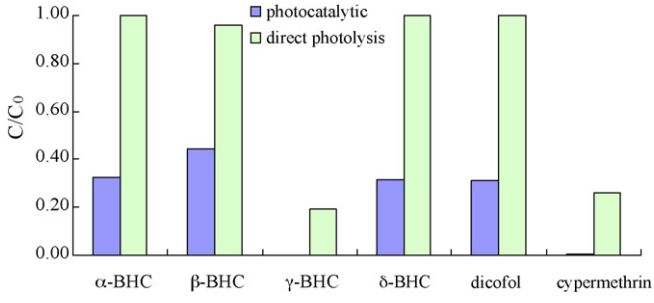

Fig. 2. Degradation efficiency of pesticides under TiO_2 photocatalysis and direct photolytic irradiation. *Conditions*: 2.24 mg cm^{-2} TiO_2 coated film; amount of organochlorine pesticide, 20 μg; irradiation time, 10 min.

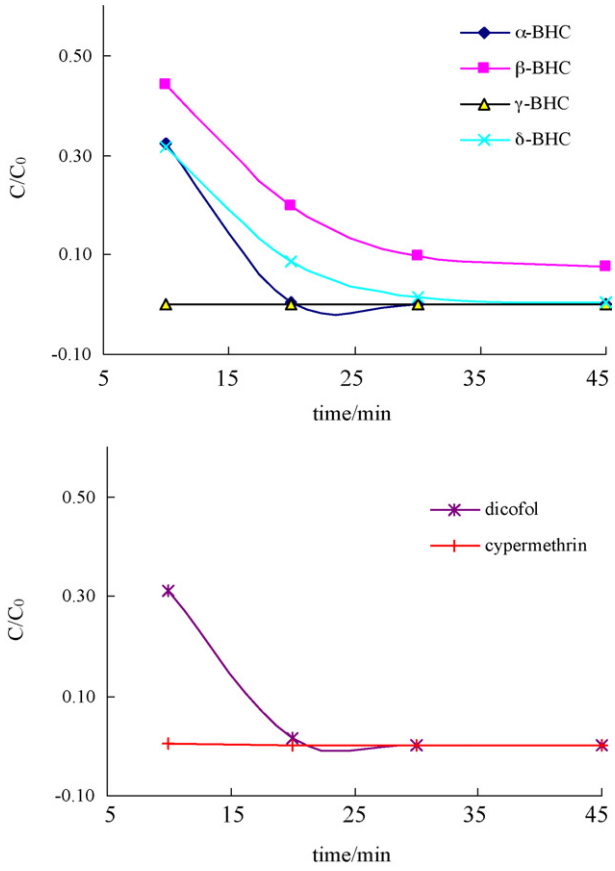

Fig. 3. Relationship between irradiation time and degradation of organochlorine pesticides. *Conditions*: 2.24 mg cm^{-2} TiO_2 coated film; amount of organochlorine pesticides, 20 μg.

aeeeee style, respectively. Generally, the cleavage of C–Cl bond with aaaeee style needs less irradiation energy. The changes of the energy, enthalpy and Gibbs free energies for the chlorine-deleted mechanism from the C sites of BHC isomers, were calculated and listed in Table 2. The calculation results show that C–Cl bond scission of γ-BHC isomer needs the lowest Gibbs free energies (ΔG°) of 45.84 kcal mol^{-1}. For the BHC isomers, the facility of chlorine-deleted follows the order

Table 2
Energetics and thermodynamic values (kcal mol^{-1}) for different C–Cl bond scission channels of BHC isomers derived from B3LYP/6-31G(d) method

Isomers	Sites	C1	C2	C3	C4	C5	C6
α-BHC	ΔE	58.89	56.84	59.70	59.70	56.84	58.89
	ΔH	59.68	57.64	60.49	60.49	57.64	59.68
	ΔG	50.51	48.46	51.35	51.35	48.46	50.51
β-BHC	ΔE	59.01	59.01	59.01	59.01	59.01	59.01
	ΔH	59.90	59.90	59.90	59.90	59.90	59.90
	ΔG	50.07	50.07	50.07	50.07	50.07	50.07
γ-BHC	ΔE	53.88	55.55	60.42	55.55	53.88	57.73
	ΔH	54.68	56.36	61.18	56.36	54.68	58.45
	ΔG	45.84	47.52	52.67	47.52	45.85	49.87
δ-BHC	ΔE	59.03	57.30	60.00	57.37	60.00	57.30
	ΔH	59.90	58.08	60.80	58.19	60.80	58.08
	ΔG	50.24	49.33	51.90	49.02	51.90	49.33

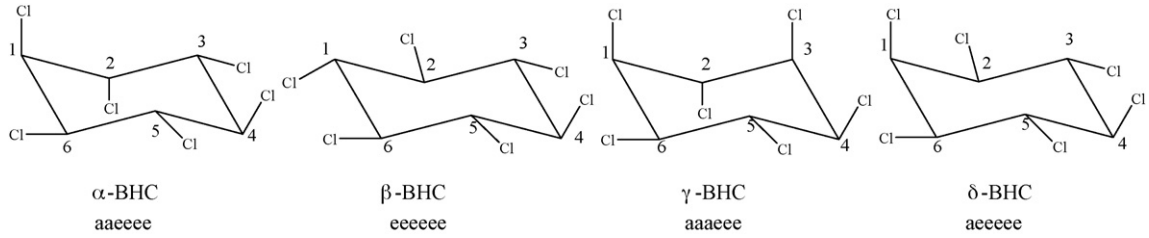

Fig. 4. Structures of the BHC isomers.

as γ-BHC > α-BHC > δ-BHC > β-BHC. The present explanation could be further confirmed by the following experimental results. In the photocatalytic degradation of BHC isomers, dicofol, γ-BHC and cypermethrin could be completely photocatalyticly degraded within 10 min, because γ-BHC exhibited its most unstable character among the BHC isomers [13] and the ester structure of cypermethrin caused a cleavage of ester three-ring bond. α-BHC and dicofol could be photocatalytically degraded within 20 min, but it was 45 min for β-BHC.

3.3. Effect of UV irradiation intensity

The effect of irradiation intensity was studied by using mercury lamps with a power of 16 and 400 W as irradiation source. Based on the experimental results as shown in Fig. 5, the irradiation intensity played an important role for the photocatalytic degradation of organochlorine pesticides. According to analytical results for the residual amounts of pesticides by GC, obvious degradation of a-BHC and dicofol occurred after a 60 min irradiation under a 400 W mercury lamp irradiation, whereas there was little change for α-BHC and only 25% degradation for dicofol under a 16 W mercury lamp. As for cypermethrin, degradation could be done completely within 10 and 60 min under the irradiations from 400 and 16 W lamps, respectively. Apparently, the above results revealed that the photocatalytic degradation of organochlorine pesticides on the nano-TiO_2 film were greatly enhanced by using the higher power UV lamp and resulted in a full conversion for the pesticides within 60 min irradiation from the 400 W lamp.

3.4. FT-IR analysis

FT-IR was applied to the study of the photocatalytic degradation process of organochlorine pesticides in the presence of TiO_2. After degradation, the residual pesticides were extracted by solvents, and the solution was then concentrated into 200 μL. The contracted solution was scanned and analyzed by FT-IR. In Fig. 6a, with the increase of irradiation time for α-BHC, the IR peaks of C–Cl with 600–800 cm^{-1} and C–H with 2991 cm^{-1} were obviously dropped. It could be concluded that the cleavages of C–Cl and C–H bonds occurred, and chlorine was further converted into chloride. In Fig. 6b, the IR spectrum for pure dicofol showed five major peaks at 767.58, 829.78, 1658.33, 1588.96 and 1486.06 cm^{-1}, respectively. Correspondingly, the first and second peaks were ascribed to C–Cl and 1,4-benzene substitution, and the last three peaks were contributed by the benzene special vibration. The intensity of the major peaks decreased and even disappeared after the UV irradiation, which indicated the aromatic ring of dicofol was destroyed in the photocatalytic degradation. The same phenomenon was observed on the cypermethrin degradation. Cypermethrin presented several peaks on the IR spectra, including C=O (ester) vibration at 1740 cm^{-1}, benzene special vibration at 1586, 1468, 1448 cm^{-1}, C–O–C at 1152 cm^{-1} and C–Cl at 692.89 cm^{-1}. After 10 min irradiation, all major peaks disappeared which meant that cypermethrin was characteristic of quick degradation.

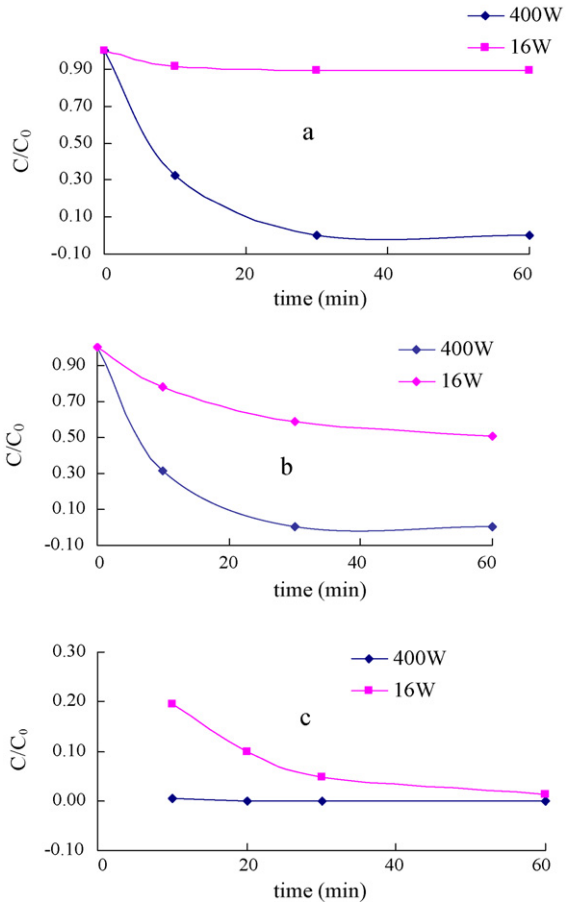

Fig. 5. Relationship between light intensity and degradation conversion of pesticides as a function of irradiation time (a) α-BHC, (b) dicofol and (c) cypermethrin. *Conditions*: 2.24 mg cm^{-2} TiO_2 coated film; amount of organochlorine pesticides, 20 μg.

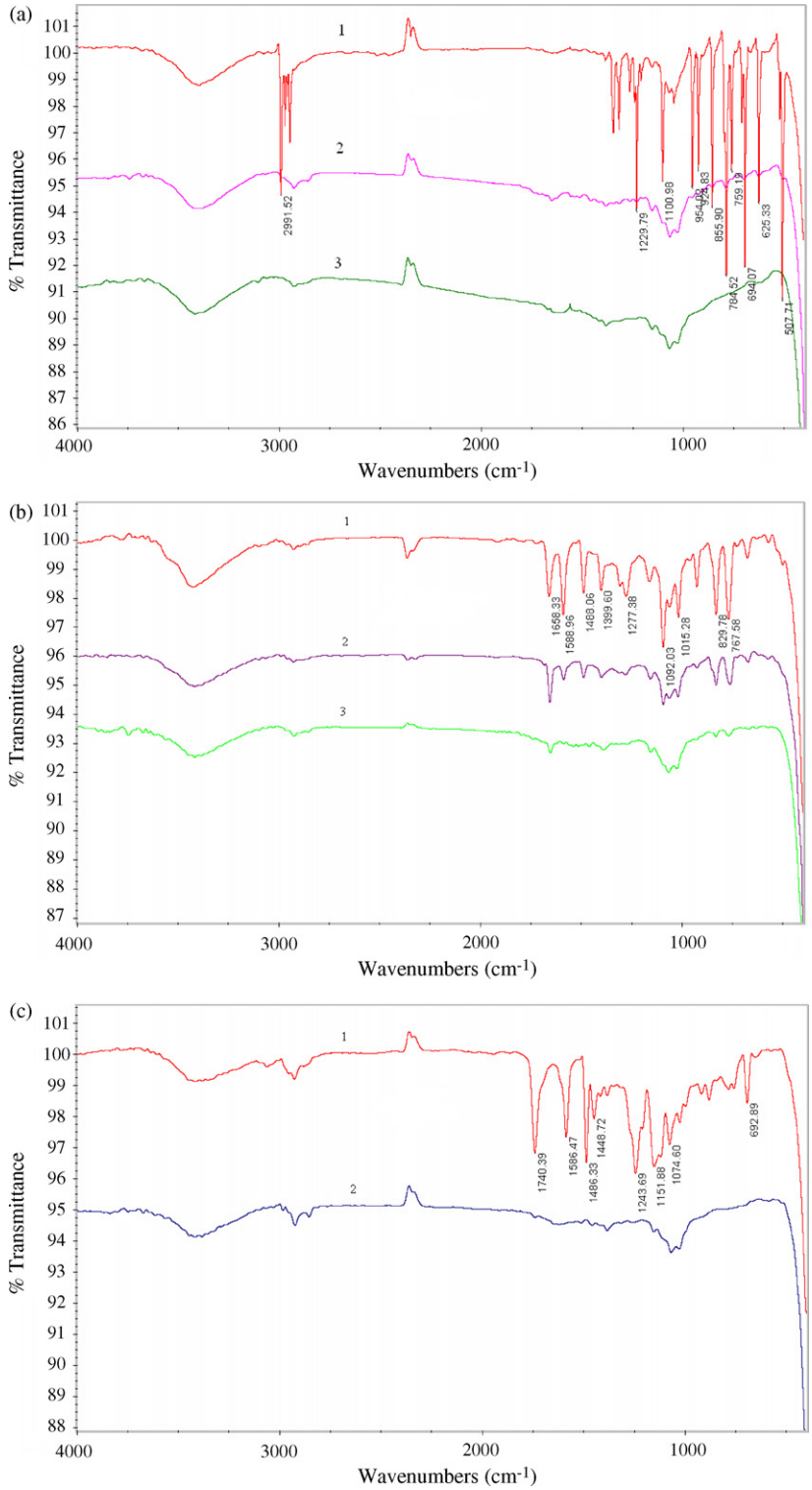

Fig. 6. FTIR spectra of pesticides with different irradiation time. (a) α-BHC 1, 0 min; 2, 10 min; 3, 30 min. (b) Dicofol 1, 0 min; 2, 10 min; 3, 30 min. (c) Cypermethrin 1, 0 min; 2, 10 min; (a) C—Cl: 600–800 cm^{-1}; C—H: 2991 cm^{-1}. (b) C—Cl: 767.58 cm−1; 1, 4-benzene substitution: 829.78 cm^{-1}; benzene special vibration: 1658.33, 1588.96, 1486.06 cm^{-1}. (c) C═O (ester): 1740 cm^{-1}; benzene special vibration: 1586, 1468, 1448 cm^{-1}; C—O: 1243 cm^{-1}; C—O—C: 1152 cm^{-1}; C—Cl: 692.89 cm^{-1}.

3.5. EDS analysis

The EDS analysis results of α-BHC are given in Table 3, which revealed the content change of titanium, oxygen, carbon and chlorine during the photocatalytic degradation. The contents of titanium and oxygen, which were presented by the ratios of weight and atomic number in the table, were kept constant, and the atomic ratio of Ti/O was nearly 1:2 in the irradiation. Hiskia

Table 3
EDS analysis results of α-BHC

Sample	Ti		O		C		Cl	
	Wt.%	Atm.%	Wt.%	Atm.%	Wt.%	Atm.%	Wt.%	Atm.%
TiO_2 coated film	61.25	35.57	36.70	63.82				
TiO_2-α-BHC (0 min irradiation)	58.94	32.57	38.82	64.24	1.04	2.28	1.21	0.90
TiO_2-α-BHC (10 min irradiation)	58.79	32.42	39.92	65.91	0.49	1.07	0.81	0.60
TiO_2-α-BHC (30 min irradiation)	60.05	33.54	38.99	65.20	0.36	0.80	0.61	0.46

et al. [14] reported that lindane was photodegraded to CO_2 and HCl in the presence of polyoxometallate ($PW_{12}O_{40}^{3-}$). Moreover, trichloroethylene was converted into CO_2 and HCl during gas–solid photocatalytic oxidation [15]. In our experiment, the carbon and chlorine of α-BHC were transformed and volatilized in the forms of CO_2 and HCl, resulting in a remarkable decrease of C and Cl contents on the TiO_2 film with the increase of the irradiation time. These results accorded with those from IR experiments.

3.6. Morphology of TiO_2 film

SEM images of TiO_2 coated film are shown in Fig. 7. As displayed in Fig. 7a, most of nano-TiO_2 particles remained to their original shapes, keeping their size around 30–50 nm. Except a few content of TiO_2 particles reunited together, there was no significant size change of the TiO_2 particles before and after absorbed on glass. The large amounts of cavities appearing on the film surface in Fig. 7b proved the porous character of TiO_2 film, which made a convenient absorption for pesticides. And Fig. 7c shows a cross-sectional view with a film thickness of 13.42 μm, which caused a stable property of film and good degradation efficiency as its high density. Under a suitable light energy, a density with 2.24 mg cm^{-2} of nano-TiO_2 on the film was most feasible to degrade pesticides on the TiO_2 surface.

3.7. Mechanism of nano-TiO_2 photocatalytic degradation

In the study of photocatalytic degradation mechanism, a quartz tube of 15 mm inner diameter with caps on the both ends was selected as a reactor. The 20 μg α-BHC or cypermethrin was pipetted on the nano-TiO_2 coated film. The film was then flatly put inside the quartz tube. Considering an important role of oxygen in the photocatalytic degradation of organochlorine pesticides, we selected the air, nitrogen or oxygen gas with a flow rate of 400 mL min^{-1} as a reaction gas. The degradation situations of α-BHC and cypermethrin in the individual gas were tested and presented in Fig. 8. After the 20 min irradiation, only 33.1% of α-BHC was degraded in the nitrogen atmosphere, but 76.5% in the air and 72.6% in oxygen. Analogously, compared to that of 39.6% residual cypermethrin in nitrogen gas, the degradation efficiency in the air or oxygen atmosphere were higher. Correspondingly, only 14.4 and 15.5% residual cypermethrin were found under the same conditions as the α-BHC degradation. These results showed that the presence of oxygen observably increased the photocatalytic degradation efficiency

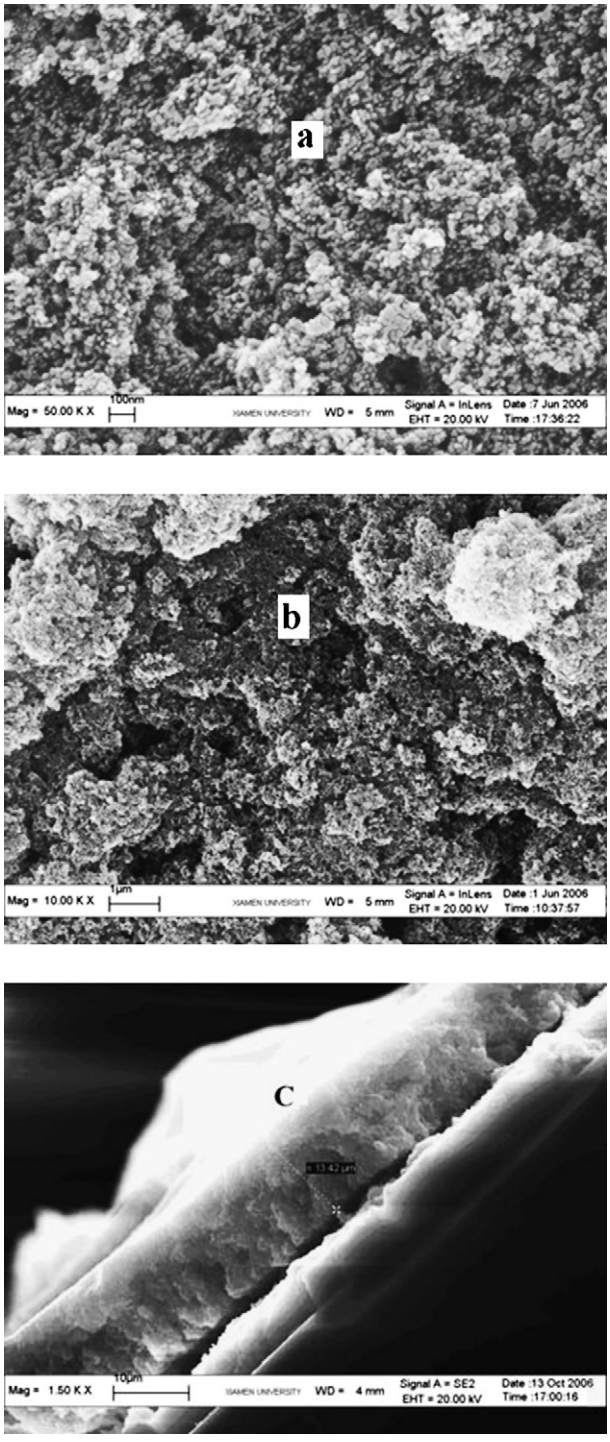

Fig. 7. SEM images of TiO_2 film. (a) Surface view, high magnification. (b) Surface view, low magnification. (c) Cross-sectional view.

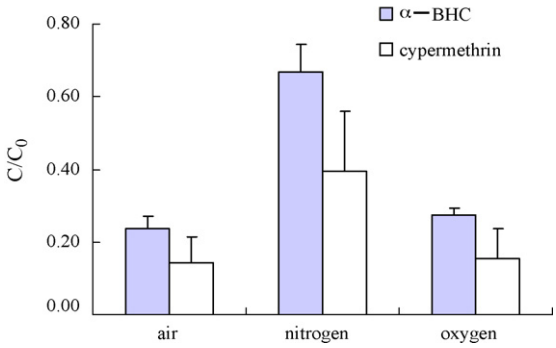

Fig. 8. Degradation efficiency of α-BHC as a funtion of gas. *Conditions*: 2.24 mg cm^{-2} TiO_2 coated film; amount of organochlorine pesticides, 20 μg.

of organochlorine pesticide. Furthermore, the content of oxygen in the air is high enough for the degradation of 20 μg pesticides since the degradation efficiency in the air was similar with that in oxygen. Hence, all the experiments were performed in the ambient air.

It is well established that conductive band electrons (e^-_{CB}) and valence band holes (h^+_{VB}) are generated when TiO_2 is irradiated with light energy greater than its band gap energy (3.2 eV) [16,17].

$$TiO_2 + h\nu \rightarrow h^+_{VB} + e^-_{CB} \quad (1)$$

As Linsebigler et al. reported [18], in the air or oxygen atmosphere, O_2 suppressed the electron-hole recombination processes leading to more efficient photoactivity.

$$O_2 + e^-_{CB} \rightarrow {}^{\bullet}O_2^- \quad (2)$$

Although the carrier gas was treated with silica gel, a certain amount of water in the gas existed. To be considered, H_2O in the air played a role in the degradation of organochlorine pesticides by a pathway of the generation of hydroxyl radical ($^{\bullet}OH$). Simultaneity, peroxide radical ($^{\bullet}OOH$) was generated in the reaction of ${}^{\bullet}O_2^-$ and H_2O. Since at low water vapor pressure, the photocatalysis rate is independent of the water partial pressure in the air [18].

$$H_2O + h^+ \rightarrow {}^{\bullet}OH + H^+ \quad (3)$$

$$OH^- + h^+ \rightarrow {}^{\bullet}OH \quad (4)$$

$${}^{\bullet}O_2^- + H_2O \rightarrow {}^{\bullet}OOH + OH^- \quad (5)$$

The degradation pathways of organic compounds on illuminated TiO_2 surface generally involved a series of electron or hole transfer reactions [18]. Peroxide radicals (${}^{\bullet}O_2^-$, $^{\bullet}OOH$) and hydroxyl radical ($^{\bullet}OH$) were responsible for the TiO_2 photodegradation of organic substrates. The degradation of pesticides on TiO_2 could be initiated by two paths including an attraction by peroxide or hydroxyl radical and electron transfer [16,17]. In general, the oxidative path including hole transfer or ${}^{\bullet}O_2^-$($^{\bullet}OOH$, $^{\bullet}OH$) radical attack initiated the degradation of organochlorine pesticides, the reductive dechlorination through CB electron transfer was the only feasible initial pathway for destroying organochlorine pesticides [17].

$$RX+ \rightarrow \text{products} \rightarrow \ldots \quad (6)$$

$$RX+e^-_{CB} \rightarrow R^{\bullet}+X^- \quad (7)$$

4. Conclusions

This study demonstrated an effective and convenient method for the degradation of organochlorine pesticides by a nano-TiO_2 coated film. The characters of the TiO_2 film were investigated. Under the selected conditions, all pesticides could be completely degraded within 45 min on the film. The presented reaction mechanism of the TiO_2 photocatalytic degradation included an attraction by peroxide or hydroxyl radical and electron transfer. The radicals was generated from the illuminated nano-TiO_2 surface by the reactions between band electrons (e^-_{CB}) or valence band holes (h^+_{VB}) with O_2 or H_2O. In addition, a simple and rapid analytical approach for chloric anion, a final degradation product of organochlorine pesticides, could be considered and developed, by which organochlorine pesticides could be determined indirectly.

Acknowledgements

This research work was financially supported by the Science and Technology Project of Fujian Province (No. 2005-I-030, 2006Y0026) and Program for New Century Excellent Talents in University of China (NCET), which are gratefully acknowledged. We also express our sincere thanks to Professor Xiaoqing Yang from College of Foreign Languages and Cultures, Xiamen University, for her kind revision.

References

[1] A.J. Reviejo, J.M. Pingarron, L.M. Polo, Talanta 39 (8) (1992) 899–906.
[2] A. Zaleska, J. Hupka, M. Wiergowski, M. Biziuk, J. Photochem. Photobiol. A 135 (2000) 213–220.
[3] A.J. Reviejo, A.R. Barrio, J.M. Pingarron, L.M. Polo, Anal. Chim. Acta 246 (1991) 293–300.
[4] L. Fang, Chin. J. Appl. Ecol. 11 (1) (2000) 249–252.
[5] A.K. Hall, J.M. Harrowfield, R.J. Hart, P.G. Mccormick, Environ. Sci. Technol. 30 (12) (1996) 3401–3407.
[6] M. Kim, P.W. Okeefe, Chemosphere 41 (2000) 793–800.
[7] G.H. Liu, Y.F. Zhu, X.R. Zhang, B.Q. Xu, Anal. Chem. 74 (24) (2002) 6279–6284.
[8] W. Choi, S.J. Hong, Y.S. Chang, Y. Cho, Environ. Sci. Technol. (34) (2000) 4810–4815.
[9] L. Zan, W.J. Fa, S.L. Wang, Environ. Sci. Technol. 40 (2006) 1681–1685.
[10] A.D. Becke, J. Chem. Phys. 98 (7) (1993) 5648–5653.
[11] C. Lee, W. Yang, P.G. Parr, Phys. Rev. B. 37 (2) (1988) 785–789.
[12] M.J. Frisch, G.W. Trucks, H.B. Schlegel, G.E. Scuseria, M.A. Robb, J.R. Cheeseman, J.A. Montgomery, T. Vreven, K.N. Kudin, J.C. Burant, J.M. Millam, S.S. Iyengar, J. Tomasi, V. Barone, B. Mennucci, M. Cossi, G. Scalmani, N. Rega, G.A. Petersson, H. Nakatsuji, M. Hada, M. Ehara, K. Toyota, R. Fukuda, J. Hasegawa, M. Ishida, T. Nakajima, Y. Honda, O. Kitao, H. Nakai, M. Klene, X. Li, J.E. Knox, H.P. Hratchian, J.B. Cross, V. Bakken, C. Adamo, J. Jaramillo, R. Gomperts, R.E. Stratmann, O. Yazyev, A.J. Austin, R. Cammi, C. Pomelli, J.W. Ochterski, P.Y. Ayala, K. Morokuma, G.A. Voth, P. Salvador, J.J. Dannenberg, V.G. Zakrzewski, S. Dapprich, A.D. Daniels, M.C. Strain, O. Farkas, D.K. Malick, A.D. Rabuck, K. Raghavachari, J.B. Foresman, J.V. Ortiz, Q. Cui, A.G. Baboul,

S. Clifford, J. Cioslowski, B.B. Stefanov, G. Liu, A. Liashenko, P. Piskorz, I. Komaromi, R.L. Martin, D.J. Fox, T. Keith, M.A. Al-Laham, C.Y. Peng, A. Nanayakkara, M. Challacombe, P.M.W. Gill, B. Johnson, W. Chen, M.W. Wong, C. Gonzalez, J.A. Pople, Gaussian 03, RevisionC. 02, Gaussian Inc., Wallingford, CT, 2004.

[13] C.H. Chen, G.M. Dai, Chin. Acta Sci. Circumstantiae 4 (3) (1984) 266–274.

[14] A. Hiskia, A. Mylonas, D. Tsipi, E. Papaconstantinou, Pestic. Sci. 50 (1997) 171–174.

[15] L.A. Dibble, G.B. Raupp, Environ. Sci. Technol. 26 (1992) 492–495.

[16] I.K. Kongstantinou, T.M. Sakellarides, V.A. Sakkas, T.A. Albanis, Environ. Sci. Technol. 35 (2001) 398–405.

[17] W. Choi, M.R. Hoffmann, Environ. Sci. Technol. 29 (1995) 1646–1654.

[18] A.L. Linsebigler, G. Lu, J.T. Yates, Chem. Rev. 95 (1995) 735–758.

Available online at www.sciencedirect.com
ScienceDirect
Talanta 72 (2007) 1630–1636
Talanta
www.elsevier.com/locate/talanta

β-Cyclodextrin modified filter paper based solid phase extraction–room temperature phosphorimetry for preconcentration and determination of nitrogen heterocyclic compounds in water samples

Ruohua Zhu [a,*], Peilong Wang [a,b], Xiangfeng Wang [a], Xiaoou Su [b]

[a] *Department of Chemistry, Capital Normal University, Beijing 100037, PR China*
[b] *Institute of Quality Standards and Testing Technique for Agricultural Products, China Agricultural Academy of Science, Beijing 100081, PR China*

Received 11 January 2007; received in revised form 1 April 2007; accepted 27 April 2007
Available online 10 May 2007

Abstract

A highly selective method for the preconcentration and the determination of nitrogen heterocyclic compounds (NHCs) by solid phase extraction–room temperature phosphorimetry (SPE–RTP) was described. The β-cyclodextrin (β-CD) coated filter paper was synthesized and used as the SPE membrane and the substrate for the measurement of RTP emission of NHCs in water samples. The RTP characteristics of NHCs on the coated filter paper were studied. The conditions for the measurement of RTP intensities of NPAHs were discussed and optimized in detail. Several experimental parameters related to the preconcentration of NHCs on the coated filter paper were also examined. The experimental results showed that the β-CD coated filter paper could selectively extract NHCs containing three benzene rings with a high enrichment efficiency. The limit of detections of carbazole, 7,8-benzoquinoline and phenanthridine were found to be 9.1×10^{-14}, 8.3×10^{-13} and 7.8×10^{-13} mol mL^{-1}, respectively. The proposed method was applied to the analysis of NHCs in water samples. The recoveries of carbazole, 7,8-benzoquinoline and phenanthridine in water samples was in the range of 86.1–109.3%.

Keywords: Room temperature phosphorimetry; Solid-phase extraction; β-Cyclodextrin Modified filter paper; Nitrogen heterocyclic compounds; Carbazole; 7,8-Benzoquinoline; Phenanthridine

1. Introduction

Nitrogen heterocyclic compounds (NHCs) are of industrial, environmental and biological importance. NHCs such as quinoline, carbazole and their derivatives occur in the waste water generated in the coke plant in the coal coking, coal gas purification and by-product recovery processes [1]. Many of NHCs have been reported to be carcinogenic or increase the carcinogenic activity of benzo[a]pyrene [1,2]. Therefore, the development of a selective and sensitive analytical method for fast screening and determination of trace NHCs in water samples is of great importance.

Because of its simplicity, high selectivity and sensitivity, the solid substrate–room temperature phosphorescence (SS–RTP) has been proved as a useful analytical technique for the determination of trace toxic pollutants such as polycyclic aromatic hydrocarbons (PAHs), polychlorinated biphenyls (PCBs) and NHCs in environmental samples [3,4]. However, the concentration detection limits of SS–RTP normally are in the range of 10^{-6}–10^{-8} mol L^{-1} [5,6] which are not sensitive enough for the analysis of pollutants in water samples although the mass detection limits are very low (in the range of picogram per spot). To improve the sensitivity of SS–RTP, Chen and Hurtubise [7] reported a novel SS–RTP method in which a solid phase extraction (SPE) procedure was combined with SS–RTP. In their work, the Whatman 1PS paper was used to extract analytes from aqueous solution and then the RTP signal was measured. Because a preconcentration procedure was involved, RTP intensities of analytes were greatly increased and their detection limits were decreased to sub ng ml^{-1}. The method was further improved by Hagestuen et al. [8]. They developed a very convenience system for SPE–RTP: the commercial SPE membranes (C8 or C18) were put in a filter holder and a syringe or a vacuum pump was used to load sample solutions. Because the RTP analysis

* Corresponding author.
E-mail address: zhurh@mail.cnu.edu.cn (R. Zhu).

0039-9140/$ – see front matter © 2007 Elsevier B.V. All rights reserved.
doi:10.1016/j.talanta.2007.04.050

of analytes is directly performed on the extraction membrane, the drawbacks associated with elution steps in SPE procedure is no longer existed and limits of detection can be substantially improved by the high preconcentration factors of SPE. SPE–RTP has shown its great potential in the analysis of trace levels of organic pollutants and has been applied to the determination or recognition of PAHs [9], polychlorinated biphenyls [10] and polychlorinated dibenzofurans [11]. The sensitivities were obtained in the range of sub ng mL^{-1} to pg mL^{-1} or even lower.

So far, the SPE membranes used in SPE–RTP are limited to the hydrophobic materials such as Whatman 1PS filter paper, C8 or C18 membrane, and silicon treated filter paper [12] which are suitable for the extraction of non-polar compounds. However, these membranes are not suitable for polar compounds such as NHCs.

Cyclodextrines (CDs) are well known steroselectors and widely applied to various analytical techniques to increase the selectivity and sensitivity. With CDs treated filter paper as the substrate, the RTP intensities of target analytes could be intensified selectively [13,14] due to the formation of the inclusion complex of the cyclodextrin and the analyte with proper size. The formation of the inclusion comlplex could protect phosphorescence molecules from quenching of oxygen or other small molecules. Our previous work [15] has shown that the β-CD coated filter paper could extract PAHs containing three benzene rings selectively from water samples. The enrichment factors of fluorene and acenaphthene were 280 and 117, respectively and LODs for fluorene and acenaphthene could be achieved as low as 10 pg mL^{-1}.

In this work, the β-CD coated filter paper was used as the SPE membrane for the preconcentration of NHCs. We found that the β-CD coated filter paper could not only extract some of NHCs selectively, but also enhance their RTP intensities. The coated filter paper showed the high extraction efficiencies to some NHCs.

2. Experimental

2.1. Instrumentation

All measurements were performed with a F-4500 Fluorescence Spectrophotometer (Hitachi, Japan) equipped with a solid samples holder. The SPE experiment was carried out on the solid phase extraction device (Supelco, VISIPREPT-MDL, America) equipped with a vacuum pump. A filter holder with 13 mm in diameter (Sartorius, Germany) was used for SPE. The modified or non-modified filter papers were cut into discs with diameter of 10 mm and were placed in the filter holder. 0.5–10 μL precise pipette (Thermo Labsystems Oy, Helsinki, Finland) was used for sampling and an oven (DHG-9023A, YIHENG laboratory instrument Factory, Shanghai, China) was used for drying the filter paper. An ultrasonic device (KQ-250B, Kunshan Ultrasonic Instrument Factory, China) was used for the synthesis of β-CD coated filter paper.

2.2. Materials and reagents

Chromatography filter papers used in the experiment are made in Hangzhou Xinhua paper mill (China). β-CD, epichlorohydrin, dimethylsulfoxide, orthophenanthrolene, quinoline, isoquinoline, acridine, carbazole, 7,8-benzoquinoline were obtained from Beijing Chemical Reagent Corporation and in analytical-reagent grade. Fluorene, acenaphthene, phenanthridine were obtained from J&Kchemica and used without further purification. All other chemicals were in analytical reagent grade and from official suppliers. Sub-boiled water was used throughout. Stock solutions of NHCs were prepared in acetone and working solutions were prepared by appropriate dilution with acetone: water = 1:1 (V/V) or with water only if the concentration below 10^{-7} mol L^{-1} daily before use.

Note: extreme cautions should be taken when handling NHCs, PAHs and other organic chemicals that are known to be extremely toxic.

2.3. Coated filter paper preparation

The β-CD modified paper was prepared according to the method descried in [15]. The chromatography filter paper was cut into appropriate size (about 40 mm × 20 mm) and put in 5 mol L^{-1} sodium hydroxide solution in a conical flask about 30 min, then the mixture reagent solution of sodium hydroxide (5 mol L^{-1}): dimethylsulfoxide: epichlorohydrin of 2:4:5 (V/V/V) was added in the flask. The reaction was carried out in the ultrasonic bath for 2 h at 45 °C. After the reaction was finished, filter papers were rinsed with pure water two times and putted in a beaker containing 0.3 mol L^{-1} β-CD and 5 mol L^{-1} sodium hydroxide. The beaker was put in the ultrasonic bath for 5 h at 45 °C. After the reaction finished, the modified filter paper was washed by pure water until the pH value was 7 or so. Finally the modified filter paper was treated with the acetone and dried at ambient temperature. The prepared paper was put in the desiccator for use.

2.4. RTP measurement

The modified filter paper was cut into circles of 10 mm in diameter by a puncher. 10 μL of heavy atom solution was spotted on the modified filter paper and preheated about 30s on 95 °C, and then 10 μL of the sample solution were dotted on the modified filter paper and dried about 4 min under the same temperature. The drying paper was put in the solid sample holder and the RTP was measured immediately.

2.5. SPE–RTP procedure

The modified filter paper was placed in the filter holder and preconditioned with 10 mL pure water before use. The filter holder was mounted on the SPE device which connected to a vacuum pump. The water sample was eluted through the modified filter paper at the rate of 0.16 ml s^{-1} under the vacuum of −9 kPa. After extraction, the filter paper was removed from the filter holder carefully and the potassium iodide was dotted on

the paper. The paper was dried at 95 °C for 4 min and the RTP intensity was measured directly.

2.6. Water sample analysis

Tap water was directly analyzed without any pre-treatment. The river water sample was collected from Kunyu river in Beijing and Fenhe river in Taiyuan city, the capital city of Shanxi province where is famous for the large production of coal and coke in China. River water samples were analyzed without any other previous treatment except filtration through a general filter paper. An appropriate aliquot of stock solution of standards was spiked in the water sample for recovery studies. 50 mL of sample solutions were then analyzed according to the procedure of 2.5.

3. Results and discussion

3.1. RTP behavior of NHCs on the modified and non-modifed filter paper

The RTP properties of several NHCs absorbed on the β-CD modified and non-modified filter papers were examined and results were shown in Table 1. It can be seen in Table 1 that the RTP intensities of 7,8-benzoquinoline (BQ), carbazole (CAR), phenanthridine (PND) and isoquinoline could be selectively increased more than five times on the modified filter paper compared with that on non-modified paper. Most likely, the proper size and structure of the BQ, CAR and CAR (see Fig. 1) make them possible to form inclusion complexes with β-CD [14,16]. Because of the formation of the inclusion complexes, it could be observed that the excitation and emission wavelengths of BQ, CAR and PND were blue or red shift. It can be seen in Table 1 that the RTP intensity of isoquinoline on the coated paper was increased about 14 times higher than that on the non-modified paper. However, the RTP emission of isoquinoline was still much lower than that of other NHCs and was not of analytical significance. For the other compounds such as acridine, orthophenanthrolene and quinoline, their sizes are either too large or too small to form the stable inclusion complex with β-CD so that the large enhancements of RTP intensities were not observed. The RTP spectra of CAR, BQ and PND on the non-modified and modified filter paper were shown in Fig. 2.

If filter papers were soaked in the β-CD solution and used as the solid substrate, the similar enhancement phenomena for CAR, BQ and PND were also observed. However, in this case, β-CD molecules were absorbed on the filter paper physically and could dissolve in the solution again during the SPE procedure. Therefore, the soaked paper were not suitable for the SPE (shown in Table 3) which will be discussed later.

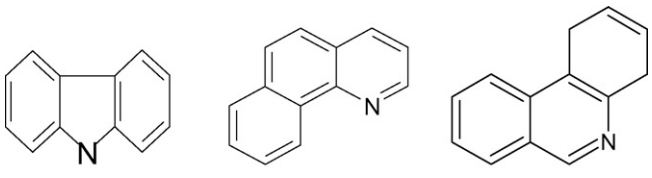

Fig. 1. The molecular structures of CAR, BQ and PND.

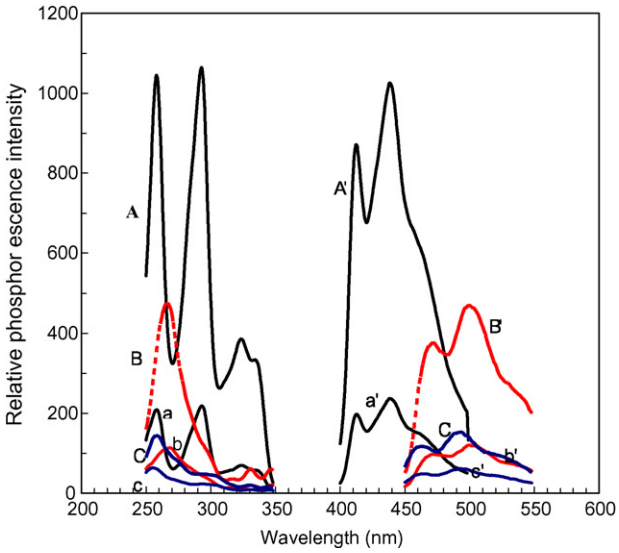

Fig. 2. RTP excitation and emission spectrum of carbazole, 7,8-benzoquinoline and phenanthridine on the β-CD coated filter paper and non-modified filter paper, the concentrations of three compounds were 4.0×10^{-5} mol L^{-1}. 10 μL of 2 mol L^{-1} KI was used as heavy atom. A, B, C and A', B', C' are excitation and emission spectra on the coated filter paper, a, b, c and a', b', c' are the RTP spectra on the non-modified filter paper. The background of the filter paper had not been subtracted.

3.2. Optimization of conditions for measurement of RTP

The addition of heavy atoms can greatly increase the RTP intensity, because heavy atom could increase the spin–orbit coupling effect and then increase the intersystem crossing rate between the lowest excitation singlet and the triplet states [17]. Different heavy atoms salts (KI, CsI, $Pb(Ac)_2$, and CsCl) were studied. The results were shown in Table 2. It can be seen in Table 2 that the CAR, BQ and PND show intense phosphorescence emission in the presence of KI. The effect of concentration of KI on the RTP intensity was examined too and the results show that proper concentration of KI solution for three compounds was 2 mol L^{-1}.

The effects of moisture and oxygen on the RTP of phosphors adsorbed on filter paper and treated filter paper have been reported [18]. It is essential to remove water completely for the measurement of SS–RTP. The drying temperature and the drying time were examined and the optimal temperature was found at 95 °C for BQ and PND and 100 °C for CAR, respectively. The drying time of the three compounds were also different. The proper drying time was 4.5 min for BQ and PND and 5 min for CAR. The appropriate preheating time was found in 0.5 min.

According to the results obtained above, the optimum experimental conditions of BQ and PND were as follows: preheated time 0.5 min, dried time 4.5 min and drying temperature 95 °C. The optimum conditions for CAR were as follows: preheated time 0.5 min, dried time 5 min and drying temperature 100 °C.

Table 1
RTP behavior of NHCs on coated and unmodified filter paper

Species	$\lambda_{ex}/\lambda_{em}$ (nm)[a]	$\lambda_{ex}/\lambda_{em}$ (nm)[b]	Relative phosphorescence intensity ratio (I_{CD}/I_0[c])
7,8-Benzoquinoline	265.2/500.2	269.4/502.8	5.97
Carbazole	295.4/441.4	293.6/440.2	4.85
Orthophenanthrolene	256.0/513.0	256.6/513.4	1.00
Quinoline	313.6/499.8	315.0/497.0	1.30
Isoquinoline	316.6/513.4	320.6/515.6	14.0
Acridine	263.0/480.4	264.0/473.6	1.60
Phenanthridine	258.4/498.6	258.8/492.2	6.76

[a] The excitation wavelength and emission wavelength of compounds on the non-modified filter paper.
[b] The excitation wavelength and emission wavelength of compounds on the modified filter paper.
[c] The ratio of RTP intensity on the modified paper to that of non-modified filter paper.

Under the optimized conditions, the linear ranges of concentrations of CAR and BQ to the RTP intensity were over three orders of magnitude (from 8×10^{-11} up to 4×10^{-8} mol mL^{-1}) with the correlation coefficient of 0.999. The concentration limit of detection for CAR and BQ were 8.6×10^{-12} and 7.76×10^{-11} mol mL^{-1}, respectively. When sampling volume was 10 μL, the absolute LODs were 14.4 pg/spot for CAR and 130.0 pg/spot for BQ.

3.3. SPE–RTP of NHCs in aqueous solutions

100 ml 8.0×10^{-8} mol L^{-1} of CAR, BQ and PND solutions was eluted through the modified paper according to the method described in the experimental part. The RTP emission spectra of three compounds before and after SPE were showed in Fig. 3. Without the SPE procedure, the intensities of RTP for three compounds were hardly observed (see Fig. 3, curves a, b and c) because their concentrations were close to the LOD. After SPE concentrated procedures, RTP intensities of target analytes were strengthened obviously (see Fig. 3 curves A, B, C).

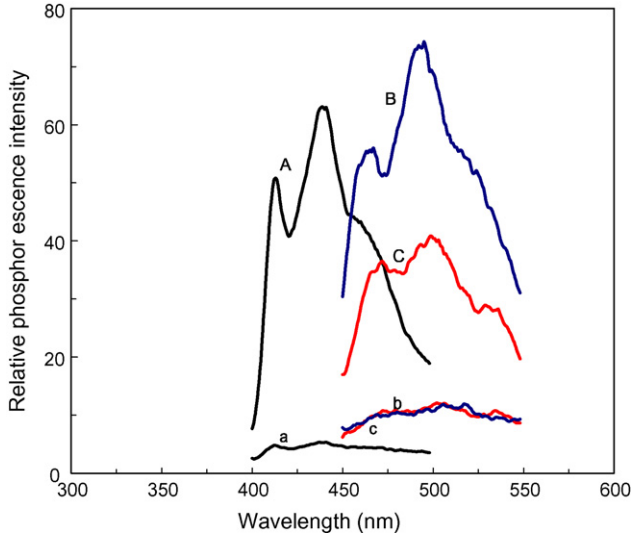

Fig. 3. Comparison of RTP intensities of carbazole, 7,8-benzoquinoline and phenanthridine before and after SPE. Concentrations of carbazole 7,8-benzoquinoline and phenanthridine all are 8.0×10^{-11} mol mL^{-1}, 10 μL of KI heavy atom salt solution was spotted on the modified filter paper after SPE. A, a, B, b and C, c are RTP emission spectra of carbazole, 7,8-benzoquinoline and phenanthridine after and before SPE, respectively.

3.4. Extraction efficiency of SPE

In the SPE procedure, factors influencing SPE efficiency include the distribution constant, the volume and concentration of analytes and the eluting rate. The distribution constants are calculated by Eq. (1) [7]

$$n_s = KV_sC_{aq} \quad (1)$$

where n_s is the amount of target compound on the paper after extraction from water solution, V_s the volume of the solid phase, C_{aq} the concentration of solution before extraction, K the distribution constant. The distribution constant K is the characteristics of the extraction material and the analyte. Large K values mean higher affinity between the extraction material and the analyte. To calculate the V_s ($V_s = \pi r^2 h$, where r is the radius of the modified paper and h the thickness of the paper), the average diameter was calculated by the average diameter of five pieces of filter paper and the average thickness was calculated from the height of 10 pieces of paper stacked together. The average radius and thickness of the modified filter paper were 10.3 and 0.17 mm, respectively. Therefore, the volume of the modified filter paper, V_s was calculated as 1.33×10^{-2} cm^3. Table 3 shows the calculated K values and the enrichment factors for different compounds on the coated filter paper, soaking filter paper and non-modified filter paper. The coated filter paper showed very good extraction ability for CAR, BQ and PND. After extraction, the enrichment factors were about 500 times for CAR, 96 times for BQ and 67 times for PND, respectively. The extrac-

Table 2
Heavy atom effect[a] on RTP emission of several NHCs deposited on the coated filter paper

Species	CAR (8.0×10^{-5} mol/L)	BQ (2.0×10^{-5} mol/L)	PND (8.0×10^{-5} mol/L)
$Pb(Ac)_2$	1.00[a]	1.00[a]	1.00[a]
KI	28.7	4.58	12.6
CsI	6.47	1.09	7.61
CsCl	6.45	0.87	3.90

[a] The ratio of RTP intensities of analytes with the heavy atom CsI, KI, CsCl and with $Pb(Ac)_2$.

Table 3
Distribution constants and enrichment efficiencies on the coated, soaking and non-modified filter paper

Analytes[d]	Modified filter paper		Soaking filter paper		Non-modified filter paper	
	K[a]	E[b]	K	E	K	E
CAR	440[d]	516	3.95	75.0	–[c]	–
BQ	75.2	96.8	6.48	21.3	–	–
PND	50.7	67.5	6.86	9.20	–	–

[a] Distribution constant.
[b] Enrichment efficiency: the enrichment efficiency was the ratio of the RTP intensities of sample solution after and before SPE.
[c] The target analytes do not show the RTP signal on the non-modified filter paper.
[d] The concentration of carbazole solution is 6.4×10^{-12} mol mL^{-1}. Concentrations of other compounds are 8.0×10^{-11} mol mL^{-1}.

tion efficiencies of β-CD soaked filter paper were poor, because β-CD molecules were physically absorbed on the filter paper and dissolved in the sample solution again during the process of extracting easily. On the non-modified filter paper, no RTP signal was observed, indicating that CAR, BQ and PND could not be extracted.

In order to study the possible losing amount of target analytes, two filter holders were connected and the solutions of CAR and BQ were successively eluted through two filter holders (see Fig. 4). From Fig. 4, the extraction proportions on the first extraction disk were about 90.2% for CAR and 86.4% for BQ, respectively. Therefore, one SPE membrane was enough for the extraction of NHCs from water samples.

3.5. Extraction capacity of the coated paper

Because of the amount of CD molecules coated on the filter paper surface are limited, the extraction capacity of the coated filter paper is limited. If solution with the certain concentration is excessive in volume, the coated paper will be saturated and the loss of analytes after the membrane being saturated will cause the error of analysis. The loading curves of CAR, BQ and PND were measured and the results were shown in Fig. 5. As shown in Fig. 5, three compounds had similar saturation volumes. When concentrations of CAR, BQ and PND were 6.4×10^{-11}, 8.0×10^{-11} and 8.0×10^{-11} mol mL^{-1}, respectively, the saturation volume was 75 ml for BQ and PND and 100 ml for CAR, respectively. If the extraction efficiency was about 80%, the mols of BQ, PND and CAR on the modified paper were almost same which were probably 4.8×10^{-9}, 4.8×10^{-9} and 5.1×10^{-9} mol, respectively. Since non-modified filter papers do not have extraction ability as mentioned above, probably only molecules those have entered the cavity of CD could be extracted on the modified paper, which implied that moles of β-CD on the filter paper may be roughly about 10^{-7}–10^{-8} mol.

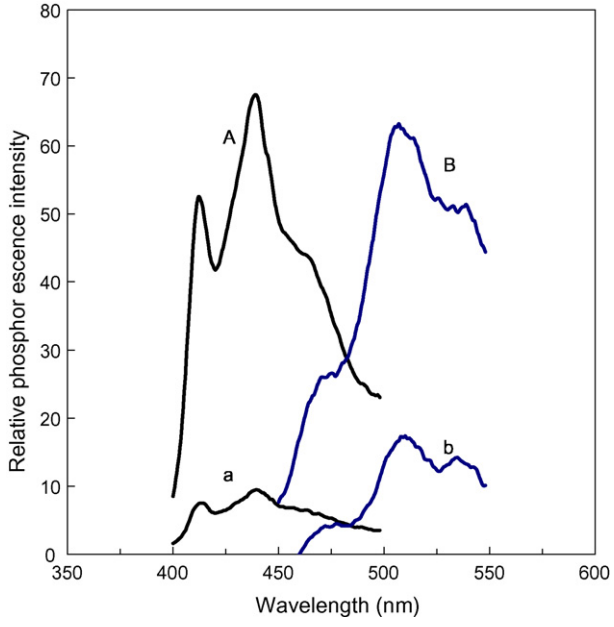

Fig. 4. Spectra of SPE–RTP of compounds with double-disks extraction. Concentrations of carbazole and 7,8-benzoquinoline all are 8.0×10^{-11} mol mL^{-1}, 10 μL of KI heavy atom salt solution was spotted on the modified filter paper after SPE. A, a are spectra of carbazole on the first disk and the second disk. B, b are the spectra of 7,8-benzoquinoline on the first disk and the second disk.

3.6. Interference study

The potential interference of concomitants such as PAHs, NHCs and so on was evaluated. The tolerant ratios of the concentration of interferences over that of analytes within the relative

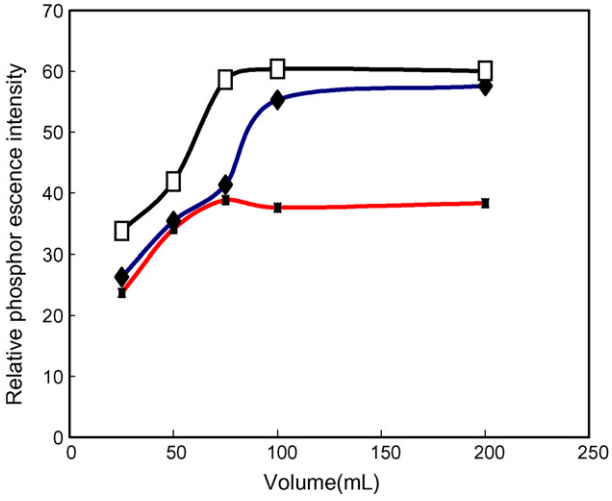

Fig. 5. Loading curves of target analytes (□) 7,8-benzoquinoline (8.0×10^{-8}mol/L), (♦) carbazole (6.4×10^{-8}mol/L), (■) phenanthridine (8.0×10^{-8}mol/L).

Table 4
The tolerant concentration ratio of interferences and analytes

Interference compounds	CBZ[a]	BQ[a]	PND[a]
Quinoline	5	10	2
Isoquinoline	5	10	2
Acridine	5	10	2
Orthophenanthrolene	5	10	2
Anthracene	2	0.5	0.5
Acenaphthylene	2	0.5	0.5
Fluoranthene	2	0.5	0.5
Acenaphthene	2	0.2	0.4
Chrysene	1	0.05	0.05
Pyrene	2	0.5	0.5
CAR	–	5	5
BQ	2	–	0.05
PND	5	0.01	–

[a] The ratio of the concentration of interference compounds and target analytes.

error ±5.0% were listed in Table 4. Each compound was individually studied for the RTP behavior on the extraction membrane. From the Table 4, the results demonstrated that quinoline, isoquinoline, acridine, and orthophenanthrolene did not interfere with the RTP measurements of CAR, BQ and PND seriously. CAR did not interfere with the RTP of BQ and PND seriously because the excitation and emission wavelength of CAR were not overlap with those of BQ and PND. However, since the spectra of BQ and PND were completely overlapped each other, BQ and PND were strongly interfered each other. The interferences of PAHs to NHCs were very strong. It is probably due to the very low polar of PAHs. Therefore, the PAHs molecules could enter into CD cavity easily and blocked the cavity of CDs to prevent NHCs molecules from entering the cavity. In addition, higher PAHs concentrations would probably cause RTP quenching due to the absorption of excitation energy. Possibly a simple liquid–liquid extraction or filtering the water sample solution with C18 SPE column prior to extracting with the modified paper would help to decrease the interference.

3.7. Analytical figures of merits (AFOM)

The SPE–RTP AFOM are shown in Table 5, SPE–RTP measurement of standards were performed with 50 ml of aqueous samples. For each concentration plotted in the calibration graph, the RTP intensity was the average of five single determinations taken from five extraction disks. The correlation coefficients of the calibration curves (R) were close to unity, indicating a linear relationship between the concentration of the three compounds and phosphorescence intensity. Because of the limitation of the saturation concentration of the extraction, the linear range was narrower than that obtained without SPE procedure. The good precision was obtained. For five measurements, the relative standard deviations (R.S.D.) were below 7.3%

The stability and repeatability of modified filter paper were satisfactory. The RSDs of RTP intensities on the modified filter paper were below 8.5% from day to day in the same batch and below 16% from batch to batch, respectively.

The LODs of three compounds were at the 10^{-12}–10^{-14} mol mL^{-1} range. These values compared favorably to the LOD estimated by the classical RTP procedure on solid substrates and other RTP methods. The improvement, which is approximately two orders of magnitude, is due to the pre-concentration of samples by SPE. It is important to note that the lower SPE–RTP LOD could be obtained by performing successive extractions of several 100 ml aliquots.

Table 5
Solid-phase extraction room temperature phosphorescence analytical figures of merit of several NCHs ($n = 5$)

Compound[a]	R^2[b]	LDR (mol mL^{-1})[c]	R.S.D. (%)	LOD (mol mL^{-1})[d]
CAR	0.9959	4.0×10^{-13}–8.0×10^{-11}	3.9	9.1×10^{-14}
BQ	0.9953	4.0×10^{-12}–8.0×10^{-10}	5.3	8.3×10^{-13}
PND	0.9934	4.0×10^{-12}–2.0×10^{-10}	7.3	7.8×10^{-13}

[a] 10 μL volume of heavy atom KI solution (2.0 mol/L) was deposited on the modified filter paper after the SPE procedure.
[b] Correlation coefficient of the calibration curve.
[c] Linear dynamic range.
[d] Limit of detection. LOD was calculated based on the equation $LOD = 3S_B/m$, S_B is the standard deviation of the blank based on 10 measurements, and m is the slope of the calibration curve based on five concentrations within the LDR.

Table 6
Recoveries of CAR, BQ and PND in water samples ($n = 5$)

Samples	CAR			BQ			PND		
	Added (mol mL^{-1})	Found (mol mL^{-1})	Recovery (%)	Added (mol mL^{-1})	Found (mol mL^{-1})	Recovery (%)	Added (mol mL^{-1})	Found (mol m^{-1})	Recovery (%)
Kunyu river water	3.2×10^{-11}	3.4×10^{-11}	106.2 ± 4.3	4.0×10^{-11}	4.1×10^{-11}	101.3 ± 4.9	1.6×10^{-11}	1.4×10^{-11}	90.4 ± 4.5
	8.0×10^{-12}	8.7×10^{-12}	109.3 ± 6.8	8.0×10^{-12}	8.6×10^{-12}	105.6 ± 4.2	8.0×10^{-12}	6.6×10^{-12}	91.3 ± 7.7
Fenhe river water	3.2×10^{-11}	3.3×10^{-11}	103.1 ± 4.1	4.0×10^{-11}	3.9×10^{-11}	97.5 ± 5.9	1.6×10^{-11}	1.4×10^{-11}	87.5 ± 4.6
	8.0×10^{-12}	8.4×10^{-12}	105.0 ± 5.3	8.0×10^{-12}	8.2×10^{-12}	102.5 ± 4.1	8.0×10^{-12}	7.6×10^{-12}	95.0 ± 5.5
Tab water	3.2×10^{-11}	3.0×10^{-11}	95.1 ± 7.8	4.0×10^{-11}	3.8×10^{-11}	94.3 ± 4.0	1.6×10^{-11}	1.4×10^{-11}	89.5 ± 5.3
	8.0×10^{-12}	7.5×10^{-12}	93.8 ± 6.1	8.0×10^{-12}	6.9×10^{-12}	86.7 ± 5.1	8.0×10^{-12}	6.9×10^{-12}	86.1 ± 8.1

3.8. Analysis of water samples

The proposed method was applied to determination of CAR, BQ and PND in water samples. River water samples were collected from Kunyu river and Fenhe river and were filtered with a general filter paper to remove the suspending dusts. Tap water sample was collected from daily tap water without any treatment. An amount of CAR, BQ and PND were spiked in 50 ml river water samples and tap water. The spiked solution directly extracted using β-CD modified filter paper and measured immediately after dotting heavy atom solution and drying. The results were shown in Table 6, as can be seen, recoveries for the determination of CAR, BQ and PND were higher than 85% with the RSD ($n = 5$) ≤8.1%. Because of the space selectivity of β-CD, larger or smaller molecules such as quinoline, isoquinoline, acridine and so on could not enter the cavity of β-CD to form an inclusion complex, and therefore could not be extracted from the water samples. In addition, some smaller phosphorescent molecules, such as naphthalene derivatives could not come into being stable inclusion complex and thus did not interfere with the RTP detection of CAR, BQ and PND.

4. Conclusions

A SPE–RTP method for preconcentration and determination of some NHCs with β-CD coated filter paper as the substrate was developed. The β-CD coated filter paper has shown the excellent abilities of enrichment and selectivity. The coated filter paper is cheap, simple and easy to prepare with good stability and reproducibility. The proposed method has the potential for screening of trace levels of some NHCs in water samples. However, the interferences of some of PAHs compounds which phosphoresce strongly are relatively high. The interference could be decreased by coupling with other CDs such as α-CD, γ-CD or derivatized CD on the filter paper or by the synchronous technique. The work on this subject is in the progress in our lab.

References

[1] J.L. Wang, X.C. Quan, L.B. Wu, Y. Qian, H. Werner, Process Biochem. 38 (2002) 777–781.
[2] M. Dong, I. Schmeltz, E. LaVoie, D. Hoffman, in: P.W. Jones, R.I. Freudenthal (Eds.), Carcinogenesis, 3, Raven Press, New York, 1978.
[3] A.D. Campiglia, D.M. Hueber, T. Vo-Dinh, Appl. Spectrosc. 50 (1996) 252–256.
[4] J. Wang, R.J. Hurtubise, Appl. Spectrosc. 50 (1996) 53–115.
[5] X.H. Feng, C.G. Gao, C. Dong, W.J. Jin, Chem. Res. Appl. 12 (2000) 440–441.
[6] W.J. Jin, C.S. Liu, J.L. Gao, X. Yang, Huaxue Shiji 15 (1993) 259–261.
[7] J. Chen, R.J. Hurtubise, Talanta 47 (1998) 971–979.
[8] E.D. Hagestuen, A.F. Arruda, A.D. Campiglia, Talanta 52 (2000) 727–737.
[9] H.A. Amanda, R.J. Hurtubise, Appl. Spectrosc. 53 (1999) 770–775.
[10] A.F. Arruda, H.C. Goicoechea, M. Santos, A.D. Campiglia, A.C. Olivieri, Environ. Sci. Technol. 37 (2003) 1385–1391.
[11] A.F. Arruda, A.D. Campiglia, Environ. Sci. Technol. 34 (2000) 4982–4988.
[12] A.H. Ackerman, R.J. Hurtubise, Anal. Chim. Acta 474 (2002) 77–89.
[13] J.M. Bello, R.J. Hurtubise, Anal. Lett. 19 (1986) 775–796.
[14] J.M. Bello, R.J. Hurtubise, Anal. Chem. 59 (1987) 2395–2400.
[15] R.H. Zhu, P.L. Wang, X.F. Wang, Luminescence 20 (2005) 382–388.
[16] L.J.S. Scypinski, C. Love, Anal. Chem. 56 (1984) 331–336.
[17] T. Vo- Dinh, Room Temperature Phosphorimetry for Chemical Analysis, Wiley, New York, 1984.
[18] R.A. Dalterio, R.J. Hurtubise, Anal. Chem. 56 (1984) 336–341.